

Republic of Iraq
Ministry of Higher Education and Scientific Research
University of Baghdad
College of Education for Pure Science (Ibn-Al-Haitham)
Department of Chemistry



*Synthesis, Structural Characterisation, Thermal properties and
Biological Activity of New Complexes Derived from Ligands
with N, O and S Donor Atoms*

A Thesis

*Submitted to the Council of College of Education for Pure Science (Ibn
Al-Haitham) /University of Baghdad in Partial Fulfillment of the
Requirements for the Degree of Master of Science in Inorganic
Chemistry*

By

Nihad Kadhum Hasan

*B.Sc. in Chemistry 2003 College of Education (Ibn Al-Haitham)
/University of Baghdad*

Supervisor

Assistant Prof. Dr. Enaam Ismail Yousif

2019AD

1441 AH



قَالُوا سُبْحَانَكَ لَا عِلْمَ لَنَا إِلَّا

مَا عَلَّمْتَنَا إِنَّكَ أَنْتَ الْعَلِيمُ

الْحَكِيمُ

(صدق الله العظيم)

(سورة البقرة/الآية 32)

Certification

I certify that, this thesis was prepared under my supervision at Department of Chemistry, College of Education for Pure Science (Ibn-Al-Haitham) / University of Baghdad in partial requirements for the Degree of Master of Science in Inorganic Chemistry, and this work has never been submitted or published anywhere else.


Signature

Name: Dr. Enaam Ismail Yousif (Supervisor)

Title: Assistant Prof

Address: Department of Chemistry, College of Education for Pure Science /(Ibn-Al-Haitham) University of Baghdad, Iraq.

Date: 2/9/2019

In the view of the available recommendation, I forward this thesis for debate by the Examination Committee.


Signature

Name: Dr. Mohamad J. Al-Jeboori


Title: Professor

Address: Head of Department of Chemistry, College of Education for Pure Science /(Ibn-Al-Haitham) University of Baghdad, Iraq.

Date: 2/9/2019


Examination Committee


We, the examination committee, after reading this thesis and examining the student (*Nihad Kadhum Hasan*), in its content, we have found it worthy to be accepted for the degree of Master in Inorganic Chemistry with (excellent).


Signature
Name: Dr. Mohamed J. Al-Jeboori
(Chairman)
Title: Professor
Address: College of Education for Pure
Science, Ibn-Alhatham, University of
Baghdad, Iraq.
Date: 4/11/2019

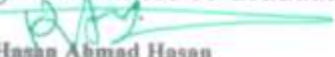


Signature
Name :Dr.Mahmoud Saleh Muter
(Member)
Title: Assistant Prof
Address: Dentistry College , University of
Anbar
Date: 4/11/2019


Signature
Name: Dr. Riyadh Mahmood Ahmed
(Member)
Title: Assistant Prof
Address: College of Education for Pure Science, Ibn-
Alhatham, University of Baghdad
Date:4/11/2019


Signature
Name: Dr. Enaam Ismail Yousif
(Supervisor)
Title: Assistant Prof.
Address: College of Education for Pure
Science, Ibn-Alhatham, University of
Baghdad, Iraq.
Date: 4/11/2019

Approved for the College Committee of Graduate Studies


Signature
Name: Dr. Hasan Ahmad Hasan
Title: Professor
Address: Dean of College of Sciences
University of Baghdad
Date: 4/11/2019

Acknowledgment

Thanks to Allah the One the Single for all this blessing during my study and all my life.

I would like to express my sincere thanks and appreciation to my supervisor **Assistant Prof. Dr. Enaam Ismail Yousif**. My grateful thanks are paid to **Assistant Prof. Dr. Riyadh Mahmood Ahmed**. Also, my grateful thanks to the staff members of the College of Education for Pure Science (Ibn al-Hiatham) especially those in the chemistry department. My thanks are due to the dean of the College **Prof. Dr. Hasan Ahmad Hasan** and the Head of the chemistry department **Prof. Dr. Mohamad J. Al-Jeboori**. I am grateful to; the Central Laboratory, College of Education for Pure Science Ibn Al-Haitham, to my friends Safaudeen, Ammar, Maha and Sabreen and all others who gave me help and sincere cooperation. I am deeply indebted and my appreciation is due to my family for their support and patience during the years of my study.

Nihad Kadhum Hasan

Baghdad, Iraq

2019 AD

Dedication

To my mother and father

To my brothers

To my beloved wife

To my dear daughters Howrah and

Rafale

To those who taught me science

with love

Summary

This research involved the preparation and characterisation of two types of ligands and their metal complexes. The first ligand (Mannich-base) was prepared using calcium chloride, HCl and EtOH, which were used as a catalyst and reaction medium, by mixing three components: 4-dimethylaminobenzaldehyde with 2-nitroaniline and dimedone and molar ratios of 1: 1: 1.

Where: $HL^1 = L^1$

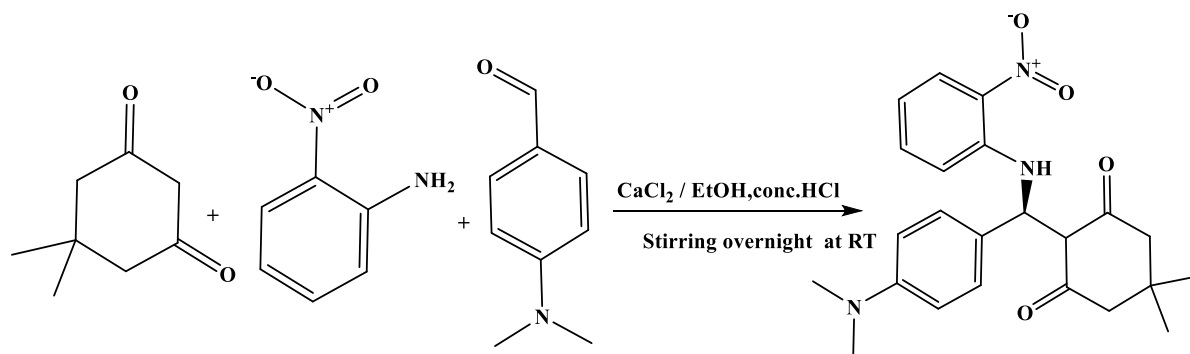
$HL^1 = R$ -2-((4-(dimethylamino)phenyl)((2-nitrophenyl)amino)methyl)-5,5-dimethylcyclohexane-1,3-dione.

While the second ligand (Schiff-base) was prepared from the reaction of the first ligand with thiosemicarbazide at molar ratios of 1: 1.

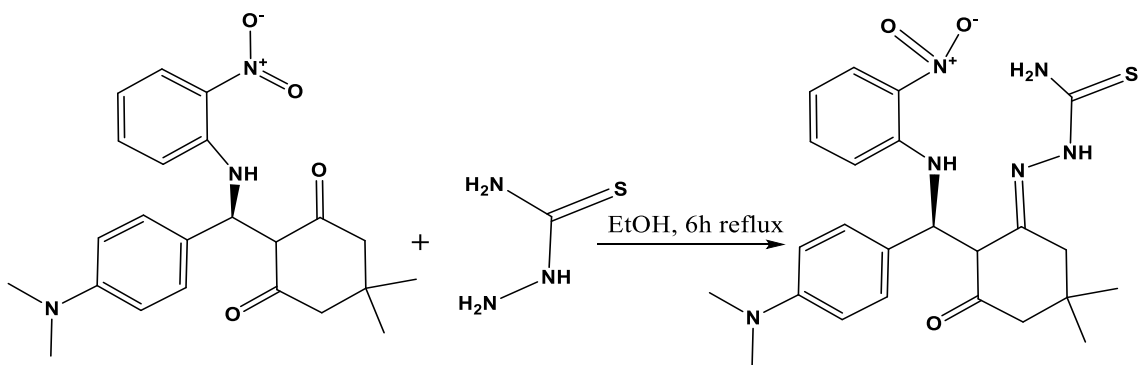
Where: $H_2L^2 = L^2$

$H_2L^2 = (E)$ -2-(2-((S)-(4-(dimethylamino)phenyl)((2-nitrophenyl)amino)methyl)-5,5-dimethyl-3-oxocyclohexylidene)hydrazine-1-carbothioamide .

The following diagrams illustrates the preparation of the ligands.



Scheme 1: General synthetic route of HL^1 .



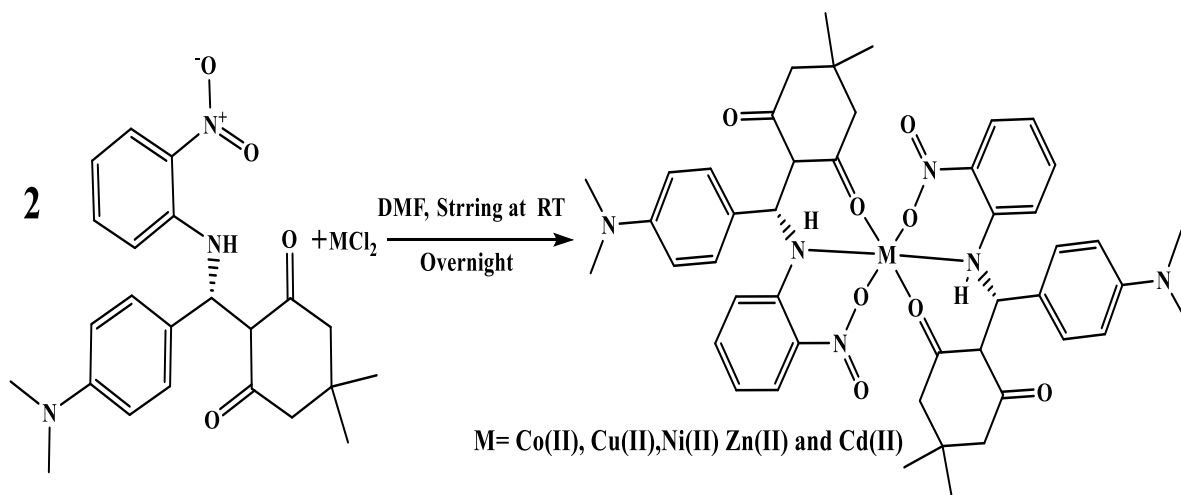
Scheme 2: General synthetic route of H_2L^2 .

Both ligands were used to prepare a series of metal complexes with metal ion: (Co(II), Ni(II), Cu(II), Zn(II) and Cd(II)), at mixing molar ratios of 1: 2 (metal: Ligand) using DMF as reaction medium. The general formula of complexes of HL^1 is $[M(HL^1)_2]$ where M= Co(II), Ni(II), Cu(II), Zn(II) and Cd(II).

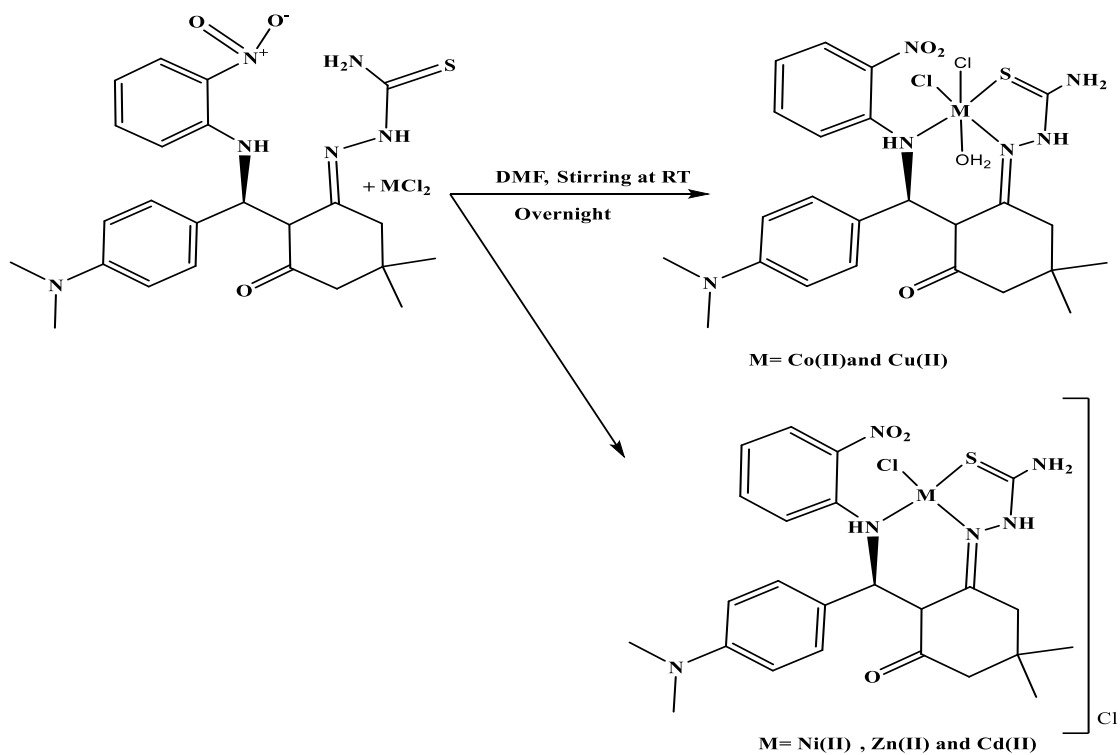
The general formula of complexes of H_2L^2 is $[M(H_2L^2)Cl_2H_2O]$ where M= Co (II) and Cu (II)

$[M(H_2L^2)Cl]Cl$ where M= Ni(II), Zn(II) and Cd(II)

Ligands and complexes were characterised using elemental analysis, melting points, metal content, chloride content, thermal analysis (for selective complexes), magnetic susceptibility, conductance, FTIR, UV-Vis and $^1H,^{13}C$ -NMR and electrospray mass spectroscopy.



Scheme 3: General synthetic route of complexes of HL¹.



Scheme 4: General synthetic route of complexes of H₂L².

Summary

Based on spectral analytical data, the following forms are proposed:

1. Distorted octahedral geometries for all of complexes min HL^1 (Co(II), Ni(II), Cu(II), Zn(II) and Cd(II)).
2. Distorted octahedral geometries for complexes of H_2L^2 with (Co(II) and Cu(II)).
3. Square planer geometry for complexes of H_2L^2 with Ni(II)
4. Tetrahedral geometries for complexes min H_2L^2 with (Zn(II) and Cd(II)).

The biological activities of all ligands and their metal complexes were characterised for two types of bacteria G positive (*Staphylococcus aureus* and *Bacillus subtilis*) and G negative (*Escherichia coli* and *Pseudomonas aeruginosa*). The activity was diagnosed in the for two types fungi namely (*Candida* and *Trichomoniasis*).

contains

	Subjects	Page
	Summary	I-IV
	List of contains	V-X
	List of tables	XI-XIII
	List of figures	XIV- XVIII
	List of schemes	XIX
	List of abbreviation	XX-XX I
Chapter one		
(1)	Introduction	
(1.1)	Schiff-bases	1
(1.2)	Chemistry of Schiff base	1
(1.2.1)	Mechanism of Azomethine	3
(1.3)	Mannich- β -amino carbonyl	4
(1.3.1)	Dimedone (5,5-Dimethylcyclohexane-1,3-dione)	5
(1.3.2)	Tautomerization	6
(1.3.3)	Mechanism of β -amino carbonyl	7
(1.4)	Schiff-base with N,O chelating system	9
(1.4.1)	Coordination compounds (nitrogen carbonyl oxygen moiety)	13
(1.4.2)	Coordination N and S in thiosemicarbazone moiety	22
(1.5)	Applications and uses of mannih reaction and Schiff-base	29
(1.5.1)	Biomedical applications	29
(1.5.1.1)	Pharmaceutical Application	29

contains

(1.5.1.2)	Biological activity	32
(1.5.2)	Analytical application	33
(1.5.3)	Industrial application (liquid crystal)	34
(1.6)	Aim of the work	36

Chapter two: Experimental		
(2.0)	Experimental section	37
(2.1)	Materials and Solvents	37
(2.2)	Physical measurement	39
(2.2.1)	Melting point	39
(2.2.2)	Fourier infrared spectra (FT-IR)	39
(2.2.3)	Electronic spectra	39
(2.2.4)	Mass spectroscopy	40
(2.2.5)	Conductivity measurements	40
(2.2.6)	Metal analysis	40
(2.2.7)	Nuclear magnetic resonance spectra (NMR)	40
(2.2.8)	Elemental microanalyses	41
(2.2.9)	Chloride content	41
(2.2.10)	Thermal analysis	41
(2.2.11)	Magnetic moment measurement	41
(2.2.12)	Anti-microbial activity	42
(2.2.13)	Molecular modelling	42
(2.3)	Ligands	43
(2.4)	Synthesis	44

contains

(2.4.1)	Synthesis of ligands	44
(2.4.1.1)	Synthesis of (R)-2-((4-(dimethylamino) phenyl) ((2-nitrophenyl)amino)methyl)-5,5-dimethylcyclohexane-1,3-dione(HL ¹)	44
(2.4.1.2)	Synthesis of (E)-2-(2- ((S)- (4-(dimethylamino)phenyl) ((2-bnitrophenyl)amino)methyl)-5,5-dimethyl-3-oxocyclohexylidene)hydrazine-1-carbothioamide (H ₂ L ²)	44
(2.5)	Complexes	45
(2.6)	Synthesis of HL ¹ Complexes	46
(2.6.1)	Synthesis of [Co(HL ¹) ₂](1)	46
(2.6.2)	Synthesis of [Ni(HL ¹) ₂](2), [Cu(HL ¹) ₂](3), [Zn(HL ¹) ₂] (4) and [Cd(HL ¹) ₂](5)	46
(2.7)	Synthesis of H ₂ L ² complexes	46
(2.7.1)	Synthesis of [Co(H ₂ L ²) ₂] (1)	46
(2.7.2)	Synthesis of [Ni(H ₂ L ²)](2), [Cu(H ₂ L ²)](3), [Zn(H ₂ L ²)](4) and [Cd(H ₂ L ²)] (5).	47
Chapter three:Results and discussion		
(3.1)	Synthesis and characterisation of ligands	49
(3.1.1)	Synthesis and characterisation of ligand HL ¹	49
(3.1.2)	Synthesis and characterisation of H ₂ L ²	50
(3.2)	FT-IR spectral data of ligands	51
(3.2.1)	FT-IR spectrum of HL ¹	51
(3.2.2)	FT-IR spectrum of H ₂ L ²	54
(3.3)	Synthesis and characterisation of metal complexes	57
(3.3.1)	Synthesis and characterisation of HL ¹ complexes	57

contains

(3.3.2)	Synthesis and characterisation of H_2L^2 complexes	60
(3.4)	FT-IR spectral data of complexes	62
(3.4.1)	FT-IR spectra of HL^1 complexes	62
(3.4.1.1)	FT-IR spectra of $[Co(HL^1)_2]$ (1), $[Ni(HL^1)_2]$ (2), $[Cu(HL^1)_2]$ (3), $[Zn(HL^1)_2]$ (4) and $[Cd(HL^1)_2]$ (5)	62
(3.4.2)	FT-IR spectral data of H_2L^2 complexes	67
(3.4.2.1)	FT-IR spectra of $[Co(H_2L^2)H_2O]Cl_2]$ (6), $[Ni(H_2L^2) Cl] Cl$ (7), $[Cu(H_2L^2)]Cl_2H_2O]$ (8), $[Zn(H_2L^2)]Cl]Cl$ (9) and $[Cd(H_2L^2)]Cl]Cl$ (10).	67
(3.5)	UV-Vis Spectral of ligands and their complexes	75
(3.5.1)	UV-Vis spectral data of ligands (HL^1 and H_2L^2)	75
(3.6)	UV-Vis Spectra of complexes	77
(3.6.1)	UV-Vis Spectra of $[Co(HL^1)_2]$ (1), $[Ni(HL^1)_2]$ (2), $[Cu(HL^1)_2]$ (3), $[Zn(HL^1)_2]$ (4) and $[Cd(HL^1)_2]$ (5) Complexes	77
(3.6.2)	UV-Vis spectra of $[Co(H_2L^2) Cl_2H_2O]$ (6), $[Ni(H_2L^2)Cl]Cl$ (7), $[Cu(H_2L^2) Cl_2H_2O]$ (8), $[Zn(H_2L^2) Cl]Cl$ (9) and $[Cd(H_2L^2) Cl]Cl$ (10) Complexes	81
(3.7)	Magnetic moment behaviour	86
(3.7.1)	Magnetic moment of HL^1 complexes	90
(3.7.1.1)	Examples for the calculation of magnetic moment	90
(3.7.2)	Magnetic moment of H_2L^2 complexes	92
(3.7.2.1)	Examples for the calculation of magnetic moment	92
(3.8)	Electrospray (+) mass spectra	95
(3.8.1)	Mass spectrum of HL^1	95
(3.8.2)	Mass spectrum of H_2L^2	97
(3.9)	Nuclear magnetic resonance (NMR) spectra of compounds.	99

contains

(3.9.1)	Nuclear magnetic resonance (NMR) spectrum of HL^1 and H_2L^2	99
(3.9.1.1)	1H -NMR spectrum of HL^1	99
(3.9.1.2)	1H -NMR spectrum of H_2L^2	100
(3.9.2.1)	^{13}C -NMR spectrum of HL^1	103
(3.9.2.2)	^{13}C -NMR spectrum of H_2L^2	104
(3.9.3)	Nuclear magnetic resonance (NMR) spectral for complexes	108
(3.9.3.1)	1H -NMR spectrum of $[Zn(HL^1)_2]$.	108
(3.9.3.2)	1H -NMR spectrum of $[Zn(H_2L^2)Cl]Cl$	110
(3.9.3.3)	^{13}C -NMR spectrum of $[Zn(HL^1)_2]$	113
(3.9.3.4)	^{13}C -NMR spectrum of $[Zn(H_2L^2)Cl]Cl$	115
(3.10)	Thermal analysis of ligands and complexes.	119
(3.10.1)	Thermal decomposition of ligands.	119
(3.10.1.1)	Thermal decomposition of HL^1 .	119
(3.10.1.2)	Thermal decomposition of H_2L^2 .	121
(3.10.2)	Thermal decomposition of some complexes.	123
(3.10.2.1)	Thermal decomposition of $[Zn(HL^1)_2]$ complex.	123
(3.10.2.2)	Thermal decomposition of $[Ni(H_2L^2)Cl]Cl$ complex.	124
(3.10.2.3)	Thermal decomposition of $[Cu(H_2L^2)Cl_2H_2O]$ complex.	125
(3.11)	Molar conductivity measurement of the complexes.	129
(4.1)	Microbiological activity.	130
(4.1.1)	Anti-bacterial activity.	130
(4.1.1.1)	Anti-bacterial activity of HL^1 and its complexes	130
(4.1.1.2)	Anti-bacterial activity of H_2L^2 and its complexes.	132
(4.1.2)	Anti-Fungi activity	138
(4.1.2.1)	Anti-fungi activity of HL^1 and its complexes.	138

contains

(4.1.2.2)	Anti-fungi activity of H_2L^2 and its complexes.	139
(3.12)	Conclusions and the proposed molecular structure of ligands and their complexes.	143
(3.12.1)	FT-IR Spectra data.	143
(3.12.2)	UV-Vis Spectra and magnetic susceptibility.	145
(3.12.3)	Conductivity measurements.	146
(3.12.4)	Microanalysis.	146
(3.12.5)	NMR data.	147
(3.12.6)	Thermal gravimetric analysis.	147
(3.12.7)	Mass spectra.	147
(3.13)	Prospective studies.	152
	References	
	الخلاصة	

contains

List of Tables

	<i>Table</i>	<i>Page</i>
(2-1a)	Table (2-1a): Organic reagents used in this work and their supplier.	37
(2-1b)	Inorganic reagents used in this work and their supplier.	38
(2-2)	Abbreviation, structure and nomenclature of the synthesised ligand.	43
(2-3)	Some physical properties of the prepared ligands.	45
(2-4)	Abbreviation, structure and nomenclature of the synthesised complexes.	45
(2-5)	Metal salts quantities, yields colours, melting points of complexes of HL^1	47
(2-6)	Metal salts quantities, yields colours, melting points of complexes of H_2L^2	48
(3-1)	The solubility of ligands in different solvents.	51
(3-2)	Micro analysis and physical properties for ligands.	51
(3-3)	The FT-IR spectral data of ligands (cm^{-1}).	56
(3-4)	The solubility of HL^1 complexes in different solvents.	58
(3-5)	Micro analysis and physical properties of HL^1 complexes.	59
(3-6)	The solubility of H_2L^2 complexes in different solvents.	61
(3-7)	Micro analysis and physical properties of H_2L^2 complexes.	61
(3-8)	The FT-IR spectral data of HL^1 complexes (cm^{-1}).	66
(3-9)	The FT-IR spectral data of H_2L^2 complexes (cm^{-1}).	74
(3-10)	Electronic spectral data for the ligands HL^1 and H_2L^2 in	76

contains

	DMSO solutions	
--	----------------	--

<i>Table</i>		
(3-11)	Electronic spectra data of HL ¹ complexes	80
(3-12)	Electronic spectra data of H ₂ L ² complexes	85
(3-13)	Pascal's constants values of cations	87
(3-14)	Pascal's constants values of atoms in covalent species.	87
(3-15)	Pascal's constants values for specific bond types	88
(3-16)	Theoretical spin only values of magnetic moments of the metal ions, d-configuration, number of unpaired electron for, octahedral , tetrahedral and square planer geometry	89
(3-17)	Values of spin only of the metal ions	89
(3-18)	Experimental data of the magnetic moment susceptibility	94
(3-19)	¹ H-NMR data for ligands measured in DMSO-d ₆ and chemical shift in ppm (δ).	102
(3-20)	¹³ C-NMR data for ligands measured in DMSO-d ₆ and chemical shift in ppm (δ).	106
(3-21)	. ¹ H-NMR data for [Zn (HL ¹) ₂] measured in DMSO-d ₆ and chemical shift in ppm (δ).	111
(3-22)	¹³ C-NMR data for [Zn(HL ¹) ₂] measured in DMSO-d ₆ and chemical shift in ppm (δ).	116
(3-23)	Thermal analysis data of ligands and some of their	127

contains

	complexes	
(3-24)	Molar conductivity measurement of the complexes	129
(4-1)	The inhibition zones (mm) of anti-bacterial activity for ligands and thier complexes.	133
(4.2)	The inhibition zones (mm) of anti-fungal activity for ligands and thier complexes.	140
(3-25)	The important bond length of $[\text{Co}(\text{HL}^1)_2]$.	149
(3.26)	The important bond length of $[\text{Co}(\text{H}_2\text{L}^2)\text{Cl}_2\text{H}_2\text{O}]$.	150
(4-27)	The important bond length of $[\text{Ni}(\text{H}_2\text{L}^2)\text{Cl}] \text{Cl}$.	151

contains

List of Figures

	<i>Figure</i>	<i>Page</i>
(1-1)	Chemical structure of dimedone	5
(1-2)	Tautomerization of the dimedone	6
(1-3)	. Crystalline dimedone in the enol form linked by hydrogen bonds.	6
(1-4)	Geometry the proposed of Co(II) complexes	9
(1-5)	Proposed structure of $[\text{Cu}_2(\text{L})_2\text{Cl}_2(\text{H}_2\text{O})_4]$ complex	10
(1-6)	Chemical geometry of complexes	11
(1-7)	Chemical geometry of Cu(II) complexes.	12
(1-8)	Chemical structure of complexes.	13
(1-9)	Chemical geometry of complexes.	14
(1-10)	Chemical structure of complexes.	15
(1-11)	Chemical structure of complexes	16
(1-12)	Structure of Schiff-base ligand ((E)-3-(phenylimino)indolin-2-one)	17
(1-13)	Chemical structure of complexes.	18
(1-14)	The structures of the complexes.	19
(1-15)	The structure of complexes.	20
(1-16)	Chemical structure of complexes.	21
(1-17)	Chemical structure of 2-(3-bromo-5-chloro-2-hydroxybenzylidene)-N-phenylhydrazinecarbothioamide	22
(1-18)	Crystal structure of the complexes $[\text{Zn}(\text{L})(\text{bpy})](1)$; and $[\text{Zn}(\text{L})(\text{phen})](2)$.	22
(1-19)	Chemical structure of Mn(II) complexes.	23

contains

(1-20)	Chemical structure of N,2-bis((E)-2-hydroxybenzylidene)hydrazine-1-carbothioamide	24
(1-21)	The structure of complexes	25
(1-22)	The structure of complexes	26
(1-23)	Chemical structure of Benzyloxybenzaldehyde-4-phenyl-3-thiosemicarbazone ligand.	27
(1-24)	The structure of complexes.	28
(1-25)	Chemical structure of complexes nickel (II).	30
(1-26)	X-Ray structures of complex (C ₃₆ H ₃₀ N ₈ NiO ₂ S ₂).	31
(1-27)	The structure of rolitetracycline.	31
(1-28)	The structure of fluoxetine.	32
(1-29)	The structure of complexes.	33
(1-30)	The structure of the azomethine.	34
(1-31)	The structure of nDMABAPB.	35
(3-1a)	The FT-IR spectrum of 2-nitroaniline	52
(3-1b)	The FT-IR spectrum of dimedone.	53
(3-1c)	The FT-IR spectrum of 4-dimeyethylaminobenzaldehyde.	53
(3-2)	The FT-IR spectrum of (R) -2- ((4-(dimethylamino) phenyl) ((2-nitrophenyl)amino)methyl)-5,5dimethylcyclohexane-1,3-dione(HL ¹).	54
(3-3)	The FT-IR spectrum of thiosemicarbazide hydrochloride	55
(3-4)	The FT-IR spectrum of (E)-2-(2-((S)-(4 (dimethylamino)phenyl)((2-nitrophenyl)amino)methyl)-5,5-dimethyl-3-oxocyclohexylidene)hydrazine-1-carbothioamide (H ₂ L ²).	56

contains

(3-5)	FT-IR spectrum of $[\text{Co}(\text{HL}^1)_2]$	63
(3-6)	FT-IR spectrum of $[\text{Ni}(\text{HL}^1)_2]$	64
(3-7)	FT-IR spectrum of $[\text{Cu}(\text{HL}^1)_2]$	64
(3-8)	FT-IR spectrum of $[\text{Zn}(\text{HL}^1)_2]$	65
(3-9)	FT-IR spectrum of $[\text{Cd}(\text{HL}^1)_2]$	65
(3-10)	FT-IR spectrum of $[\text{Co}(\text{H}_2\text{L}^2)\text{Cl}_2]$.	69
(3-11)	FT-IR spectrum of $[\text{Ni}(\text{H}_2\text{L}^2)]\text{Cl}_2$.	70
(3-12)	FT-IR spectrum of $[\text{Cu}(\text{H}_2\text{L}^2)\text{Cl}_2]$.	71
(3-13)	FT-IR spectrum of $[\text{Zn}(\text{H}_2\text{L}^2)\text{Cl}_2]$.	72
(3-14)	FT-IR spectrum of $[\text{Cd}(\text{H}_2\text{L}^2)\text{Cl}_2]$.	73
(3-15)	Electronic spectrum of HL^1 in DMSO solution	75
(3-16)	Electronic spectrum of H_2L^2 in DMSO solution.	76
(3-17)	Electronic spectrum of $[\text{Co}(\text{HL}^1)_2]$ in DMSO solution.	78
(3-18)	Electronic spectrum of $[\text{Ni}(\text{HL}^1)_2]$ in DMSO solution.	78
(3-19)	Electronic spectrum of $[\text{Cu}(\text{HL}^1)_2]$ in DMSO solution.	79
(3-20)	Electronic spectrum of $[\text{Zn}(\text{HL}^1)_2]$ in DMSO solution.	79
(3-21)	Electronic spectrum of $[\text{Cd}(\text{HL}^1)_2]$ in DMSO solution.	79
(3-22)	Electronic spectrum of $[\text{Co}(\text{H}_2\text{L}^2)\text{Cl}_2\text{H}_2\text{O}]$ in DMSO solution.	82
(3-23)	Electronic spectrum of $[\text{Ni}(\text{H}_2\text{L}^2)\text{Cl}]\text{Cl}$ in DMSO solution.	82
(3-24)	Electronic spectrum of $[\text{Cu}(\text{H}_2\text{L}^2)\text{Cl}_2\text{H}_2\text{O}]$ in DMSO solution.	83
(3-25)	Electronic spectrum of $[\text{Zn}(\text{H}_2\text{L}^2)\text{Cl}]\text{Cl}$ in DMSO solution.	83
(3-26)	Electronic spectrum of $[\text{Cd}(\text{H}_2\text{L}^2)\text{Cl}]\text{Cl}$ in DMSO solution.	84
(3-27)	The electrospray (+) mass spectrum of HL^1 .	95
(3-28)	The electrospray (+) mass spectrum of H_2L^2 .	97

contains

(3-29)	^1H NMR spectrum of HL^1 in DMSO-d_6 .	100
(3-30)	^1H -NMR spectrum of H_2L^2 in DMSO-d_6	101
(3-31)	^{13}C -NMR spectrum of HL^1 in DMSO-d_6 .	104
(3-32)	^{13}C -NMR spectrum of H_2L^2 in DMSO-d_6	105
(3-33)	^1H -NMR spectrum of $[\text{Zn}(\text{HL}^1)_2]$ in DMSO-d_6 .	109
(3-34)	^{13}C -NMR spectrum of $[\text{Zn}(\text{HL}^1)_2]$ in DMSO-d_6 .	111
(3-35)	Thermal decomposition of HL^1 in N_2 atmosphere.	114
(3-36)	Thermal decomposition of H_2L^2 in N_2 atmosphere.	116
(3-37)	Thermal decomposition of HL^1 in N_2 atmosphere.	120
(3-38)	Thermal decomposition of H_2L^2 in N_2 atmosphere.	122
(3-39)	Thermal decomposition of $[\text{Zn}(\text{HL}^1)_2]$ in N_2 atmosphere.	124
(3-40)	Thermal decomposition of $[\text{Ni}(\text{H}_2\text{L}^2)\text{Cl}]\text{Cl}$ in N_2 atmosphere	125
(3-41)	Thermal decomposition of $[\text{Cu}(\text{H}_2\text{L}^2)\text{Cl}_2 \cdot \text{H}_2\text{O}]$ in N_2 atmosphere	126
(4-1)	The microbiological activity of HL^1 and its complexes against <i>Escherichia coli</i> .	134
(4-2)	The microbiological activity of HL^1 and its complexes against <i>Pseudomonas aeruginosa</i> .	134
(4-3)	The microbiological activity of HL^1 and its complexes against <i>Bacillus subtilis</i> .	135
(4-4)	The microbiological activity of HL^1 and its complexes against <i>Staphylococcus aureus</i> .	135
(4-5)	The microbiological activity of H_2L^2 and its complexes against <i>Escherichia coli</i> .	136
(4-6)	The microbiological activity of H_2L^2 and its complexes	136

contains

	against <i>Pseudomonas aeruginosa</i> .	
(4-7)	The microbiological activity of H_2L^2 and its complexes against <i>Bacillus subtilis</i> .	137
(4-8)	The microbiological activity of H_2L^2 and its complexes against <i>Staphylococcus aureus</i> .	137
(4-9)	The microbiological activity of HL^1 and its complexes against <i>Candida</i> .	141
(4-10)	The microbiological activity of HL^1 and its complexes against <i>Trichomoniasis</i> .	141
(4-11)	The microbiological activity of H_2L^2 and its complexes against <i>Candida</i> .	142
(4-12)	The microbiological activity of H_2L^2 and its complexes against <i>Trichomoniasis</i> .	142
(3-42)	The proposed molecular structure of $[Co(HL^1)_2]$.	148
(3-43)	The proposed molecular structure of $[Co(H_2L^2)Cl_2H_2O]$.	149
(3-44)	The proposed molecular structure of $[Ni(H_2L^2)Cl] Cl$.	150

contains

List of Schemes

	<i>Scheme</i>	<i>Page</i>
(1.1)	Synthesis of the azomethine.	2
(1.2)	Reversible reaction of a azomethine.	2
(1.3)	Mechanism of azomethine.	3
(1.4)	Synthesis of the mannich- β -amino carbonyl.	4
(1.5)	Mechanism of the Mannich - β -amino carbonyl.	8
(3.1)	General synthetic route of HL^1 .	50
(3.2)	General synthetic route of H_2L^2	50
(3.3)	General synthesis route of HL^1 complexes.	57
(3.4)	General synthetic route of H_2L^2 complexes.	60
(3.5)	The fragmentation pattern and relative abundance of HL^1 fragments.	96
(3.6)	The fragmentation pattern and relative abundance of H_2L^2 fragments.	98

contains

List of Abbreviations

A.A.	Atomic absorption
¹ H-NMR	Hydrogen nuclear magnetic resonance
¹³ C-NMR	Carbon-13-nuclear magnetic resonance
DMF	Dimethyl formamide
DMSO	Dimethyl sulfoxide
M.p.	Melting point
FT-IR	Fourier transform-Infrared
UV-Vis	Ultraviolet and visible
λ	Wave length
ϵ_{\max}	Molar absorptivity
Abs	Absorbance
nm	Nanometer
MHz	Mega hertz
3D	Three dimensional
XD	Diamagnetic molar susceptibility
XP	Paramagnetic molar susceptibility
TGA	Thermal gravimetric analysis
DTG	Differential thermal gravimetric
DSC	Differential scanning calorimetry
HOMO	Highest occupied molecular orbital
LUMO	Lowest unoccupied molecular orbital
ESR	Electro spin Resonance
TLC	Thin layer chromatography

contains

EPR	Electro paramagnetic Resonance
<i>J</i>	Coupling constant
MW	Molecular Weight
TMS	Tetra methyl Saline
ESI (+)	Electro-Spray Ionization (Positive mode)
C.H.N.S	Elemental micro analyses
ppm	Part per million
δ	Chemical shift
BM	Bohr Magnetron
POM	Polarizing Optical Microscopy
LCD	Liquid crystal display

Chapter One: Introduction

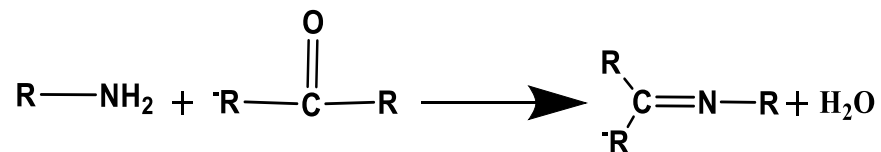
(1) Introduction

(1.1) Schiff base

Schiff bases containing the azomethine ($-RC=N-$) are generally achieved from the condensation of primary amine with carbonyl compound (ketone or aldehyde). Schiff bases are one of the widely used organic combinations. They have a wide range of applications in many fields including inorganic chemistry, biological and analytical. Schiff base ligands are important in the field of coordination chemistry, especially in the development of complexes of azomethine because these ligands are potentially proficient of making stable complexes with metal ions [1]. Azomethine ligands and their metal complexes are increasingly used as catalysts in many biological systems, dyes and polymers [2], as effective corrosion inhibitors [3], in pharmaceutical fields due to a broad spectrum of biological activities, like anti-inflammatory [4-8], analgesic [9-11], antimicrobial [12,13], anticonvulsant [14], antitubercular [15], anticancer [16, 17], antioxidant [18] and anthelmintic [19].

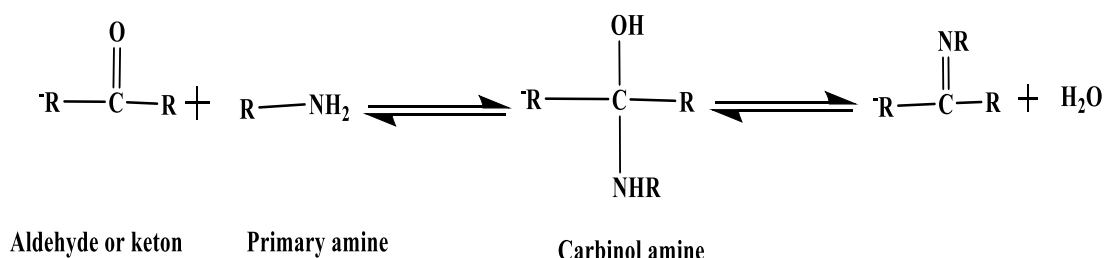
(1.2) Chemistry of Schiff base

Schiff base also known as azomethine or imine, is an analogue of an aldehyde or ketone in which the carbonyl group ($C=O$) has been substituted by an azomethine or imine group [20-25], Scheme (1.1). Azomethine is a kind of chemical compounds having a C-N double bond as functional group, where N atom linked to alkyl group or aryl group R but not to H. The azomethine is synonymous with an imine and were termed after Hugo Schiff.



Scheme (1.1) : Synthesis of the azomethine

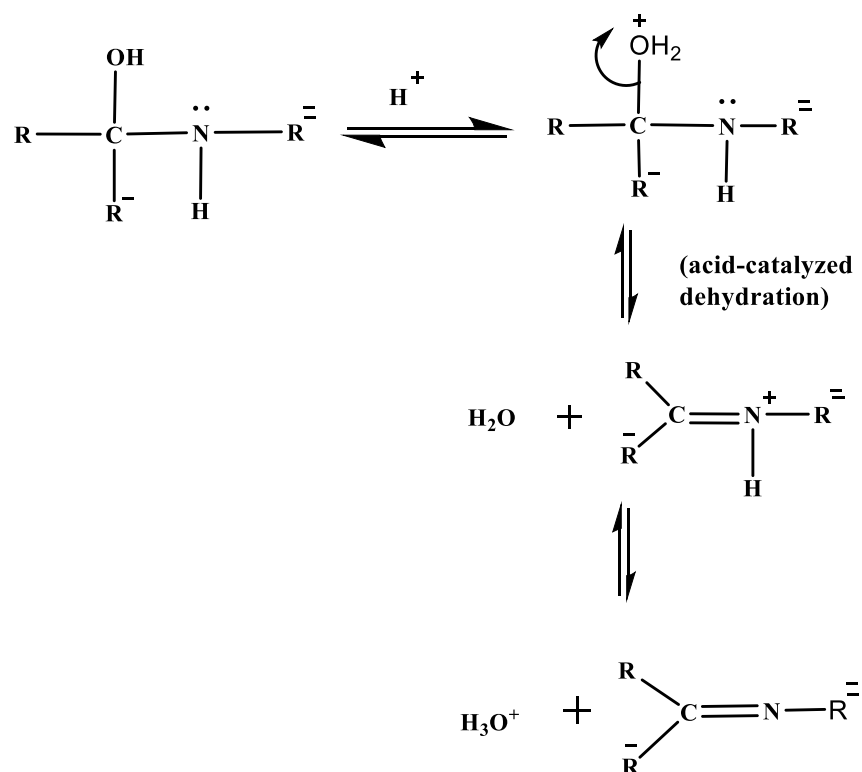
Where R is a phenyl or alkyl group which makes the azomethine a more stable imine. Azomethine is capable to stabilize several different metals in many oxidation states, which enhance the performance of metals in many catalytic transformations processes[26]. Generally, azomethine has N_2O_2 or NO donor groups with a chance that O atoms to be substituted by S, N, or Se [27]. Azomethine that contain, aryl substituents are substantially more stable and more readily synthesized, while those which contain alkyl substituents are relatively unstable. Azomethine of aliphatic aldehydes are relatively unstable and readily polymerizable [28,29], while those of aromatic aldehydes having effective conjugation, are more stable [30,31]. Many azomethines can be hydrolyzed back to their ketones or aldehydes and amines using base or aqueous acid, Scheme (1.2).



Scheme (1.2) : Reversible reaction of a azomethine

(1.2.1) Mechanism of Azomethine Formation

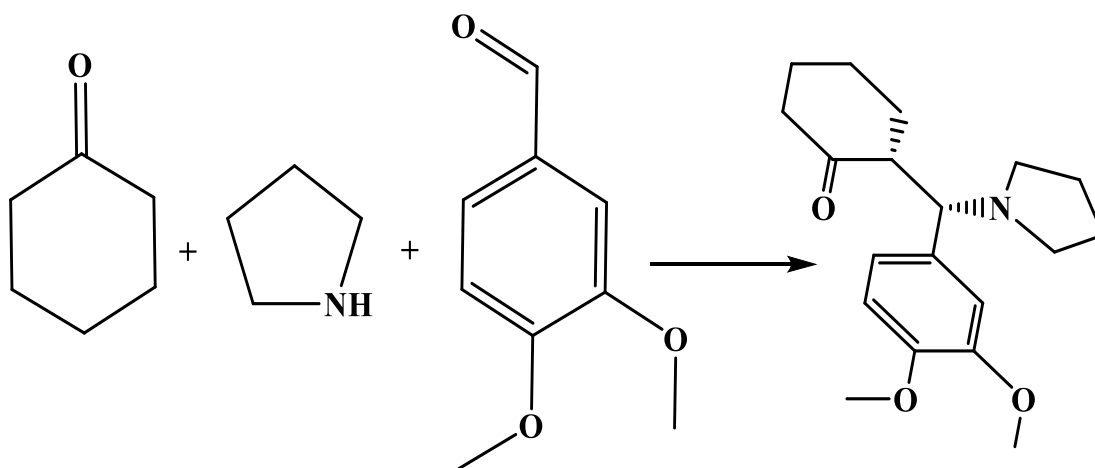
The mechanism of azomethine formation is another modification the theme of nucleophilic addition to the carbonyl group, Scheme (1.3). In this case, the nucleophile is the amine. In the first part of the mechanism, the amine reacts with the ketone or aldehyde to give an unstable addition compound called carbinolamine. The carbinolamine loses water by either acid or base catalyzed pathways. Since the carbinolamine is an alcohol, it undergoes acid catalyzed dehydration. Generally, the azomethine formation is a sequence of two types of reactions, *i.e.* addition followed by elimination [32].



Scheme (1.3): Mechanism of azomethine formation

(1.3) Mannich- β -amino carbonyl

Mannich reaction is one of the most important reactions in organic synthesis of C–C bond and medicinal chemistry [33]. In these reactions, three compounds are used as starting materials. These processes consist of two or more synthetic steps in a one-pot reaction, Scheme (1.4). They are forming rapidly, efficient, eco-friendly and acceptable for green chemistry [34,35]. Mannich reaction applied in the synthesis of antimalarial, antitumour, antimicrobial, antitubercular, antiinflammatory and anticonvulsant molecules, such as nikkomycin or neopolyoxins [36].



Scheme (1.4): Synthesis of the mannich- β -amino carbonyl.

(1.3.1) Dimedone (5,5-Dimethylcyclohexane-1,3-dione)

It is a cyclic diketone that used in organic chemistry, Fig (1.1). Is white to light yellow crystals that called also dimedone, cyclomethone, 5,5-dimethyl-1,3-cyclohexanedione, dimethyldihydroresorcinol and methone. Cyclohexanediones in general can be used as catalysts in the formation of transition-metal complexes. Other uses include, its applications in colorimetry, crystallography, luminescence and spectrophotometric analysis. The use of dimedone in green chemistry has been described for the synthesis of selective heterocyclic motifs which are both pharmacologically and industrially important [37].

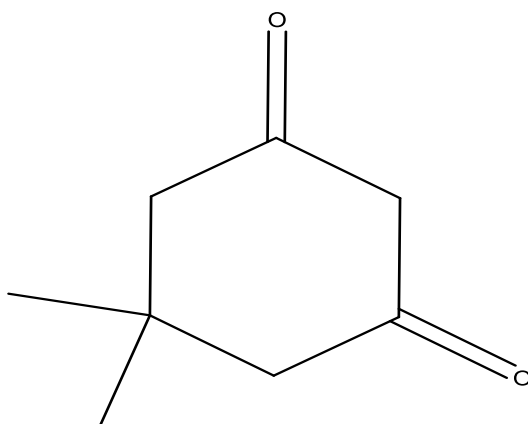


Fig (1.1): Chemical structure of dimedone

(1.3.2) Tautomerization

Dimedone in equilibrium with its tautomer in solution at a 2:1 keto to enol ratio in chloroform [38], Fig (1.2).

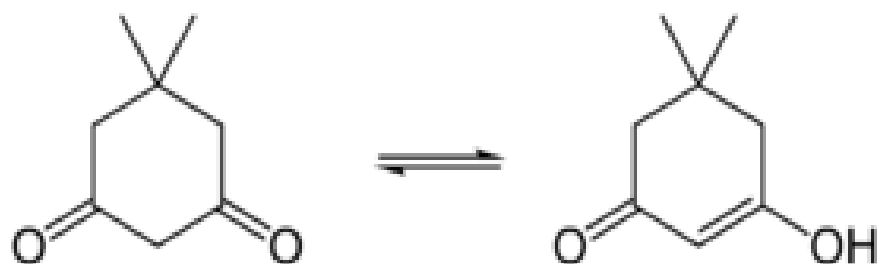


Fig (1.2): Tautomerization of the dimedone.

Crystalline dimedone contains chains of molecules, in the enol form, linked by hydrogen bonds [39], Fig (1.3).

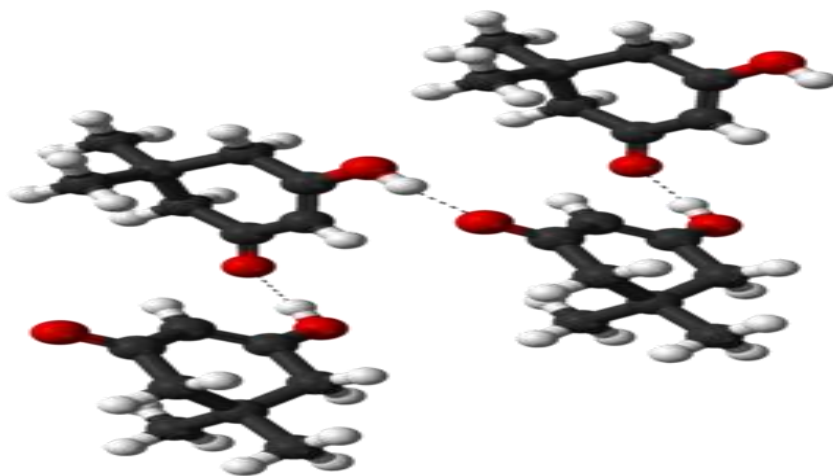
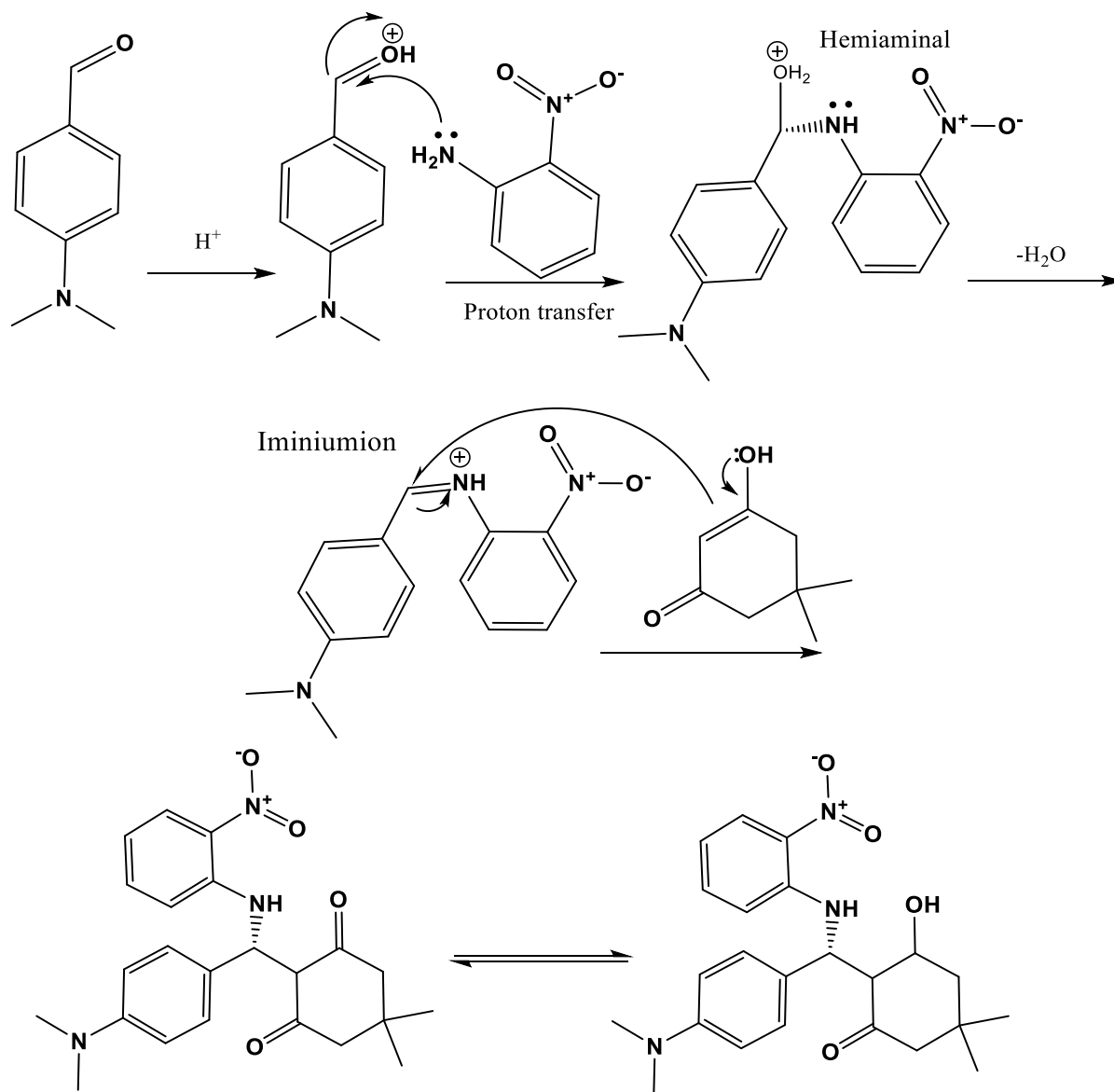


Fig (1.3): Crystalline dimedone in the enol form linked by hydrogen bonds.

(1.3.3) Mechanism of Mannich - β -amino carbonyl

The reaction can continue under both basic and acidic conditions, but acidic conditions are more common. Under acidic conditions the first step is the reaction of the amine component with the protonated nonenolizable (ketone or aldehyde) to give a hemiaminal. After proton transfer and elimination of H₂O molecule, the electrophilic iminium ion is obtained. The formed iminium ion then reacts with the enolized carbonyl compound (nucleophile) at its α -C in an aldol-type reaction to give rise to the Mannich - β -amino carbonyl. H⁺ might promote the reaction by accelerating the formation of the imine bond in the iminium ion in the rate-determining step, Scheme (1.5). It is worth noting that the ¹H Nuclear magnetic resonance spectra of the products show that in the keto–enol tautomerization, the enol is the dominant form. However, this is compatible with the fact that 1,3-dicarbonyl compounds exist predominantly in the enol form in acidic conditions [40].



Scheme (1.5): Mechanism of the Mannich - β -amino carbonyl

(1.4) Schiff-bases with N, O chelating system

The synthesis of new Schiff base ligands (1,4-phenylene-bis-(methanylylidene)-bis- (2-nitroaniline) L^1 and 4-2-nitrophenyl)imino)methyl benzaldehyde L^2 obtained from the condensation of terephthalaldehyde and ortho-nitroaniline [41], in mole ratio 1:2= L^1 , 1:1= L^2 then those ligands reacted with Co(II) metal ion. Compounds were characterized by FT-IR, UV-Visible, $^1\text{H-NMR}$, mass spectroscopy and molar conductance. Antibacterial activity of the metal complexes was found to be higher than that for the ligands. Physico-chemical techniques indicated the formation of four coordinate complexes, Fig (1.4).

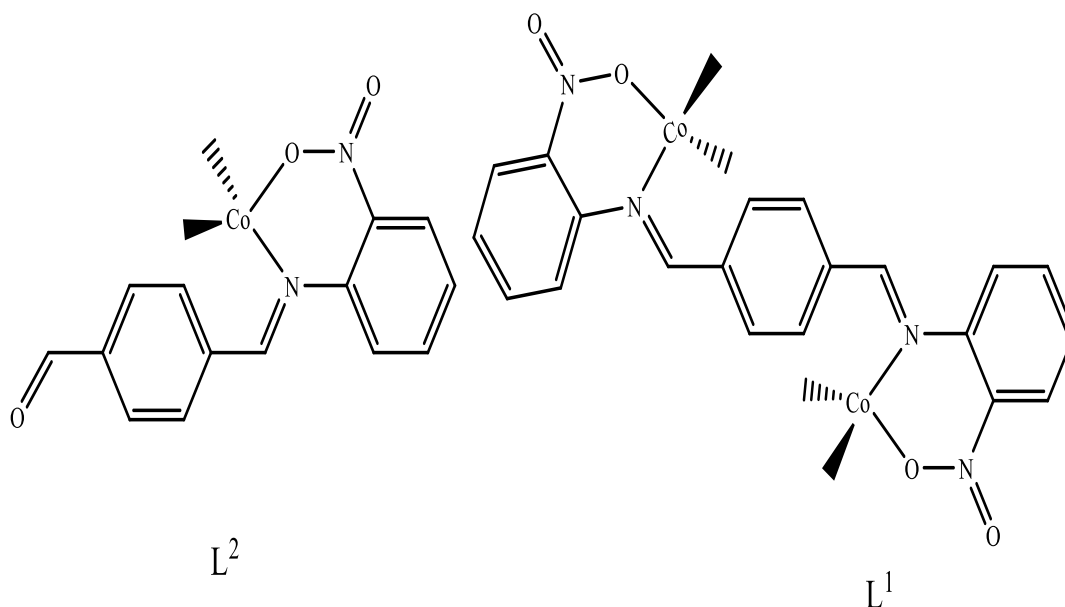


Fig (1.4): Chemical structure of Co(II) complexes.

Pahonțu *et al.* [42] have described the synthesis of ethyl 4-((E)-(2-hydroxy-4-methoxyphenyl)methyleneamino) benzoate HL. The ligand was prepared from the reaction of 2-hydroxy-4-methoxybenzaldehyde with 4-aminobenzoate. The formed ligand was then reacted with Cu(II). The Ligand and Its complex were characterised by using elemental analyses, UV-Vis, FT-IR, ^1H -, ^{13}C -NMR, mass spectram, thermal analysis and magnetic studies. The structure for Cu(II) complex is shown in Fig (1.5).

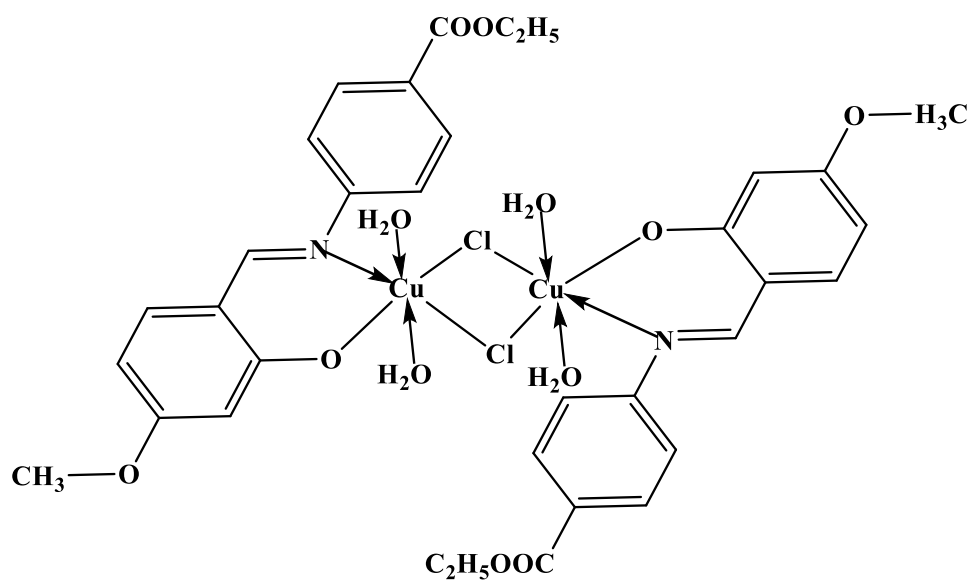
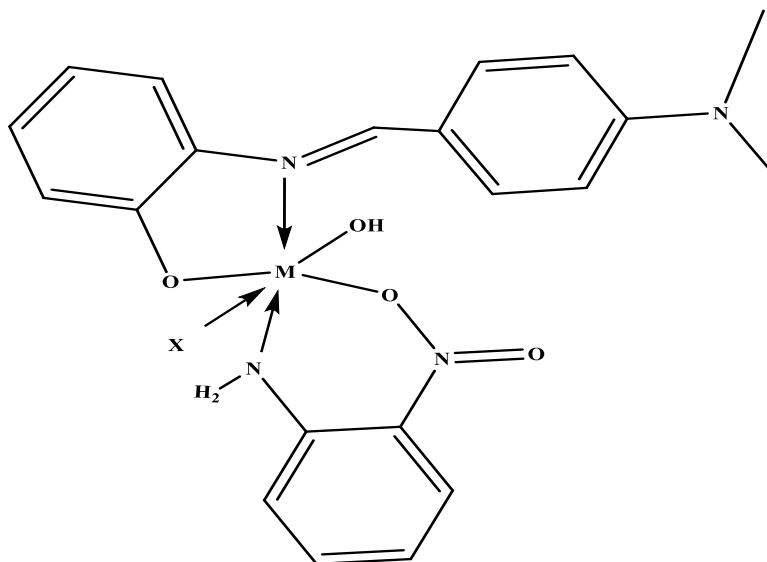


Fig (1.5): Chemical structure of $[\text{Cu}_2(\text{L})_2\text{Cl}_2(\text{H}_2\text{O})_4]$ complex.

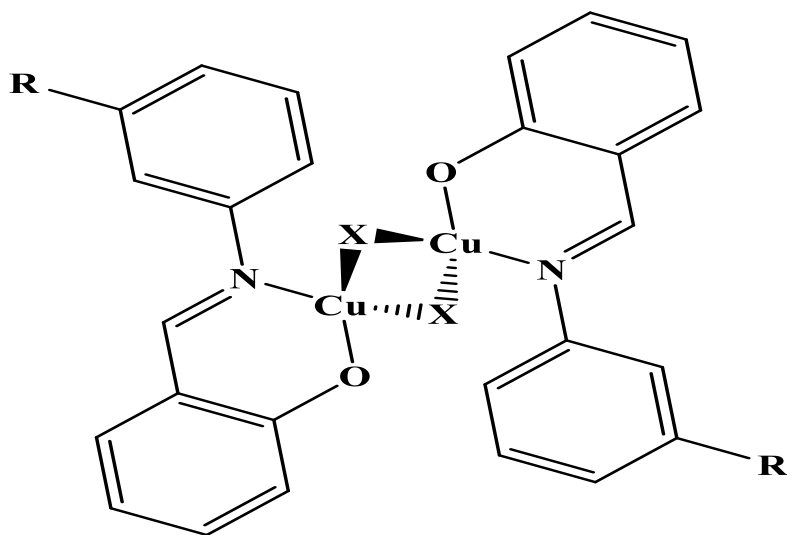
The Schiff base (E)-2-((4-(dimethylamino)benzylidene)amino)phenol was synthesised from the condensation of 4-dimethylaminobenzaldehyde with 2-aminophenol as primary ligand. Then, mixed ligand chelates was synthesised from di- and trivalent metal ions (Cr, Co, Ni, and Cu ions) and Schiff base with 2-nitroaniline [43]. Compounds have been characterized by elemental analysis, molar conductivity, magnetic moment measurements, infrared and electronic spectra, mass spectra and electron paramagnetic resonance spectrum. On the basis of the obtained data, The proposed geometry of all compounds adopt an octahedral geometry was proposed, Fig (1.6).



Where M= Cr(III), X = OH, M=Cu(II), Co(II) or Ni(II), X = H₂O

Fig (1.6): Chemical structure of complexes.

A number of Cu(II) complexes that have mixed ligands including Schiff-bases were reported [44]. This includes the synthesis of ligands from the reaction of salicylaldehyde with 2-aminophenol or 3-nitro amino benzene. Compounds were characterized by magnetic measurements, ESR, UV-VIS, FT-IR, C.H.N, and mass spectra. On the basis of the obtained data the creation of dinuclear Cu(II) complexes in which the suggested geometry is tetrahedral, Fig (1.7).



Where: $X = \text{Cl}$ or OAr , $R = 3\text{-NO}_2$ or 2-OH

Fig (1.7): Chemical structure of Cu(II) complexes.

(1.4.1) Coordination of (Nitrogen and carbonyl oxygen moiety).

In 2019, the preparation of Mannich-base ligand and its metal complexes was reported [45]. The formation of the ligand (R)-2-((R)-(4-(dimethylamino) phenyl)-(phenyl-amino) methyl) cyclohexan-1-one (HL) was achieved from the reaction of 4,4'-dimethylaminobenzaldehyde and aniline with cyclohexanone. The reaction of the ligand with the metal chloride salt gave the required complexes. The ligand and its metal complexes were characterised using a range of analytical and spectroscopic techniques including elemental microanalysis, magnetic susceptibility, conductance FT-IR, electronic spectra, electrospray mass spectroscopy and nuclear magnetic resonance (^1H , ^{13}C spectra). The characterisation data showed the six and four coordinate for complexes, Fig (1.8).

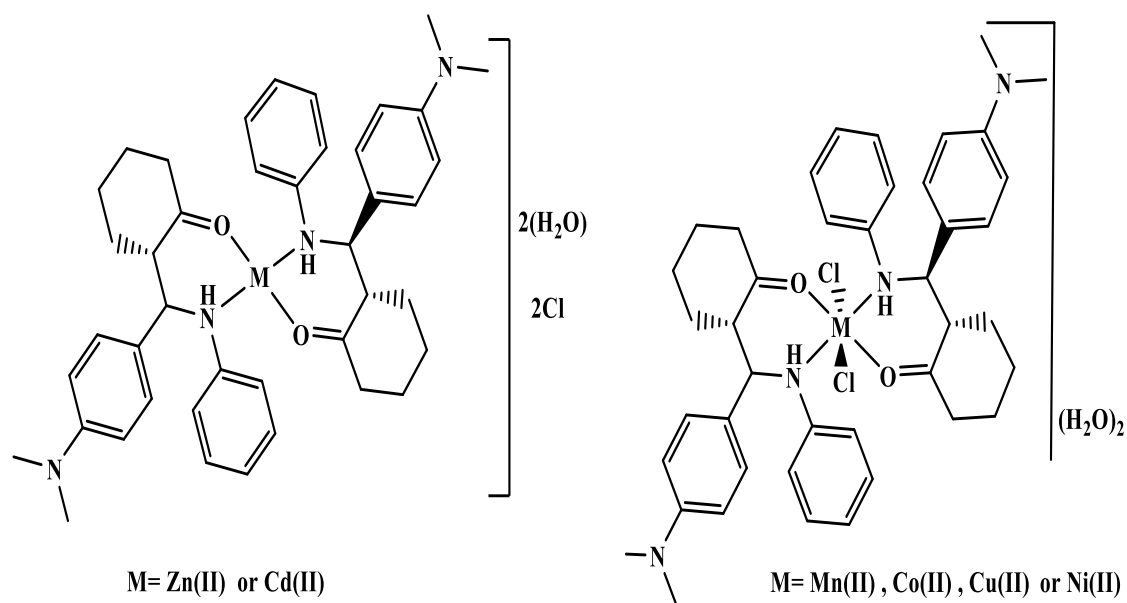
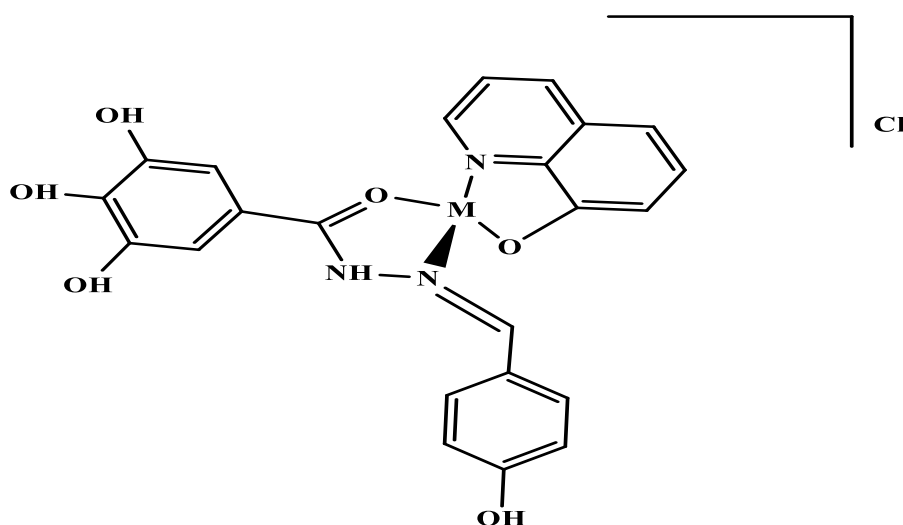


Fig (1.8): Chemical structure of complexes.

The formation and structural characterisation of mixed Schiff base and 8-hydroxyquinoline ligands and their complexes have been reported [46]. The synthesis of Schiff base ligand was done from the reaction of 3,4,5-trihydroxybenzohydrazide with 4-hydroxybenzaldehyde. Ligand and complexes were characterised by analytical and spectroscopic analyses including; FTIR, electronic and ^1H , ^{13}C -NMR spectroscopy, microanalysis, chloride content, thermal analysis, magnetic susceptibility and conductance. Physico-chemical techniques indicated the formation of complexes with four-coordinated arrangement. Biological activity of the prepared ligand and their complexes were screened for their antimicrobial activity against four bacterial species (*Staphylococcus aureus* and *Bacillus subtilis*(G+)), *Enterobacter* and *Escherichia coli* (G-). Biological data showed that complexes become potentially more active against these tested bacteria compared with the ligands, Fig (1.9).



Where M= Co(II) , Zn(II) , Cd(II) and Hg(II) .

Fig (1.9): Chemical structure of complexes.

Preparation of the Mannich base ligand (2-[(3, 4-dimethoxyphenyl)(pyrrolidin-1-yl)methyl]cyclopentanone) was performed using method one-pot,three-component. The ligand was prepared by mixing of 3,4-dimethoxybenzaldehyde and pyrrolidine with cyclopentanone in the presence of calcium chloride using ethanol as a solvent. The resulting Mannich base (L) was isolated and complexed with Cu(II), Co(II), Ni(II) and Fe(II) ions, Fig (1.10). The structures of the synthesized compounds were confirmed by IR, ^1H , ^{13}C NMR, mass spectroscopy, TGA and elemental analyses. The characterisation data indicated the isolation of four coordinate. All compounds showed poor antibacterial activities [47].

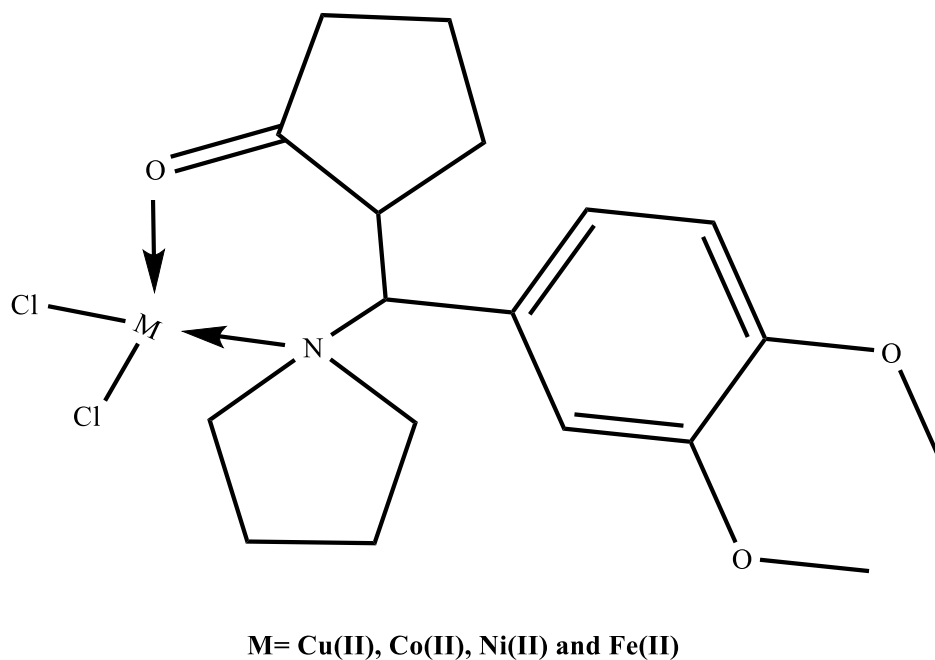


Fig (1.10): Chemical structure of complexes.

The synthesis of three different azomethen ligands[48], was performed by reacting ligands with metal chlorides to give the complexes. The ligands were synthesised from condensation of furan-2-carboxylic acid hydrazid, thiophene- 2-carboxylic acid hydrazide and 2-hydrazino pyridine and isatine. The prepared compounds were characterised by magnetic studies, conductance, metal content, (UV–Vis, FTIR, Nuclear magnetic resonance spectroscopic methods) and C.H.N, which revealed distorted octahedral structures, Fig (1.11).

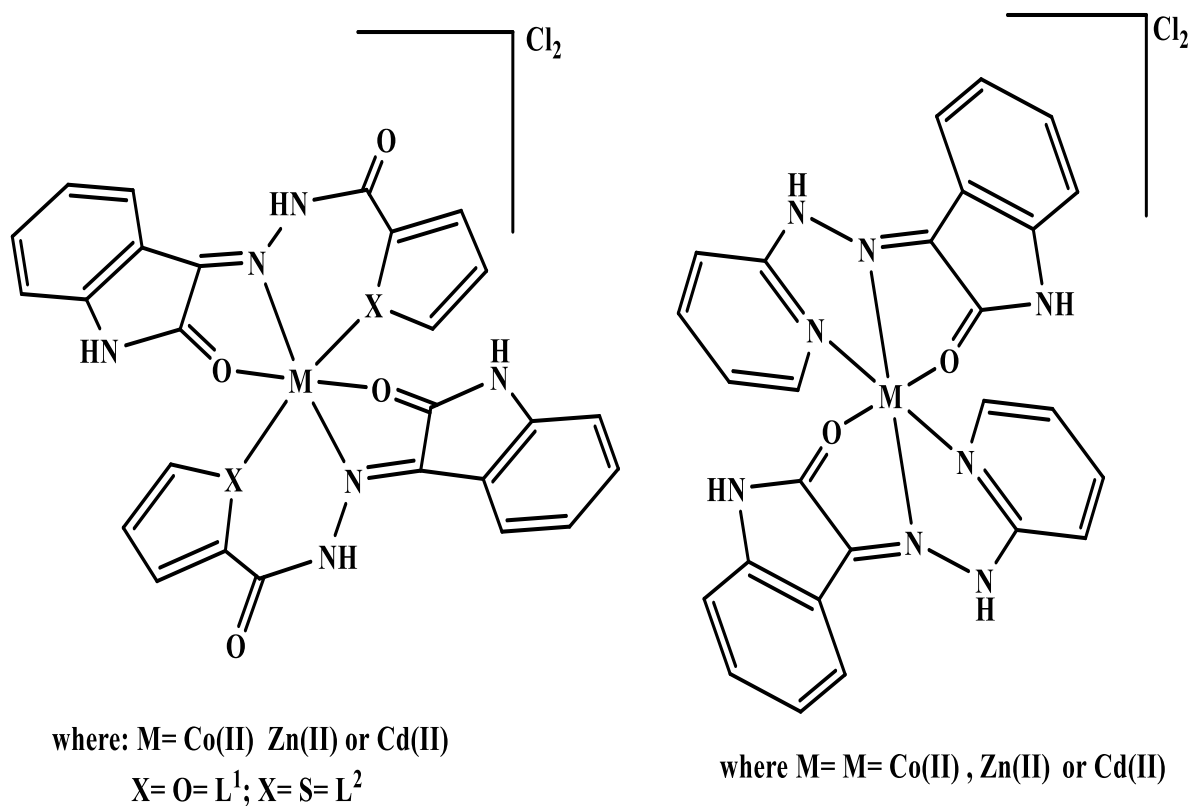


Fig (1.11): Chemical structure of complexes.

Azomethen ((E)-3-(phenylimino)indolin-2-one) was prepared from the reaction of isatin with aniline, Fig (1.12). A series of new Te (IV) complexes with the Schiff base ligand have been synthesised and characterised using some analytical and physical techniques. These techniques include; FT-IR , ^1H NMR spectroscopy, (C, H, N), conductivity and magnetic moment. These studies revealed the formation of six-coordinate Te (IV) complexes with a distorted octahedral geometry [49].

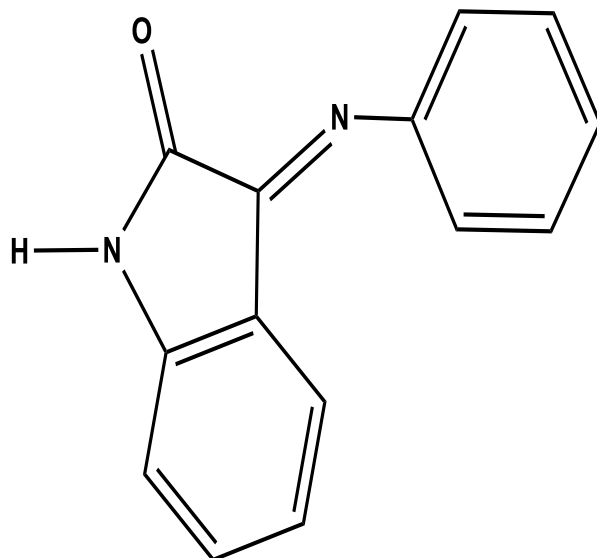


Fig (1.12): Structure of Schiff-base ligand ((E)-3-(phenylimino)indolin-2-one).

Synthesis of a novel Mannich base ((Z)-1-(2-hydroxyphenyl)-5-(piperidin-1-yl)hex-1-en-3-one) was derived from reaction of salicylidene acetone with formaldehyde and piperidine, then reacting of Mannich base with some transition metal ion [50]. The structure of the synthesised compounds were confirmed by ^1H NMR, UV-Vis and IR spectroscopic techniques. The antibacterial activity of compounds were examined and the complexes showed good activity than the Mannich base ligand. These analysis indicated a six coordinate as shown in Fig (1.13).

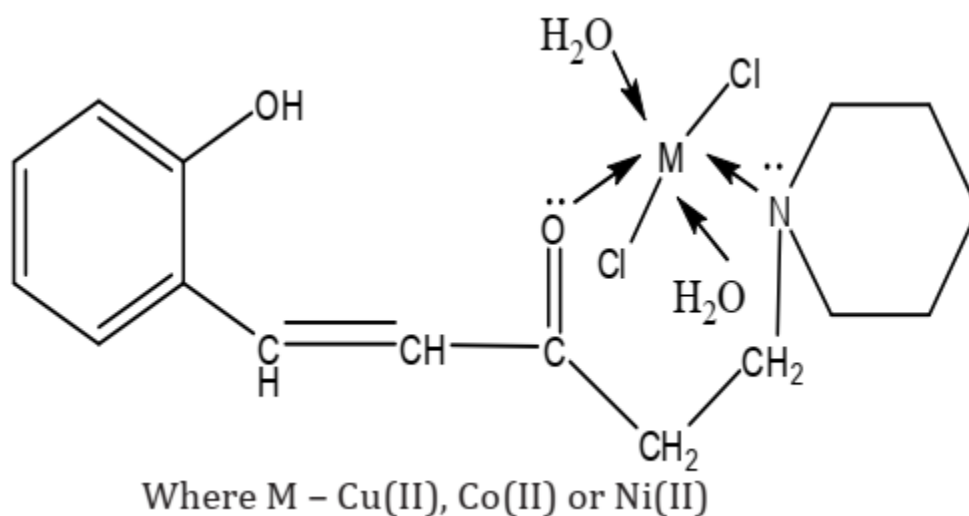


Fig (1.13): Chemical structure of complexes.

The formation of the azomethen ligands were reported [51], then reacted those ligands with Co(II) and Cd(II) metal ion. The ligands were synthesised from condensation of 3-hydroxy-4-methoxybenzaldehyde with furan-2-carboxylic acid hydrazide or thiophene-2-carboxylic acid hydrazide, respectively. The structure around the metal centres was predicted from spectroscopic and analytical data including magnetic studies, conductance, metal content, (UV-Vis, FTIR, Nuclear magnetic resonance). The studies indicated four coordinate as shown in, Fig (1.14).

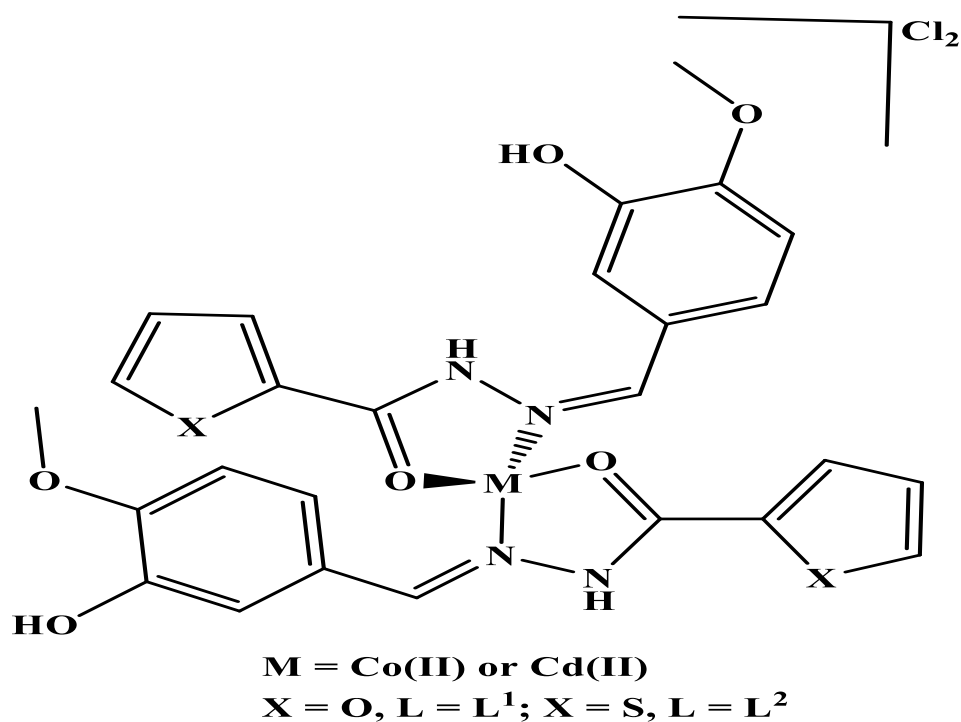
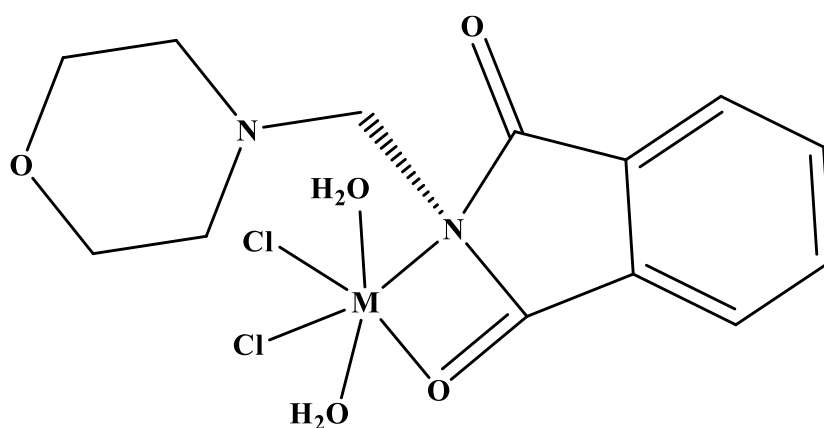


Fig (114.): The structures of the complexes.

The formation of Mannich base (2-(morpholinomethyl)isoindoline-1,3-dione) ligand derived from morpholine and formaldehyde with phthalimide. The reaction of the ligand with Zn (II) and Cd (II) ions at a 1:1 (M:L) mole ratio resulted in the formation of six coordinate complexes, Fig (1.15). C.H.N, molar conductance, UV-Vis, IR and ^1H , ^{13}C -NMR spectroscopy was used to characterise the structure of ligand and its metal complexes [52].



M= Zn (II) and Cd (II)

Fig (1.15): The structure of complexes.

Formation, characterization and antimicrobial properties of Mannich reaction ((R)-N'-(1-morpholino-2-(pyridin-2-yl)ethyl)benzohydrazide) and its metal [Co(II), Cu(II) and Mn(II)] complexes were recently reported [53]. Mannich base formation by the reaction of benzohydrazide and morpholine with pyridine-2-carboxaldehyde. Analytical methods such as TLC, melting point and spectral studies UV, ^1H , ^{13}C -NMR were employed for the characterisation. These analytical and spectroscopic analyses confirmed the formation of six and four coordinate complexes, Fig (1.16). Compounds were tested against some microorganisms for their antimicrobial activity.

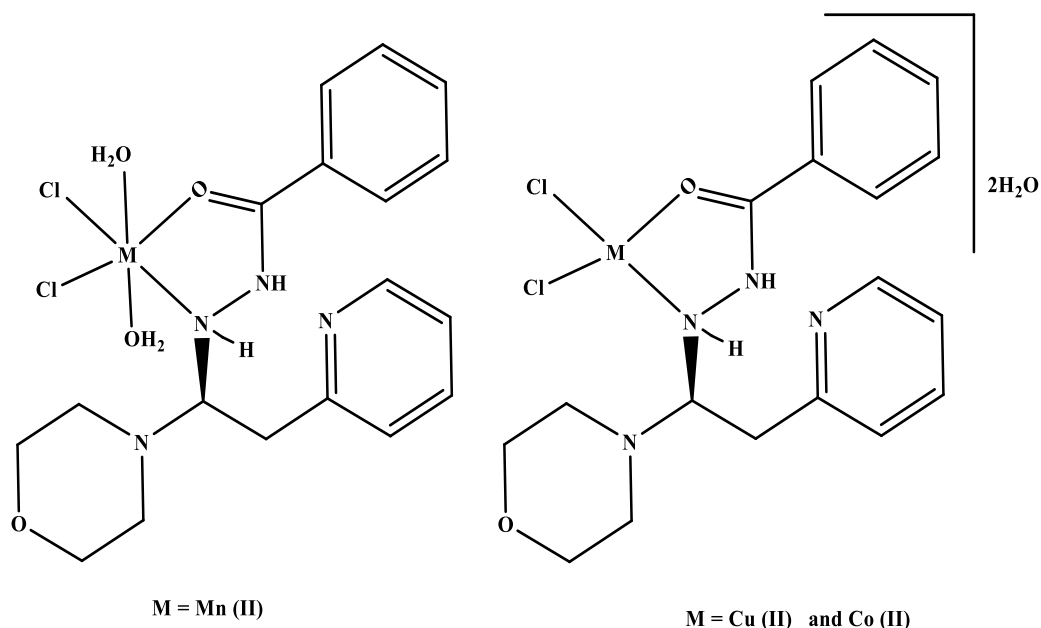


Fig (1.16): Chemical structure of complexes.

(1.4.2) Coordination of N and S in thiosemicarbazone moiety

The synthesis and characterisation of mixed ligand complex of Zn(II) with the Schiff base ligand (2-(3-bromo-5-chloro-2-hydroxybenzylidene)-N-phenylhydrazinecarbothioamide, Fig(1.17), and bipyridine or 1, 10-phenanthroline were reported [54]. Compounds were characterised by ^1H - NMR, FTIR and UV-Vis spectra. The crystal structures of complexes 1 and 2 have been determined by single crystal X-ray diffraction studies. Both complexes 1 and 2 possess square based pyramidally distorted trigonal bipyramidal geometry, Fig (1.18).

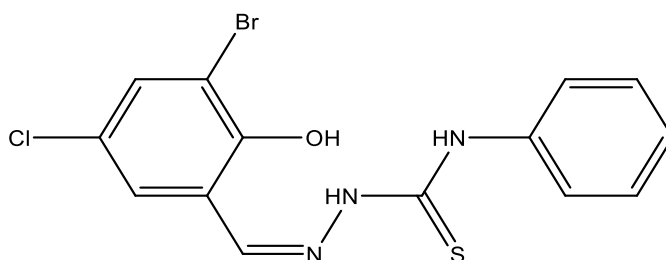


Fig (1.17): Chemical structure of 2-(3-bromo-5-chloro-2-hydroxybenzylidene)-N-phenylhydrazinecarbothioamide.

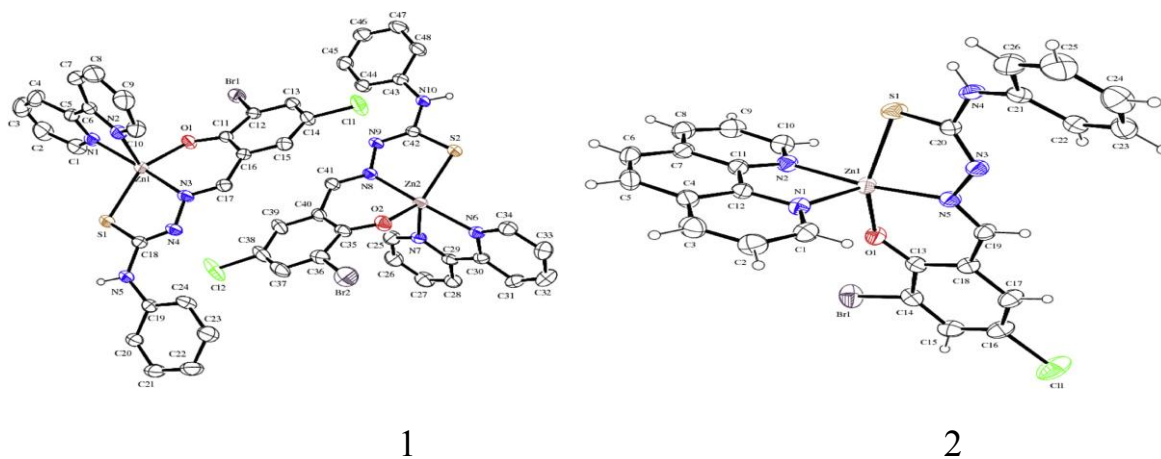


Fig (1.18): Crystal structure of the complexes $[\text{Zn}(\text{L})(\text{bpy})]$ (1); and $[\text{Zn}(\text{L})(\text{phen})]$ (2).

Mn(II) complexes with thiosemicarbaside based ligands such as 2-formyl pyridine thiosemicarbazone (L^1) and 5-methyl 2-formyl pyridine thiosemicarbazone (L^2) have been synthesised and characterised [55]. The ligands and the complexes were characterised by molar conductance, elemental analyses, magnetic susceptibility measurements, IR, UV-Visible, EPR, ^1H NMR and mass spectral studies, which revealed distorted octahedral structures, Fig (1.19).

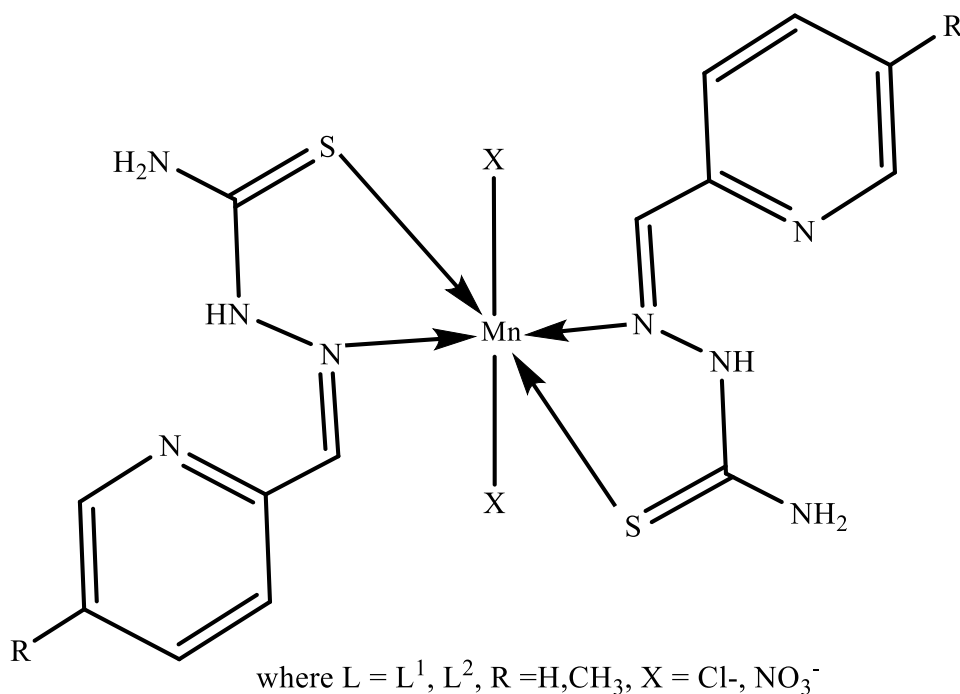


Fig (1.19): Chemical structure of Mn(II) complexes.

The Cu(II) complex was prepared with Schiff base N,2-bis((E)-2-hydroxybenzylidene)hydrazine-1-carbothioamide. Schiff base ligand was derived from the reaction of salicylaldehyde with thiosemicarbazide, Fig (1.20). The ligand and complexes were characterised by magnetic susceptibility IR, UV-Visible, $^1\text{H-NMR}$, thermal analysis The which suggested a distorted square planar structure of the complexes. The Schiff bases and their metal complexes have shown moderate to strong antimicrobial activity [56].

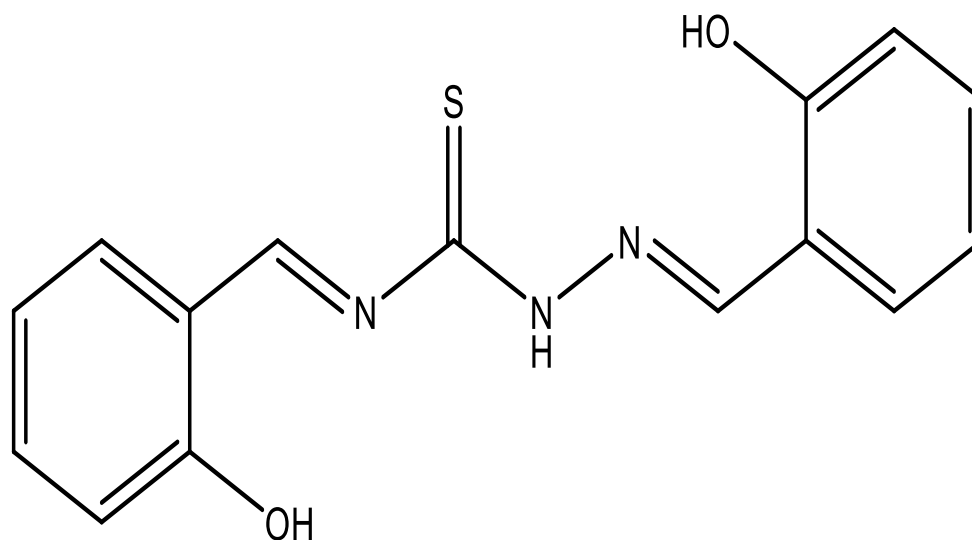


Fig (1.20): Chemical structure of N,2-bis((E)-2-hydroxybenzylidene)hydrazine-1-carbothioamide.

Monika *et al.* [57] reported the reaction of Pd(II), Pt(II), Rh(III) and Ir(III) ions with (2E,2'E)-2,2'-(pyridine-2,6-diylbis(ethan-1-yl-1-ylidene))bis(hydrazine-1-carbothioamide) ligand. The compounds have been characterised using C.H.N.S, molar conductance, magnetic susceptibility measurements, IR, NMR and electronic spectral studies. Complexes of Pd(II) and Pt(II) ions confirmed square planar structures about metal centres. Further, the complexes of Rh(III) and Ir(III) revealed octahedral arrangement. Compounds have been tested against some species of plant pathogenic fungi and bacteria in order to assess their antimicrobial properties, Fig (1.21).

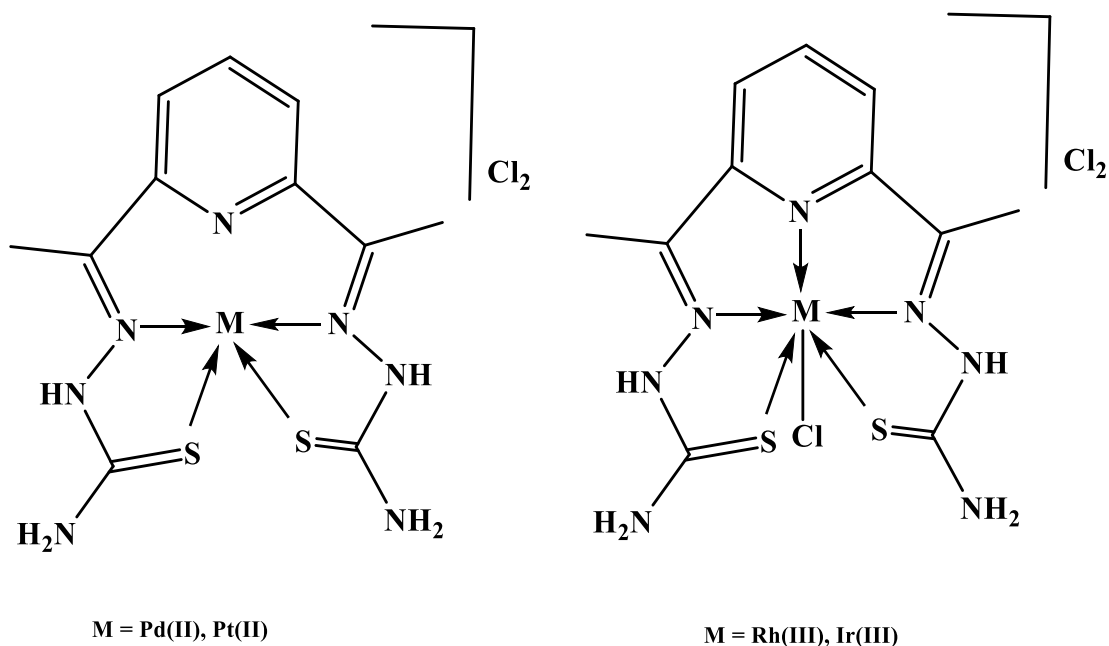


Fig (1.21): The structure of complexes.

Schiff-base ligand (2,6-bis-[(3-phenyl thiourea-imino)-methyl]- phenol) and its metal complexes with Cr(III), Mn(II), Zn(II) and Cd(II) are reported [58]. Schiff-base was derived from the reaction of (2,6-diformyl-4-methyl-phenol) with (4-phenylthiosemicarbazide). Compounds were characterised by FTIR, UV-Vis, ^1H , ^{13}C -NMR, chloride content, conductance and melting point measurements. These analysis indicated six coordinate geometries as shown in Fig (1.22). Compounds were tested against some species of bacteria in order to assess their antimicrobial properties.

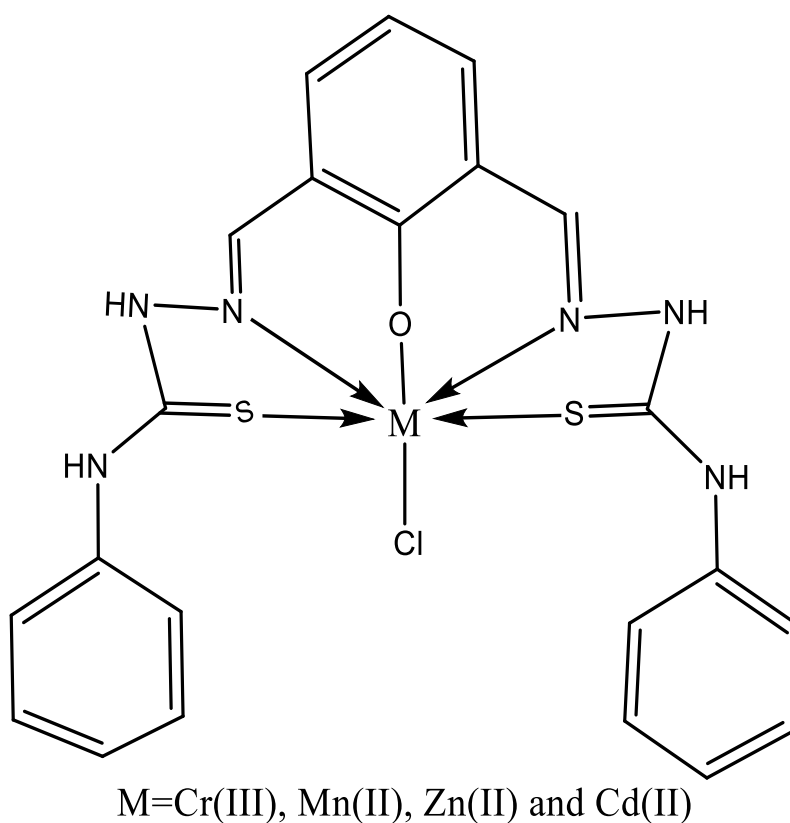
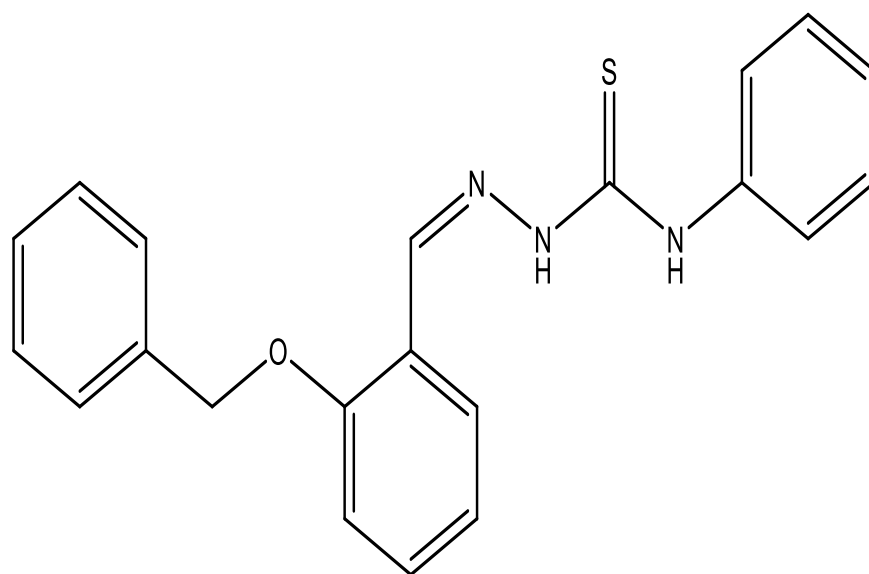


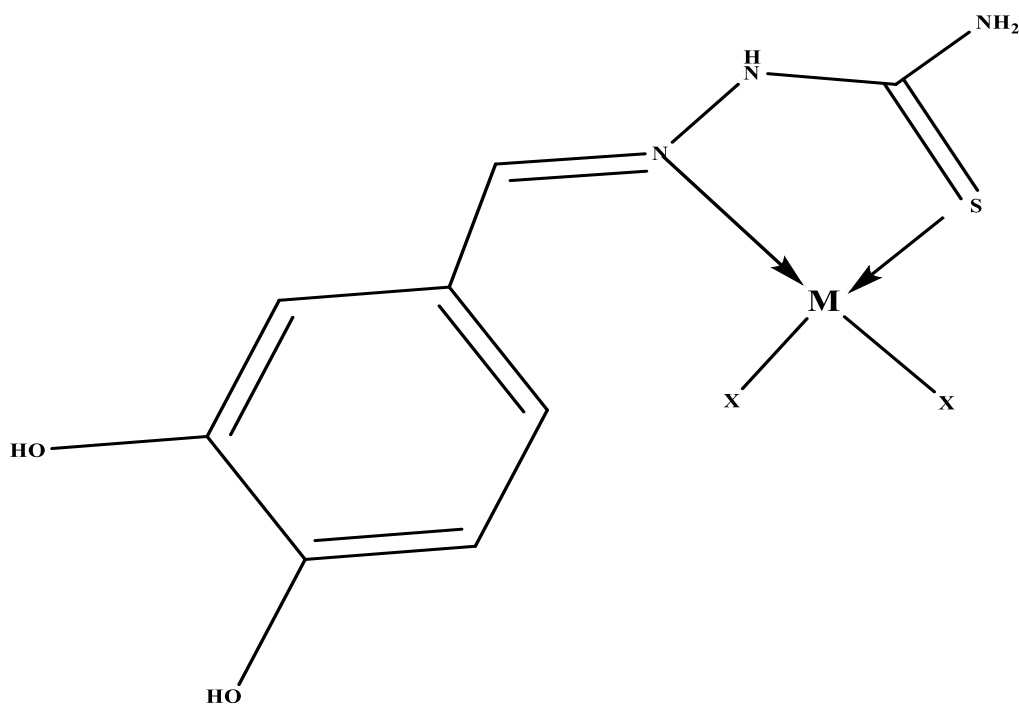
Fig (1.22.): The structure of complexes.

Benzyloxybenzaldehyde-4-phenyl-3-thiosemicarbazone ligand (L) has been synthesised from benzyloxybenzaldehyde and 4-phenyl-3-thiosemicarbazide [59]. Complexes of this ligand with chlorides of Cu(II) and Ni(II) have been prepared. Complexes were characterised by elemental analysis, EPR, IR, UV Vis and $^1\text{H-NMR}$ spectra. These analytical and spectroscopic analyses confirmed the formation of six coordinate complexes. The ligand and their metal complexes were tested in vitro for their biological effects. The prepared metal complexes exhibit higher antibacterial activities than the parent ligand, Fig (1.23).



Fig(1.23):Chemical structure of Benzyloxybenzaldehyde-4-phenyl-3-thiosemicarbazone ligand

The Schiff base (1-(3,4-dihydroxybenzylidene)thiosemicarbazide) HL and its Ni(II) and Fe(II) complexes were synthesised [60]. The ligand and their metal complexes have been characterised by elemental analysis, molar conductance, IR, UV Vis, $^1\text{H-NMR}$ and mass spectral studies resulted in the formation of four coordinate monomeric complexes. Biological activity tests showed that the complexes exhibit strong superoxygen dismutase activity and inhibitory actions toward *Escherichia coli*, *Bacillus subtilis*, *Staphylococcus aureus* and *Cryptococcus neoforms*, Fig (1.24).



$\text{M}(\text{LH})\text{X}_2 \cdot n\text{H}_2\text{O}$; $\text{M} = \text{Ni}(\text{II})$, $\text{X} = \text{OAc}$, $n = 1$; $\text{M} = \text{Fe}(\text{II})$, $\text{X} = \text{Cl}$, $n = 3$

Fig (1.24): The structure of complexes.

(1.5) Applications and uses of Mannich reaction and Schiff-base

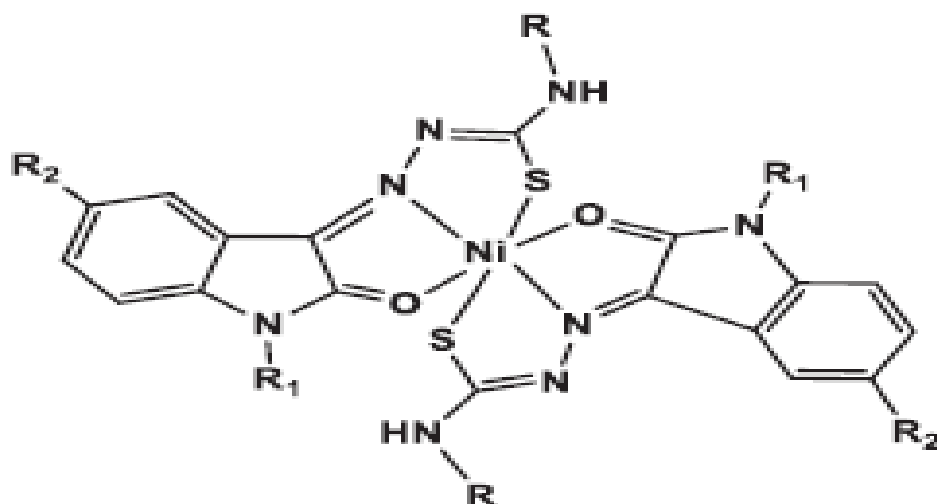
Mannich reaction and Schiff-base are useful materials that have a variety of applications in human life. These include biomedical, analytical, coordination chemistry, agriculture, industry, polymer chemistry and Environment.

1.5.1 Biomedical applications

Biomedical applications may be divided into two types;

1.5.1.1 Pharmaceutical applications

Balachandran *et al.*[61] reported the reaction of the tridentate (ONS) azomethen ligands (L^1 - L^8). The ligands were formed from the reaction of isatin with thiosemicarbazide. Complexes were synthesized from isatin thiosemicarbazone ligands with Ni(II), Fig(1.25). Compounds were characterized by magnetic susceptibility, UV-Visible, FT-IR and ^1H , ^{13}C - NMR spectroscopic. The crystal structure of compounds was confirmed by single crystal X-ray diffraction technique. The compounds were examined for their anticancer activity against a panel of five cell lines such as HepG2, MOLM-14, U937, IM-9 and Vero. Complex Ni(II) ($\text{C}_{36}\text{H}_{30}\text{N}_8\text{NiO}_2\text{S}_2$), Fig (1.26) showed promising anticancer activity against IM-9 cells and induced morphological changes, nuclear condensation, apoptosis and cell cycle arrest at G1 phase in IM-9 cells. In addition, apoptosis was also confirmed by Western blot analysis. Cleavage of plasmid DNA was effectively promoted after its exposure to complex nickel(II) ($\text{C}_{36}\text{H}_{30}\text{N}_8\text{NiO}_2\text{S}_2$). The overall results suggested that complex may be developed as a good candidate for the treatment of leukemia cancer in the future.



R	R ₁	R ₂	Ligand	Complex
H		H	L ¹	1
CH ₃		H	L ²	2
		H	L ³	3
		H	L ⁴	4
CH ₃	H	H	L ⁵	5
CH ₃	CH ₃	H	L ⁶	6
CH ₃	H	Br	L ⁷	7
CH ₃		H	L ⁸	8

Fig (1.25): Chemical structure of complexes nickel (II).

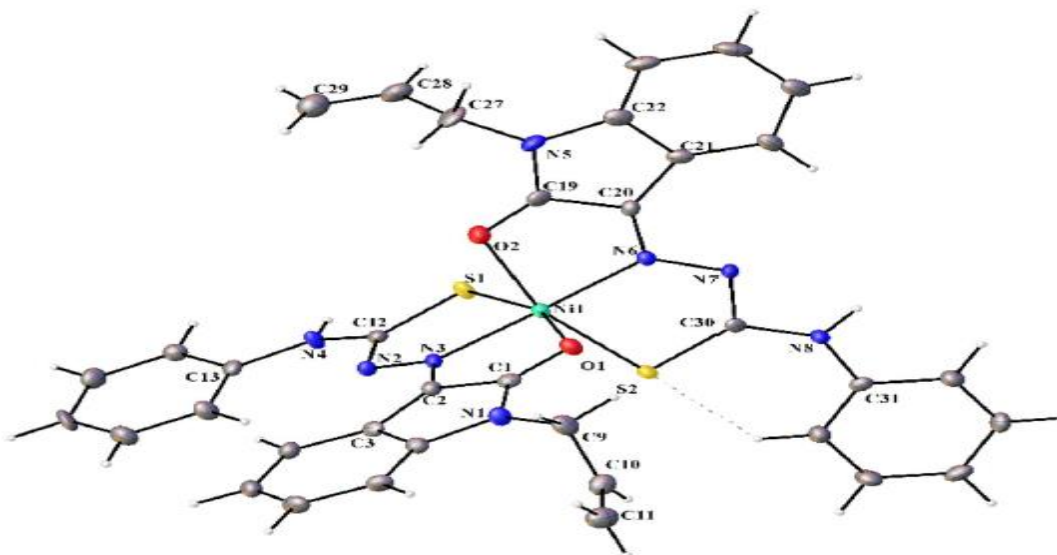


Fig (1.26): X-Ray structures of complex ($C_{36}H_{30}N_8NiO_2S_2$)

Many antibiotics are formed from mannich bases for example, the mannich base of tetracycline a broad-spectrum antibiotic is Rolitetracycline, Fig (1.27). The mannich reaction is used in the synthesis of many pharmaceutical drugs. One example is the use of this reaction in the production of fluoxetine, Fig (1.28), a powerful antidepressant.[62].

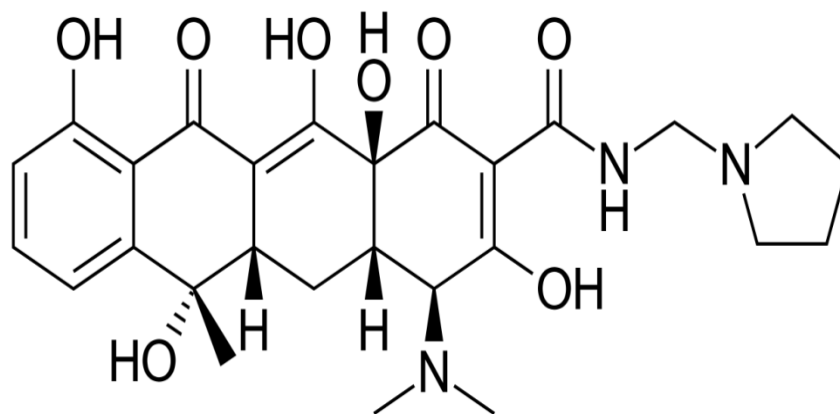


Fig (1.27): The structure of rolitetracycline.

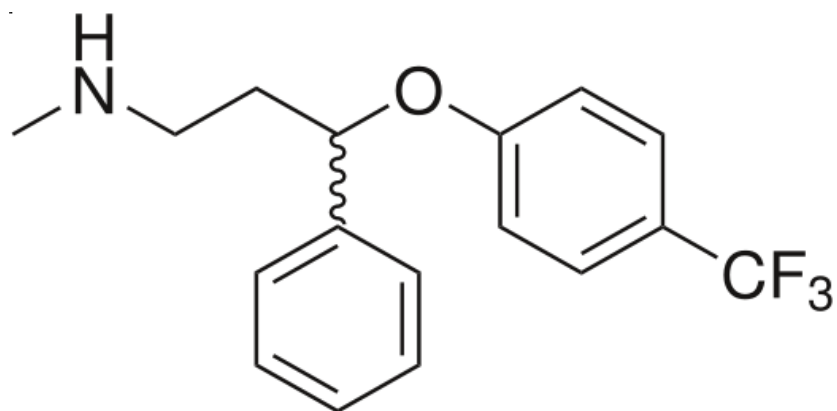


Fig (1.28): The structure of fluoxetine.

(1.5.1.2) Biological activity

The synthesis of a novel Mannich base (1-((dicyclohexylamino)-12-methyl)-3-hydroxy-1H-2(1H)-pyridazin-6(3H)-one) and its transition metal complexes was performed [63]. The ligand was prepared from the reaction of maleic hydrazide with formaldehyde and dicyclohexylamine, three transition metal complexes were also prepared using this ligand. All the compounds are characterized by physical and spectral studies. Mannich base behaves as a bidentate chelating agent and the spectroscopic data resulted in the formation of six coordinate, Fig(1.29). The antimicrobial property of the complexes were studied and the antibacterial activity against certain pathogenic bacteria using disc diffusion method at concentration of 10 μ g/ ml in DMSO using gram positive *Bascillus subtilis*, *Staphaylococcus aureus* and gram negative *Proteus vulgaris*, *Klesiella pneumonia*. It was found that the metal complexes exhibit higher antibacterial property than that of the Mannich base ligand.

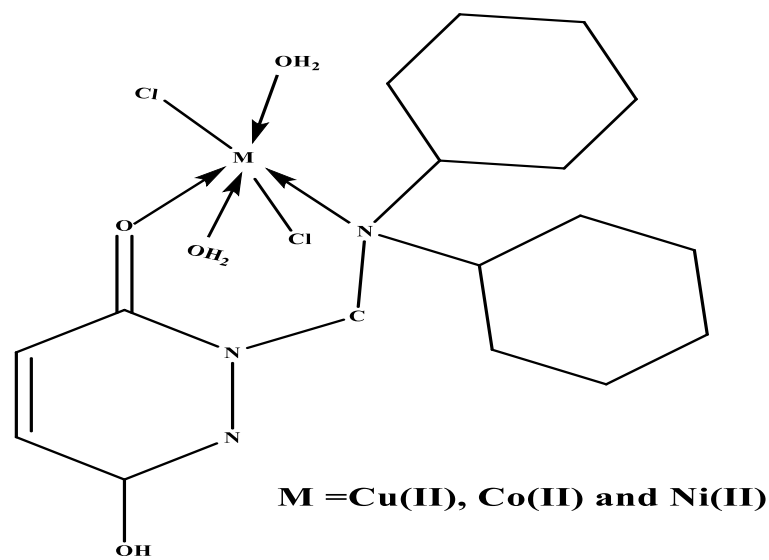


Fig (1.29): The structure of complexes.

(1.5.2) Analytical applications

Formation, characterisation and studying of the fluorescence properties for Schiff bases (N,N -bis(salicylidene)-2,3-pyridinediamine) was reported [64]. Azomethine ligand resulted from the reaction of the aminopyridine with salicylaldehyde. Compounds can be used for spectrofluorimetric monitoring of small pH changes as well as for sensitive metal ion determinations. As analysis of Cu(II) is presented, determination of Cu(II) was based on the quenching effect of CuII on the fluorescence of N,N -bis(salicylidene)-2,3-pyridinediamine, Fig (1.30). The process was fast, simple and reproducible. It has been characterized by high sensitivity and satisfactory selectivity.

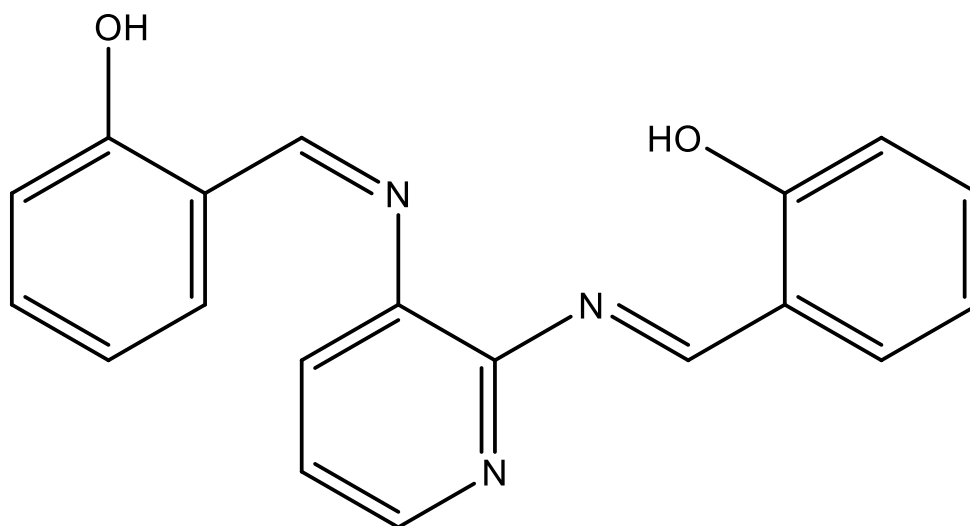


Fig (1.30): The structure of the azomethine

(1.5.3) Industrial applications (liquid crystal)

Schiff bases are very beneficial in liquid crystal research due to its rich polymorphism and low temperature of phase transitions [65]. A range of azomethine ester, 4-((4-(dimethylamino)benzylidene)amino)phenyl-4-(alkanoxyloxy)benzoates, nDMABAPB, Fig (1.31), where n denotes the number of C in the straightalkyl chain ($n = 10, 12, 14, 16$ and 18), were synthesized, characterized and the mesomorphic properties were investigated. The products were synthesized in two main steps. The first step involved condensation of 4-aminophenol with 4-(dimethylamino)benzaldehyde which formed the imine linkage. The second step of the synthesis involved the Steglich esterification between the nDMABAP and the 4-allyloxy benzoic acids, nABA. The structures of the synthesized compounds were confirmed by IR, ^1H , ^{13}C -Nuclear magnetic resonance, as well as Mass (EI-MS) spectroscopic techniques. Differential scanning calorimetry (DSC) and polarising optical microscopy (POM) were used to study the thermal and mesomorphic properties of the compounds. All the

compounds of nDMABAPB (where $n = 10, 12, 14$ and 16), exhibited a thread-like texture nematic phase on cooling from the isotropic liquid only. However, for 18DMABAPB, it exhibited both smectic and nematic phases upon cooling. The most common application of liquid crystal technology is liquid crystal displays. A liquid crystal display (LCD) are used in a wide range of applications, including computer monitors, television, instrument panels, aircraft cockpit displays, signage [66].

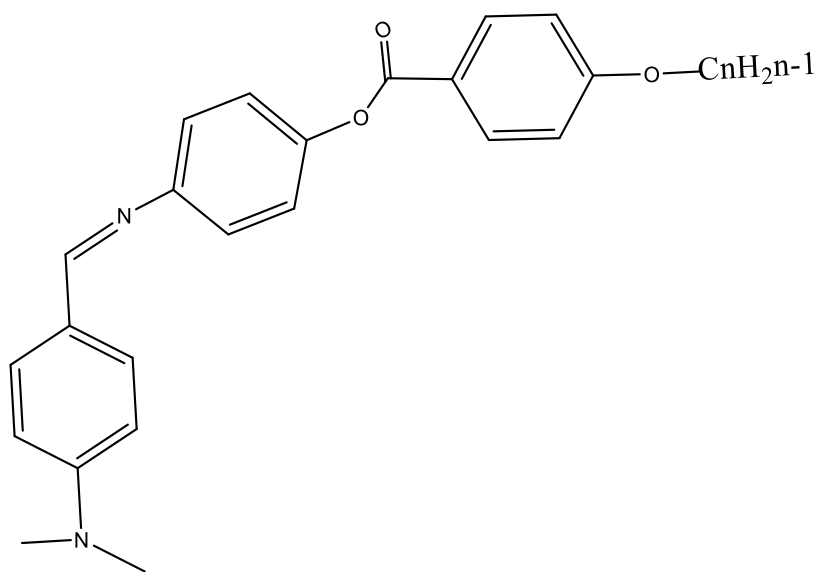


Fig (1.31): The structure of nDMABAPB

(1.6) Aim of the work

This study aims to synthesis, structural characterisation and microbiological activity studies of Mannich reaction and Schiff base ligands and their metal complexes. Consequently this work involved:

1. The formation step(1) of new Mannich-base ligand (R)-2-((4-(dimethylamino)phenyl)((2-nitrophenyl)amino)methyl)-5,5-dimethylcyclohexane-1,3-dione (HL¹) from the reaction of 4-dimethylaminobezaldehyde, 2-nitroaniline and dimedone.
2. The formation step(2) of new Schiff-base ligand (E)-2-(2-((S)-(4-(dimethylamino)phenyl)((2-nitrophenyl)amino)methyl)-5,5-dimethyl-3-oxocyclohexylidene)hydrazine-1-carbothioamide (H₂L²) was acheivd from the reaction of (R)-2-((4-(dimethylamino)phenyl)((2-nitrophenyl)amino)methyl)-5,5-dimethylcyclohexane-1,3-dione (HL¹) and thiosemicarbazide.
3. Complexes of the ligands with some transition metal ions were synthesised.
4. Studying the possible structures and the stereochemistry of the prepared complexes.
5. Studying the microbiological activity of ligands and their complexes against G⁺ and G⁻ strains of bacteria and two types of fungi.

Chapter Two: Experimental

(2) Experimental

(2.1) Materials and Solvents

All reagents (chemicals and solvents) that used in this work were commercially available, Tables (2-1a and 2-1b). They used without further purification.

Table (2-1a): Organic reagents used in this work and their suppliers.

No.	Material	Supplier	Purity %
1	4-(Dimethylamino)benzaldehyde	B.D.H	99
2	Dimedone	England	99
3	2-Nitroaniline	B.D.H	98
4	CHCl ₃	Merk	98
5	Diethyl ether	C.D.H	99
6	C ₆ H ₆	Sigma Aldrich	99.8
7	DMF	B.D.H	99
8	DMSO	B.D.H	99
9	MeCN	Sigma Aldrich	99.8
10	Ethanol	Sigma Aldrich	99
11	Methanol	Sigma Aldrich	99
12	Thiosemicarbazide	Thomas Baker	99

Table (2-1b): Inorganic reagents used in this work and their suppliers.

No.	Material	Supplier	Purity %
1	Cadmium (II) chloride dihydrate	B.D.H	99
2	Calcium chloride (anhydrous)	Merck	99
3	Cobalt (II) chloride hexahydrate	B.D.H	99
4	Copper (II) chloride dihydrate	Fluka	99
5	HCl (36%)	G.C.C	98
6	Zinc (II) chloride (anhydrous)	B.D.H	99
7	Nickel (II) chloride hexahydrate	B.D.H	99
8	Potassium hydroxide	Scharlau	99

(2.2) Physical measurements

A range of physico-chemical measurements was used to characterise ligands and their metal complexes and as follows;

(2.2.1) Melting point

An Electrothermal Stuart SMP₄₀ apparatus was used to determine the melting points of compounds at College of Education for Pure Science (Ibn Al-Haitham), Chemistry Department, Baghdad University.

(2.2.2) Fourier Transform Infrared Spectra (FT-IR)

Biotic 600 FT-IR spectrophotometer was used to obtain Infrared spectra for the prepared compounds in the range 4000-400 cm⁻¹ as potassium bromide at College of Education for Pure Science (Ibn al-Haitham), Baghdad University and as CsI discs in the range 4000-200 cm⁻¹ on Shimadzu 8400s FT-IR at College of Science, Baghdad University.

(2.2.3) Electronic spectra

The electronic spectra of compounds were obtained using a (UV-Vis) spectrophotometer type Shimadzu UV-160 in the range (200-1000 nm) using quartz cell of (1.0) cm length with concentration 10⁻³ mol.L⁻¹ of samples in DMSO at 25°C. The samples were tested at Ibn Siena Enterprise / Iraqi Ministry of Industry.

(2.2.4) Mass spectroscopy

Mass spectra for the ligands were obtained using a positive mode Electrospray mass spectrophotometer (+) (Sciex Esi mass analysis). The spectra were recorded at Mashhad / Islamic Republic of Iran.

(2.2.5) Conductivity measurements

Conductivity measurements of the complexes were recorded at 25 °C for 10^{-3} M solutions of the samples in DMSO using an Eutech Instruments Cyberscan con 510 digital conductivity meter. The recorded conductivity measurements were done at College of Education for Pure Science (Ibn Al-Haitham), Chemistry Department, University of Baghdad.

(2.2.6) Metal analysis

Metal content for complexes were measured using a Shimadzu atomic absorption spectrophotometer (A.A) 680G in Ibn Sina Company, Ministry of Industry, Baghdad, Iraq.

(2.2.7) Nuclear magnetic resonance spectra (NMR)

NMR spectra (^1H - and ^{13}C -NMR) for the compounds were recorded in DMSO- d^6 using a Bruker 300 MHz for ^1H -NMR and 75 MHz for ^{13}C -NMR, respectively, with a tetramethylsilane (TMS) as an internal reference. The samples were acquired at Tehran University / Islamic Republic of Iran.

(2.2.8) Elemental microanalyses

Elemental microanalysis was performed using a (C.H.N.S) analyzer, (Eager 300 for EA1112). The samples were recorded at Central Laboratory/ University of Tehran, Islamic Republic of Iran.

(2.2.9) Chloride content

The chloride content for complexes was determined using potentiometric titration method on 686–Titro Processor–665 Dosim A–Metrohm/Swiss. The samples were recorded at Ibn Siena Enterprise / Iraqi Ministry of Industry.

(2.2.10) Thermal analysis

Thermogravimetric analysis was carried out using Differential Scanning Calorimetry (DSC) on SDT Q600 V20.9 Build 20. The samples were recorded at Beam Gostar Taban Lab/ Tehran, Islamic Republic of Iran.

(2.2.11) Magnetic moment measurement

Magnetic moments at 308K were determined using a magnetic susceptibility balance (Sherwood Scientific). Samples were recorded at College of Sciences, Al-Mustansiriyah University.

(2.2.12) Anti-microbial Activity

The evaluation of ligands and their metal complexes against four bacterial species (*Escherichia coli*, *Pseudomonas aeruginosa*, *Staphylococcus aureus* and *Bacillus*) and two types of fungi (*Candida* and *trichomoniasis*) were performed using agar-well diffusion. In this method, the wells were dug in the media using a sterile metallic borer with centres at least 6 mm. Recommended concentration (100 μL) of the test sample 1 mg/mL in DMSO was introduced in the respective wells. The plates were incubated immediately at 37°C for 24 h. Activity was evaluated by measuring the diameter of inhibition zones (mm). The samples were recorded at Market Researches and Consumer Protection Center/ University of Baghdad

(2.2.13) Molecular modelling

CS Chem 3D Ultra Molecular Modelling and Analysis Program was performed using 3D molecular modelling to predict the proposed structure for the synthesised complexes.

(2.3) Ligands

Chemical structure, symbol and nomenclature of ligands are presented in Table (2.2).

Table (2.2): Abbreviation, structure and nomenclature of the synthesised ligands.

Symbol	Chemical structure	Nomenclature
HL ¹		(R)-2-((4-(dimethylamino)phenyl)((2-nitrophenyl)amino)methyl)-5,5-dimethylcyclohexane-1,3-dione
H ₂ L ²		(E)-2-(2-((S)-4-(dimethylamino)phenyl)((2-nitrophenyl)amino)methyl)-5,5-dimethyl-3-oxocyclohexylidene)hydrazine-1-carbothioamide

(2.4) Synthesis

(2.4.1) Synthesis of ligands

(2.4.1.1) Synthesis of (R)-2-((4-(dimethylamino) phenyl) ((2-nitrophenyl)amino)methyl)-5,5-dimethylcyclohexane-1,3-dione(HL¹)

Ligand was prepared according to a conventional method that mentioned in [67-70], which based on Mannich approach and as follows;

To a mixture of anhydrous CaCl₂ (0.5g, 5mmol) in EtOH (10ml), three drops of conc.HCl. was added successively. Dimedone (0.7g, 5mmol) and 4-dimethylaminobezaldehyde (0.74g, 5mmol), and 2-Nitroaniline (0.69g, 5mmol) was. The reaction mixture was allowed to stir overnight at RT and a yellow solid was formed. This solid product was filtered off and washed with EtOH (25ml) and H₂O (25ml) then dried in air. Yield: 0.9g, (44%) and m.p = 217-219°C.

(2.4.1.2) Synthesis of (E)-2-(2- ((S)- (4-(dimethylamino)phenyl) ((2-bnitrophenyl)amino)methyl)-5,5-dimethyl-3- oxocyclohexylidene)hydrazine-1-carbothioamide (H₂L²)

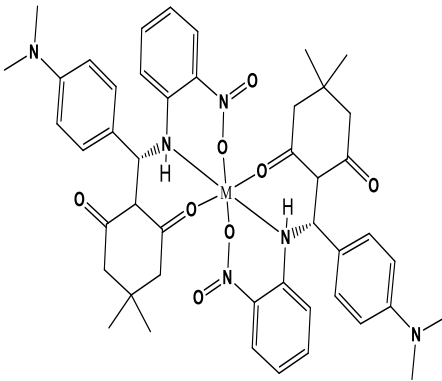
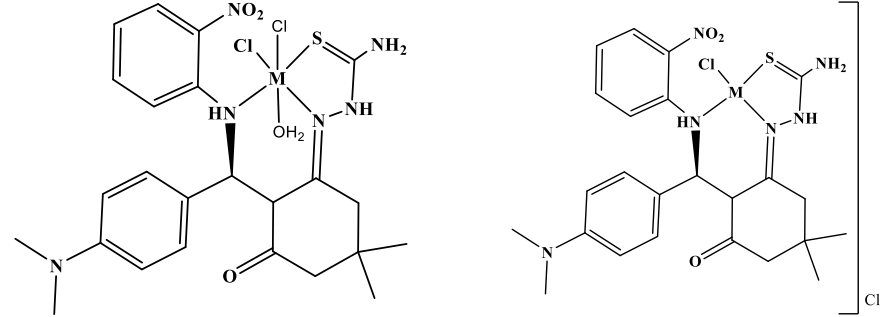
To a mixture of HL¹ (0.5g, 1.22mmol) in 15ml of hot EtOH was added with stirring a solution of thiosemicarbazide (0.11g, 1.22mmol) in 15ml of EtOH with 3drops of glacial acetic acid. The reaction mixture was heated at reflux for 6h, to give a yellowish-white powder, which washed with cold ethanol (5ml) and then dried air. Yield: 0.4g (68%), m.p = 181-183°C.

Table (2.3): Some physical properties of the prepared ligands.

Comp	Colour	Melting point °C
HL ¹	Yellow powder	217-219
H ₂ L ²	Yellowish-white powder	181-183

2.5 Complexes

Table (2.4): Abbreviation, structure and nomenclature of the synthesised complexes.

Comp	Chemical structure
HL ¹	 <p>M= Co(II), Ni(II) , Cu(II) , Zn(II) and Cd(II)</p>
H ₂ L ²	 <p>M=Co(II) and Cu(II)</p> <p>M= Ni(II) Zn(II) and Cd(II) .</p>

(2.6) Synthesis of HL¹ complexes

(2.6.1) Synthesis of [Co(HL¹)₂] (1)

To a solution of HL¹ (0.4g, 0.97mmol) in 5ml DMF was add CoCl₂.6H₂O (0.11g, 0.46mmol). The mixture was stirred overnight at RT. The solution was evaporated slowly at RT and the solid powder was filtered off and washed with 15ml of ethanol. The compound was recrystallised from ethanol to give the pure product. Yield: 0.21g (50%), m.p 255°C.

(2.6.2) Synthesis of [Ni(HL¹)₂](2), [Cu(HL¹)₂](3), [Zn(HL¹)₂] (4) and [Cd(HL¹)₂] (5).

The procedure described for (1) that mentioned in (2.6.1) was used to synthesis [Ni(HL¹)₂](2), [Cu(HL¹)₂](3), [Zn(HL¹)₂] (4) and [Cd(HL¹)₂] (5). Table (2.5) shows the physical properties of the complexes and their reactant quantity.

(2.7) Synthesis of H₂L² complexes

(2.7.1) Synthesis of [Co (H₂L²) Cl₂ H₂O] (1)

A mixture of H₂L² (0.2g, 0.5mmol) and CoCl₂.6H₂O (0.098g, 0.065mmol) in 5ml DMF medium was stirred overnight at RT. A dark green powder was crushed out of the solution, which washed with ethanol 15ml and 10ml of diethyl ether then dried in air. Yield: 0.046g (67%), m.p = 360 dec.

(2.7.2) Synthesis of $[\text{Ni}(\text{H}_2\text{L}^2)\text{Cl}]\text{Cl}$ (2), $[\text{Cu}(\text{H}_2\text{L}^2)\text{Cl}_2 \cdot \text{H}_2\text{O}]$ (3), $[\text{Zn}(\text{H}_2\text{L}^2) \text{Cl}]\text{Cl}$ (4) and $[\text{Cd}(\text{H}_2\text{L}^2) \text{Cl}]\text{Cl}$ (5).

A similar procedure which used to synthesis $[\text{Ni}(\text{H}_2\text{L}^2)\text{Cl}]\text{Cl}$ (2), $[\text{Cu}(\text{H}_2\text{L}^2)\text{Cl}_2 \cdot \text{H}_2\text{O}]$ (3), $[\text{Zn}(\text{H}_2\text{L}^2) \text{Cl}]\text{Cl}$ (4) and $[\text{Cd}(\text{H}_2\text{L}^2) \text{Cl}]\text{Cl}$ (5). Table (2.6) shows the physical properties of the complexes and their reactant quantity.

Table (2.5): Metal salts quantities, yields Colours, melting points of complexes of HL^1

Complex	Weight of metal salt(g)	Weight of complex(g)	Yield (%)	Colour	m.p. °C
$[\text{Co}(\text{HL}^1)_2]$	0.11	0.21	50	Pale green	255
$[\text{Ni}(\text{HL}^1)_2]$	0.11	0.2	50	Greenish-yellow	360*
$[\text{Cu}(\text{HL}^1)_2]$	0.083	0.25	57	Pale brown	287
$[\text{Zn}(\text{HL}^1)_2]$	0.066	0.18	41	Yellow	197
$[\text{Cd}(\text{HL}^1)_2]$	0.11	0.23	50	Pale yellow	296

*= Decomposed.

Table (2.6): Metal salts quantities, yields Colours, melting points of complexes of H_2L^2

Metal ion	Weight of metal salt(g)	Weight of complex(g)	Yield (%)	Colour	m.p. °C
$[Co(H_2L^2)Cl_2H_2O]$	0.098	0.253	67	Dark green	360*
$[Ni(H_2L^2) Cl] Cl$	0.098	0.253	68	Pale gray	223
$[Cu(H_2L^2)Cl_2H_2O]$	0.07	0.25	50	Red	233
$[Zn(H_2L^2) Cl] Cl$	0.056	0.25	47	White	360*
$[Cd(H_2L^2) Cl] Cl$	0.094	0.27	46	Pale yellow	265

*= Decomposed.

Chapter Three: Results & Discussion

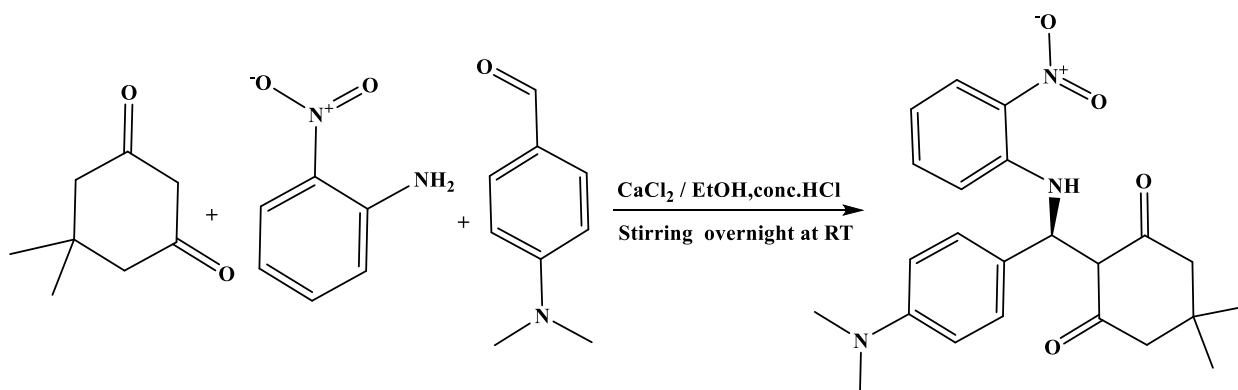
(3) Results and discussion

(3.1) Synthesis and characterisation of ligands

The synthesis of the two ligands: (i) Mannich β -amino carbonyl ligand from reaction of the dimedone with 2-nitroaniline and 4-dimethylaminobenzaldehyde resulted in the formation of the (R)-2-((4-(dimethylamino) phenyl) ((2-nitrophenyl) amino) methyl)-5,5-dimethylcyclohexane-1,3-dione (HL^1) (ii) Schiff base ligand from the reaction of (R)-2-((4-(dimethylamino)phenyl)((2-nitrophenyl)amino)methyl)-5,5-dimethylcyclohexane-1,3-dione (HL^1) with thiosemicarbazide resulted in the formation of (E)-2-(2-((S)-(4-(dimethylamino)phenyl)((2-nitrophenyl)amino)methyl)-5,5-dimethyl-3-oxocyclohexylidene)hydrazine-1-carbothioamide (H_2L^2).

(3.1.1) Synthesis and characterisation of HL^1 ligand:.

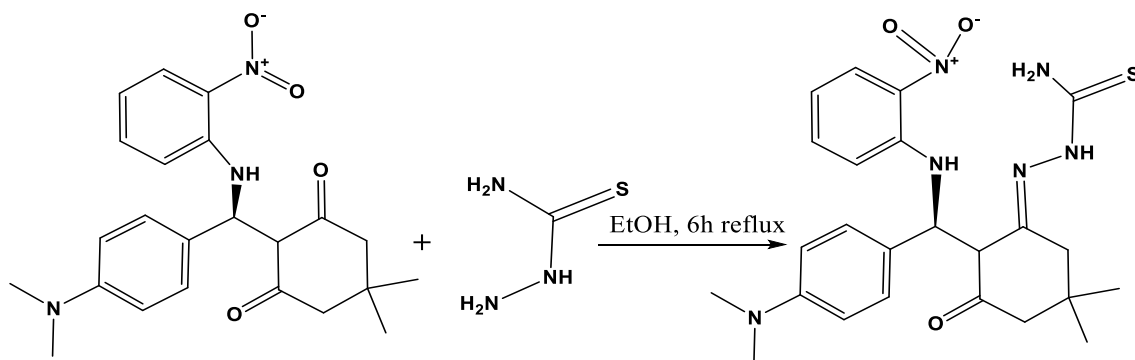
The preparation of HL^1 was based on a published method using a three component *via* a one pot approach [67-70]. In this approach, anhydrous calcium chloride, HCl and EtOH were used as a catalyst and reaction medium, respectively. The reaction of dimedone, 2-nitroaniline and 4-dimethylaminobenzaldehyde in a 1:1:1 mole ratio in EtOH. 1mole of anhydrous calcium chloride as a catalyst resulted in the formation of HL^1 in moderate yield (Scheme (3.1)). The ligand is soluble in DMSO and DMF, Table(3.1). The ligand was confirmed by melting point, C.H.N (Table (3.2)), Fourier Transform Infrared Spectrum (Table(3.3)), electrospray mass spectroscopy and 1H , ^{13}C -NMR spectra.



Scheme (3.1): General synthetic route of HL¹.

(3.1.2) Synthesis and characterisation of H₂L² ligand:.

The preparation of the thiosemicarbazide ligand (H₂L²) was accomplished using a condensation approach [71]. HL¹ was used as a precursor to form H₂L². The synthesis was based on the addition of thiosemicarbazide to HL¹ in a 1:1 mole ratio in EtOH, Resulted in the formation of H₂L² in moderate yield (Scheme 3.2). The ligand is soluble in dimethyl sulfoxide and dimethylformamide, Table (3-1). The chemical structure of the ligand was established using; Elemental microanalysis Table (3.2), FT-IR Table (3.3), electrospray mass spectroscopy and ¹H, ¹³C-NMR spectra.



Scheme (3.2): General synthetic route of H₂L².

Table (3.1): The solubility of ligands in different solvents.

Compound	H ₂ O	MeOH	EtOH	DMF	DMSO	MeCN	C ₆ H ₆
HL ¹	-	÷	÷	+	+	-	-
H ₂ L ²	-	÷	÷	+	+	-	-

(÷) sparingly, (+) soluble, (-) in soluble

Table (3.2): Micro-analysis and physical properties for ligands.

Compound	Empirical Formula	M.W	Yield (%)	Colour	Microanalysis found, (calc)%			
					C	H	N	S
HL ¹	C ₂₃ H ₂₇ N ₃ O ₄	409	44	Yellow	67.02 (67.46)	6.23 (6.65)	10.00 (10.26)	-
H ₂ L ²	C ₂₄ H ₃₀ N ₆ O ₃ S	483	68	Yellowish -white	59.22 (59.73)	5.93 (6.27)	17.19 (17.41)	6.15 (6.64)

(calc) = Calculated

(3.2) FT-IR spectral data of ligands

(3.2.1) FT-IR spectrum of HL¹

The FT-IR spectrum of HL¹, Fig (3.2), is compared with that of the starting materials, 2-nitroanilinedimedone and 4-dimethylaminobezaldehyde, (Fig 3.1 (a, b and c, respectively)). The HL¹ spectrum revealed a broad peak at 3433 cm⁻¹ assigned to the overlap of (NH) peaks of the secondary amine and OH enol of the carbonyl group, which was formed as a result of tautomerazim between carbonyl-dimedone with a proton of adjucted carbonyl [38,40], compared with the twin peaks of the

primary amine of 2-nitroaniline at 3355 and 3479cm^{-1} (the asymmetric and symmetric $\nu(\text{N-H}_2)$). This peak confirmed the involvement of the 2-nitroaniline moiety in the formation of the Mannich base. The spectrum exhibited a band at 1647cm^{-1} assigned to $\nu(\text{C=O})$ carbonyl group of amide, compared with that at 1616 and 1694cm^{-1} of the carbonyl groups of the free dimedone and 4-dimethylaminobezaldehyde, respectively. The appearance of a one carbonyl band and its value indicated the involvement of the ketone and aldehyde groups in the formation of the Mannich base. Bands at 1601 and 1510cm^{-1} assigned to $\delta(\text{N-H})$ and $\nu(\text{C=C})_{\text{aromatic}}$, respectively. The assignment and values of the prominent bands are listed in Table(3.3).

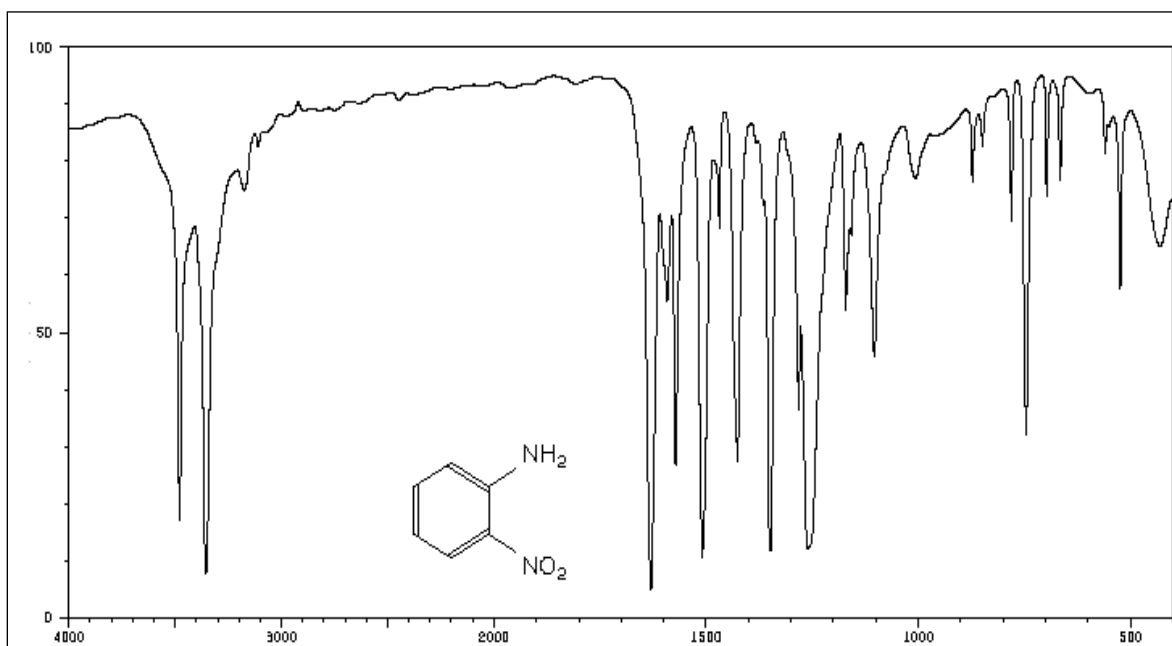


Fig (3.1a): The FT-IR spectrum of 2-nitroaniline.

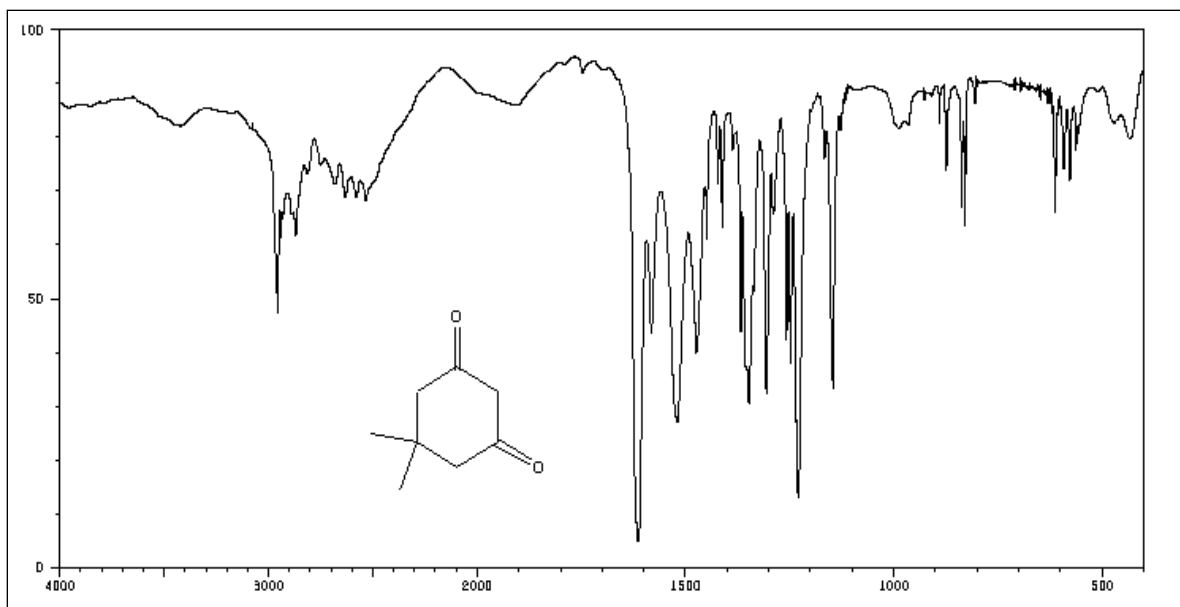


Fig (3.1b): The FT-IR spectrum of dimedone.

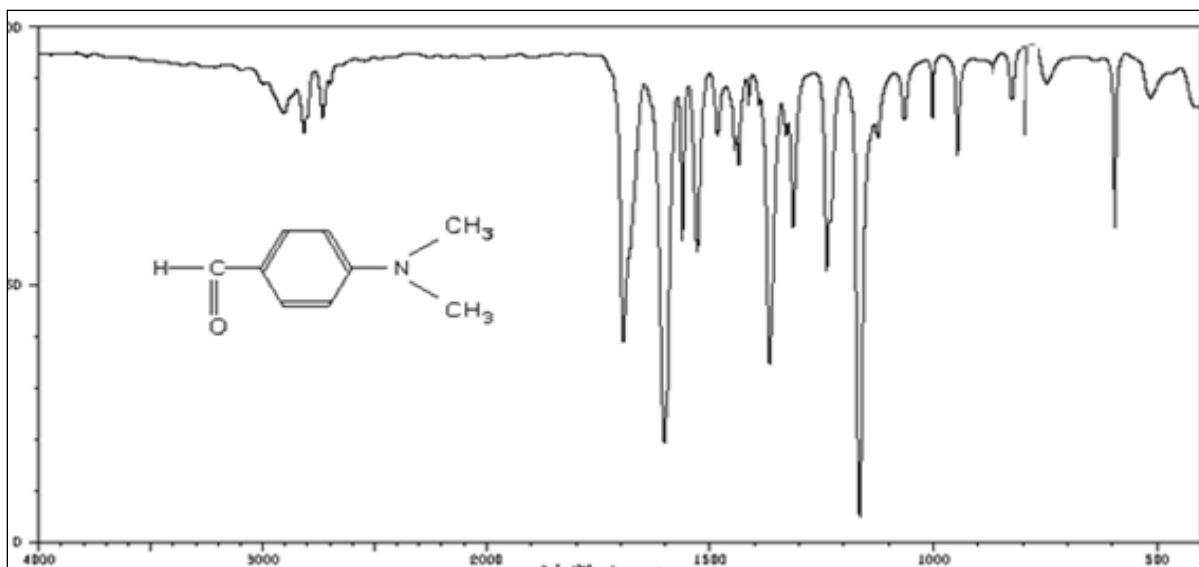


Fig (3.1c): The FT-IR spectrum of 4-dimethylaminobenzaldehyde.

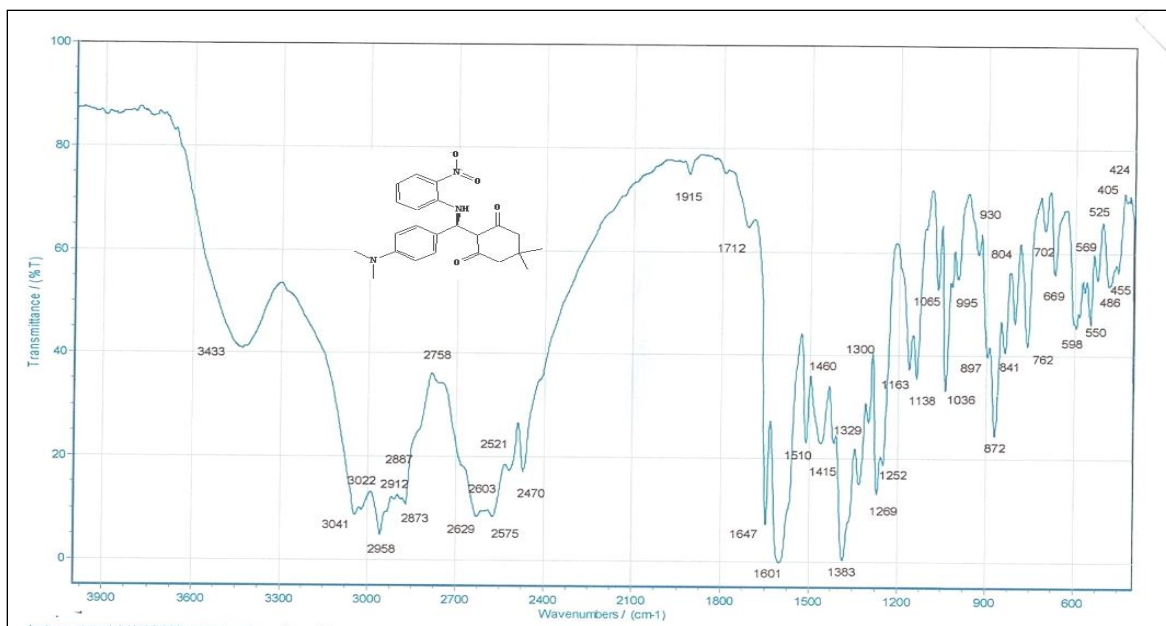


Fig (3.2):The FT-IR spectrum of (R) -2- ((4-(dimethylamino) phenyl) ((2-nitrophenyl)amino)methyl)-5,5dimethylcyclohexane-1,3-dione(HL¹).

(3.2.2) FT-IR spectrum of H₂L²

The FT-IR spectrum of H₂L², Fig (3.4), is correlated with the FT-IR spectra of the starting materials; (R) -2-((4-(dimethylamino) phenyl) ((2-nitrophenyl)amino)methyl)-5,5dimethylcyclohexane-1,3-dione, Fig (3.2), and thiosemicarbazide, Fig (3.3). The H₂L² spectrum revealed peaks at 3442 and 3371cm⁻¹ which are assigned to $\nu(\text{N-H})$ of the hydrazinic segment and the $\nu(\text{N-H})$ of the secondary amine, respectively. The asymmetric and symmetric bands of $\nu(\text{N-H}_2)$ of the thiosemicarbazide appeared at 3263 and 3174cm⁻¹, respectively. The spectrum showed a new band at 1622cm⁻¹ which assigned to $\nu(\text{C=N})_{\text{imine}}$ group. The appearance of this band and the disappearance of the carbonyl ketone band at 1647cm⁻¹.The spectrum revealed a peak at 1664cm⁻¹ assigned to carbonyl ketone group (Fig (3.2)) confirmed the condensation and the formation of the thiosemicarbazone

Schiff-base. The appearance a band at 1198cm^{-1} related to $\nu(\text{C}=\text{S})$ is another indication for the formation of the thiosemicarbazone ligand. Further, the spectrum showed a new band at 995cm^{-1} that is related to $\nu(\text{N}-\text{N})$ of the hydrazinic group. The assignment and values of the prominent peaks are listed in Table (3.3).

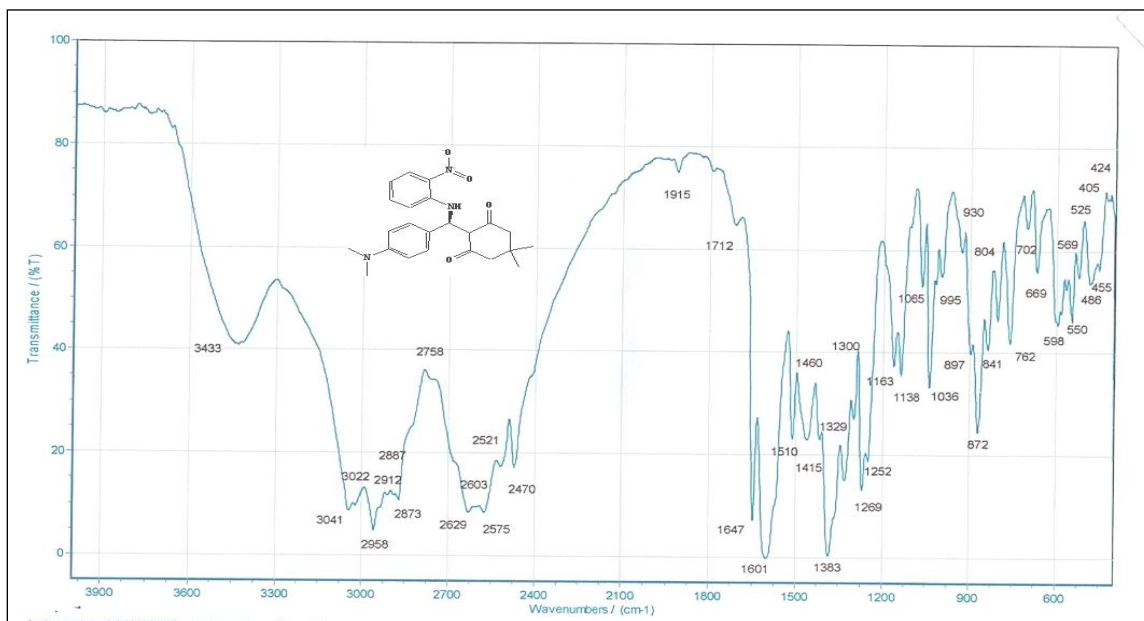


Fig (3.2):The FT-IR spectrum of **(R)-2-((4-(dimethylamino) phenyl)((2-nitrophenyl)amino)methyl)-5,5dimethylcyclohexane-1,3-dione(HL¹)**.

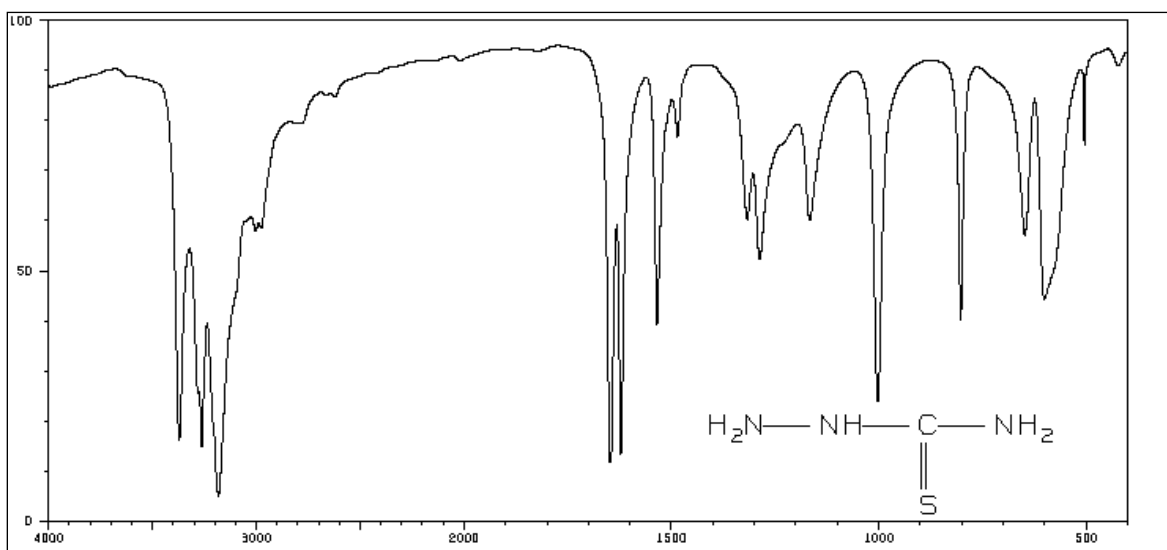


Fig (3.3): The FT-IR spectrum of thiosemicarbazide hydrochloride

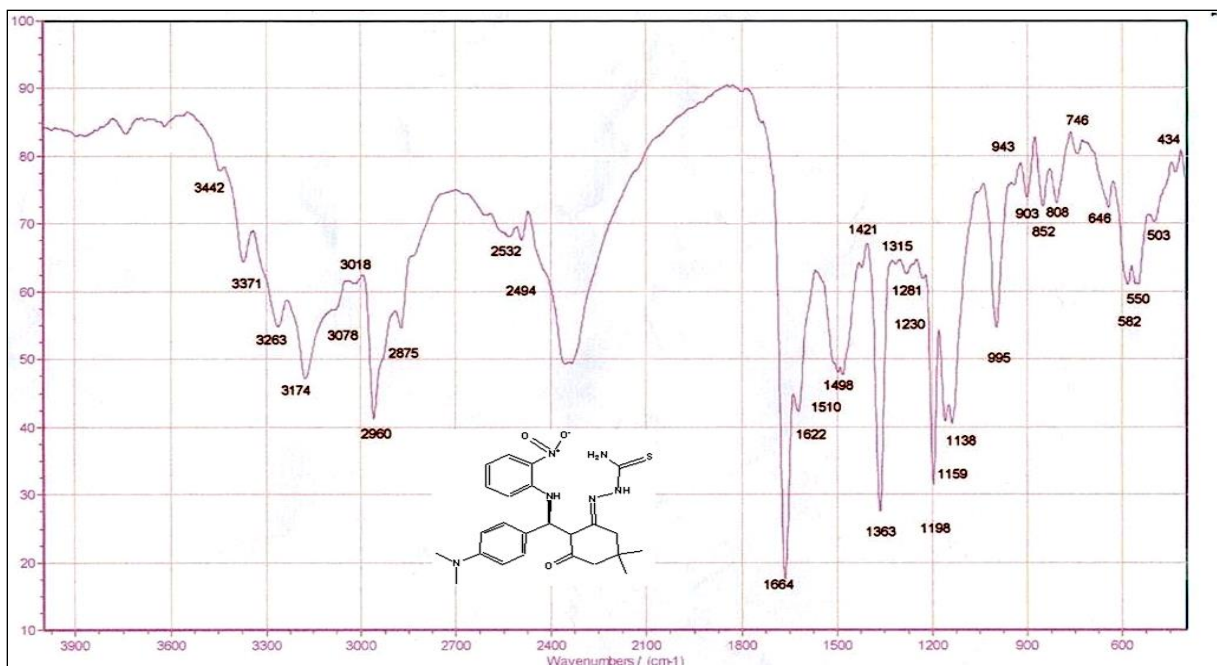


Fig (3.4): The FT-IR spectrum of (E)-2-(2-((S)-4-(dimethylamino)phenyl)((2-nitrophenyl)amino)methyl)-5,5-dimethyl-3-oxocyclohexylidene)hydrazine-1-carbothioamide (H_2L^2).

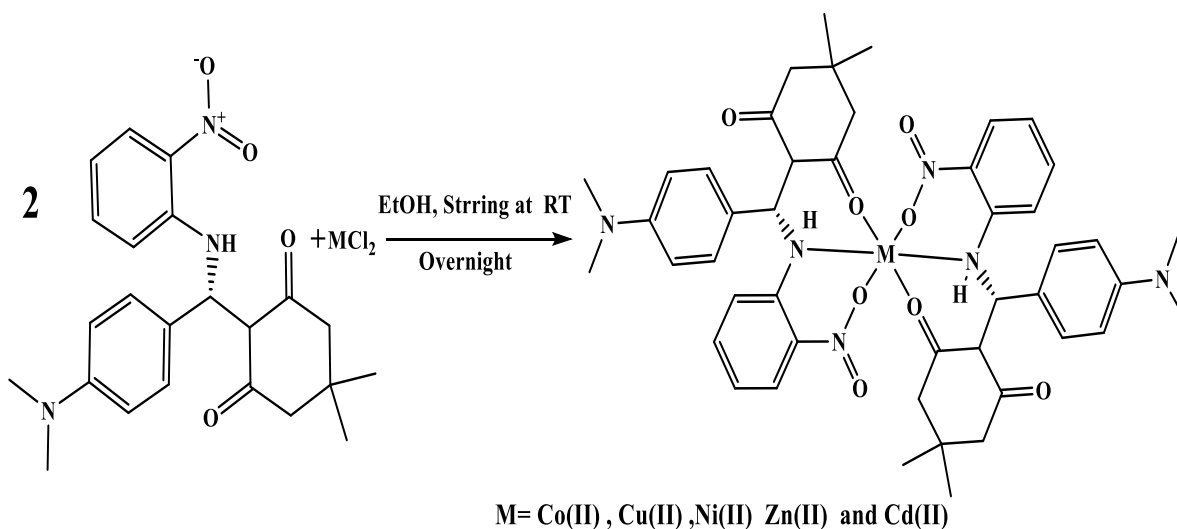
Table (3.3): The FT-IR spectral data of ligands(cm^{-1}).

Ligand	$\nu(NH)$	$\nu(NH)_{am}$	$\nu(NH_2)_{sy,asy}$	$\nu(C-H)_{ar}$	$\nu(C-H)_{al}$	$\nu(C=O)_{ket.}$	$\nu(C=N)$	$\nu(C=C)_{aro.}$	$\nu(NO_2)$	$\nu(C=S)$
HL^1	3433	-	-	3043,3022	2958,2912, 2887,2873	1647	-	1510	1460	-
H_2L^2	3442	3371	3263, 3174	3078, 3018	2960, 2875	1664	1622	1510	1460	1198

(3.3) Synthesis and characterisation of metal complexes

(3.3.1) Synthesis and characterisation of HL¹ complexes

The complexes were prepared implementing a similar method, Scheme (3.3), that based on the addition of metal chloride of Co(II), Ni(II), Cu(II), Zn(II) and Cd(II) ions to the ligand in a 1:2 (M:L) mole ratio. The reaction was carried out in DMF medium. The ligand behaves as a neutral tridentate moiety. The obtained results indicated the formation of six-coordinate for all complexes.



Scheme (3.3): General synthesis route of HL¹ complexes.

The solubility of the complexes was checked in different solvents, Table (3.4). A range of physico-chemical analysis were used to characterised complexes. Micro-analysis, metal and chloride ratio, Table (3.5). Further, spectroscopic methods include; fourier transform infrared spectra, electronic spectra, ^1H , ^{13}C -nuclear magnetic resonance spectra, along with molar conductivity and melting point were used to characterise the complexes.

Table (3.4): The solubility of HL^1 complexes in different solvents.

Complex	H_2O	MeOH	EtOH	DMF	DMSO	CHCl_3	MeCN	C_6H_6
$[\text{Co}(\text{HL}^1)_2]$	–	÷	÷	÷	+	–	–	–
$[\text{Ni}(\text{HL}^1)_2]$	–	÷	÷	÷	+	–	–	–
$[\text{Cu}(\text{HL}^1)_2]$	–	÷	÷	÷	+	–	–	–
$[\text{Zn}(\text{HL}^1)_2]$	–	÷	÷	÷	+	–	–	–
$[\text{Cd}(\text{HL}^1)_2]$	–	÷	÷	÷	+	–	–	–

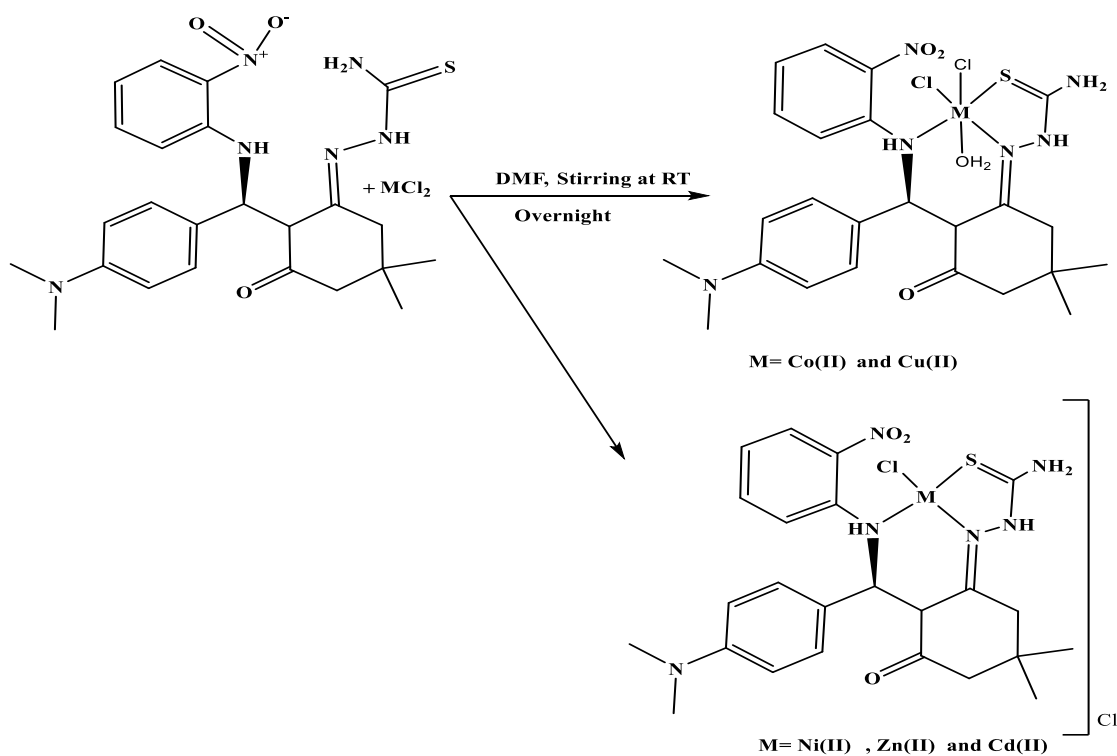
Table (3.5): Micro analysis and physical properties of HL¹ complexes.

Complex	Molecular formula	M.Wt	Colour	m.p.°C	Yield (%)	Micro analysis calculated			
						found (%)			
						C	H	N	M
[Co(HL ¹) ₂]	C ₄₆ H ₅₄ CoN ₆ O ₈	877.97	Pale green	255	50	(62.34) 62.93	(6.00) 6.21	(9.22) 9.56	(6.45) 6.67
[Ni(HL ¹) ₂]	C ₄₆ H ₅₄ NiN ₆ O ₈	877.74	Greenish-yellow	360*	50	(62.24) 62.94	(6.96) 6.21	(9.24) 9.57	(6.34) 6.68
[Cu(HL ¹) ₂]	C ₄₆ H ₅₄ CuN ₆ O ₈	882.58	Pale brown	287	57	(62.18) 62.60	(5.97) 6.17	(9.11) 9.51	(7.00) 7.19
[Zn(HL ¹) ₂]	C ₄₆ H ₅₄ ZnN ₆ O ₈	884.45	Yellow	197	41	(62.23) 62.46	(5.98) 6.16	(9.26) 9.49	(7.15) 7.39
[Cd(HL ¹) ₂]	C ₄₆ H ₅₄ CdN ₆ O ₈	931.99	Pale yellow	296	50	(59.27) 59.28	(6.53) 5.85	(8.92) 9.01	(12.00) 12.11

* = Decomposed

(3.3.2) Synthesis and characterisation of H_2L^2 complexes

The complexes were prepared from reaction of metal chlorides (CoII, NiII, CuII, ZnII and CdII ions) with the ligand in a 1:1 (M:L) mole ratio, Scheme (3.4). The solubility of the complexes in different solvents is listed in Table (3.6). The complexes were characterised by analytical and spectroscopic techniques including; micro-analysis, metal and chloride ratio, Table(3.7). In addition, fourier transform infrared spectra, electronic spectra, 1H , ^{13}C -Nuclear magnetic resonance spectra, along with molar conductivity and melting point were used to characterise the complexes. The obtained results indicated the formation of four-coordinate and six-coordinate complexes with (CoII, NiII, CuII, ZnII and CdII ions).



Scheme (3.4): General synthetic route of H_2L^2 complexes.

Table (3.6): The solubility of H_2L^2 complexes in different solvents.

Complex	H ₂ O	MeOH	EtOH	DMF	DMSO	CHCl ₃	MeCN	C ₆ H ₆
[Co(H ₂ L ²)Cl ₂ H ₂ O]	–	÷	÷	÷	+	-	-	-
[Ni(H ₂ L ²) Cl]Cl	–	÷	÷	÷	+	-	-	-
[Cu(H ₂ L ²) Cl ₂ H ₂ O]	–	÷	÷	÷	+	-	-	-
[Zn(H ₂ L ²) Cl] Cl	–	÷	÷	÷	+	-	-	-
[Cd(H ₂ L ²) Cl] Cl	–	÷	÷	÷	+	-	-	-

Table (3.7): Micro analysis and physical properties of H_2L^2 complexes.

Complex	Molecular formula	M.Wt	Colour	m.p. °C	Yield (%)	Micro analysis calculated					
						found (%)					
						C	H	N	S	Cl	M
[Co(H ₂ L ²) Cl ₂ H ₂ O]	C ₂₄ H ₃₂ C ₆ N ₆ O ₄ S ₂ Cl	630.45	Dark green	360*	67	(45.52)	(5.1)	(13.3)	(5.06)	(11.23)	(9.13)
						45.72	5.126	13.33	5.09	11.25	9.35
[Ni(H ₂ L ²)Cl] Cl	C ₂₄ H ₃₀ NiN ₆ O ₃ S ₂ Cl	612.228	Pale gray	223	68	(47.00)	(4.81)	(13.50)	(5.00)	(11.50)	(9.22)
						47.08	4.95	13.72	5.23	11.58	9.58
[Cu(H ₂ L ²) Cl ₂ H ₂ O]	C ₂₄ H ₃₂ CuN ₆ O ₄ S 2Cl	635.06	Red	233	50	(45.00)	(5.04)	(13.12)	(4.96)	(11.00)	(9.92)
						45.39	5.08	13.23	5.05	11.16	10.01
[Zn(H ₂ L ²) Cl]Cl	C ₂₄ H ₃₀ ZnN ₆ O ₃ .S 2Cl	618.94	White	360*	47	(46.12)	(4.56)	(13.23)	(5.00)	(11.23)	(10.21)
						46.57	4.89	13.57	5.18	11.45	10.56
[Cd(H ₂ L ²) Cl]Cl	C ₂₄ H ₃₀ CdN ₆ O ₃ .S 2Cl	665.94	Pale yellow	265	46	(43.10)	(4.26)	(12.33)	(4.67)	(10.58)	(16.76)
						43.28	4.54	12.61	4.81	10.64	16.87

*= Decomposed.

(3.4) FT-IR spectral data of complexes

(3.4.1) FT-IR spectra of HL¹ complexes

(3.4.1.1) FT-IR spectra of [Co(HL¹)₂](1), [Ni(HL¹)₂](2), [Cu(HL¹)₂](3), [Zn(HL¹)₂](4) and [Cd(HL¹)₂](5)

The FT-IR spectra of complexes 1, 2, 3, 4 and 5 are shown in Fig. (3.5 to 3.9). The band at 1645 cm^{-1} related to $\nu(\text{C}=\text{O})_{\text{keto}}$ in free ligand was shifted to higher frequency at $1653, 1662, 1666, 1660$ and 1651 cm^{-1} in complexes, respectively. The shifting of the carbonyl moiety may be attributed to the coordination of the oxygen atom of the carbonyl to the metal centre in a similar fashion to that reported in literature [72-74]. The change in the position and the shape of the N-H band in the FT-IR spectra of the complexes is an indication of the involvement of the nitrogen atom in the complexation [74]. The spectra of the metal complexes showed new bands. These bands are attributed to $\nu(\text{M}-\text{O})$ and $\nu(\text{M}-\text{N})$ moiety. Bands observed in the range of $(548-598)\text{ cm}^{-1}$ assigned to $\nu(\text{Co}-\text{O})$, $\nu(\text{Ni}-\text{O})$, $\nu(\text{Cu}-\text{O})$, $\nu(\text{Zn}-\text{O})$ and $\nu(\text{Cd}-\text{O})$, respectively [74,75]. The FT-IR spectra showed bands in the range of $(471-498)\text{ cm}^{-1}$ attributed to $\nu(\text{Co}-\text{N})$, $\nu(\text{Ni}-\text{N})$, $\nu(\text{Cu}-\text{N})$, $\nu(\text{Zn}-\text{N})$ and $\nu(\text{Cd}-\text{N})$, respectively [72,74]. These peaks supported the coordination of the ligand to the metal centre through nitrogen and oxygen. Finally, the spectra of complexes revealed additional peaks at $3425, 3440, 3433, 3441$ and 3438 cm^{-1} in the complexes of Co(II), Ni(II), Cu(II), Zn(II) and Cd(II) respectively. The FT-IR spectra of Co(II) and Cu(II) complexes showed bands can be attributed to H₂O molecule. The presence of these peaks may be related to intramolecular hydrogen bonding between secondary amine and

OH enol of the carbonyl group for complexes [40]. The assignment of the characteristic bands is summarised in Table (3.8).

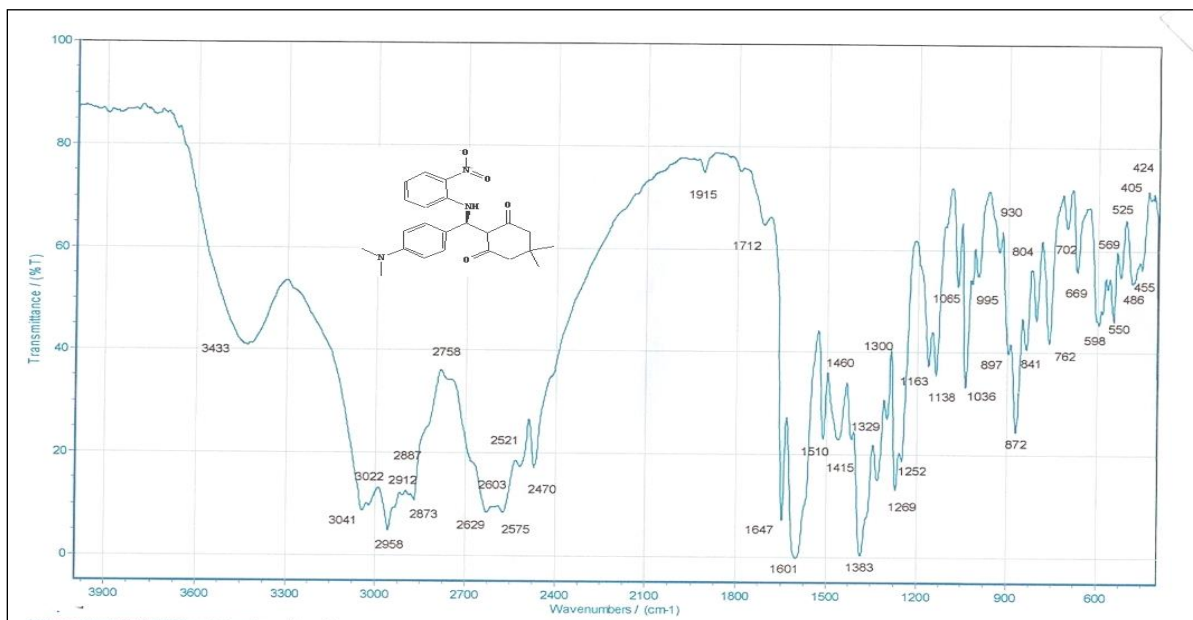


Fig (3.2):The FT-IR spectrum of (R)-2-((4-(dimethylamino) phenyl)((2-nitrophenyl)amino)methyl)-5,5dimethylcyclohexane-1,3-dione(HL¹).

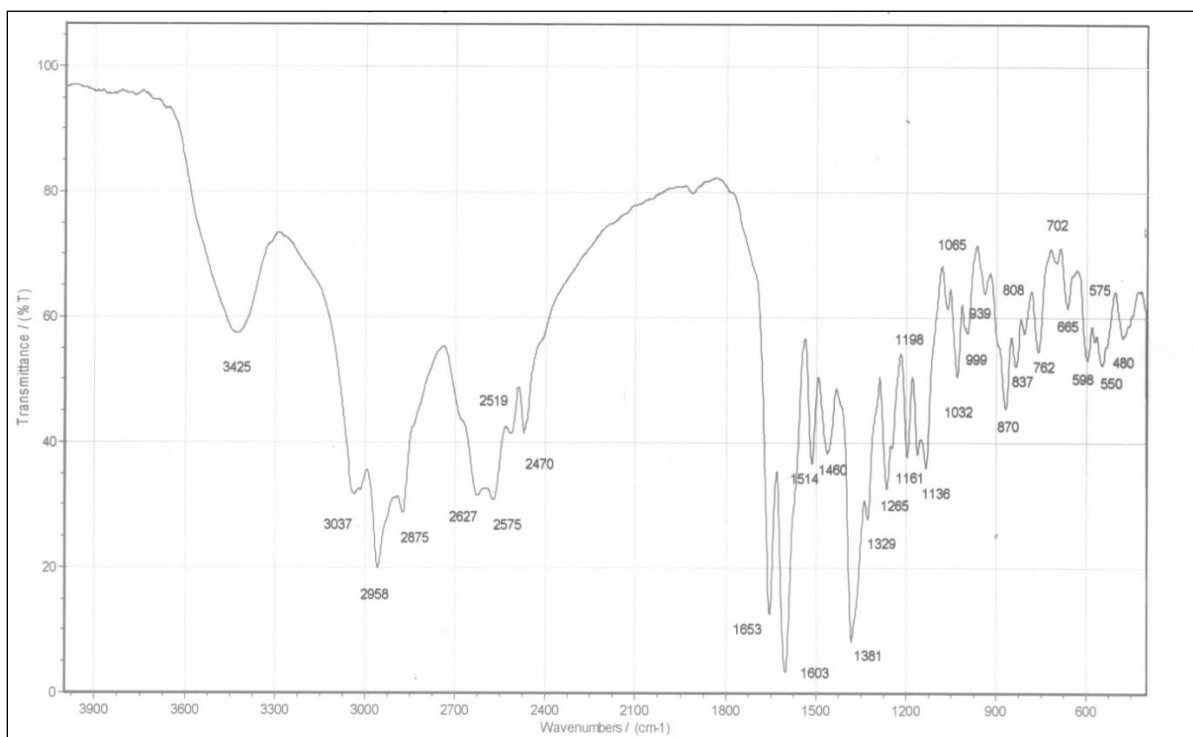


Fig (3.5): FT-IR spectrum of [Co(HL¹)₂]

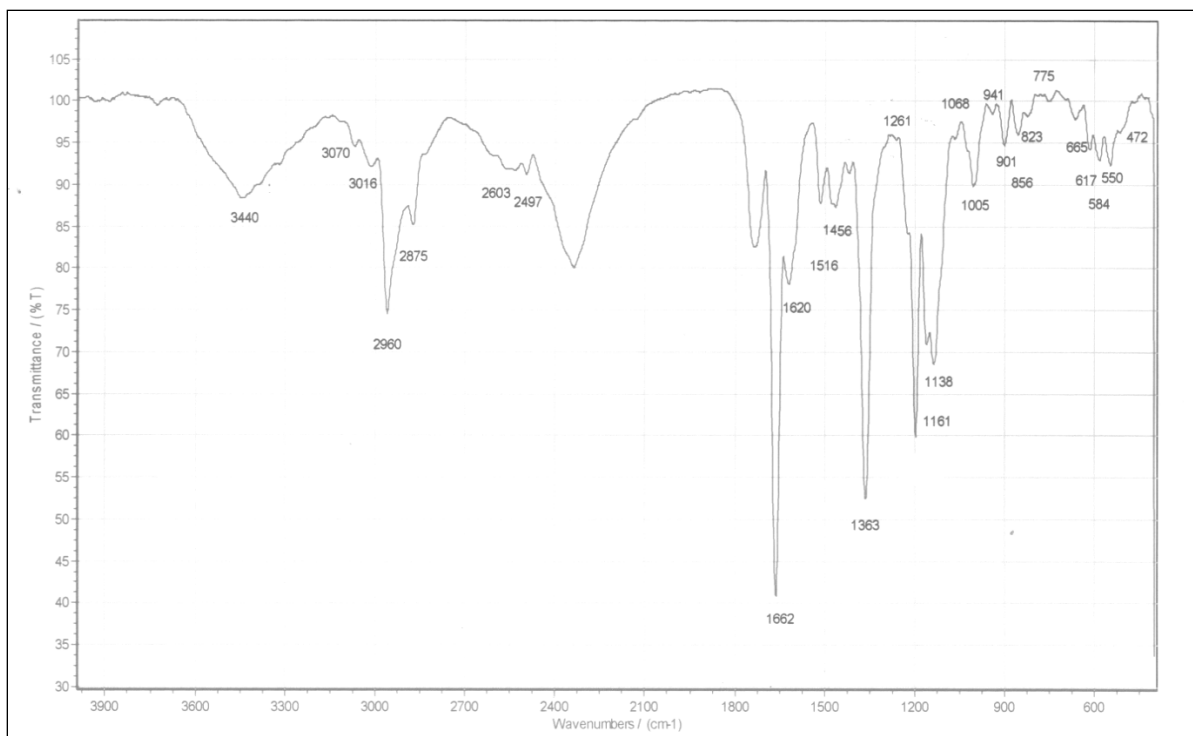


Fig (3.6): FT-IR spectrum of [Ni(HL¹)₂]

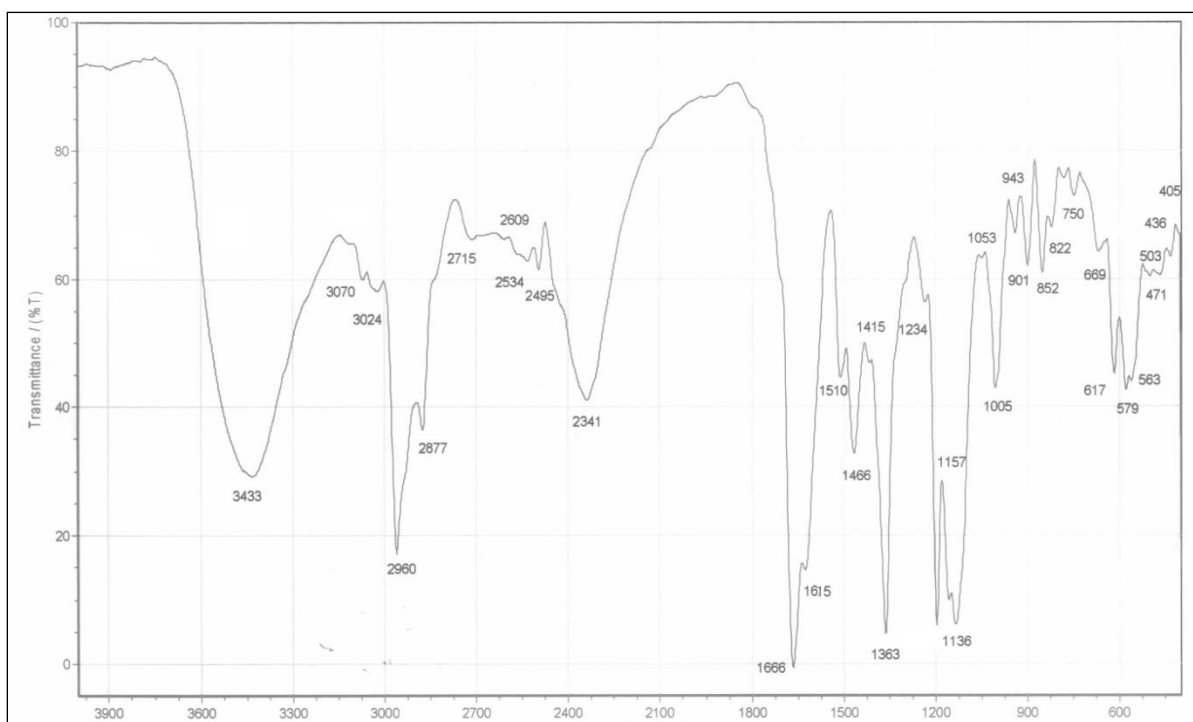


Fig (3.7): FT-IR spectrum of [Cu(HL¹)₂]

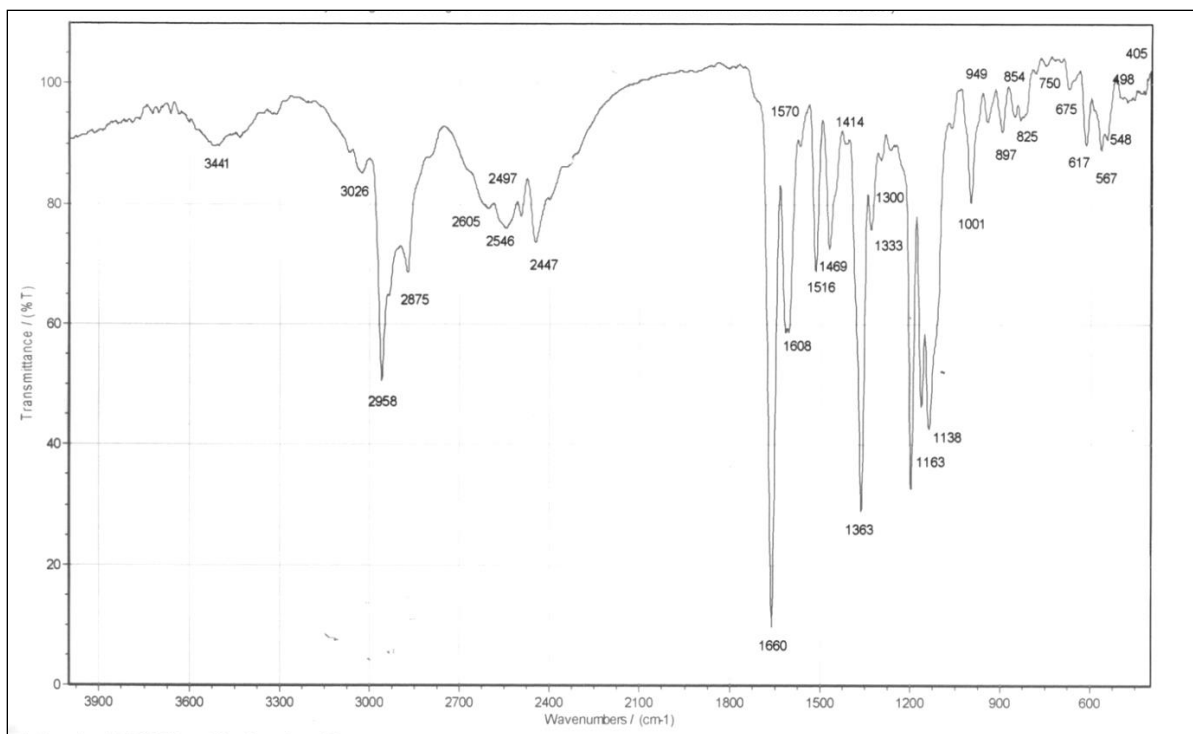


Fig (3.8): FT-IR spectrum of [Zn(HL¹)₂]

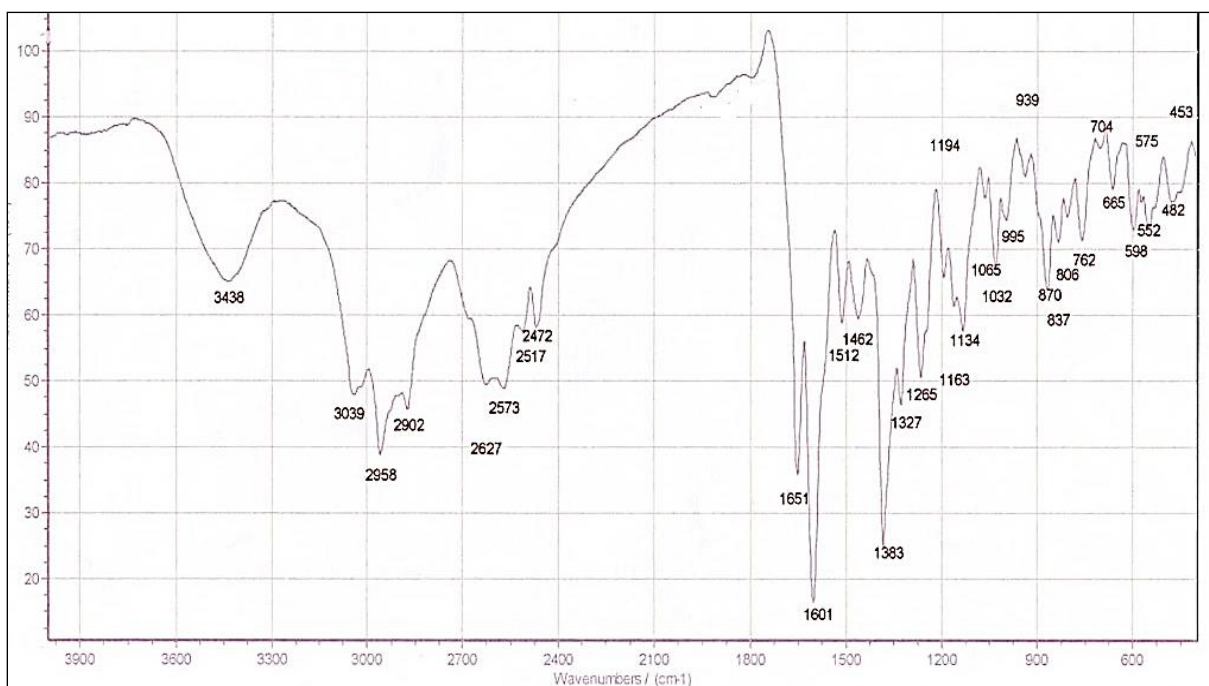


Fig (3.9): FT-IR spectrum of [Cd(HL¹)₂]

Table (3.8): The FT-IR spectral data of HL¹ complexes (cm⁻¹).

Compounds	$\nu(\text{NH})$ $\nu(\text{OH})$	$\nu(\text{C-H})_{\text{ar}}$	$\nu(\text{C-H})_{\text{al}}$	$\nu(\text{C=O})_{\text{ket.}}$	$\delta(\text{N-H})$	$\nu(\text{C=C})_{\text{aro.}}$	$\nu(\text{NO}_2)$	$\nu(\text{M-O})$	$\nu(\text{M-N})$
[Co(HL ¹) ₂]	3425	3037,3020	2958, 2875	1653	1603	1514	1460	598.575	480
[Ni(HL ¹) ₂]	3440	3070,3016	2960, 2875	1662	1620	1516	1456	584.550	472
[Cu(HL ¹) ₂]	3433	3070,3024	2960, 2877	1666	1615	1510	1466	579.563	471
[Zn(HL ¹) ₂]	3441	3030,3026	2958, 2875	1660	1608	1516	1469	567.548	498
[Cd(HL ¹) ₂]	3438	3039,3010	2958, 2902	1651	1601	1512	1462	598.575	482

(3.4.2) FT-IR spectral data of H_2L^2 complexes

(3.4.2.1) FT-IR spectra of $[Co(H_2L^2)]Cl_2 \cdot H_2O$ (6), $[Ni(H_2L^2)Cl]Cl$ (7), $[Cu(H_2L^2)]Cl_2 \cdot H_2O$ (8), $[Zn(H_2L^2)]Cl]Cl$ (9) and $[Cd(H_2L^2)]Cl]Cl$ (10).

The FT-IR spectra of complexes 6, 7, 8, 9 and 10 are placed in Fig. (3.10 to 3.14). The band at 1664cm^{-1} which is referred to $\nu(C=O)$ in the free ligand, Fig (3.2), While in the complexes were appeared at 1660, 1658, 1658, 1666 and 1660cm^{-1} for complexes 6, 7, 8, 9 and 10 respectively, this may be explained by non-participation of $\nu(C=O)$ oxygen atoms in complexes formation [71,74]. Further, the spectra of 6, 7, 8, 9 and 10 showed bands at 1612, 1612, 1616, 1618 and 1614cm^{-1} are attributed to the imine group $\nu(C=N)$, which and shifted to lower frequency. The shift to lower frequency may be related to delocalisation of metal electron density into the ligand π -system, HOMO \rightarrow LUMO [76,77]. The shifting to lower frequency indicates strong bonding nature between the metal ions and the iminic (C=N) group. The shift in the $\nu(C=N)$ confirmed the coordination of the ligand through nitrogen atoms of imine moieties to the metal ions [78-80]. The spectra of complexes revealed peaks that related to $\nu(N-H)$ stretching of the secondary amine at range of $3309-3366\text{cm}^{-1}$ in 6, 7, 8, 9 and 10, respectively, and shifted to lower frequency. The shift in the $\nu(N-H)$ confirmed the coordination of the ligand through nitrogen atoms to the metal ions.

Furthermore, the spectra of the metal complexes showed new bands allocated between $600\text{-}200\text{cm}^{-1}$ that are attributed to $\nu(\text{M-O})$, $\nu(\text{M-N})$, $\nu(\text{M-S})$ and $\nu(\text{M-Cl})$ moiety. The FT-IR spectra exhibited bands at range $(536\text{-}585)\text{cm}^{-1}$ assigned to $\nu(\text{Co-O})$ and $\nu(\text{Cu-O})$, bands at range $(498\text{-}405)\text{cm}^{-1}$ assigned to $\nu(\text{Co-N})$, $\nu(\text{Ni-N})$, $\nu(\text{Cu-N})$, $\nu(\text{Zn-N})$ and $\nu(\text{Cd-N})$, respectively. Bands at range of $(370\text{-}395)\text{cm}^{-1}$ are assigned to $\nu(\text{Co-S})$, $\nu(\text{Ni-S})$, $\nu(\text{Cu-S})$, $\nu(\text{Zn-S})$ and $\nu(\text{Cd-S})$, respectively, Band that belongs to $\nu(\text{M-Cl})$ moiety reported at range $(275\text{-}233)\text{cm}^{-1}$ is for (Co-Cl) , (Ni-Cl) , (Cu-Cl) , (Zn-Cl) and $\nu(\text{Cd-Cl})$, respectively [71,74]. The assignment of characteristic bands is summarised in Table (3.9).

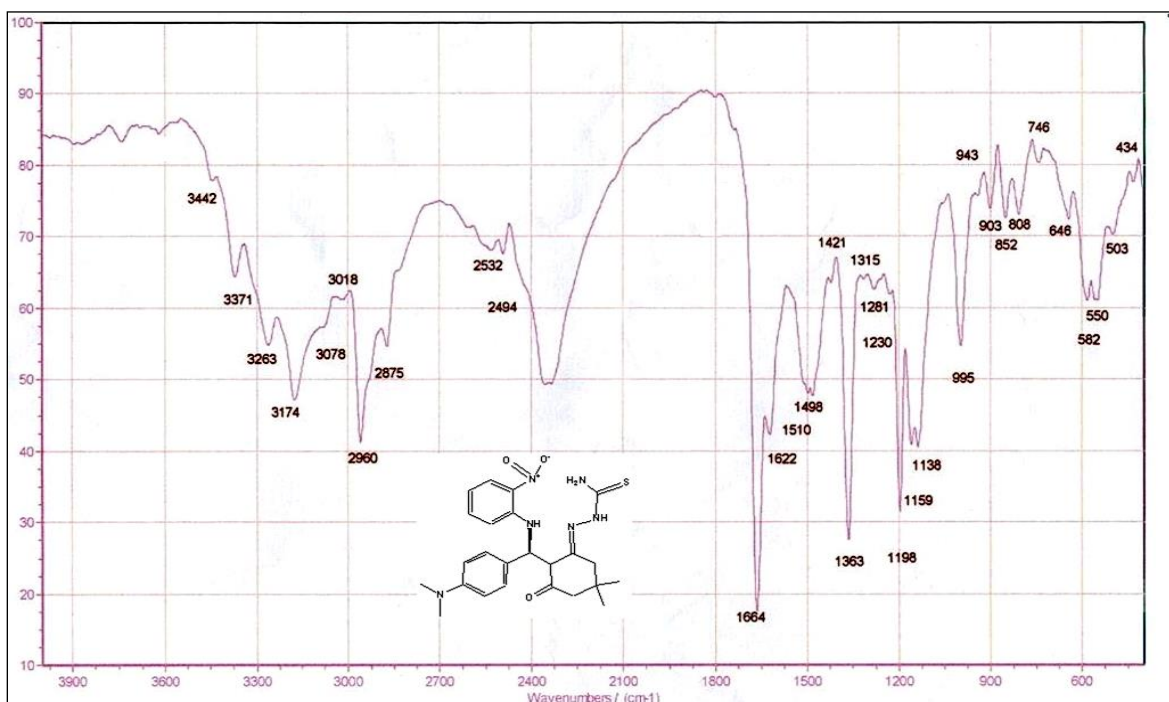


Fig (3.4): The FT-IR spectrum of (E)-2-(2-((S)-(4 (dimethylamino)phenyl)((2-nitrophenyl)amino)methyl)-5,5-dimethyl-3-oxocyclohexylidene)hydrazine-1-carbothioamide (H_2L^2).

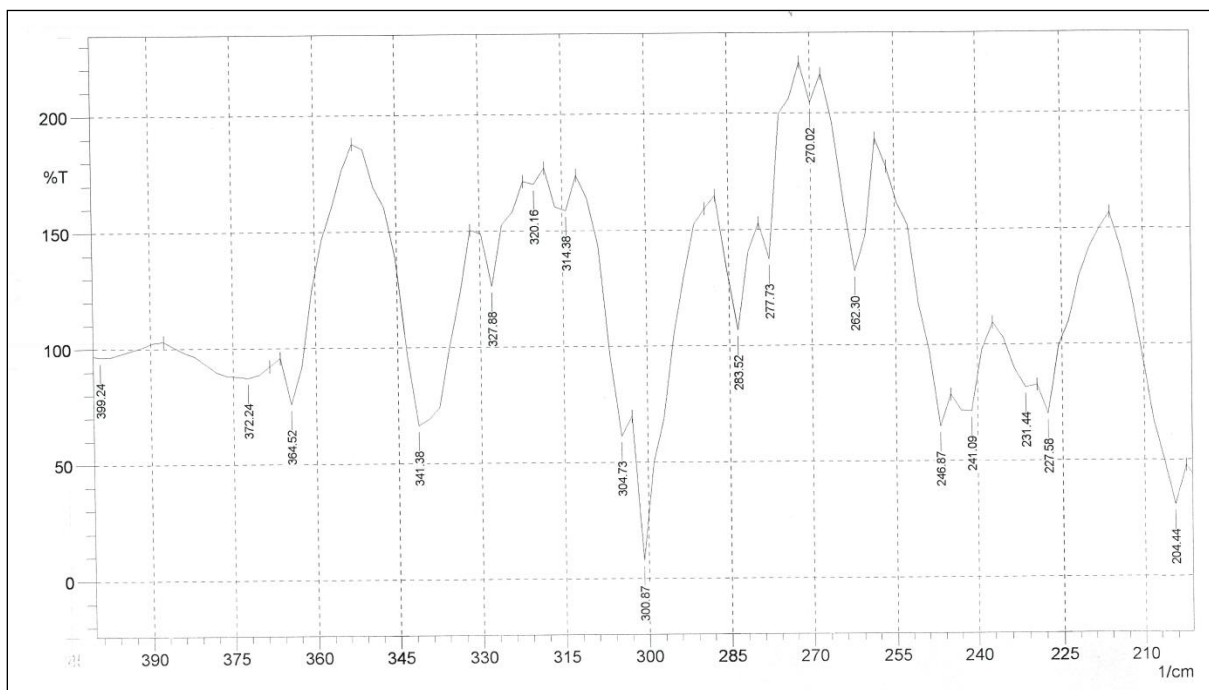
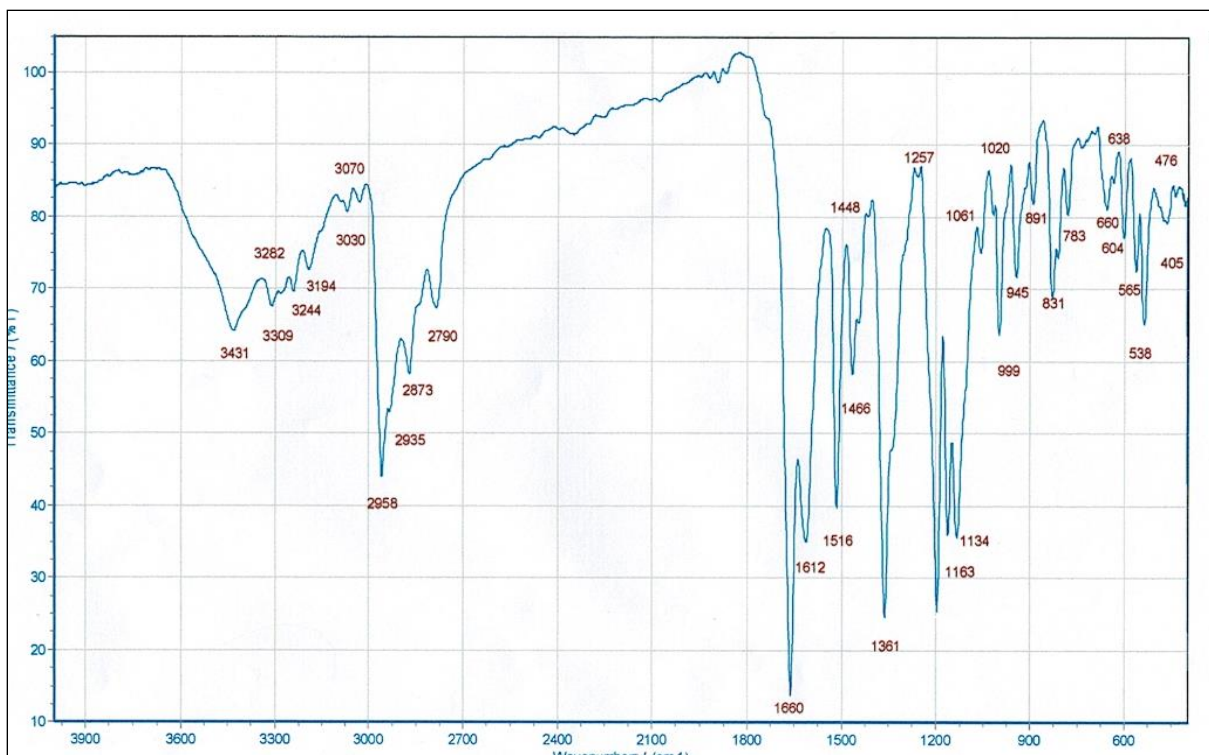


Fig (3.10): FT-IR spectrum of $[\text{Co}(\text{H}_2\text{L}^2)\text{Cl}_2 \cdot \text{H}_2\text{O}]$.

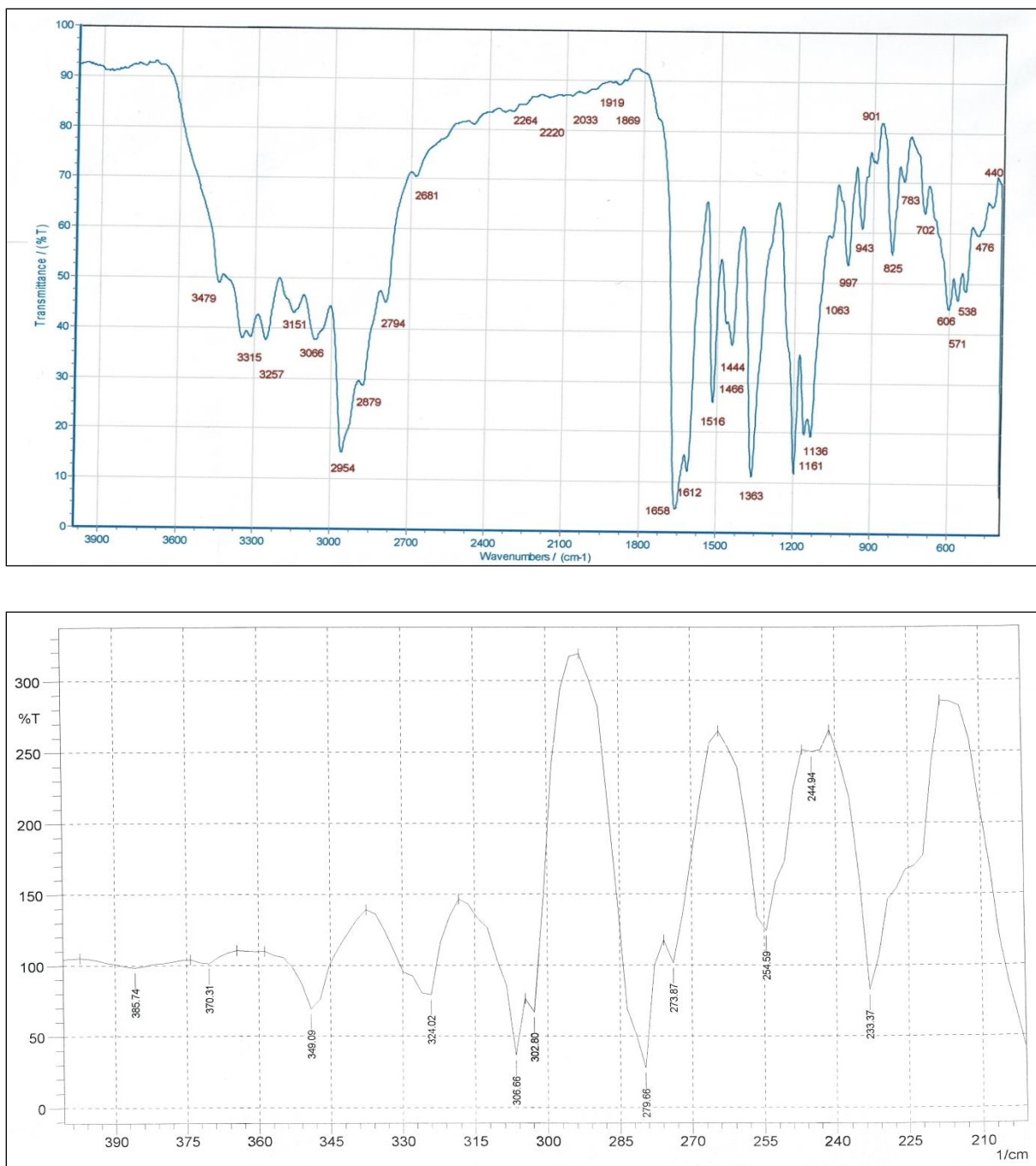


Fig (3.11): FT-IR spectrum of [Ni(H₂L²)Cl]Cl.

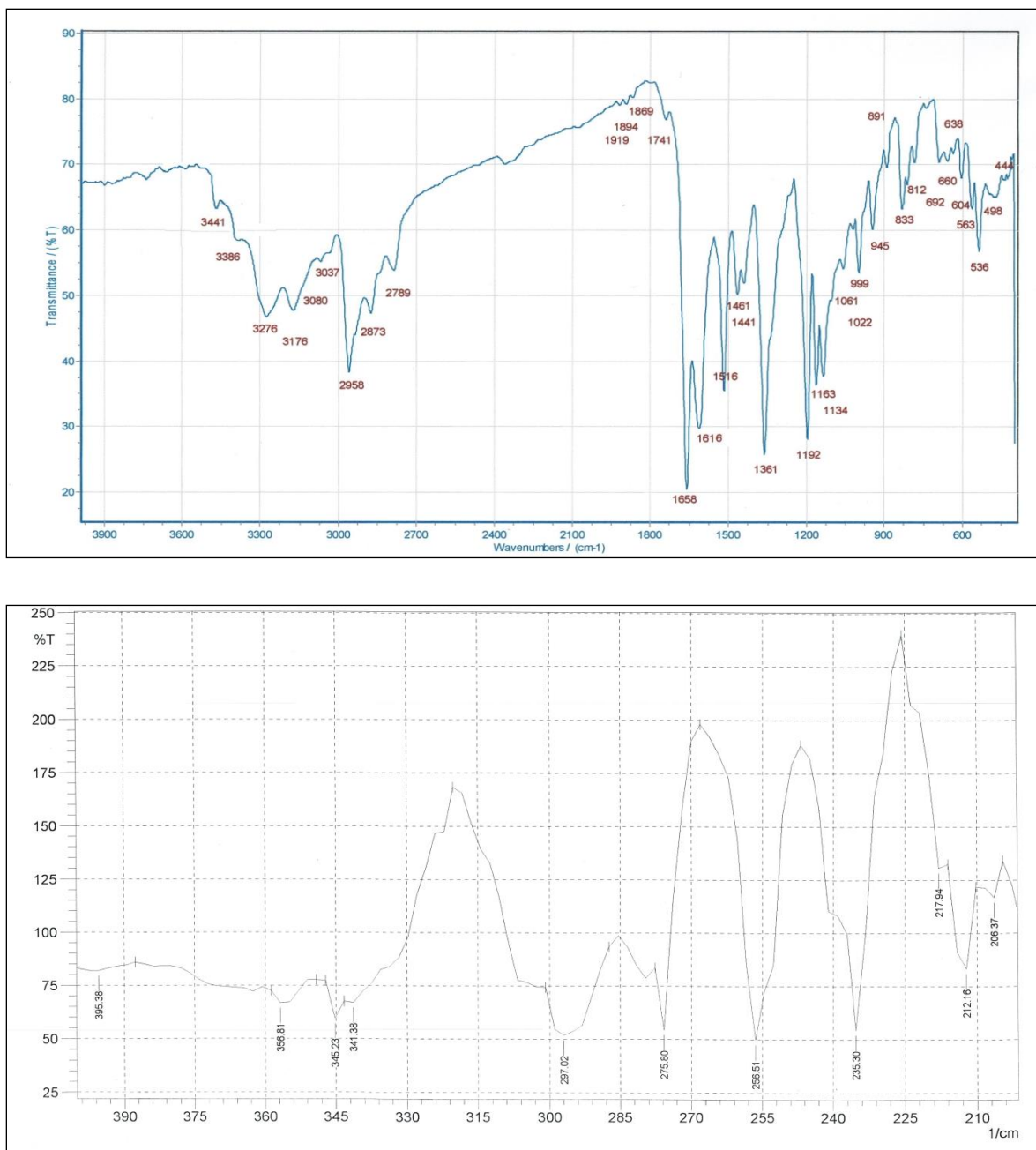


Fig (3.12): FT-IR spectrum of $[\text{Cu}(\text{H}_2\text{L}^2)\text{Cl}_2 \cdot \text{H}_2\text{O}]$.

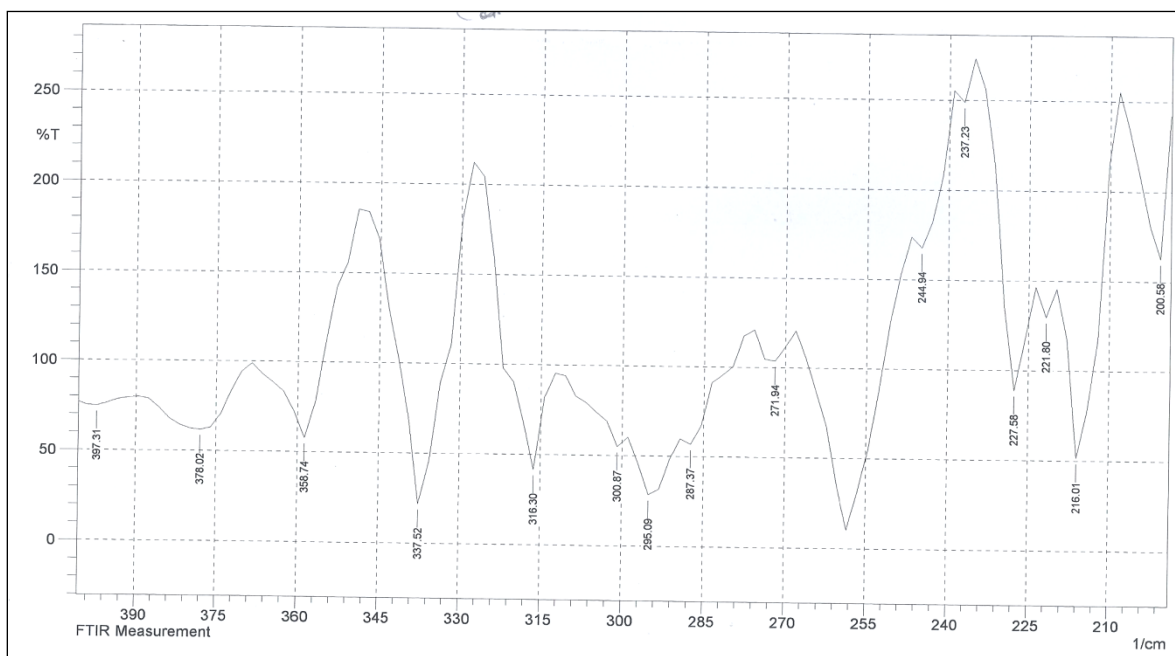
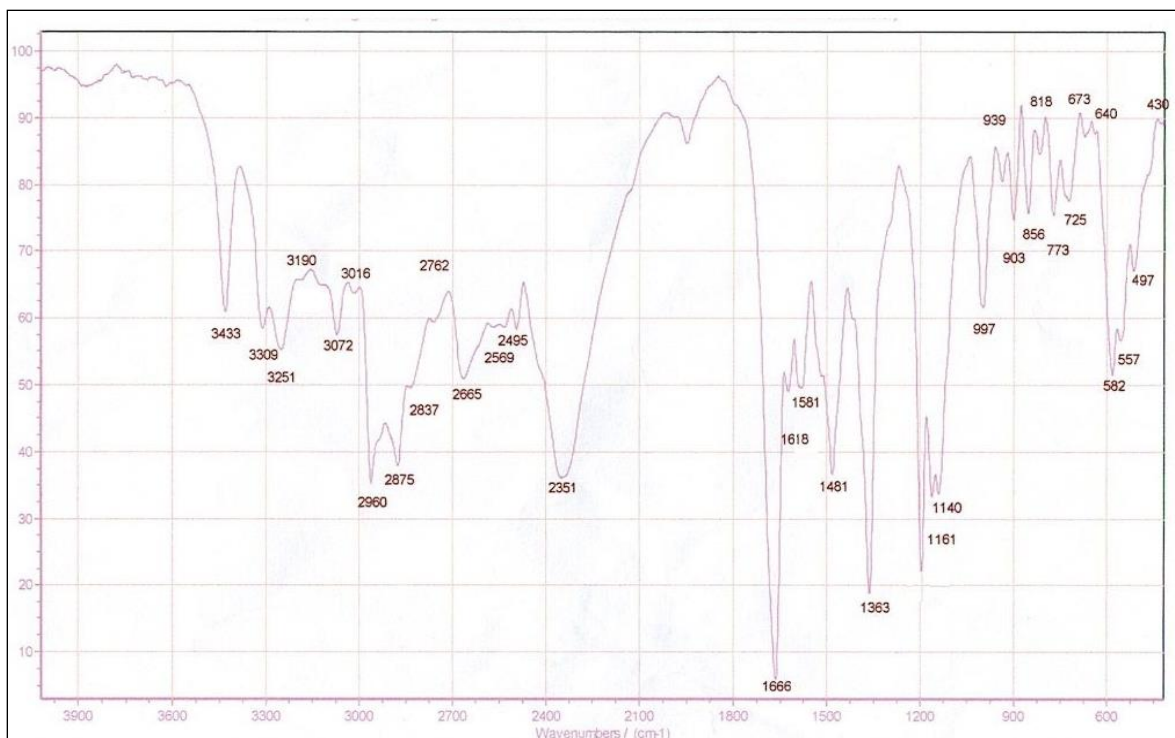


Fig (3.13): FT-IR spectrum of [Zn(H₂L²)Cl]Cl.

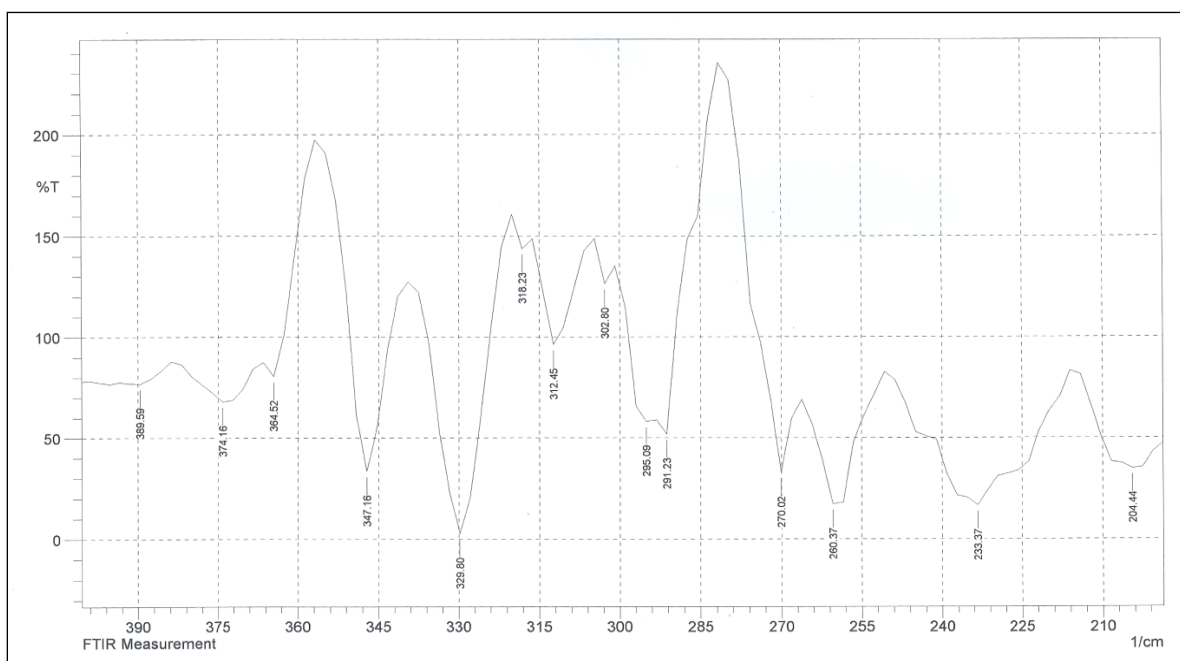
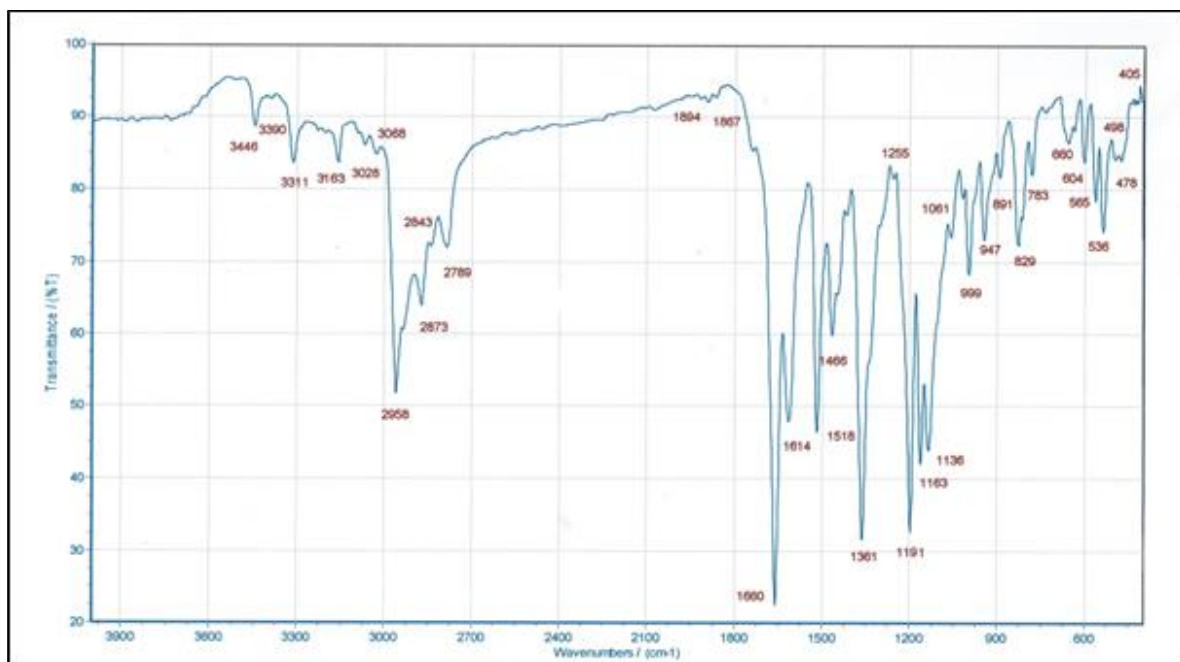


Fig (3.14): FT-IR spectrum of [Cd(H₂L²)Cl]Cl.

Table (3.9): The FT-IR spectral data of H_2L^2 complexes (cm^{-1}).

Compounds	$\nu(NH)$	$\nu(NH)_{am}$	$\nu(NH_2)_{sy,asy}$	$\nu(C=O)$	$\nu(C=N)$	$\nu(C=C)$	$\nu(NO_2)$	$\nu(M-O)$	$\nu(M-N)$	$\nu(M-S)$	$\nu(M-Cl)$
$[Co(H_2L^2)Cl_2H_2O]$	3431	3309	3282, 3194	1660	1612	1516	1466	565	476,405	372	262, 246
$[Ni(H_2L^2)Cl]Cl$	3479	3315	3257, 3151	1658	1612	1516	1466	-	476,440	370	273
$[Cu(H_2L^2)Cl_2H_2O]$	3441	3386	3276, 3176	1658	1616	1516	1461	536	498,444	395	275, 256
$[Zn(H_2L^2)Cl]Cl$	3433	3309	3251, 3190	1666	1618	1581	1481	-	497,430	378	271
$[Cd(H_2L^2)Cl]Cl$	3446	3390	3211, 3163	1660	1614	1518	1456	-	478,406	374	270

(3.5) UV-Vis Spectral of ligands and their complexes

(3.5.1) UV-Vis spectral data of ligands (HL¹ and H₂L²)

The UV-Vis spectra of HL¹ and H₂L² in DMSO solution are shown in Fig. (3.15) and (3.16). The spectra reveals absorption peaks at (269nm = 37174cm⁻¹, ϵ_{\max} = 1432 molar⁻¹ cm⁻¹) and (301nm = 33222cm⁻¹, ϵ_{\max} = 1532 molar⁻¹ cm⁻¹), While H₂L² reveals absorption peaks at (275nm = 36363cm⁻¹, ϵ_{\max} = 1132 molar⁻¹ cm⁻¹) and (313nm = 31948cm⁻¹, ϵ_{\max} = 932 molar⁻¹ cm⁻¹), which are assigned to $\pi \rightarrow \pi^*$ and $n \rightarrow \pi^*$ transitions, respectively [81,82]. The U.V-Vis absorption peaks of the ligands (HL¹ and H₂L²) are summarised in Table (3.10).

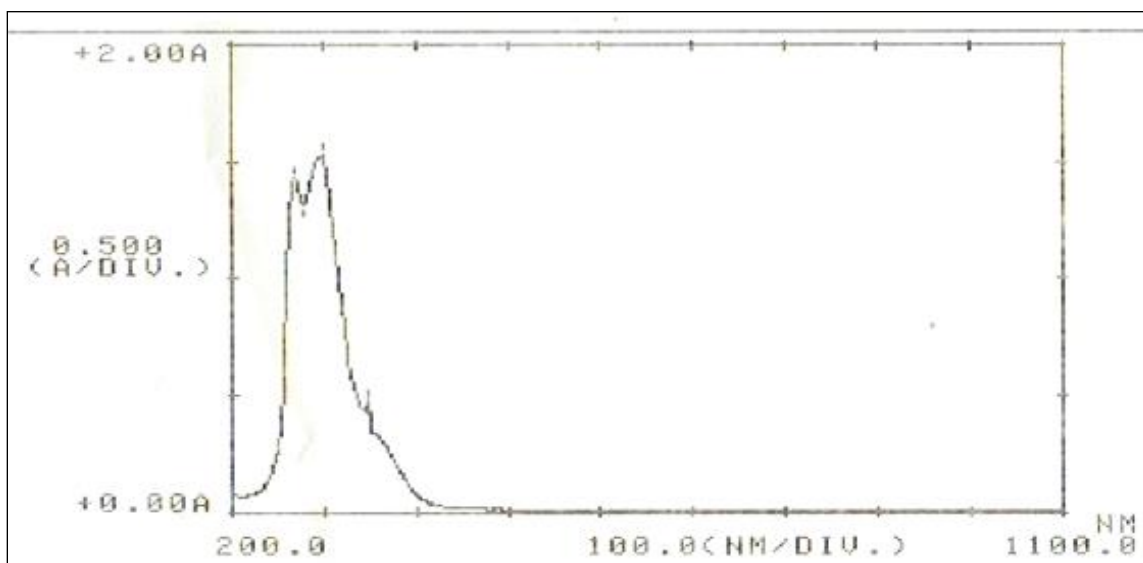


Fig (3.15): Electronic spectrum of HL¹ in DMSO solution

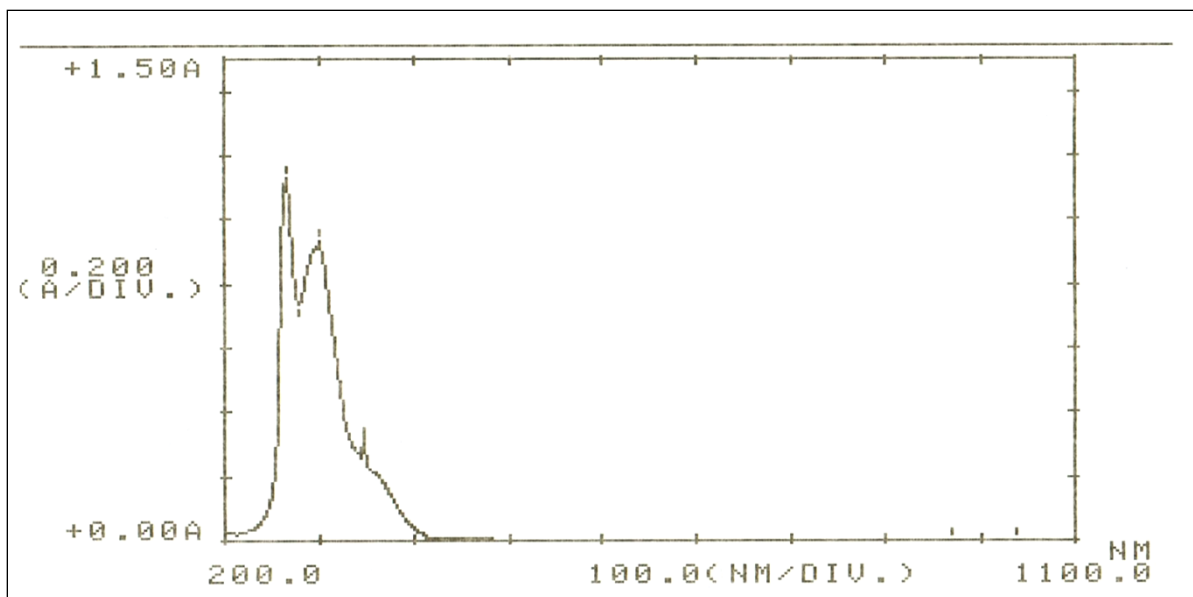


Fig (3.16): Electronic spectrum of H_2L^2 in DMSO solution

Table (3.10): Electronic spectral data for the ligands HL^1 and H_2L^2 in DMSO solutions

Comp.	Band Position λ_{nm}	Wave number (cm^{-1})	Extinction coefficient $\epsilon_{max} (dm^3 mol^{-1} cm^{-1})$	Assignment
HL^1	269	37174	1432	$\pi \rightarrow \pi^*$
	301	33222	1532	$n \rightarrow \pi^*$
H_2L^2	275	36363	1131	$\pi \rightarrow \pi^*$
	313	31948	932	$n \rightarrow \pi^*$

(3.6) UV-Vis Spectra of complexes

(3.6.1) UV-Vis Spectra of $[\text{Co}(\text{HL}^1)_2](1)$, $[\text{Ni}(\text{HL}^1)_2](2)$, $[\text{Cu}(\text{HL}^1)_2](3)$, $[\text{Zn}(\text{HL}^1)_2](4)$ and $[\text{Cd}(\text{HL}^1)_2](5)$ Complexes

The electronic spectra of HL^1 and its metal complexes with $\text{Co}(\text{II})$, $\text{Ni}(\text{II})$, $\text{Cu}(\text{II})$, $\text{Zn}(\text{II})$ and $\text{Cd}(\text{II})$ are displayed in Fig. (3.17 to 3.21), respectively. The electronic spectra for the complexes exhibited peaks in the range 291-297nm are related to the ligand field ($\pi \rightarrow \pi^*$ and $n \rightarrow \pi^*$) transition, The Peaks in the range 345-445nm related to charge transfer transitions (C.T) [83-85]. The spectrum of $\text{Co}(\text{II})$ complex displays the bands that detected in the d-d region at 613 and 665nm when could be correlated to ${}^4\text{T}_{1g}^{(F)} \rightarrow {}^4\text{T}_{2g}^{(F)}$ and ${}^4\text{T}_{1g}^{(F)} \rightarrow {}^4\text{A}_{2g}^{(F)}$, respectively indicating a distorted octahedral structure about the cobalt centre [86,87]. The electronic spectrum of the $\text{Ni}(\text{II})$ complex confirmed an octahedral arrangement about $\text{Ni}(\text{II})$ atom. Band at 612nm attributed to ${}^1\text{A}_{1g}^{(F)} \rightarrow {}^1\text{A}_{2g}^{(F)}$ [87]. The spectrum of $\text{Cu}(\text{II})$ complex revealed peaks at 597 and 645nm, which attributed to ${}^2\text{B}_{1g} \rightarrow {}^2\text{B}_{2g}$, respectively. These transitions are characteristic for Cu -complexes with distorted octahedral structures [87]. The spectra of the $\text{Zn}(\text{II})$ and $\text{Cd}(\text{II})$ complexes exhibited peak assigned to ligand $\pi \rightarrow \pi^*$ and $\text{M} \rightarrow \text{L}$ charge transfer [87]. It is well known that the six-coordinate number is one of the most detected coordination numbers for transition metals. There are many factors that have influence the formation of this coordination number. These related to the metal ions, ligands and steric type and electronic interaction that happened between ligands and metal ion upon complex formation [88]. The U.V-Vis absorption peaks of the complexes are summarised in Table (3.11).

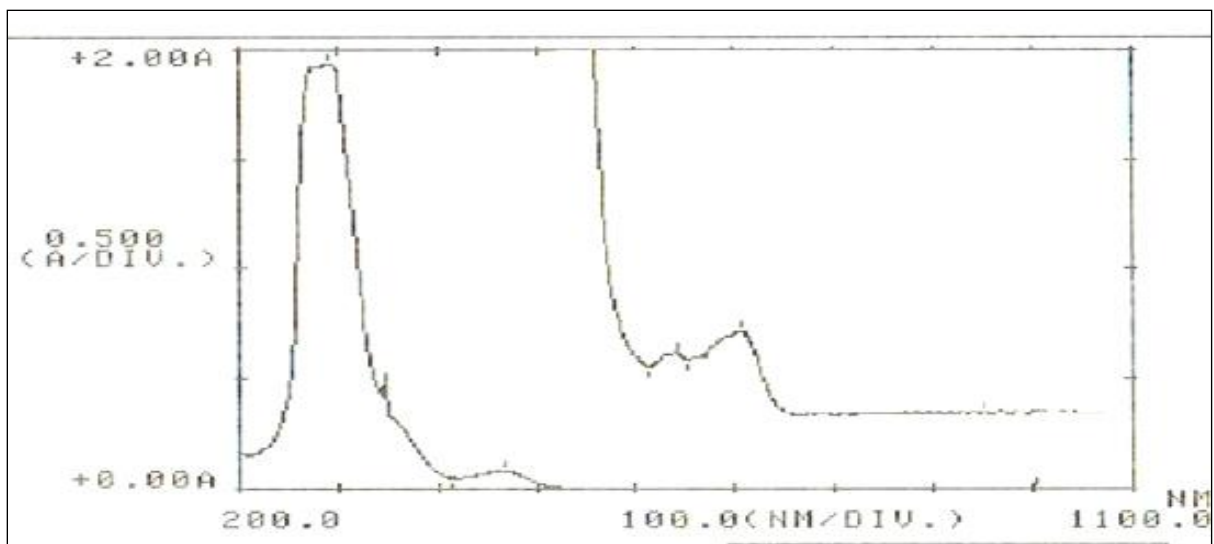


Figure (3.17): Electronic spectrum of [Co(HL¹)₂] in DMSO solution.

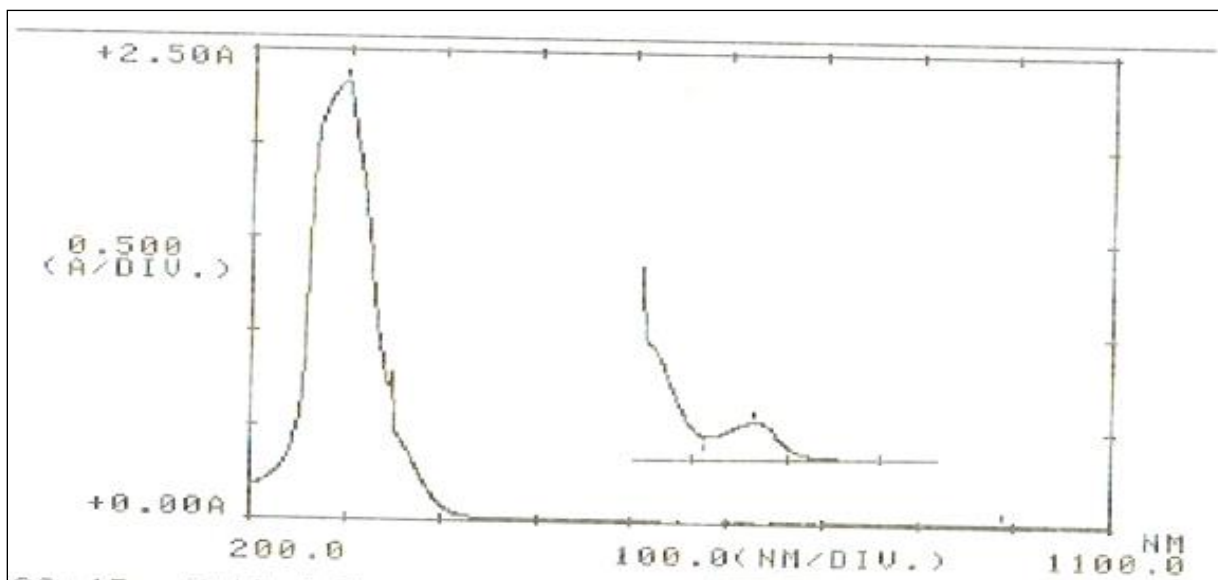


Fig (3.18): Electronic spectrum of [Ni(HL¹)₂] in DMSO solution.

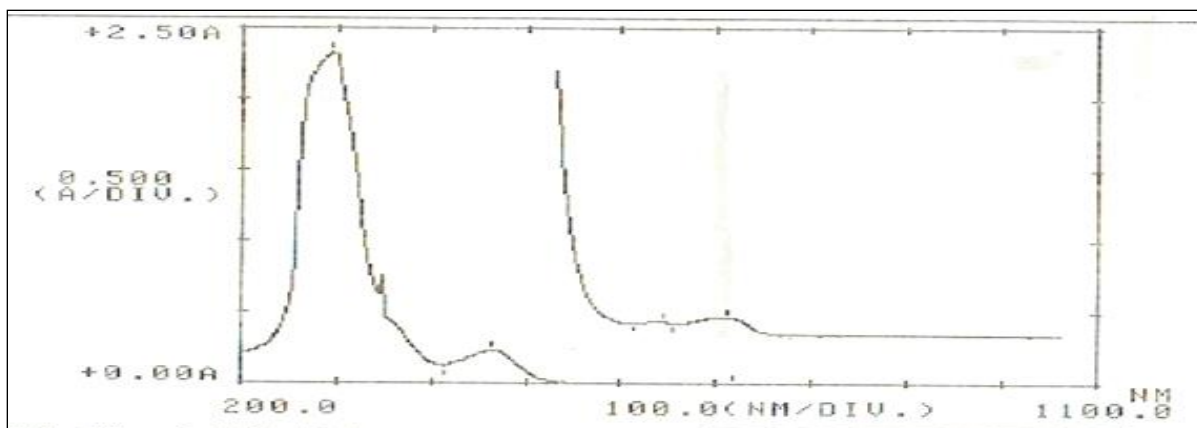


Fig (3.19): Electronic spectrum of [Cu(HL¹)₂] in DMSO solution.

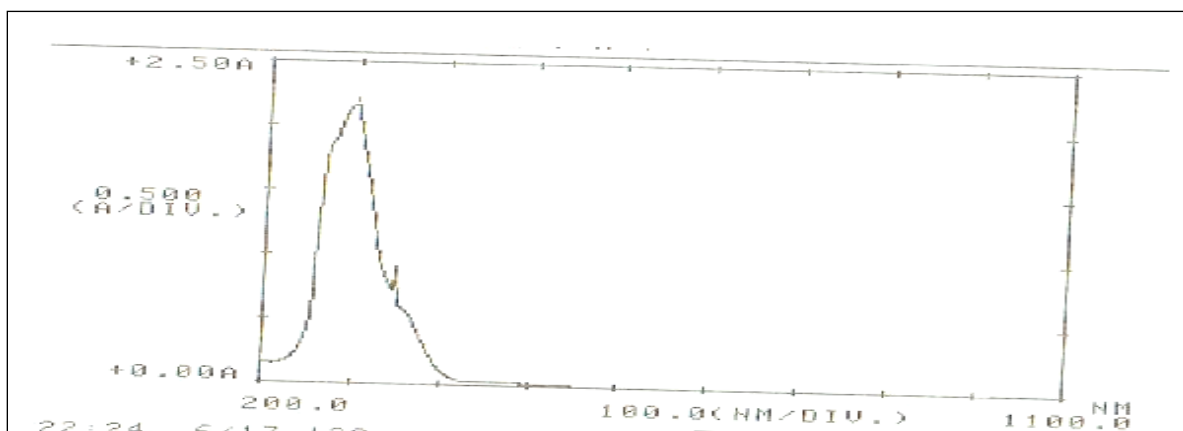


Fig (3.20): Electronic spectrum of [Zn(HL¹)₂] in DMSO solution.

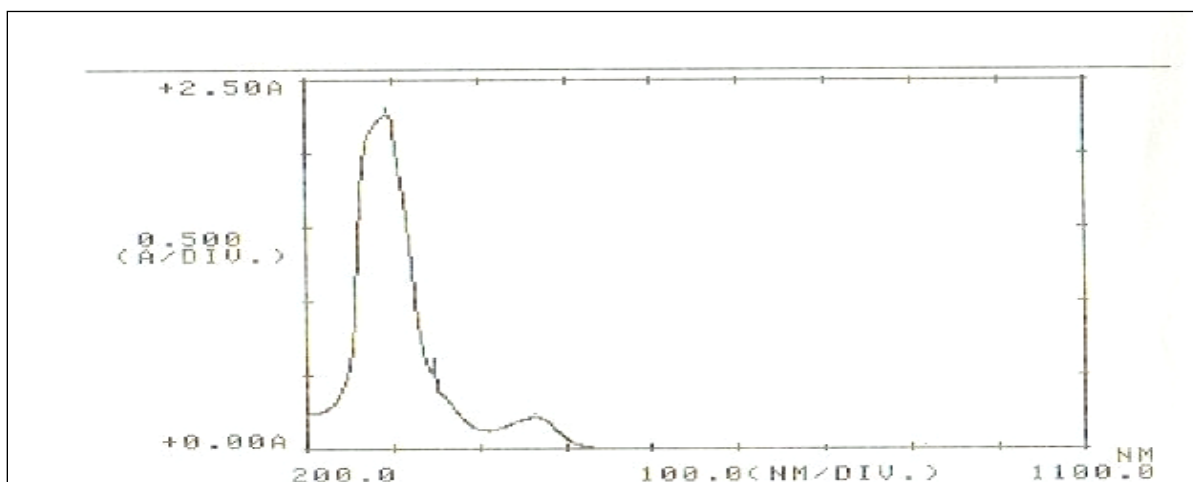


Fig (3.21): Electronic spectrum of [Cd(HL¹)₂] in DMSO solution.

Table (3.11): Electronic spectral data of HL¹ complexes.

Complex	λ_{nm}	ϵ_{max} ($dm^3 \cdot mol^{-1} \cdot cm^{-1}$)	Assignment	Suggested geometry
[Co(HL ¹) ₂]	291	1935	L.F	Distorted octahedral
	399	1955	C.T	
	445	120	C.T	
	613	92	${}^4T_{1g}^{(F)} \rightarrow {}^4T_{2g}^{(F)}$	
	665	117	${}^4T_{1g}^{(F)} \rightarrow {}^4A_{2g}^{(F)}$	
[Ni(HL ¹) ₂]	297	2333	L.F	Distorted octahedral
	388	1697	C.T	
	612	45	${}^3A_{1g}^{(F)} \rightarrow {}^3A_{2g}^{(F)}$	
[Cu(HL ¹) ₂]	295	2322	L.F	Distorted octahedral
	378	2380	C.T	
	597	108	${}^2B_{1g} \rightarrow {}^2B_{2g}$	
	645	80	${}^2B_{1g} \rightarrow {}^2B_{2g}$	
[Zn(HL ¹) ₂]	296	2163	L.F	Distorted octahedral
	345	2350	C.T	
[Cd(HL ¹) ₂]	293	2257	L.F	Distorted octahedral
	412	215	C.F	

(3.6.2) UV-Vis spectra of $[\text{Co}(\text{H}_2\text{L}^2)\text{Cl}_2 \cdot \text{H}_2\text{O}]$ (6), $[\text{Ni}(\text{H}_2\text{L}^2)\text{Cl}]\text{Cl}$ (7), $[\text{Cu}(\text{H}_2\text{L}^2)\text{Cl}_2 \cdot \text{H}_2\text{O}]$ (8), $[\text{Zn}(\text{H}_2\text{L}^2)\text{Cl}]\text{Cl}$ (9) and $[\text{Cd}(\text{H}_2\text{L}^2)\text{Cl}]\text{Cl}$ (10) Complexes

The electronic spectra of H_2L^2 and its metal complexes with Co(II), Ni(II), Cu(II), Zn(II) and Cd(II) are displayed in Fig (3.22 to 3.26) respectively. The electronic spectra of the complexes exhibited peaks in the range (267-289)nm are related to the ligand field $\pi \rightarrow \pi^*$ and $n \rightarrow \pi^*$ transition, The peaks in the range of (301-442)nm related to the charge transfer transitions (C.T) [83-85]. The spectrum of Co(II) complex displays the bands that detected in the d-d region at 526 and 614nm could be correlated to ${}^4\text{T}_{1g}^{(F)} \rightarrow {}^4\text{A}_{1g}^{(P)}$ and ${}^4\text{T}_{1g}^{(F)} \rightarrow {}^4\text{A}_{2g}^{(F)}$, respectively indicating a distorted octahedral structure about the cobalt centre [86,87]. The electronic spectrum of the Ni(II) complex confirmed an distorted square planar arrangement about Ni(II) atom. Band at 618nm attributed to ${}^1\text{A}_{1g} \rightarrow {}^1\text{A}_{2g}$ [87]. The spectrum of Cu(II) complex revealed peaks at 615 and 675nm, which attributed to ${}^2\text{B}_{1g} \rightarrow {}^2\text{B}_{2g}$, respectively. These transitions are characteristic for Cu-complex with distorted octahedral structure [87]. The spectra of the Zn(II) and Cd(II) complexes exhibited peak assigned to ligand $\pi \rightarrow \pi^*$ and M \rightarrow L charge transfer. The spectra showed no bands in the d-d region, as the two metal ions belong to d^{10} configuration. Accordingly, the isolated complexes exhibit tetrahedral geometries around metal atoms. The U.V-Vis absorption peaks of the complexes are summarised in Table (3.12).

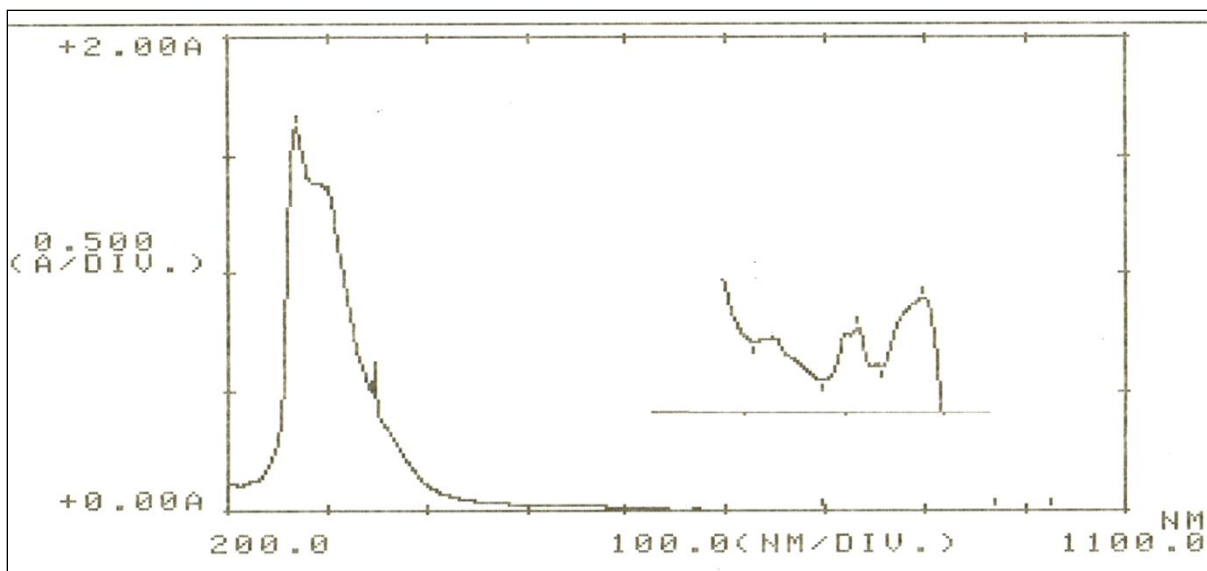


Fig (3.22):Electronic spectrum of $[\text{Co}(\text{H}_2\text{L}^2)\text{Cl}_2] \cdot \text{H}_2\text{O}$ in DMSO solution.

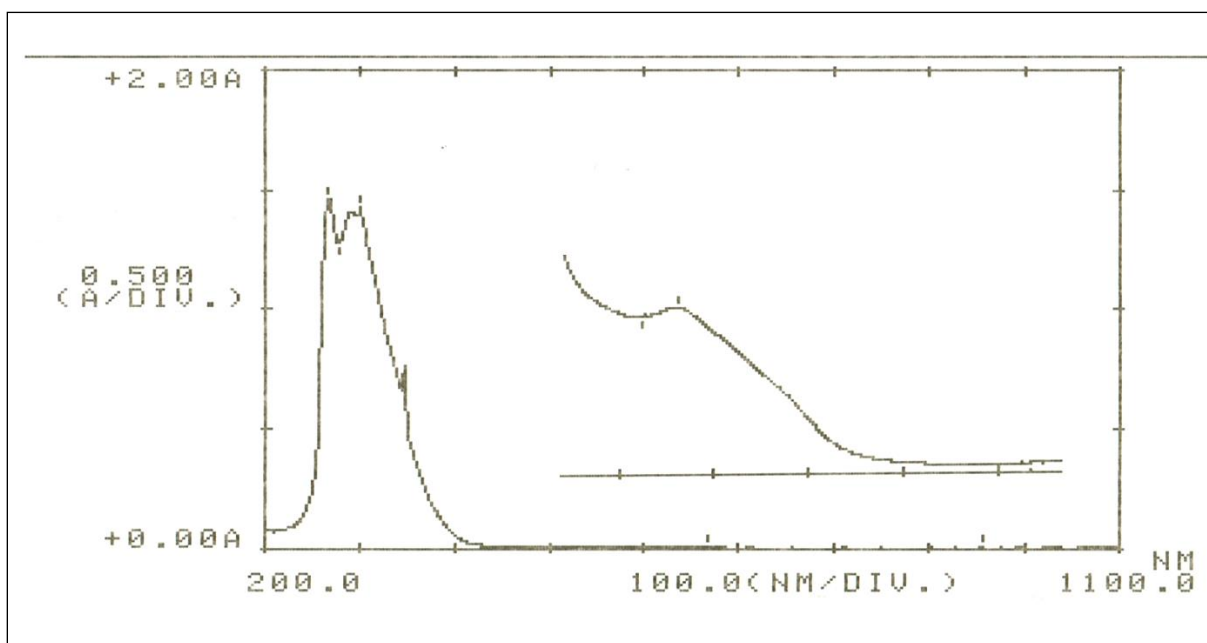


Fig (3.23): Electronic spectrum of $[\text{Ni}(\text{H}_2\text{L}^2)\text{Cl}]\text{Cl}$ in DMSO solution.

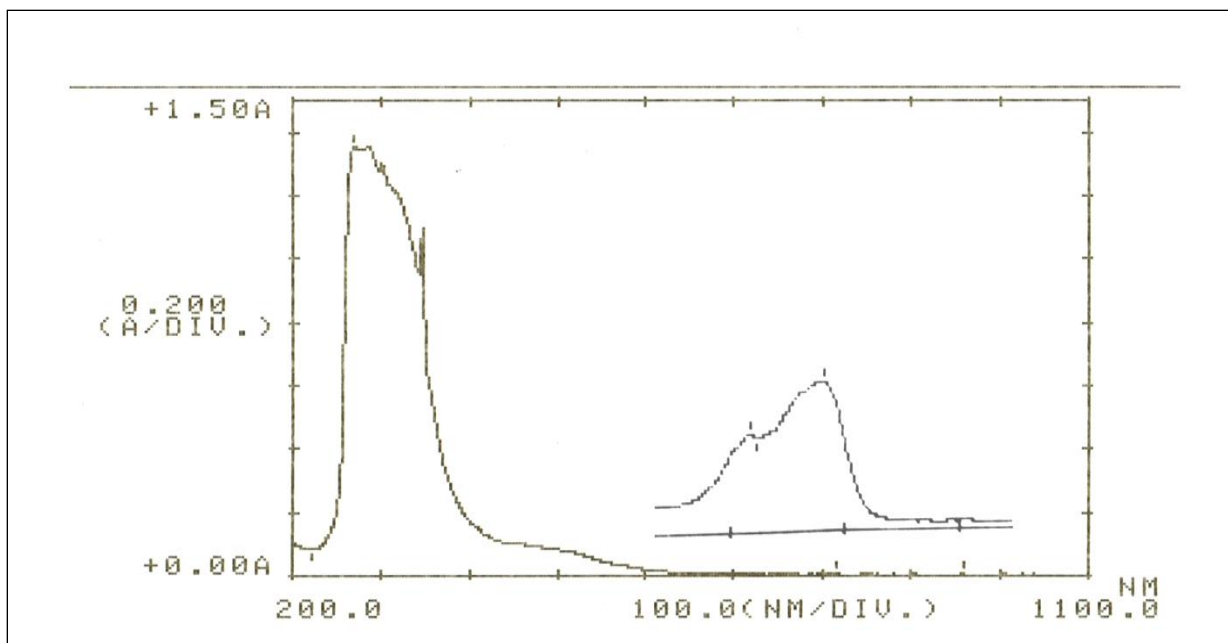


Fig (3.24): Electronic spectrum of [Cu(H₂L²)Cl₂ H₂O] in DMS solution.

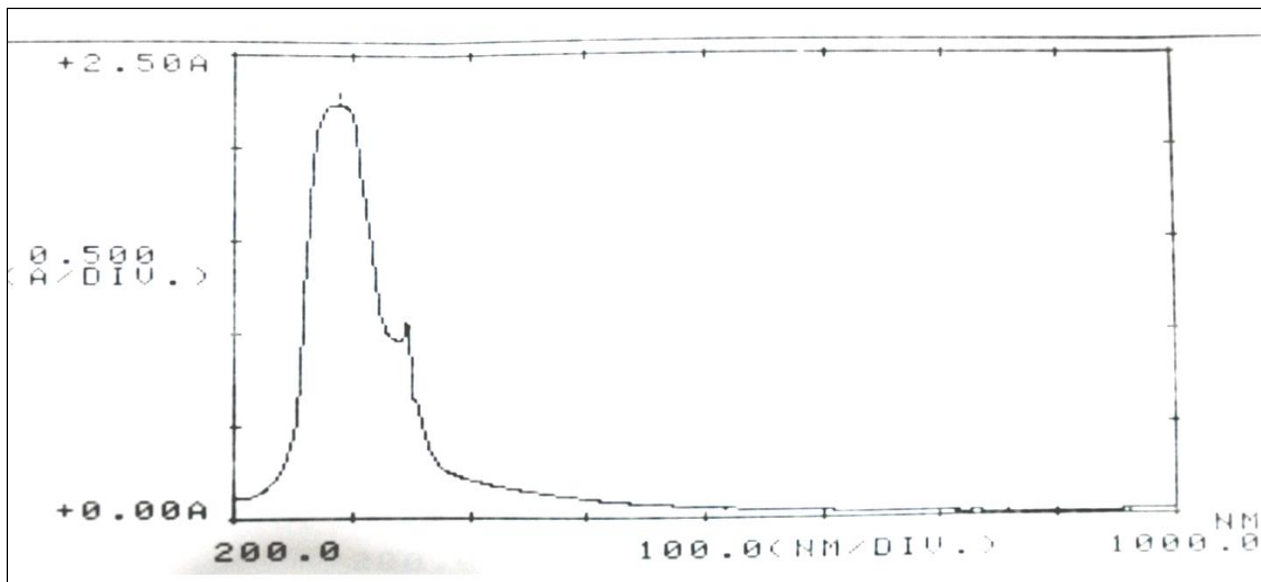


Fig (3.25): Electronic spectrum of [Zn(H₂L²)Cl] Cl in DMSO solution.

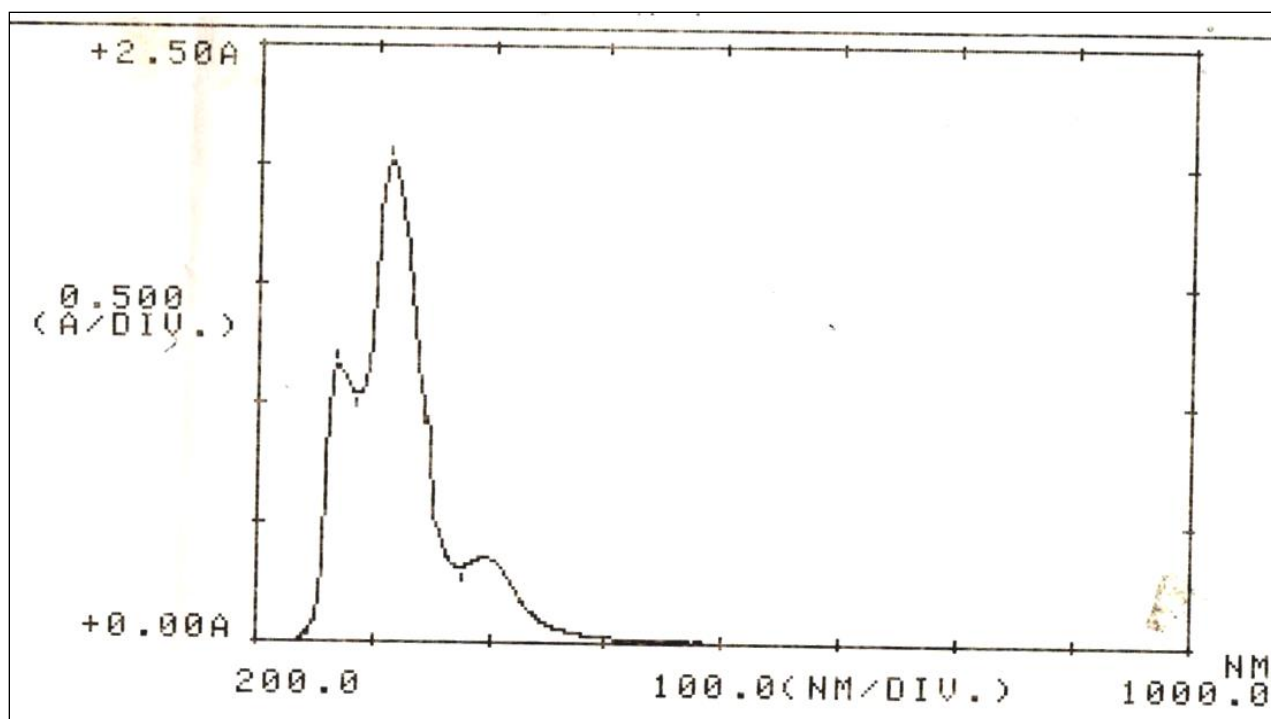


Fig (3.26):Electronic spectrum of [Cd(H₂L²)Cl] Cl in DMSO solution.

Table (3.12): Electronic spectra data of H_2L^2 complexes.

Complex	λ_{nm}	ϵ_{max} ($dm^3 mol^{-1} cm^{-1}$)	Assignment	Suggested geometry
[Co(H_2L^2)Cl ₂ H ₂ O]	268	1621	L.F	Distorted octahedral
	375	1830	C.T	
	442	2500	C.T	
	526	72	${}^4T_{1g}^{(F)} \rightarrow {}^4A_{1g}^{(P)}$	
	614	102	${}^4T_{1g}^{(F)} \rightarrow {}^4A_{2g}^{(F)}$	
[Ni(H_2L^2) Cl]Cl	267	1467	L.F	distorted Square planer
	301	1431	C.T	
	618	19	${}^1A_{1g} \rightarrow {}^1A_{2g}$	
[Cu(H_2L^2)Cl ₂ H ₂ O]	270	1356	L.F	Distorted octahedral
	388	1341	C.T	
	615	108	${}^2B_{1g} \rightarrow {}^2B_{2g}$	
	675	80	${}^2B_{1g} \rightarrow {}^2B_{2g}$	
[Zn(H_2L^2) Cl]Cl	289	2236	L.F	Tetrahedral
	385	1114	C.T	
[Cd(H_2L^2) Cl]Cl	278	1157	L.F	Tetrahedral
	325	2011	C.F	

(3.7) Magnetic moment behaviour

Magnetic measurements give us an important information to elucidate proposed geometry around metal ion in complexes. Also, magnetic moment values for complexes may be used to predict the monomeric and/or their polymeric entity of species. The magnetic susceptibility measurements were determined using a Guoy balance. Magnetic moment may be calculated implementing the following equation:

$$\mu = 2.83 (X_p T)^{1/2}$$

where: X_p is the molar magnetic value that corrected for diamagnetism of atoms in the complex using Pascal's constant. T is temperature in Kelvin (k).

$$X_p = X_M - X_D$$

The multiplying of the mass susceptibility by the molecular mass of the sample gives the molar magnetic (X_M) value:

$$X_M = M X_g$$

where: X_M = molar magnetic susceptibility

M = molecular mass of the sample in $\text{g}\cdot\text{mol}^{-1}$ unit

X_g = mass magnetic susceptibility

Diamagnetic corrections values obtained by calculating molar magnetic susceptibility. These values are due to ligand electron pairs, counter ion electron and core paired electrons central metal ion [89].

$$X_D = [X_D (\text{core}) + X_D (\text{ligand}) + X_D (\text{counter ion})] [90]$$

The diamagnetic correction factors are agreed values, called Pascal's constant, Tables (3-13) to (3-15) [91].

The magnetic moment values were calculated using

$$\mu = 2.83 (X_p T)^{1/2} \text{ Equation.}$$

Table (3.13): Pascal's constants values of cations.

Cation	$X_{Di} (1 \times 10^{-6} \text{ emu mol}^{-1})$
Co^{+2}	-12
Ni^{+2}	-12
Cu^{+2}	-11

Table (3.14): Pascal's constants values of atoms in covalent species.

Atom	$X_{Di}(1 \times 10^{-6} \text{ emu mol}^{-1})$
C_{ring}	-6.24
H	-2.93
C	-6
N	-5.57
O	-4.6
S	-15.0
Cl^-	23.4

Table (3.15): Pascal's constants values for specific bond types.

Bond	λ (1×10^{-6} emu mol ⁻¹)
C=N	8.15
C-N	-13
C=O	6.3
C-C	0.8
C=C	5.5
Ar-NR ₂	+1
Ar-NO ₂	-0.5
C ₆ H ₆	-1.4
(C.H.)cyclohexanone	3

Table (3.16): Theoretical spin only values of magnetic moments of the metal ions, d-configuration, number of unpaired electron for, octahedral, tetrahedral and square planer geometry [92].

Metal ion	d-configuration	General spin only of the metal ions		Octahedral geometry		Tetrahedral geometry		Square planer
		Number of unpaired electron	Value of magnetic moment μ_{eff}	No. of unpaired Electron	Magnetic moment (B.M)	No. of unpaired Electron	Magnetic moment (B.M)	Magnetic moment (B.M)
Co ²⁺	d ⁷	3	3.87	3 high spin 1 low spin	4.3-5.2 2.0-2.7	3 high spin	4.2-4.8	1.80
Ni ²⁺	d ⁸	2	2.83	2	2.9-3.3	2	3.7-4.0	Diamagnetic
Cu ²⁺	d ⁹	1	1.73	1	1.8-2.1	1	Depend on	1.87

Table (3.17): Values of spin only of the metal ions.

Number of unpaired electron	Value of magnetic moment μ_{eff}
1	1.73
2	2.83
3	3.87
4	4.96
5	5.92

(3.7.1) Magnetic moment of HL¹ complexes

(3.7.1.1) Examples for the calculation of magnetic moment

The complex [Co (HL¹)₂] is used as an example for the calculation of the magnetic susceptibility and as follows:

$$X_{Di} (\text{ligand}) = [12 * X_{Di} (\text{C-ring}) + 11 * X_{Di} (\text{C}) + 2 * X_{Di} (\text{N}) + 27 * X_{Di} (\text{H}) + X_{Di} (\text{NO}_2^-) + 2 * X_{Di} (\text{O}_{\text{keto}}) + 2 * \lambda (\text{C=O}) + \lambda (\text{Ar-NO}_2) + \lambda (\text{Ar-NR}_2) + 9 * \lambda (\text{C-C}) + \lambda (\text{C-H}) \text{ cyclohexanone} + 6 * \lambda (\text{C=C}) + 2 * \lambda (\text{C-N}) + 8 * \lambda (\text{C}_6\text{H}_6)] \times 10^{-6} \text{ emu mol}^{-1}.$$

$$X_{Di} = [12 * X_{Di} (-6.24) + 11 * X_{Di} (-6) + 2 * X_{Di} (-5.57) + 27 * X_{Di} (-2.93) + X_{Di} (-10) + 2 * X_{Di} (-4.61) + 2 * \lambda (6.3) + \lambda (-0.5) + \lambda (3) + \lambda (1) + 9 * \lambda (0.8) + 6 * \lambda (5.5) + 2 * \lambda (-13) + 8 * \lambda (-1.4)] \times 10^{-6} \text{ emu mol}^{-1}.$$

$$X_{Di} = -0.00024385$$

The reaction was performed in a 2:1 (L:M) mole ratio of the ligand and complex. Therefore, the X_D equation becomes:

$$X_{Di} = [X_D (\text{core}) + 2 (X_D (\text{ligand}))] \text{ emu mol}^{-1}$$

$$X_{Di} = [(-12 * 10^{-6} + 2(-0.00024385))] \text{ emu mol}^{-1}$$

$$X_{Di} = -0.0004997 \text{ emu mol}^{-1}$$

$$X_g = 0.0000093$$

$$X_M = MX_g$$

$$X_M = 878 * 0.0000093$$

$$= 0.0081654 \text{ emu mol}^{-1}$$

$$X_P = X_M - X_D$$

$$= (0.0081654) - (-0.0004997)$$

$$= 0.0086651 \text{ emu mol}^{-1}$$

$$X_P T = 0.0086651 \times 308 \text{ K}$$

$$= 2.6688508 \text{ K.mol}^{-1}$$

$$\mu = 2.83 (X_P T)^{1/2}$$

$$= 2.83 (2.6688508)^{1/2}$$

$$= 4.6 \mu_B$$

By implementing similar calculation approach for other complexes, the calculated magnetic moment values related the HL¹ complexes are 4.6, 2.9 and 1.9 BM for Co(II), Ni(II) and Cu(II) complexes, respectively. These values agreed well with the summation of the spin's moment indicating a weak field and the hybridization of complexes is sp³d². These values proved the formation of high spin monomeric complexes with distorted octahedral geometries.

(3.7.2) Magnetic moment of H_2L^2 complexes

(3.7.2.1) Examples for the calculation of magnetic moment

The complex $[Co(H_2L^2)Cl_2H_2O]$ is used as an example for the calculation of the magnetic susceptibility and as follows:

$$X_{Di}(\text{ligand}) = [12 * X_{Di}(\text{C-ring}) + 12 * X_{Di}(\text{C}) + 5 * X_{Di}(\text{N}) + 30 * X_{Di}(\text{H}) + X_{Di}(\text{NO}_2^-) + X_{Di}(\text{C=N}) + X_{Di}(\text{S}) + X_{Di}(\text{O}_{\text{keto}}) + \lambda(\text{C=O}) + \lambda(\text{Ar-NO}_2) + \lambda(\text{Ar-NR}_2) + 9 * \lambda(\text{C-C}) + \lambda(\text{C-H}) \text{ cyclohexanone} + 6 * \lambda(\text{C=C}) + 4 * \lambda(\text{C-N}) + 8 * \lambda(\text{C}_6\text{H}_6)] \times 10^{-6} \text{ emu mol}^{-1}.$$

$$X_{Di} = [12 * X_{Di}(-6.24) + 12 * X_{Di}(-6) + 5 * X_{Di}(-5.57) + 30 * X_{Di}(-2.93) + X_{Di}(-10) + X_{Di}(8.15) + X_{Di}(-15) + X_{Di}(-4.6) + \lambda(6.3) + \lambda(-0.5) + \lambda(1) + 9 * \lambda(0.8) + \lambda(3) + 4 * \lambda(-13) + 6 * \lambda(5.5) + 8 * \lambda(-1.4)] \times 10^{-6} \text{ emu mol}^{-1}.$$

$$X_{Di} = -0.00029728$$

The reaction was performed in a 1:1 (L:M) mole ratio of the ligand and complex. Therefore, the X_D equation becomes:

$$X_{Di} = [X_D(\text{core}) + X_D(\text{ligand}) + 2 * X_D(\text{Chloride}) + X_D(\text{H}_2\text{O})] \text{ emu mol}^{-1}$$

$$X_{Di} = [(-12 * 10^{-6}) + (-0.00029728) + 2(-23.4 * 10^{-6}) + (-13 * 10^{-6})] \text{ emu mol}^{-1}$$

$$X_{Di} = -0.00036828 \text{ emu mol}^{-1}$$

$$X_g = 0.0000039$$

$$X_M = M X_g$$

$$X_M = 630.45 * 0.0000039$$

$$= 0.002458755 \text{ emu mol}^{-1}$$

$$X_P = X_M - X_D$$

$$= (0.002458755) - (-0.00036828)$$

$$= 0.002827035 \text{ emu mol}^{-1}$$

$$X_P T = 0.002827035 \times 308 \text{ K}$$

$$= 0.87072678 \text{ emu K mol}^{-1}$$

$$\mu = 2.83 (X_P T)^{1/2}$$

$$= 2.83 (0.933127419)$$

$$= 2.6$$

By implementing similar calculation approach for other complexes, the calculated magnetic moment values related the H_2L^2 complexes 2.5 and 1.9 BM for Co(II) and Cu(II) complexes, respectively. While the experimental magnetic values of Ni(II) complex indicate square planer geometry about Ni atom. These values agreed well with the summation of the spin moment indicating a strong field and the hybridization of complexes is d^2sp^3 except nickel complex is dsp^2 . These values proved the formation of low spin monomeric complexes with distorted octahedral geometries.

Table (3.18): Experimental data of the magnetic moment susceptibility.

Complexes	$X_D(-1 \times 10^{-6})$	$X_g \times 10^{-6}$	$X_P \times 10^{-2}$	$X_P T$	μ_B
[Co(HL ¹) ₂]	499.7	9.3	0.28	0.88	4.6
[Ni(HL ¹) ₂]	499.7	3.5	0.35	1.10	2.9
[Cu(HL ¹) ₂]	498.7	1.2	0.15	0.47	1.9
[Co(H ₂ L ²) Cl ₂ H ₂ O]	368.28	3.9	0.28	0.87	2.6
[Ni(H ₂ L ²)Cl]Cl	Diamagnetic				
[Cu(H ₂ L ²) Cl ₂ H ₂ O]	367.28	2.00	0.16	0.50	2.0

(3.8) Electrospray (+) mass spectra

(3.8.1) Mass spectrum of HL¹

The electrospray (+) mass spectrum of HL¹, Fig (3.27), reveals the parent ion peak at $M/Z=409.49$ amu. This peak is related to $(M+H)^+$. The assignment of the successive fragmentation ions of the compound along with their relative abundance is shown in Scheme (3.5).

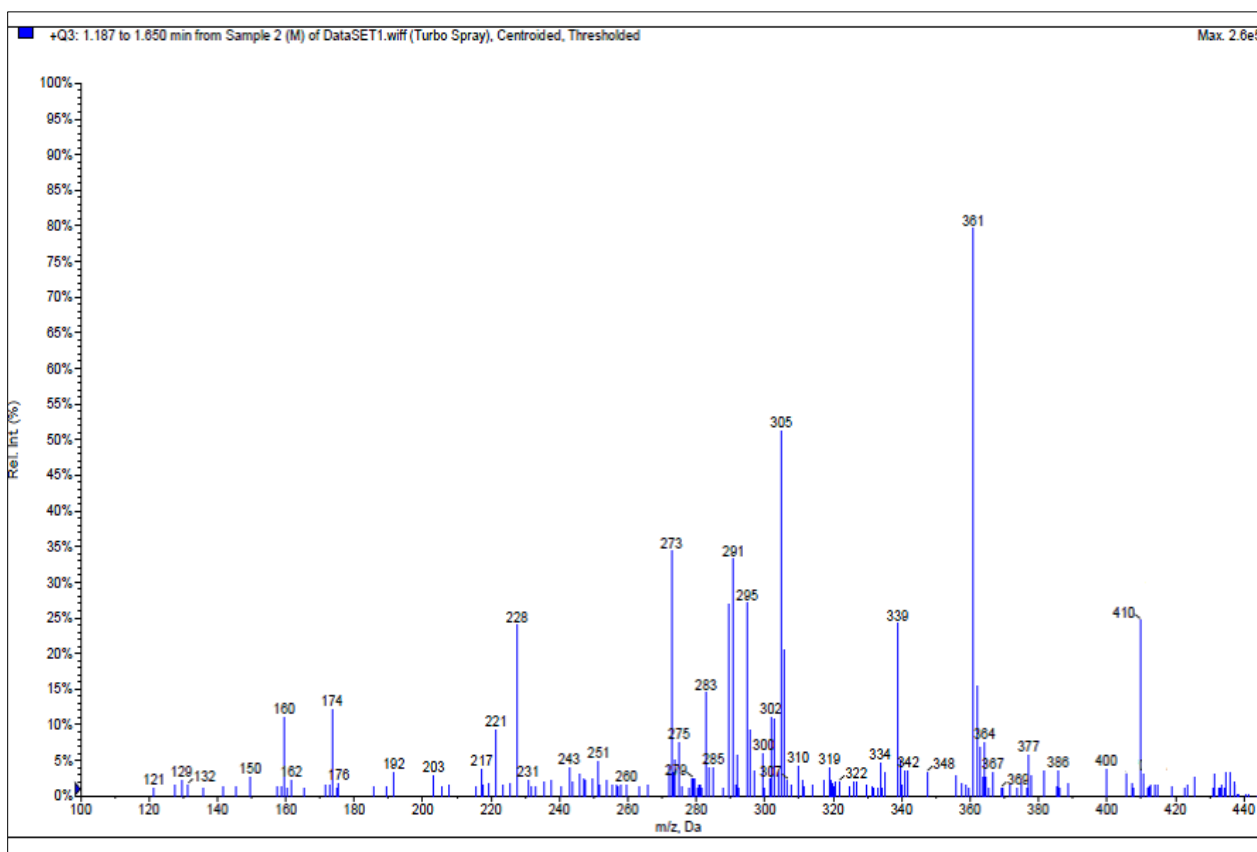
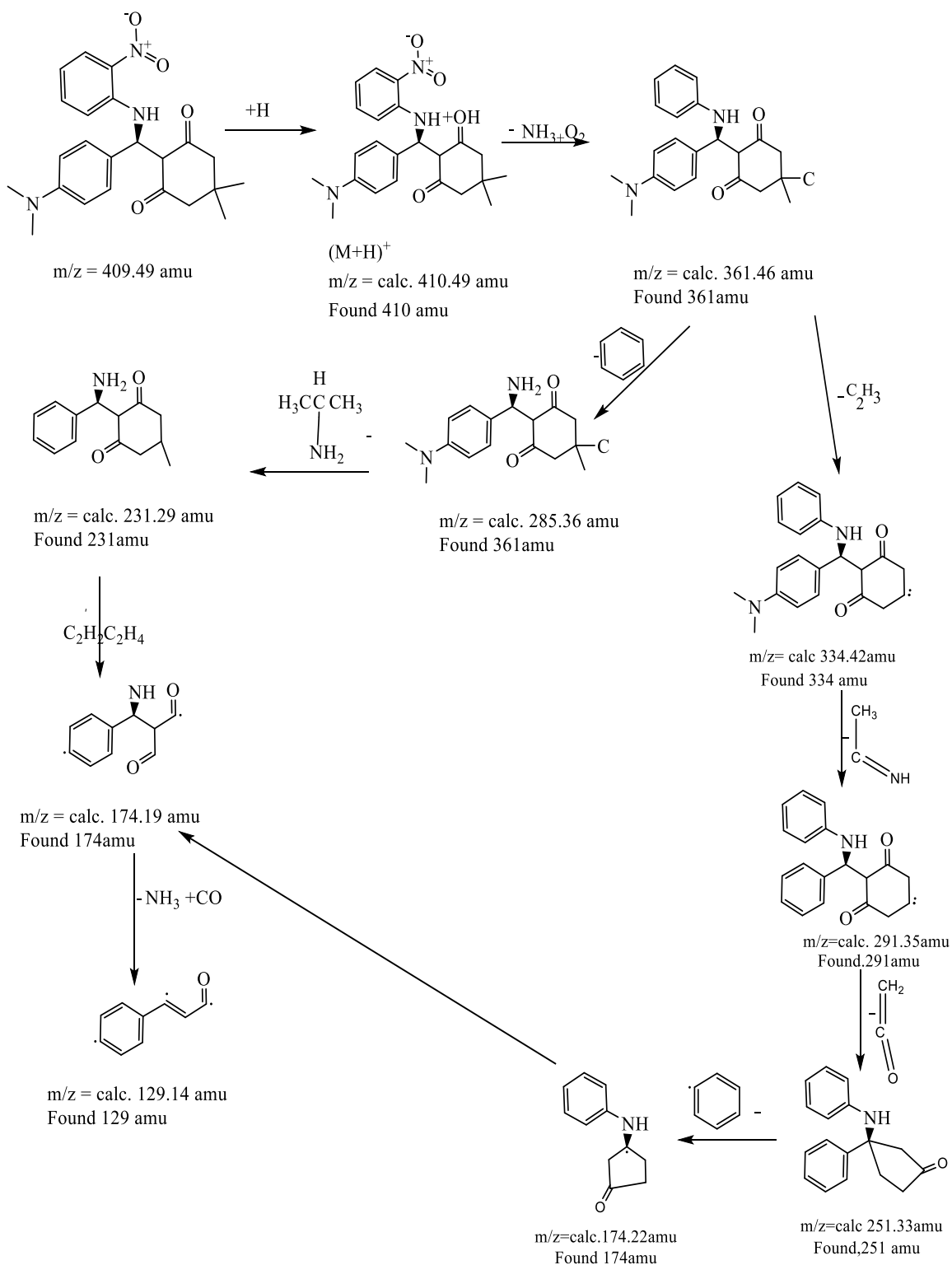


Fig (3.27): The electrospray (+) mass spectrum of HL¹.



Scheme (3.5): The fragmentation pattern and relative abundance of HL¹ fragments.

(3.8.2) Mass spectrum of H_2L^2

The electrospray (+) mass spectrum of H_2L^2 , Fig (3.28), displays the parent ion peak at $M/Z=482.60$ amu. This peak is related to $(M+H)^+$. The assignment of the fragmentation ions and their relative abundance is shown in Scheme (3.6).

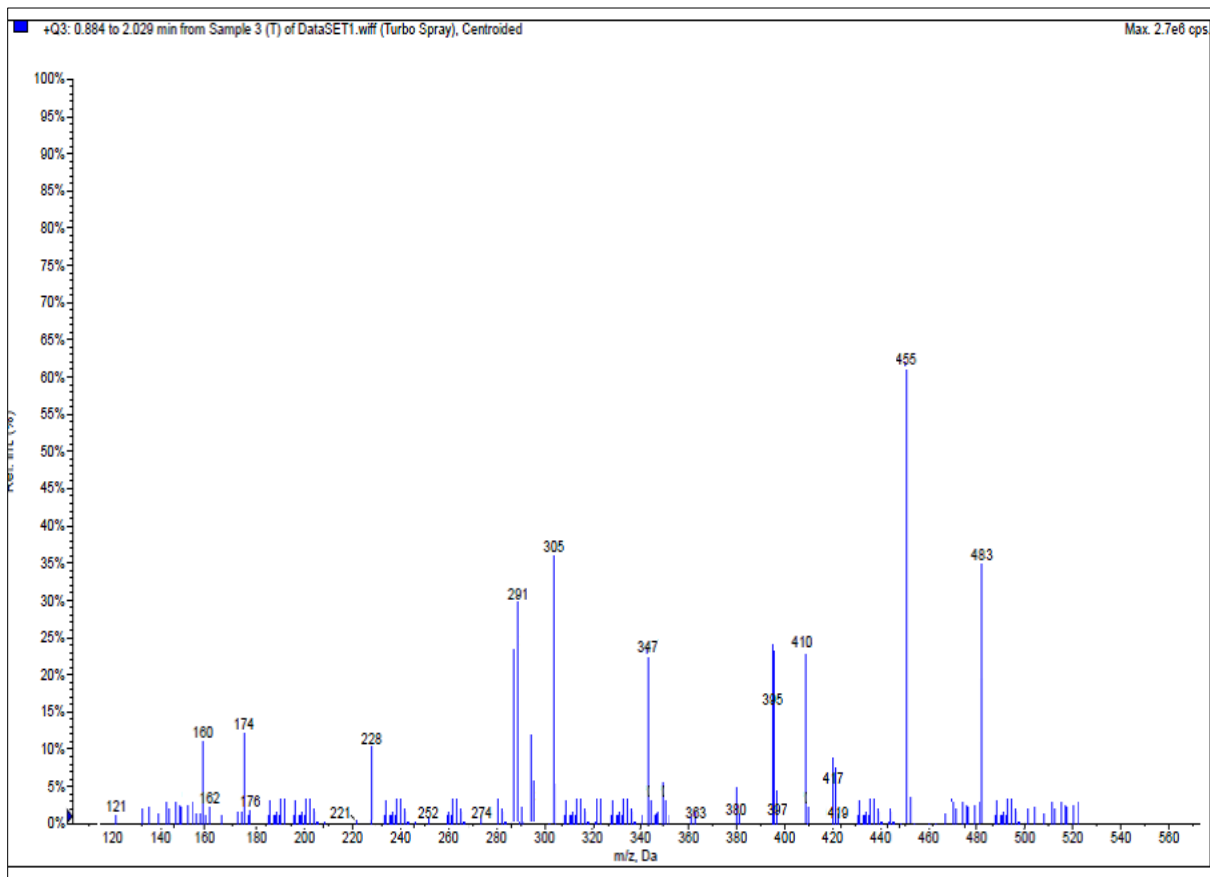
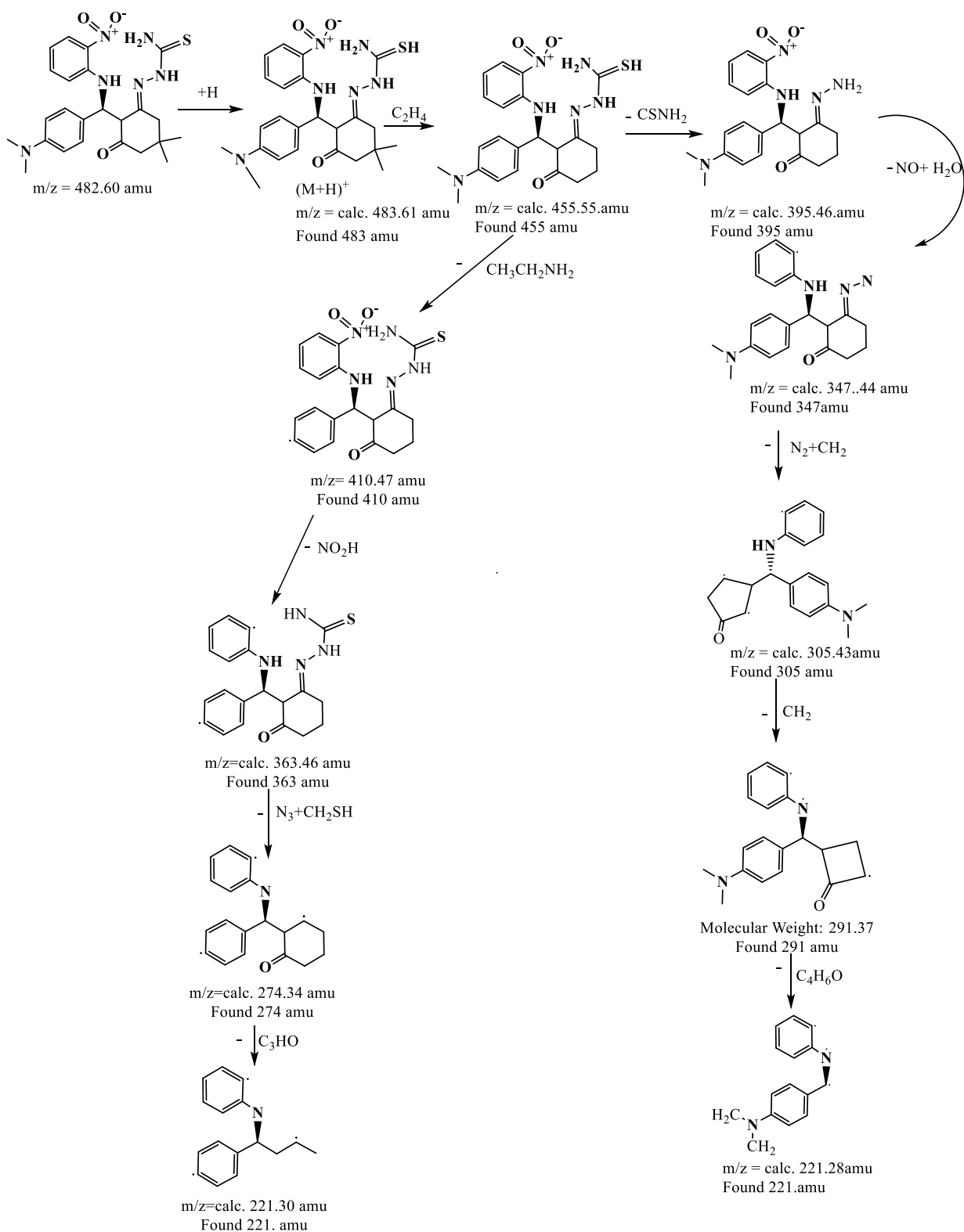


Fig (3.28): The electrospray (+) mass spectrum of H_2L^2 .



Scheme (3.6): The fragmentation pattern and relative abundance of H_2L^2 fragments.

(3.9) Nuclear magnetic resonance (NMR) spectra of compounds

NMR technique was used to elucidate the structure of compounds and their purity. The NMR data include the ^1H , ^{13}C -NMR spectra [93].

(3.9.1) Nuclear magnetic resonance (NMR) spectrum of HL^1 and H_2L^2

The ^1H -NMR analysis was used to characterise the ligands (HL^1 and H_2L^2). The spectra were recorded in DMSO-d_6 solvent.

(3.9.1.1) ^1H -NMR spectrum of HL^1

The ^1H -NMR spectrum of HL^1 is depicted in Fig (3.29). The spectrum displays chemical shift at $\delta = 0.85\text{-}1.98\text{ppm}$ (6H, s, $-\text{C}(\text{Me})_2$) which are attributed to ($\text{C}_{1,1}$ -H) of the two methyl groups protons. The chemical shift at $\delta = 2.01\text{-}2.47\text{ppm}$ (4H, s, CH_2) that appeared as a multiplete and equivalent to four protons which are assigned to ($\text{C}_{3,3}$ -H). More, the spectrum displays chemical shift at $\delta = 2.56\text{-}3.17\text{ppm}$ (6H, s, $-\text{N}(\text{Me})_2$) are attributed to ($\text{C}_{10,10}$ -H) of the two methyl groups protons. The peak at $\delta = 3.44\text{-}3.91\text{ppm}$ (H, d, CH), which equivalent to one proton is related to (C_4 -H). The peak at $\delta = 4.31\text{-}4.55\text{ppm}$ (H, t, CH), which equivalent to one proton is related to (C_5 -H). The signal at $\delta = 6.01\text{-}6.00\text{ppm}$ (H, d, $J_{\text{HH}} = 3\text{Hz}$) belongs to N-H which equivalent to one proton. Resonances at $\delta = 6.94\text{-}7.08\text{ppm}$ (2H, d, CH) assigned to ($\text{C}_8,8$ -H), $7.10\text{-}7.23\text{ppm}$ (H, t, CH) are assigned to (C_{13} -H), $7.25\text{-}7.30\text{ppm}$ (2H, d, $J_{\text{HH}} = 15\text{Hz}$) assigned to ($\text{C}_7,7$ -H), $7.32\text{-}7.34\text{ppm}$ (H, d, $J_{\text{HH}} = 6\text{Hz}$) assigned to (C_{11} -H), $7.60\text{-}7.62\text{ppm}$ (H, t, $J_{\text{HH}} = 6\text{Hz}$) assigned to (C_{12} -H) and $7.64\text{-}7.66\text{ppm}$ (H, d, $J_{\text{HH}} = 6\text{Hz}$) assigned to (C_{14} -H) of the aromatic ring protons, respectively.

The signal at 13.35 ppm that belongs to O-H which equivalent to one proton is related to (H, s, OH). The appearance more than one signal for CH₃, CH₂ CH and some group can be attributed to appearance two isomer in solution. The spectrum revealed peaks at 2.51-2.52 and 3.27ppm related to the DMSO-d₆ solvent and the traces of water molecules in the solvent, respectively. The chemical shifts data are summarised in Table (3.19).

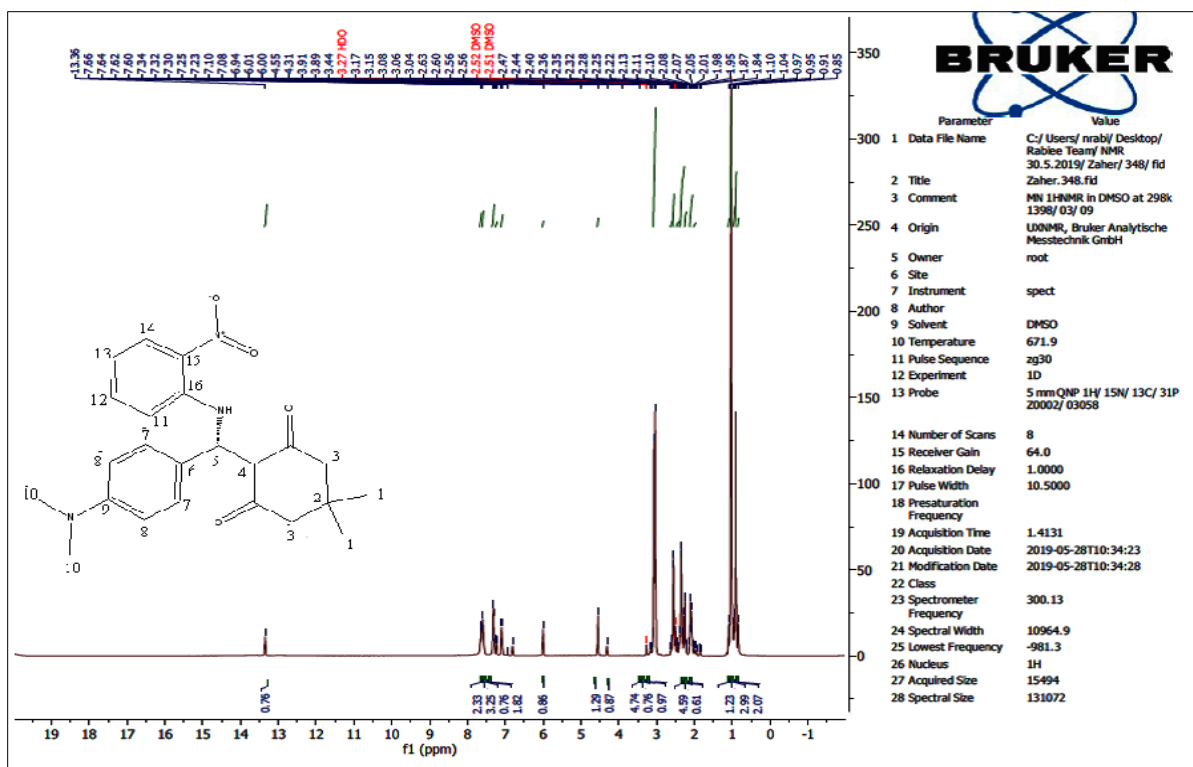


Fig (3.29): ¹H NMR spectrum of HL¹ in DMSO-d₆.

(3.9.1.2) ¹H-NMR spectrum of H₂L²

The ¹H-NMR spectrum of H₂L² is depicted in Fig (3.30). The spectrum displays chemical shift at $\delta = 0.85-1.04$ ppm (6H, s-C-(Me)₂) which are attributed to (C₁, ₁'-H) of the Two methyl group protons. The chemical shift at $\delta = 2.08-2.11$ ppm (2H, s, CH₂, J_{HH} = 9 Hz) that appeared as a singlet and equivalent to two protons which assigned to (C₄-H). The chemical

shift at $\delta = 2.25\text{-}2.28\text{ppm}$ (2H, s, CH₂, $J_{\text{HH}} = 9$ Hz) that appeared as a singlet and equivalent to Two protons which assigned to (C₃-H). More, the spectrum displays chemical shift at $\delta = 2.36\text{-}2.51\text{ppm}$ (6H, s, -N-(Me)₂) are attributed to (C_{11, 11'}-H) of the two methyl groups protons. The peak at $\delta = 2.56\text{-}2.59\text{ppm}$ (H, d, CH, $J_{\text{HH}} = 9$ Hz), which equivalent to one proton is related (C₅-H). The peak at $\delta = 4.53\text{-}4.80\text{ppm}$ (H, t, CH), which equivalent to one proton is related (C₆-H). The signal at $\delta = 5.59\text{ppm}$ (H, d, NH) that belongs to N-H which equivalent to one proton. Resonances at $\delta = 7.09\text{ppm}$ (2H, d, CH) assigned to (C_{9, 9'}-H), 7.22ppm (H, t, CH) are assigned to (C₁₄-H), 7.23ppm (2H, d, CH) assigned to (C_{8, 8'}-H), 7.24ppm (H, d) assigned to (C₁₂-H), 7.31ppm (H, t) assigned to (C₁₃-H) and 8.01ppm (H, d) assigned to (C₁₅-H) of the aromatic ring protons, respectively. The peak at 10.23-10.03ppm that belongs to N-H₂ which equivalent to two protons is related to (H, s, NH₂). The signal at 11.08 ppm that belongs to N-H which equivalent to one proton is related to (H, s, NH). The spectrum revealed peaks at 2.55 and 2.99-3.93ppm is related to the DMSO-d₆ solvent and the traces of water molecules in the solvent, respectively. The chemical shifts data are summarised in Table (3.19).

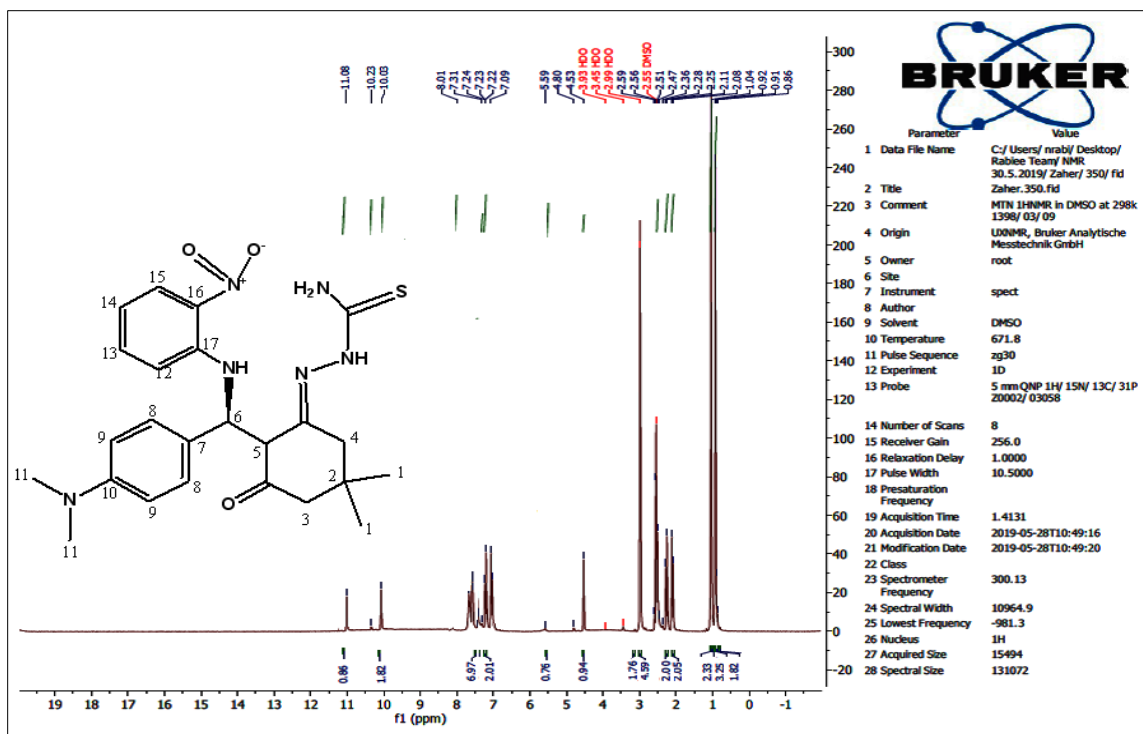


Fig (3.30): $^1\text{H-NMR}$ spectrum of H_2L^2 in DMSO-d_6 .

Table (3.19): $^1\text{H-NMR}$ data for ligands measured in DMSO-d_6 and chemical shift in ppm (δ).

ligand	Fund. group	δ (ppm)
HL^1	$(\text{C}_{1,1}-\text{H})$	0.85-1.98 (6H, s, $-\text{C}(\text{Me})_2$)
	$(\text{C}_{3,3}-\text{H})$	2.01 -2.47 (4H, s, CH_2)
	$(\text{C}_{10,10}-\text{H})$	2.56 -3.17 (6H, s, $-\text{N}(\text{Me})_2$)
	(C_4-H)	3.44-3.91 (H, d, CH)
	(C_5-H)	4.31-4.55 (H, t, CH)
	(N-H)	6.01-6.00 (H, d, $J_{\text{HH}}= 3\text{Hz}$)
	$(\text{C}_{8,8}-\text{H})$	6.94 -7.08 (2H, d, CH)
$(\text{C}_{13}-\text{H})$	7.10-7.23 (H, t,CH)	

	(C _{7,7} -H)	7.25-7.30 (2H, d, J _{HH} = 15 Hz)
	(C ₁₁ -H)	7.32-7.34 (H, d, J _{HH} = 6 Hz)
	(C ₁₂ -H)	7.60-7.62 (H, t, J _{HH} = 6 Hz)
	(C ₁₄ -H)	7.64-7.66 (H, d, J _{HH} =6Hz)
	(O-H)	13.35(H, s, OH).
H ₂ L ²	(C _{1,1} -H)	0.85-1.04 (6H, s-C-(Me) ₂)
	(C ₄ -H)	2.08-2.11 (2H, s, CH ₂ , J _{HH} = 9 Hz)
	(C ₃ -H)	2.25-2.28 (2H, s, CH ₂ , J _{HH} = 9 Hz)
	(C _{11,11} -H)	2.36 -2.51 (6H, s, -N-(Me) ₂)
	(C ₅ -H)	(2.56-2.59 (H, d, CH, J _{HH} = 9 Hz))
	(C ₆ -H)	4.53-4.80 (H, t, CH)
	(N-H) _{mannich}	5.59(H, d)
	(C _{9,9} -H)	7.09 (2H, d, CH)
	(C ₁₄ -H)	7.22 (H, t,CH)
	(C _{8,8} -H)	7.23 (2H,dCH)
	(C ₁₂ -H)	7.24 (H, d,CH)
	(C ₁₃ -H)	7.31 (H, t.CH)
	(C ₁₅ -H)	8.01 (H, d.CH)
	(N-H)	10.23-10.03(H, s, NH ₂).
	(N-H)	11.08 (H, s, NH).

(3.9.2.1) ^{13}C -NMR spectrum of HL¹

The ^{13}C -NMR spectrum of HL¹ is depicted in Fig (3.31). The Resonances at $\delta = 149.45$ and 144.01ppm were assigned to (C₉) and (C₁₆), respectively. Signals related to (C₁₂), (C₆) and (C₁₅) were detected at 132.17 , 129.34 and 128.83ppm , respectively. Resonances assigned for (C_{7,7}⁻), (C₁₄), (C₁₃), (C₁₁) and (C_{8,8}⁻) were observed at 128.82 , 127.22 , 119.22 , 113.46 and 113.33ppm , respectively. The chemical shifts that appeared at 56.55 , 49.80 and 45.01ppm are assigned to (C₄), (C₃) and (C₅), respectively. The two methyl groups, N-(C_{10,10}⁻), appeared as a one peak at 44.84ppm . The peaks of (C₂) and (C₁) are resonances appeared at 32.81ppm and 28.64ppm , respectively. Finally, the C=O of the carbonyl group appears as expected downfield at $\delta=200.07$ and 208.64ppm . The spectrum revealed peak at 39.52 - 38.52ppm which is related to the DMSO-d₆ solvent. The ^{13}C -NMR results are summarised in Table (3.20).

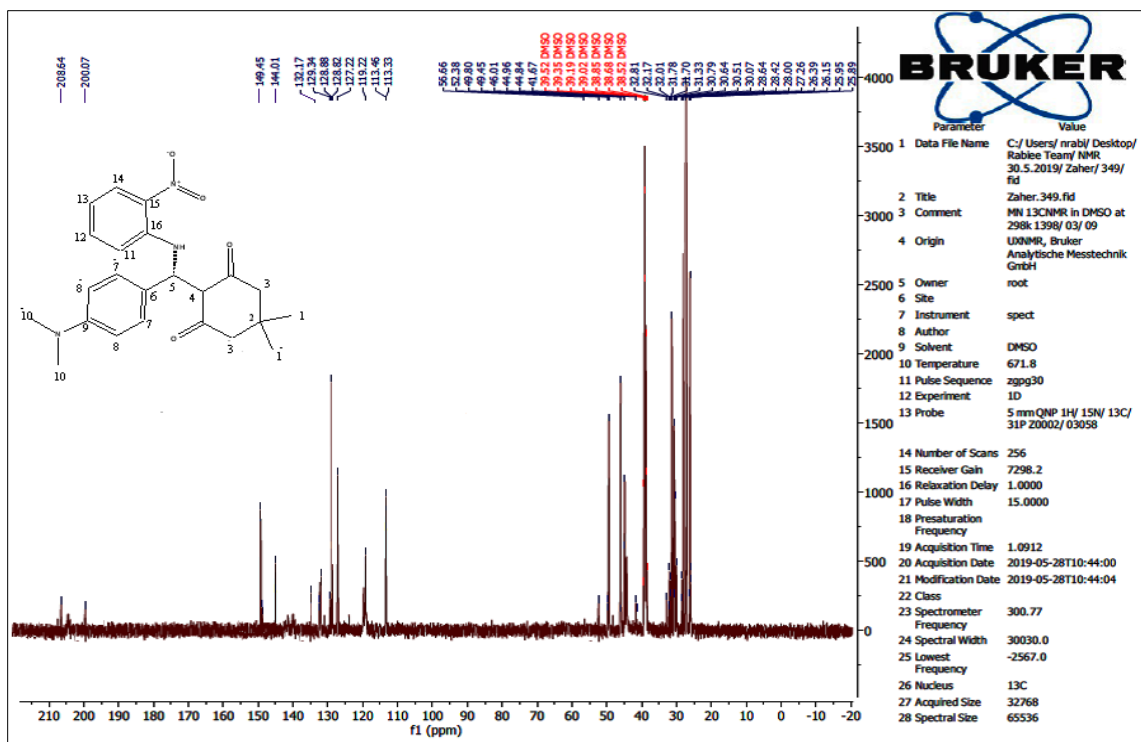


Fig (3.31): ^{13}C -NMR spectrum of HL^1 in DMSO-d_6 .

(3.9.2.2) ^{13}C -NMR spectrum of H_2L^2

The ^{13}C -NMR spectrum of H_2L^2 is depicted in Fig (3.32). The resonances at $\delta = 149.18$ and 144.00 ppm were assigned to (C_{10}) and (C_{17}), respectively. Signals related to (C_{13}), (C_7) and (C_{16}) were detected at 131.73 , 131.28 and 129.29 ppm, respectively. Resonances assigned for ($\text{C}_{8,8}$), (C_{15}), (C_{14}), (C_{12}) and ($\text{C}_{9,9}$) were observed at 128.70 , 128.49 , 127.07 , 113.70 and 100.53 ppm, respectively. The chemical shifts that appeared at 53.82 , 53.37 and 53.13 ppm are assigned to (C_5), (C_3) and (C_6), respectively. The two methyl groups, $\text{N}-(\text{C}_{11,11})$, were appeared as a one peak at 49.52 ppm. The peaks of (C_4), (C_2) and (C_1) resonances appeared at 31.99 , 30.76 ppm and 28.07 ppm, respectively. The chemical shifts that appeared at 169.00 ppm is assigned to $\text{C}=\text{N}$. The chemical shift that appeared at 186.75 ppm is assigned to $\text{C}=\text{S}$. Finally, the $\text{C}=\text{O}$ of the carbonyl group appears as expected

downfield at $\delta=195.55\text{ppm}$. The spectrum revealed peak at $39.61\text{-}38.89\text{ppm}$ is related to the DMSO-d_6 solvent. The $^{13}\text{C-NMR}$ results are summarised in Table (3.20).

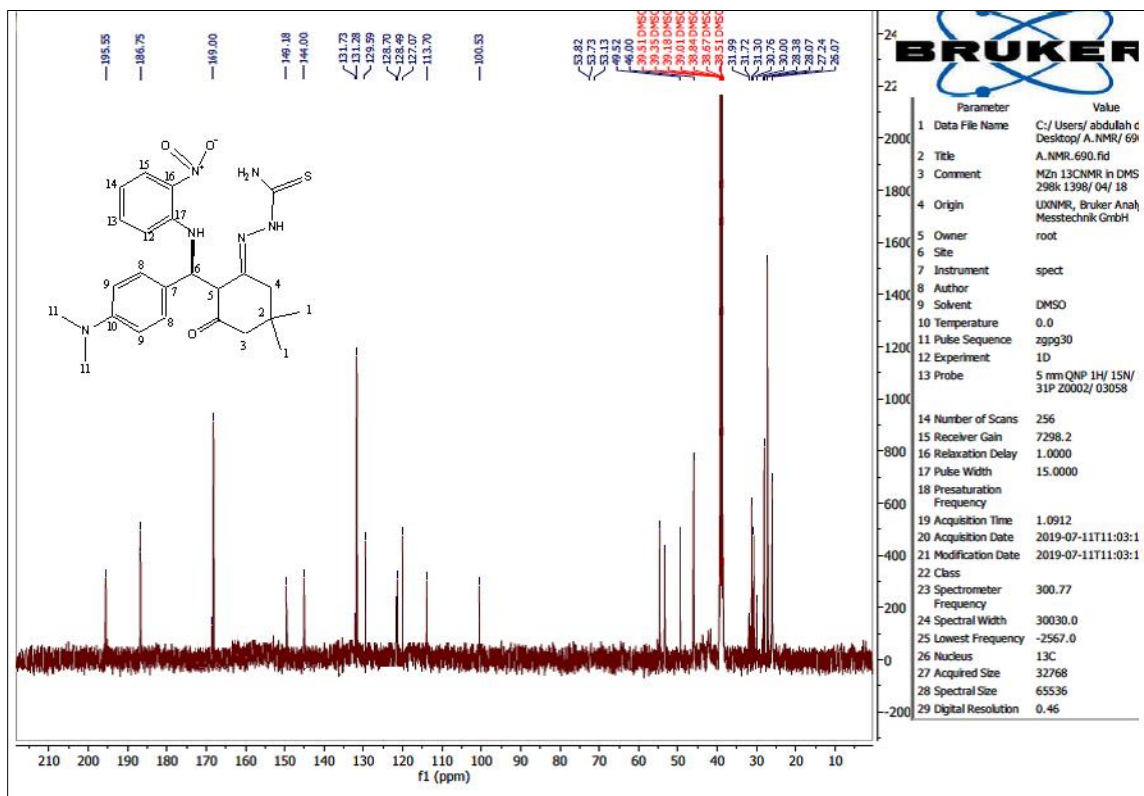


Fig (3.32): $^{13}\text{C-NMR}$ spectrum of H_2L^2 in DMSO-d_6 .

Table (3.20): ^{13}C -NMR data for ligands measured in DMSO- d_6 and chemical shift in ppm (δ).

ligand	Fund. group	δ (ppm)
HL ¹	(C ₉)	149.45
	(C ₁₆)	144.01
	(C ₁₂)	132.17
	(C ₆)	129.34
	(C ₁₅)	128.83
	(C _{7,7})	128.82
	(C ₁₄)	127.22
	(C ₁₃)	119.22
	(C ₁₁)	113,46
	(C _{8,8})	113.33
	(C ₄)	56.55
	(C ₃)	49.80
	(C ₅)	45.01
	N-(C _{10,10})	44.84
	(C ₂)	32.81
(C ₁)	28.64	
	C=O	200.07 and 208.64

H_2L^2	(C ₁₀)	149.18
	(C ₁₇)	144.00
	(C ₁₃)	131.73
	(C ₇)	131.28
	(C ₁₆)	129.59
	(C _{8,8})	128.70
	(C ₁₅)	128.49
	(C ₁₄)	127.07
	(C ₁₂)	113.70
	(C _{9,9})	100.53
	(C ₅)	53.82
	(C ₃)	53.73
	(C ₆)	53.13
	N-(C _{11,11})	49.52
	(C ₄)	31.99
	(C ₂)	30.76
	(C _{1,1})	28.07
	C=N	169.00
	C=S	186.75
	C=O	195.55

(3.9.3) Nuclear magnetic resonance (NMR) spectral for complexes

(3.9.3.1) ^1H -NMR spectrum of $[\text{Zn}(\text{HL}^1)_2]$

The ^1H -NMR spectrum of $[\text{Zn}(\text{HL}^1)_2]$ is depicted in Fig (3.33). The spectrum displays chemical shift at $\delta = 0.85$ - 1.97 ppm (6H, s, $-\text{C}(\text{Me})_2$) are attributed to ($\text{C}_{1,1}$ -H) of the two methyl groups protons for both ligands. The chemical shift at $\delta = 2.00$ - 2.55 ppm (4H, s, CH_2) that appeared as a multiplete and equivalent to four protons is assigned to ($\text{C}_{3,3}$ -H) for each ligands. More, the spectrum displays chemical shift at $\delta = 2.61$ - 3.14 ppm (6H, s, $-\text{N}(\text{Me})_2$) are attributed to ($\text{C}_{10,10}$ -H) of the two methyl groups protons for each ligands. The peak at $\delta = 3.64$ - 3.89 ppm (H, d, CH), which equivalent to one proton, is related to (C_4 -H). The peak at $\delta = 4.30$ - 4.48 ppm (H, t, CH), which equivalent to one proton is related to (C_5 -H) for each ligands. The signal at $\delta = 5.94$ ppm (H, d) that belongs to N-H which equivalent to one proton also for both ligands. Resonances at $\delta = 6.89$ - 7.07 ppm (2H, d, CH) is assigned to (C_8 -H), 7.15 - 7.18 ppm (H, t, CH $J_{\text{HH}} = 9$ Hz) assigned to (C_{13} -H), 7.20 ppm (2H, d) assigned to ($\text{C}_{7,7}$ -H), 7.25 ppm (H, d) assigned to (C_{11} -H), 7.27 ppm (H, t) assigned to (C_{12} -H) and 7.38 ppm (H, d) assigned to (C_{14} -H) of the aromatic ring protons for each ligands, respectively. The spectrum revealed peaks at 2.59 and 3.23 ppm is related to the DMSO- d_6 solvent and the traces of water molecules in the solvent, respectively. The chemical shifts data are summarised in Table (3.21).

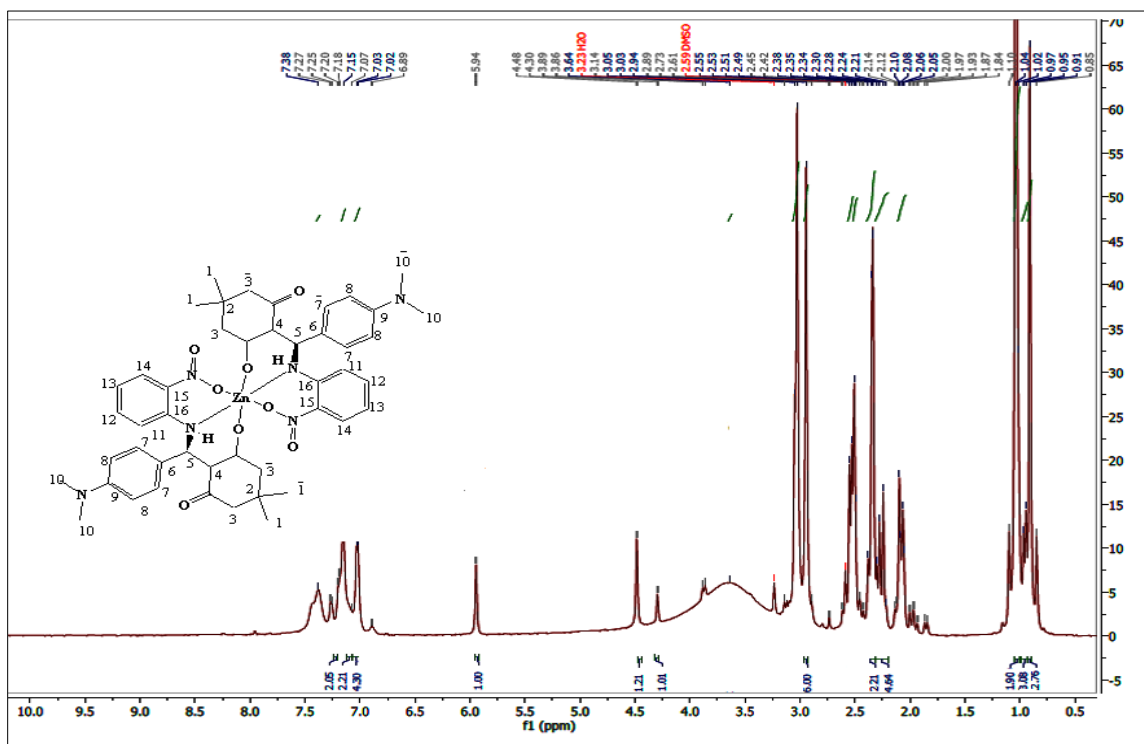


Fig (3.33): $^1\text{H-NMR}$ spectrum of $[\text{Zn}(\text{HL})_2]$ in DMSO-d_6 .

(3.9.3.2) $^1\text{H-NMR}$ spectrum of $[\text{Zn}(\text{H}_2\text{L}^2)\text{Cl}]\text{Cl}$

The $^1\text{H-NMR}$ spectrum of $[\text{Zn}(\text{H}_2\text{L}^2)\text{Cl}]\text{Cl}$ is depicted in Fig. (3.34). The spectrum displays chemical shift at $\delta = 0.93\text{--}1.04\text{ppm}$ (6H, s) are attributed to ($\text{C}_{1,1}\text{-H}$) of the two methyl groups protons. The chemical shift at $\delta = 1.10\text{--}2.09\text{ppm}$ (2H, s, CH_2) that appeared as a single and equivalent to two protons which assigned to ($\text{C}_4\text{-H}$). The chemical shift at $\delta = 2.23\text{--}2.26\text{ppm}$ (2H, s, CH_2 $J_{\text{HH}} = 9$ Hz) that appeared as a single and equivalent to two protons which assigned to ($\text{C}_3\text{-H}$). More, The spectrum displays chemical shift at $\delta = 2.53\text{--}2.57$ ppm (6H, s, $-\text{N}(\text{Me})_2$ $J_{\text{HH}} = 12$ Hz) are attributed to ($\text{C}_{11,11}\text{-H}$) of the two methyl group protons. The peak at $\delta = 4.26\text{ppm}$ (H, d, CH), which equivalent to one proton is related ($\text{C}_5\text{-H}$). The peak at $\delta = 4.43\text{ppm}$ (H, t, CH), which equivalent to one proton is related ($\text{C}_6\text{-H}$). The signal at $\delta = 5.73\text{ppm}$ (H, d, NH) that belongs to N-H which

equivalent to one proton. Resonances at $\delta = 6.46$ ppm (2H, d, CH) assigned to (C_9 , η -H), 6.53 ppm (H, t, CH) assigned to (C_{14} -H), 7.22-7.32 ppm (2H, d, CH) assigned to (C_8 , δ -H), 7.33-7.47 ppm (H, d) assigned to (C_{12} -H), 7.48 ppm (H, t) assigned to (C_{13} -H) and 7.95 ppm (H, d) assigned to (C_{15} -H) of the aromatic ring protons, respectively. The peak at 10.13 ppm that belongs to N-H₂ which equivalent to two protons is related to (H, s, NH₂). The signal at 12.96 ppm that belongs to N-H which equivalent to one proton is related to (H, s, NH). The spectrum revealed peaks at 2.51 and 2.82-3.23 ppm related to the DMSO-d₆ solvent and the traces of water molecules in the solvent, respectively. The chemical shifts data are summarised in Table (3.21).

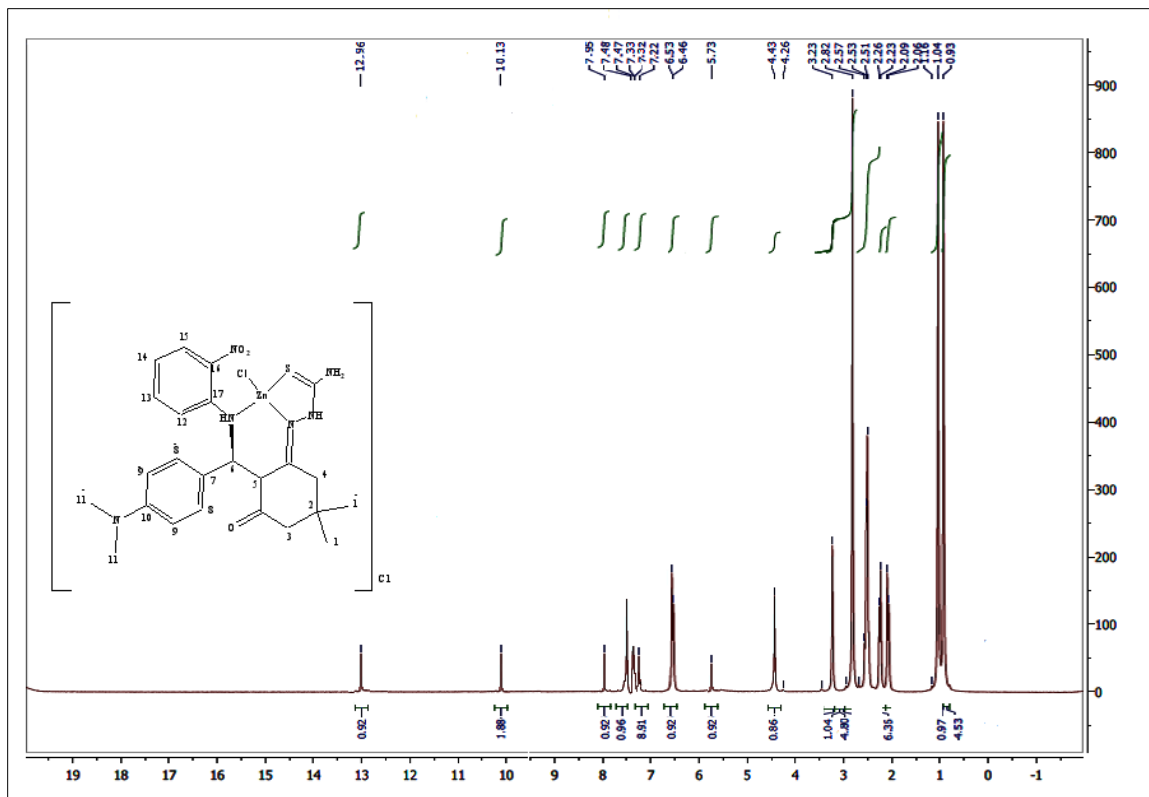


Fig (3.34): ¹H-NMR spectrum of [Zn(H₂L²)Cl]Cl in DMSO-d₆.

Table (3.21): $^1\text{H-NMR}$ data for complexes measured in DMSO-d_6 and chemical shift in ppm (δ).

complexes	Fund. group	δ (ppm)
[Zn(HL ¹) ₂]	(C _{1,1} ^{-H})	0.85-1.97 (6H, s, -C-(Me) ₂)
	(C _{3,3} ^{-H})	2.00 -2.55 (4H, s, CH ₂)
	(C _{10,10} ^{-H})	2.61 -3.14 (6H, s, -N-(Me) ₂)
	(C ₄ -H)	3.64-3.89(H, d, CH)
	(C ₅ -H)	4.30-4.48 (H, t, CH)
	(N-H)	5.94 (H, d)
	(C _{8,8} ^{-H})	6.89 -7.07 (2H, d, CH)
	(C ₁₃ -H)	7.15-7.18 (H, t,CH $J_{\text{HH}}=9\text{Hz}$)
	(C _{7,7} ^{-H})	7.20 (2H, d)
	(C ₁₁ -H)	7.25 (H, d)
	(C ₁₂ -H)	7.27 (H, t)
	(C ₁₄ -H)	7.38 (H, d)
[Zn(H ₂ L ²)Cl]Cl	(C _{1,1} ^{-H})	0.93-1.04 (6H, s)
	(C ₄ -H)	1.10-2.2.09 (2H, s, CH ₂)
	(C ₃ -H)	2.23-2.26(2H,s,CH ₂ $J_{\text{HH}}=9\text{Hz}$)
	(C _{11,11} ^{-H})	2.53-2.57 (6H, s, -N-(Me) ₂ $J_{\text{HH}}=12\text{Hz}$)

(C ₅ -H)	4.26 (H, d, CH)
(C ₆ -H)	4.43 (H, t, CH)
(N-H) _{mannich}	5.73 (H, d, NH)
(C _{9,9'} -H)	6.46 (2H, d, CH)
(C ₁₄ -H)	6.53 (H, t, CH)
(C _{8,8'} -H)	7.22-7.32 (2H, d, CH)
(C ₁₂ -H)	7.33-7.47 (H, d)
(C ₁₃ -H)	7.48 (H, t, CH)
(C ₁₅ -H)	7.95 (H, d)
(N-H)	10.13 (H, s, NH ₂)
(N-H)	12.96 (H, s, NH)

(3.9.3.3) ¹³C-NMR spectrum of [Zn(HL¹)₂]

The ¹³C-NMR spectrum of [Zn(HL¹)₂] is depicted in Fig. (3.35). The Resonances at $\delta = 149.60$ and 145.26 ppm were assigned to (C₉) and (C₁₆), respectively. Signals related to (C₁₂), (C₆) and (C₁₅) were detected at 129.34, 128.88 and 128.82 ppm, respectively. Resonances assigned for (C_{7,7'}), (C₁₄), (C₁₃), and (C_{8,8'}) were observed at 127.22, 119.22, 113.33 and 100.57 ppm, respectively. The chemical shifts that appeared at 56.55, 49.80 and 45.01-44.96 ppm are assigned to (C₄), (C₃) and (C₅), respectively. The two methyl groups, N-(C_{10,10'}), were appeared as a one peak at 44.84 ppm. The peaks of

(C₂) and (C₁) resonances appeared at 32.81 and 30.79 ppm, respectively. Finally, the C=O of the carbonyl group appears as expected downfield at δ =199.55 and 211.22 ppm. The spectrum revealed peak at 39.52-38.52 ppm is related to the DMSO-d₆ solvent. The ¹³C-NMR results are summarised in Table (3.22).

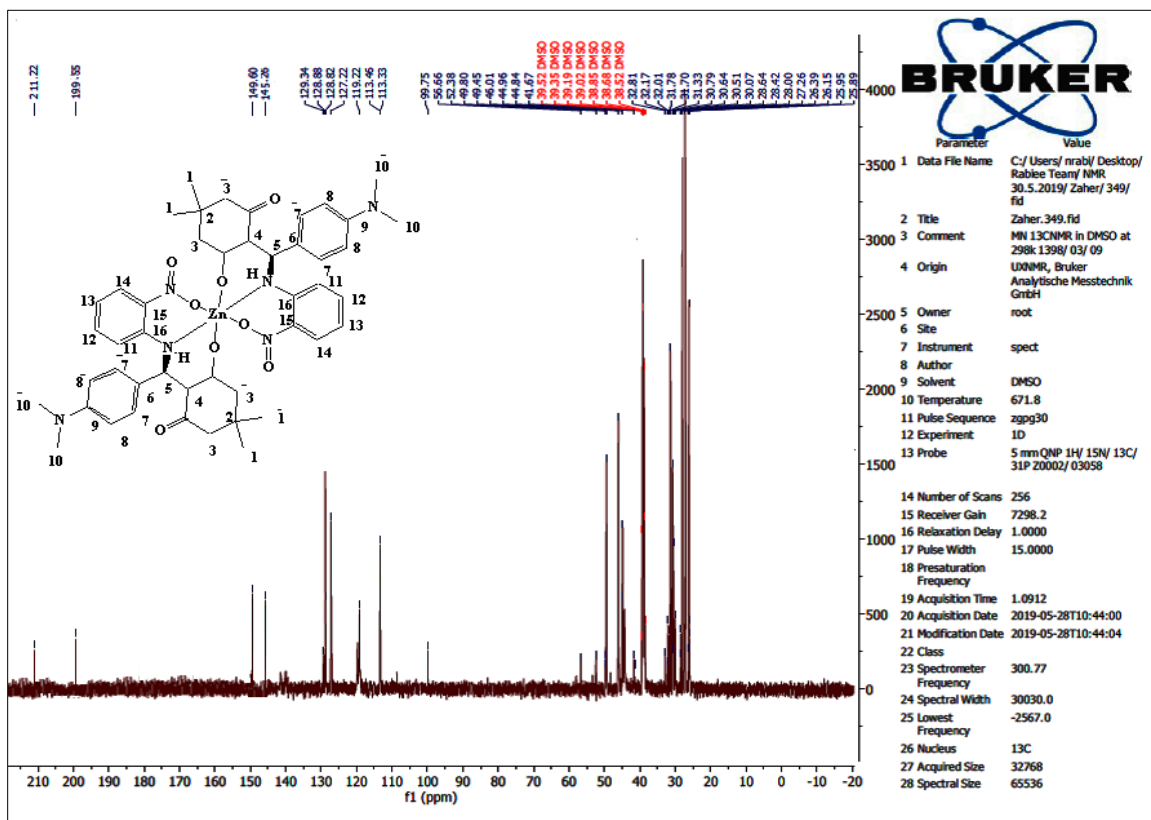


Fig (3.35): ¹³C-NMR spectrum of [Zn(HL¹)₂] in DMSO-d₆.

(3.9.3.4) ^{13}C -NMR spectrum of $[\text{Zn}(\text{H}_2\text{L}^2)\text{Cl}]\text{Cl}$

The ^{13}C -NMR spectrum of $[\text{Zn}(\text{H}_2\text{L}^2)\text{Cl}]\text{Cl}$ is depicted in Fig. (3.36). The Resonances at $\delta = 149.29$ and 144.00ppm were assigned to (C_{10}) and (C_{17}), respectively. Signals related to (C_{13}), (C_7) and (C_{16}) were detected at 131.66 , 129.34 and 128.88ppm , respectively. Resonances assigned for ($\text{C}_{8,8}$), (C_{15}), (C_{14}), (C_{12}) and ($\text{C}_{9,9}$) were observed at 128.82 , 127.22 , 119.22 , 113.46 and 113.33ppm , respectively. The chemical shifts that appeared at 56.66 , 52.38 and 49.80ppm are assigned to (C_5), (C_3) and (C_6), respectively. The two methyl groups, N-($\text{C}_{11,11}$), were appeared as a one peak at 49.62ppm . The peaks of (C_4), (C_2) and (C_1) resonances appeared at 29.41 , 28.17ppm and 26.00ppm , respectively. The chemical shifts that appeared at 161.00ppm is assigned to $\text{C}=\text{N}$. The chemical shifts that appeared at 181.68ppm is assigned to $\text{C}=\text{S}$. Finally, the $\text{C}=\text{O}$ of the carbonyl group appears as expected downfield at $\delta=198.55\text{ppm}$. The spectrum revealed peak at 39.61 - 38.89ppm is related to the DMSO-d_6 solvent. The ^{13}C -NMR results are summarised in Table (3.22).

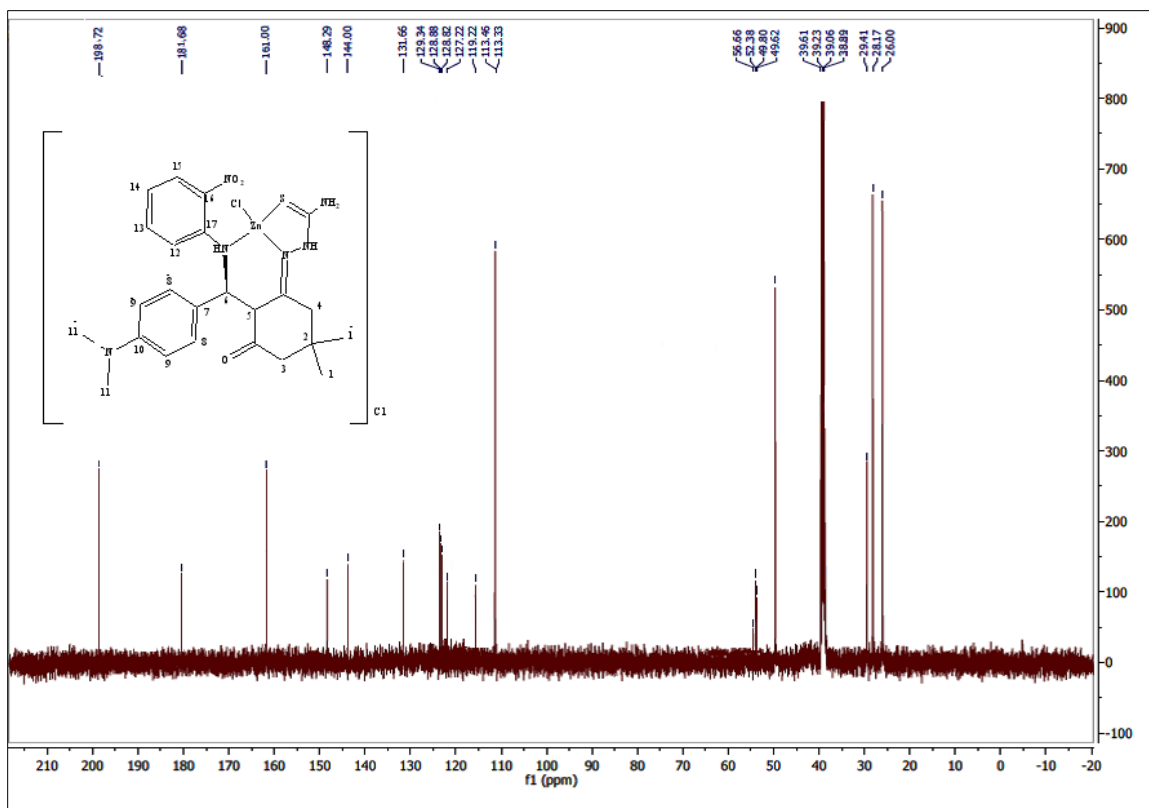


Fig (3.36): ^{13}C -NMR spectrum $[\text{Zn}(\text{H}_2\text{L}^2)\text{Cl}]\text{Cl}$ in DMSO-d_6 .

Table (3.22): ^{13}C -NMR data for complexes measured in DMSO-d_6 and chemical shift in ppm (δ).

complex	Fund. group	δ (ppm)
$[\text{Zn}(\text{HL}^1)_2]$	(C ₉)	149.60
	(C ₁₆)	145.26
	(C ₁₂)	129.34
	(C ₆)	128.88
	(C ₁₅)	128.82
	(C _{7,7})	127.22
	(C ₁₄)	119.22

	(C ₁₃)	113.45
	(C ₁₁)	113.33
	(C _{8,8} ⁻)	100.57
	(C ₄)	56.55
	(C ₃)	49.80
	(C ₅)	45.01
	N-(C _{10,10} ⁻)	44.84
	(C ₂)	32.81
	(C ₁)	30.79
	C=O	199.55 and 211.22
[Zn(H ₂ L ²)Cl]Cl	(C ₁₀)	149.29
	(C ₁₇)	144.00
	(C ₁₃)	131.66
	(C ₇)	129.34
	(C ₁₆)	128.88
	(C _{8,8} ⁻)	128.82
	(C ₁₅)	127.22
	(C ₁₄)	119.22
	(C ₁₂)	113,46
	(C _{9,9} ⁻)	113.33

	(C ₅)	56.66
	(C ₃)	52.38
	(C ₆)	49.80
	N-(C _{11,11})	49.62
	(C ₄)	29.41
	(C ₂)	28.17
	(C _{1,1})	(26.00)
	C=N	161.00
	C=S	181.68
	C=O	195.55

(3.10) Thermal analysis of ligands and complexes.

Thermal decomposition data for the ligands and some of their metal complexes are summarised in Table(3.23). Analysis curves Thermogravimetric analysis (TGA) and Differential scanning calorimetry (DSC) of compounds are studied and interpreted as follows:

(3.10.1) Thermal analysis of ligands.

(3.10.1.1) Thermal decomposition of HL¹

The thermogram of HL¹ is depicted in Fig (3.37). The first exothermic peak detected at 205-275 °C may be attributed to the loss of a molecule of the (NH₃+ NH₂+ CO₂+ H₂CO + (CH₃)) segment; (obs.=0.648mg, 30.26%; calc. =0.639mg, 29.80%). The second step occurred at 280-625 °C indicated the loss of (CO + NH₂ + C₂H₂ + C₆H₂ +C₇H₃) fragment; (obs.=1.22mg, 56.92%; calc.=1.21mg, 56.47 %). The third step recorded at 630-1000 °C indicated the loss of (4H₂) fragment, (obs.= 0.044mg, 2.055%; calc.=0.042mg, 1.97%). The final residue of the (4C) calc.= 48mg, 11.735%. The TGA indicated several peaks at 205, 219, 404 and 457 °C. The second peak may indicate the melting point of the ligand. In the DSC analysis, peaks at 205, 404 and 457 °C are correlated to exothermic decompositions process. However, the peak at 219 °C refers to endothermic decompositions process. The exothermic and endothermic peaks may indicate combustion of the organic ligand in nitrogen atmosphere [94, 95].

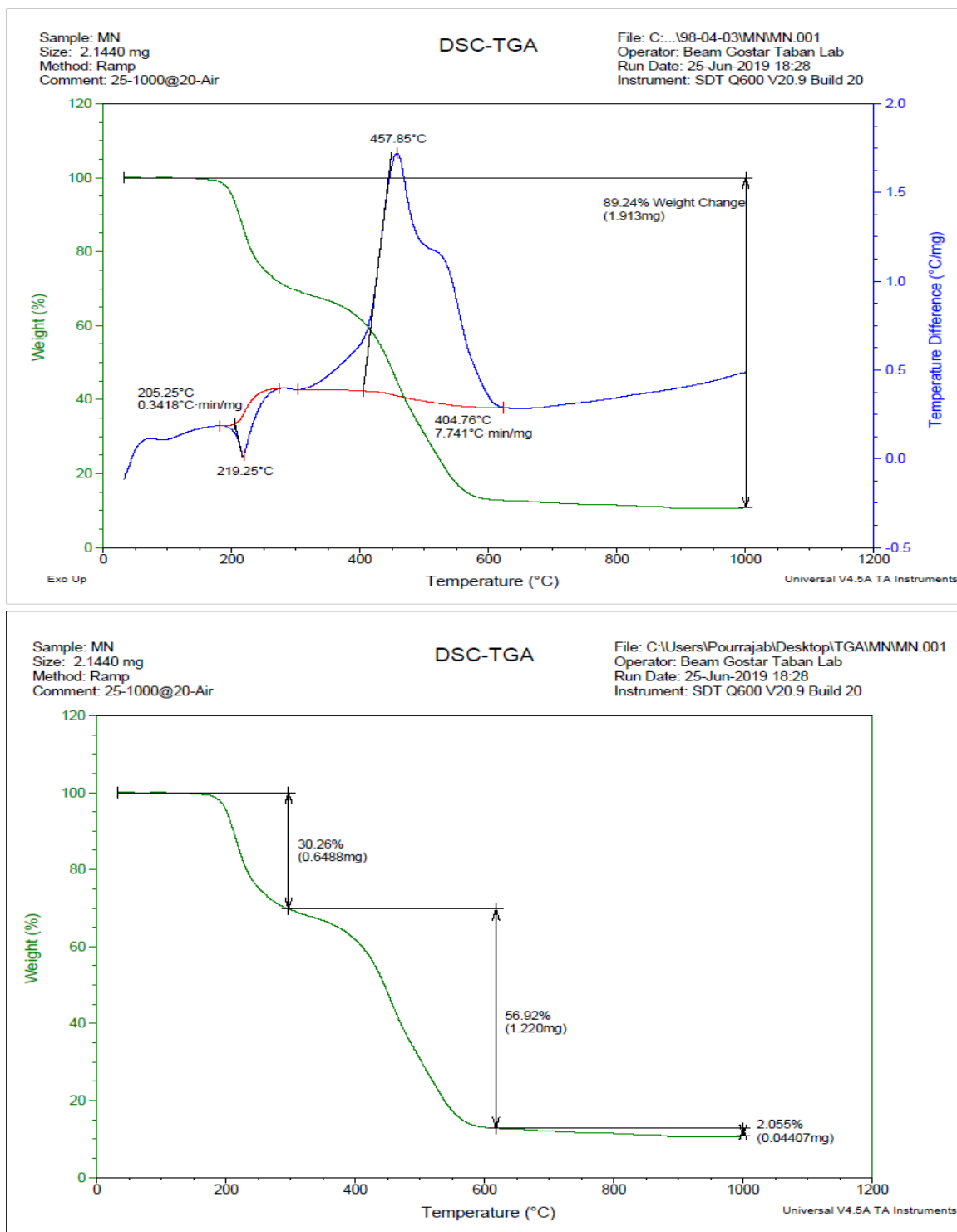


Fig (3.37): Thermal decomposition of HL¹ in N₂ atmosphere.

(3.10.1.2) Thermal decomposition of H_2L^2

The thermogram of H_2L^2 is depicted in Fig. (3.38). The first exothermic peak detected at 181-315°C may be attributed to the loss of a molecule of the (CO + NO + NH₂ + NH₃ + H₂S + H₂CO + CH₄) segments; (obs. =0.8497mg, 35.05%; calc. = 0.848mg, 35.02). The second step occurred at 320-660°C indicated the loss of (4NH₂ + C₄H₂ + C₇H₂ + C₈H₃) fragment; (obs.=1.347mg, 55.55%; calc.=1.340mg, 55.30%). The third step recorded at 665-1000°C indicated the loss of (NH₃+H₂) fragment, (obs.= 0.112mg, 4.61%; calc.=0.0955mg, 3.94%). The final residue of the (C₂H) calc.= 25.01mg, 5.18%. The DTGA indicated several peaks at 210, 221, 441, 459, 509 and 542°C. In the DSC analysis, peaks at 210, 441, 459, 509 and 542°C correlated to exothermic decompositions process. However, the peak at 221°C refers to endothermic decompositions process. The exothermic and endothermic peaks may indicate the combustion of the organic ligand in nitrogen atmosphere.

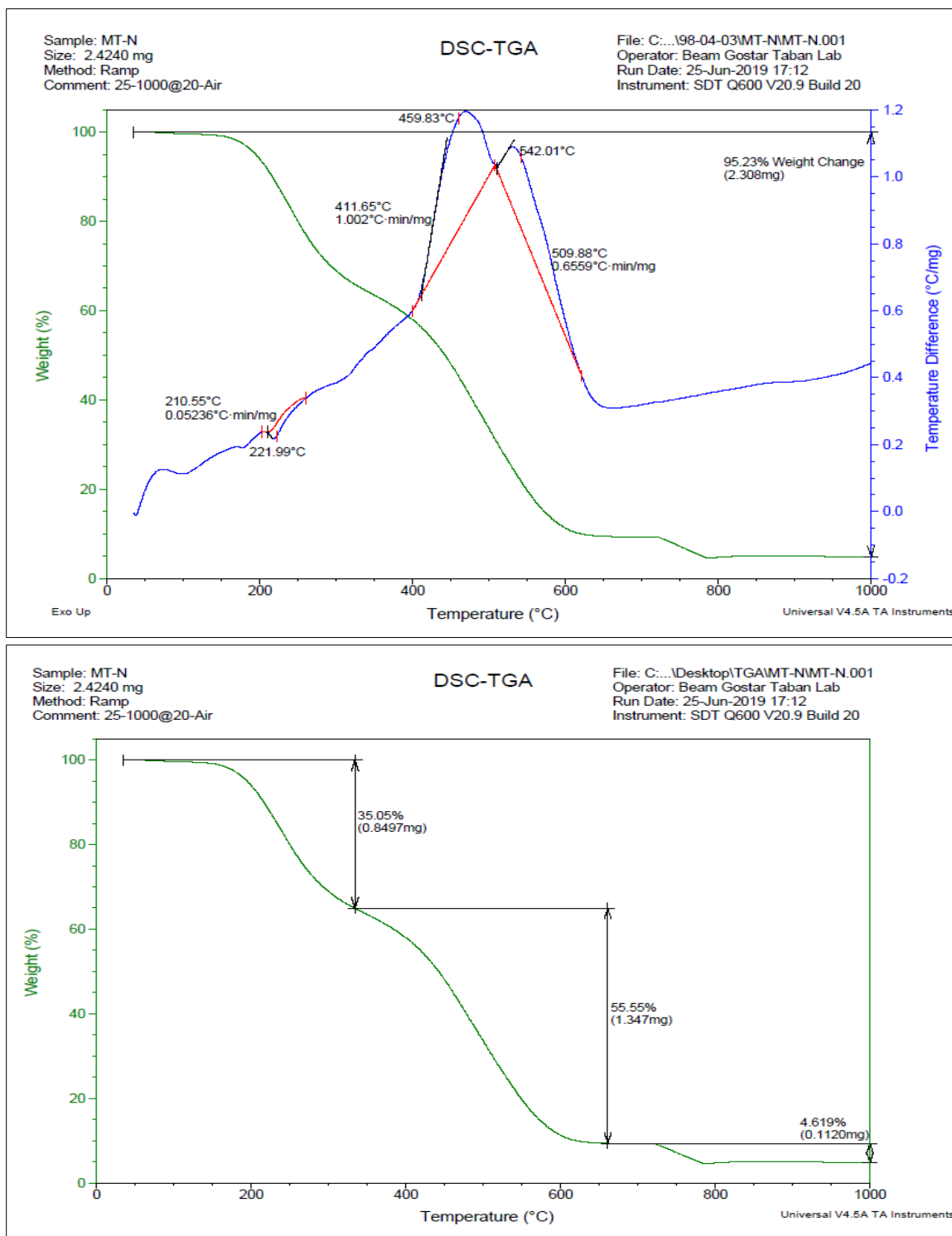


Fig (3.38): Thermal decomposition of H_2L^2 in N_2 atmosphere.

(3.10.2) Thermal decomposition of some the complexes.

(3.10.2.1) Thermal decomposition of $[\text{Zn}(\text{HL}^1)_2]$ complex

The thermogram of $[\text{Zn}(\text{HL}^1)_2]$ is depicted in Fig(3.39). The first exothermic peak detected at 197-270°C may be attributed to the loss of a molecule of the $(2\text{NO} + 2\text{NH}_2 + 2\text{CO} + \text{C}_5\text{H}_3 + \text{C}_5\text{H}_5)$ segments; (obs.=1.272mg, 28.82%; calc. =1.23 mg, 28.05). The second step occurred at 275-540°C indicated the loss of $(\text{O}_2 + 2\text{CN}^- + \text{CO}_2 + \text{C}_5\text{H}_4 + \text{C}_8\text{H}_4 + \text{C}_4\text{H}_2)$ fragment; (obs.=1.691mg, 38.32%; calc.=1.68mg, 38.23%). The third step recorded at 550-1000°C indicated the loss of $(\text{C}_2\text{H}_2 + \text{C}_4\text{H}_5 + \text{C}_6\text{H}_5)$ fragment, (obs.=0.7855mg, 17.80%; calc.=0.780mg, 17.65%). The final residue of the $(6\text{H}_2 + \text{C}_2\text{H}_6 + \text{ZnO})$ calc.= 107.56mg, 12.16%. The DTGA indicated several peaks at 197, 214, 270 and 995°C. In the DSC analysis, peaks at 197°C are correlated to exothermic decompositions process. However, the peak at 214, 270 and 995°C refer to endothermic decompositions process. The exothermic and endothermic peaks may indicate the combustion of the organic ligand in nitrogen atmosphere.

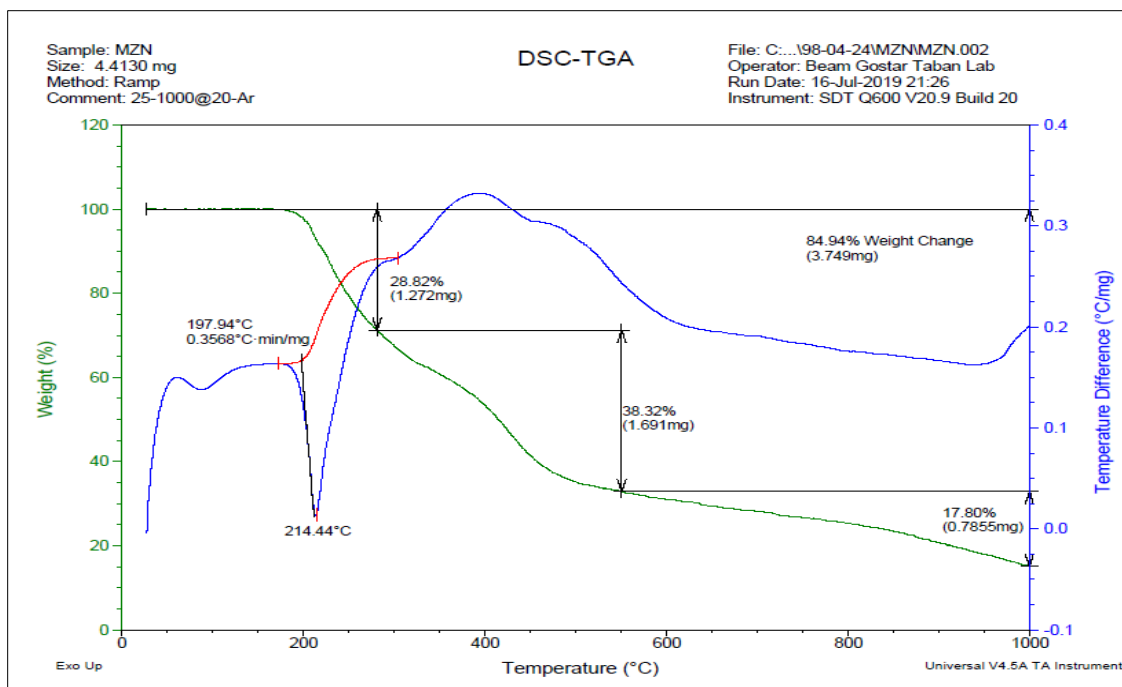


Fig (3.39): Thermal decomposition of $[\text{Zn}(\text{HL}^1)_2]$ in N_2 atmosphere

(3.10.2.2) Thermal decomposition of $[\text{Ni}(\text{H}_2\text{L}^2)\text{Cl}]\text{Cl}$ complex

The thermogram of $[\text{Ni}(\text{H}_2\text{L}^2)]\text{Cl}_2$ is depicted in Fig (3.40). The first exothermic peak detected at 223-500°C may attribute to the loss of a molecule of the $(2\text{NO} + \text{H}_2\text{S} + \text{Cl}_2 + \text{CH} + \text{CO})$ segment; (obs.=3.145mg, 66.53%; calc.= 3.13mg, 66.30). The second step occurred at 510-1000 °C indicated the loss of $(2\text{NH}_3 + \text{C}_6\text{H}_9)$ fragment; (obs.=0.8918mg,18.87%; calc.=0.888mg,18.80%). The final residue of the $(\text{C}_2\text{H}_7 + \text{NiO})$ calc.= 89.7634mg, 14.662%. The DTGA indicated several peaks at 223, 231 and 500°C. In the DSC analysis, peaks pointed at 223°C correlated to exothermic decompositions process. However, the peak 231 and 500°C refer to endothermic decompositions process. The exothermic and endothermic peaks may indicate combustion of the organic ligand in nitrogen atmosphere.

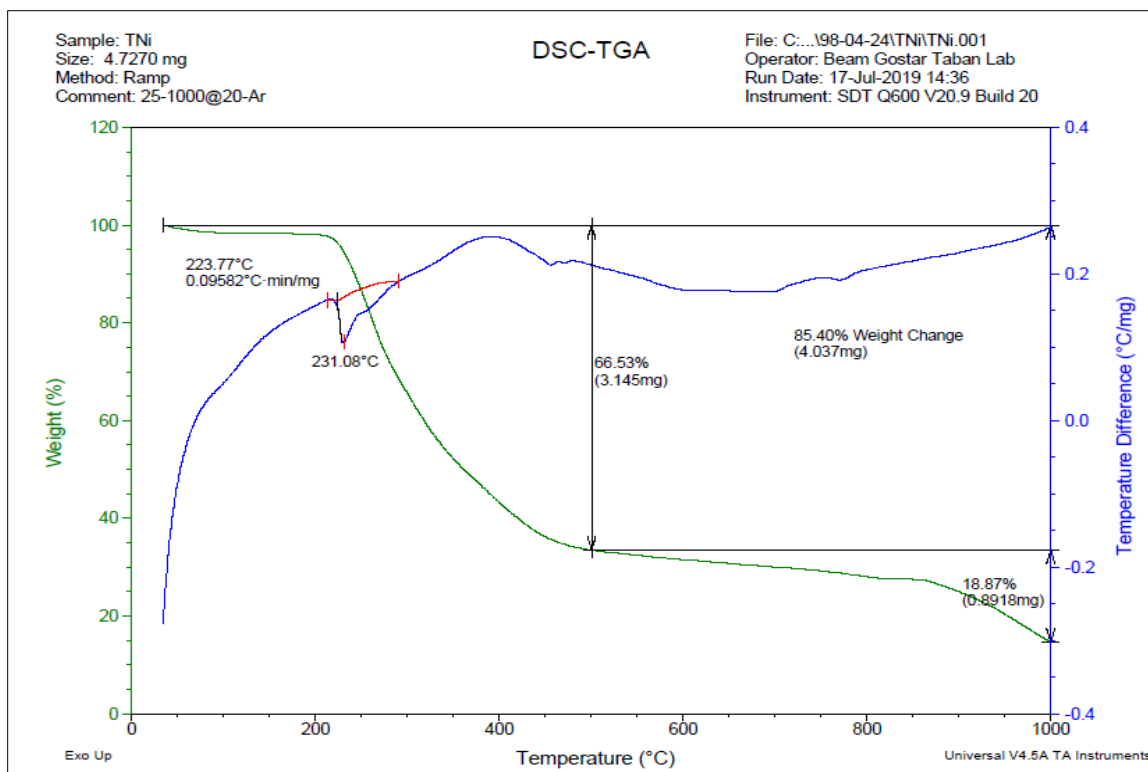
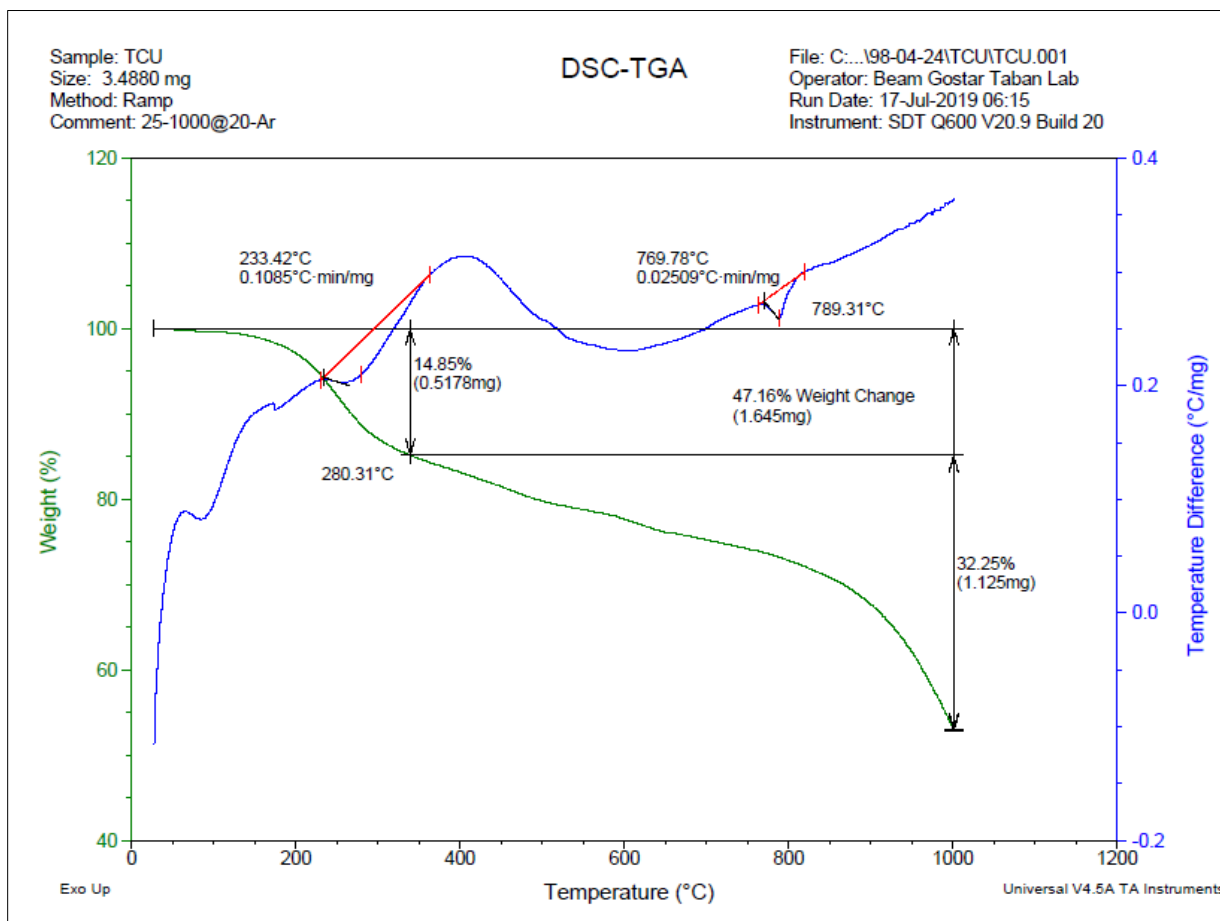


Fig (3.40): Thermal decomposition of $[\text{Ni}(\text{H}_2\text{L}^2)\text{Cl}]\text{Cl}$ in N_2 atmosphere.

(3.10.2.3) Thermal decomposition of $[\text{Cu}(\text{H}_2\text{L}^2)\text{Cl}_2\text{H}_2\text{O}]$ complex

The thermogram of $[\text{Cu}(\text{H}_2\text{L}^2)\text{Cl}_2\text{H}_2\text{O}]$ is depicted in Fig (3.41). The first exothermic peak detected at 140-320°C may be attributed to the loss of a molecule of the $(\text{H}_2\text{O} + \text{H}_2\text{S} + \text{CO}_2 + \text{CO})$ segments; (obs.= 0.5178mg, 14.85%; calc.=0.5164mg, 14.81). The second step occurred at 325-1000°C indicated the loss of $\text{C}_3\text{H}_8 + \text{Cl}_2 + \text{N}_2\text{H}_4 + \text{C}_2\text{H}_6$ fragment; (obs.=1.125mg, 32.25%; calc.=1.120mg, 32.13%). The final residue of the $(\text{C}_6\text{H}_4\text{N}_2 + \text{C}_6\text{H}_3\text{N} + \text{C}_5\text{H}_3\text{N} + \text{CuO})$ calc.= 33.553mg, 52.52%. The TGA indicated several peaks at 233, 280, 320, 769 and 789°C. In the DSC analysis, peaks at 233 and 789°C are correlated to exothermic decompositions process.

However, the peak at 280, 320 and 769 °C. refers to endothermic decompositions process. The exothermic and endothermic peaks may indicate the combustion of the organic ligand in nitrogen atmosphere



Fig(3.41):Thermal decomposition of $[\text{Cu}(\text{H}_2\text{L}^2)\text{Cl}_2 \cdot \text{H}_2\text{O}]$ in N_2 atmosphere

Table (3.23): Thermal analysis data of ligands and some of their complexes.

Comp	Stable up to °C	Stage	Decomposition Temperature Initial-Final (°C)	Nature of Transformation/Intermediate Formed % mass found (calc.)	Nature of DSC peak and Temp. °C
HL ¹	205	1	205-275	0.648 (0.639)	205, 404, 457 Exo 219 Endo
		2	280-625	1.22 (1.21)	219,457 Endo
		3	630-1005	0.044(0.042)	650 Endo
H ₂ L ²	181	1	181-315	0.8497(0.848)	210 Exo 221Endo
		2	320-660	1.347(1.340)	441, 459, 509 , 542 Exo
		3	665-1000	0.112 (0.0955)	660Endo
[Zn(HL ¹) ₂]	197	1	197-270	1.27 (1.23)	197 Exo 214, 270 Endo
		2	275-540	1.691 (1.68)	-
		3	550-1000	0.785 (0.780)	995 Endo

[Ni(H ₂ L ²) Cl]Cl	223	1	223-500	3.145 (3.13)	223 Exo
		2	510-1000	0.891 (0.888)	231 Endo
[Cu(H ₂ L ²) Cl ₂ H ₂ O]	140	1	140-320	0.5178 (0.513)	233,280 Exo
		2	325-1000	1.125 (1.125)	789 Endo

(3.11) Molar conductivity measurement of the complexes

The electro-conductivity measurement values of complexes were determined to revealed conductance of (electrolyte or non-electrolyte) [96,97]. The molar electro-conductivity of the complexes in DMSO were summarised in Table (3.24).

Table (3.24): The molar conductivity of the complexes.

Comp.	$\Lambda_m \text{ S.cm}^2.\text{mole}^{-1}$
$[\text{Co}(\text{HL}^1)_2]$	10.51
$[\text{Ni}(\text{HL}^1)_2]$	21.4
$[\text{Cu}(\text{HL}^1)_2]$	8.62
$[\text{Zn}(\text{HL}^1)_2]$	16.74
$[\text{Cd}(\text{HL}^1)_2]$	14.94
$[\text{Co}(\text{H}_2\text{L}^2)\text{Cl}_2 \cdot \text{H}_2\text{O}]$	20.4
$[\text{Ni}(\text{H}_2\text{L}^2) \text{Cl}]\text{Cl}$	36.3
$[\text{Cu}(\text{H}_2\text{L}^2)\text{Cl}_2 \cdot \text{H}_2\text{O}]$	17.3
$[\text{Zn}(\text{H}_2\text{L}^2)\text{Cl}] \text{Cl}$	38.4
$[\text{Cd}(\text{H}_2\text{L}^2)\text{Cl}] \text{Cl}$	32.7

Chapter Four: Bacterial activity

(4.1) Microbiological activity

The synthesised ligands and their metal complexes were screened for their microbiological activity against two strains of bacterial species: G⁺ positive (*Staphylococcus aureus* and *Bacillus subtilis*) and G⁻negative (*Escherichia coli* and *Pseudomonas aeruginosa*). Additional to two types of fungi were explored (*Candida* and *Trichomoniasis*).

(4.1.1) Anti-bacterial activity

(4.1.1.1) Anti-bacterial activity of HL¹ and its complexes

The Mannich-base ligand and its complexes with Co(II), Ni(II), Cu(II), Zn(II) and Cd(II) ions were screened against two bacterial strains G⁺ positive (*Staphylococcus aureus* and *Bacillus subtilis*) and G⁻negative (*Escherichia coli* and *Pseudomonas aeruginosa*), using Kirby-Bauer method. DMSO, has shown no activity against any bacterial strains [98]. The obtained results are listed in Table (4.1) and Fig. (4.1 to 4.4). The strains of bacteria, under this study, revealed high resistant against HL¹, which means that the ligand showed no activity against all type of bacteria. However, the metal complexes have shown antimicrobial activity against several bacteria species, compared with the free ligand. The high activity of the complexes could be discussed on the basis of chelation theory and Overtone's model [99]. According to the chelation hypothesis, the complex has the ability to move and across the cell membrane of organism. This may be related to the decrease of the polarity of the metal ion, by the partial sharing of metal positive charge with donor groups. Subsequently, this will enhance the lipophilic property of the chelation system of metal allowing the complex to

cross the lipid layer of the cell tissue. The anti-bacterial activity of the different complexes against different organisms depends on [100,101]:

1. Their impermeability of the microbial cells.
2. The difference in the ribosome of the microbial cells.

Table (4.1) displays the evolution of diameter zone (mm) of HL¹-complexes, inhibition against the growth of various bacterial strains, the following conclusions are observed;

1. The ligand showed no any activity against tested bacteria.
2. The Co(II), Ni(II) and Cu(II) complexes indicated no activity towards all tested bacteria. This may be related to the size of the metal ion or the stability of the complex in the tested medium, the complex suffers decomposition in the medium.
3. The Zn(II) and Cd(II) complexes indicated inhibition activity against all bacterial species; (*Staphylococcus aureus*, *Bacillus stubtilis*, *Escherichia coli* and *Pseudomonas aeruginosa*).

(4.1.1.2) Anti-bacterial activity of H_2L^2 and its complexes

The synthesised thiosemicarbazone ligand and its metal complexes were examined to assess their antimicrobial activity against four bacterial species (*Staphylococcus aureus*, *Bacillus subtilis*, *Escherichia coli* and *Pseudomonas aeruginosa*). DMSO showed no activity against any bacterial strains [98]. The tests results against the growth of different bacterial strains are listed in Tables (4.1). Fig (4.5 to 4.8) displays the effect of the synthesised ligand and its complexes towards all bacteria under study. From the obtained results, the ligand showed no activity against all type of bacteria compared with its complexes. This may be related to the nature of the prepared complexes. From the obtained results, the following conclusion could be derived:

1. The ligand didn't show any activity against tested bacteria.
2. The complexes of Ni(II) showed no activity against any type of the bacterial strains.
3. The Co(II)-complex exhibits antibacterial activity against *Escherichia coli*.
4. The Cu(II)-complex exhibits antibacterial activity against (*Escherichia coli*.and *Bacillus subtilis*).
5. The Zn(II)-complex exhibits antibacterial activity against (*Staphylococcus aureus* and *Bacillus subtilis*).
6. The Cd(II)-complex indicated inhibition activity against all bacterial species; (*Staphylococcus aureus*, *Bacillus subtilis*, *Escherichia coli* and *Pseudomonas aeruginosa*).

Table (4.1): The inhibition zones (mm) of anti-bacterial activity for ligands and thier complexes.

Compounds	<i>Escherichia coli</i> (G ⁻)	<i>Pseudomonas aeruginosa</i> (G ⁻)	<i>Bacillus stubtilis</i> (G ⁺)	<i>Staphylococcus aureus</i> (G ⁺)
HL ¹	-	-	-	-
[Co(HL ¹) ₂]	-	-	-	-
[Ni(HL ¹) ₂]	-	-	-	-
[Cu(HL ¹) ₂]	-	-	-	-
[Zn(HL ¹) ₂]	8	6	9	3
[Cd(HL ¹) ₂]	12	17	11	6
H ₂ L ²	-	-	-	-
[Co(H ₂ L ²) Cl ₂ H ₂ O]	16	-	-	-
[Ni(H ₂ L ²) Cl] Cl	-	-	-	-
[Cu(H ₂ L ²) Cl ₂ H ₂ O]	13	-	15	-
[Zn(H ₂ L ²) Cl] Cl	-	-	18	11
[Cd(H ₂ L ²) Cl] Cl	18	24	27	22

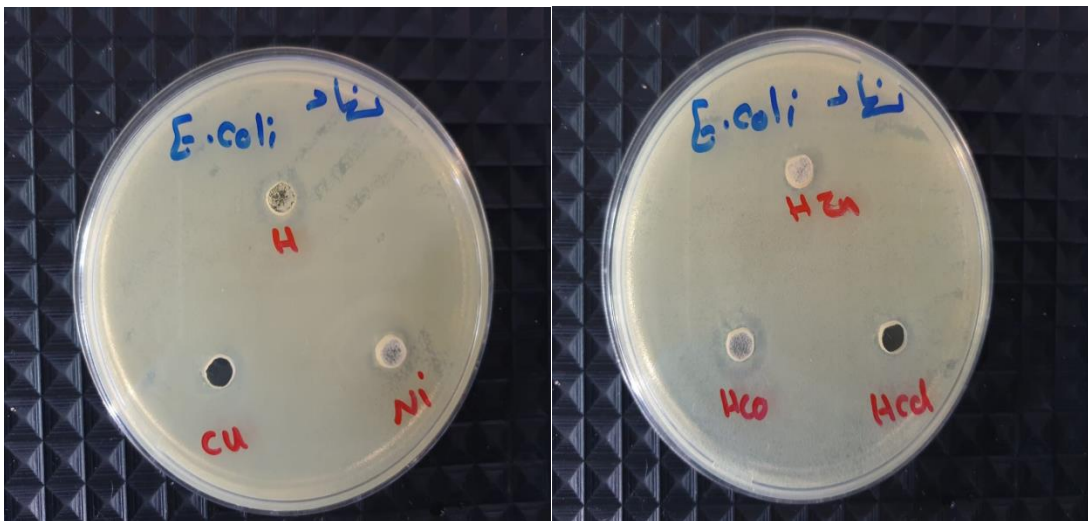


Fig (4.1): The microbiological activity of HL¹ and its complexes against *Escherichia coli*.

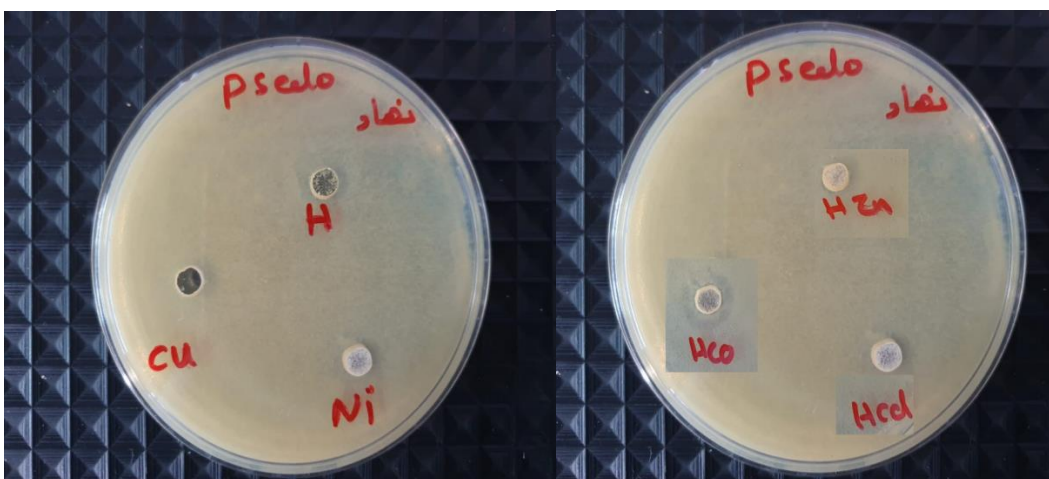


Fig (4.2): The microbiological activity of HL¹ and its complexes against *Pseudomonas aeruginosa*.

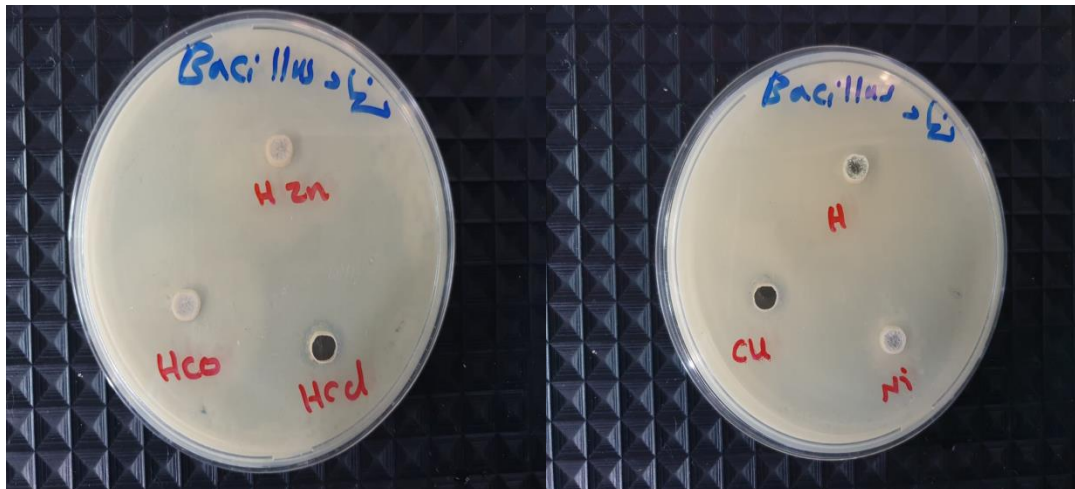


Fig (4.3): The microbiological activity of HL¹ and its complexes against *Bacillus subtilis*.

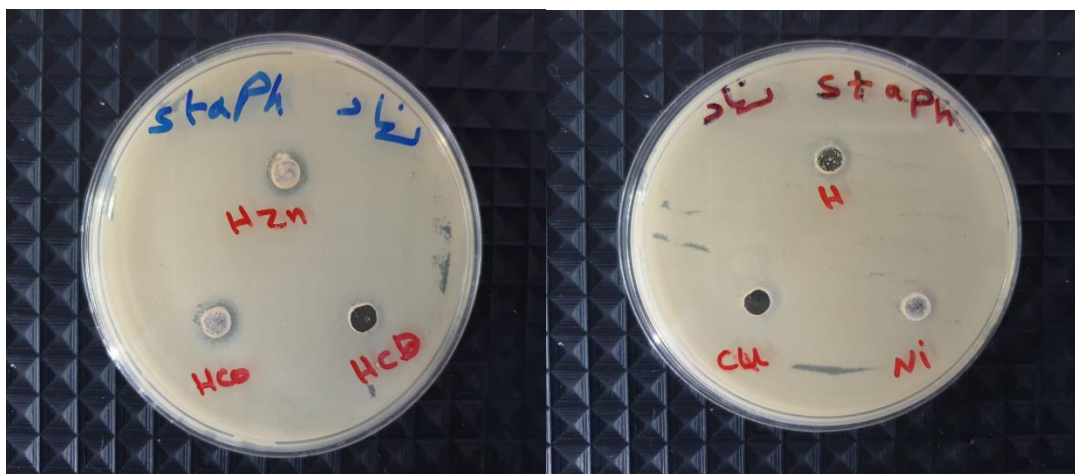


Fig (4.4): The microbiological activity of HL¹ and its complexes against *Staphylococcus aureus*.

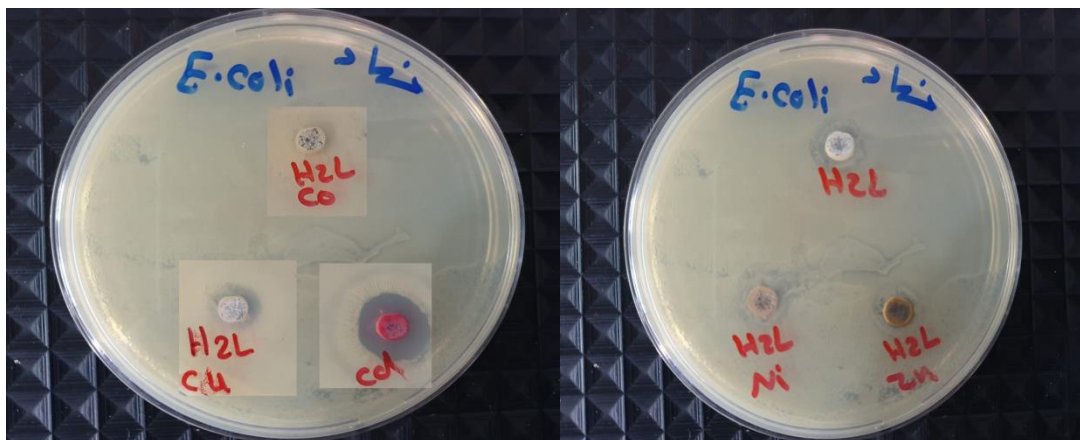


Fig (4.5): The microbiological activity of H_2L^2 and its complexes against *Escherichia coli*.

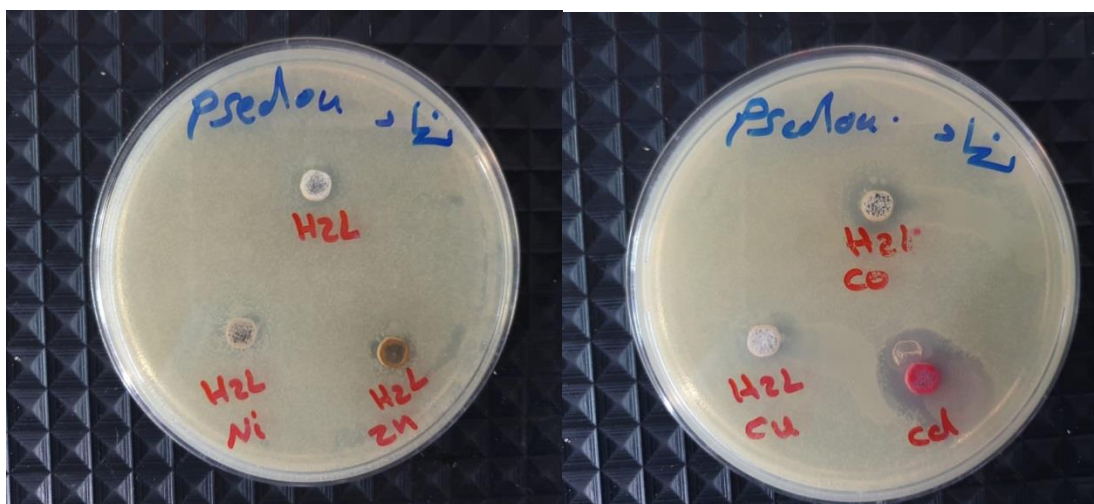


Fig (4.6): The microbiological activity of H_2L^2 and its complexes against *Pseudomonas aeruginosa*.

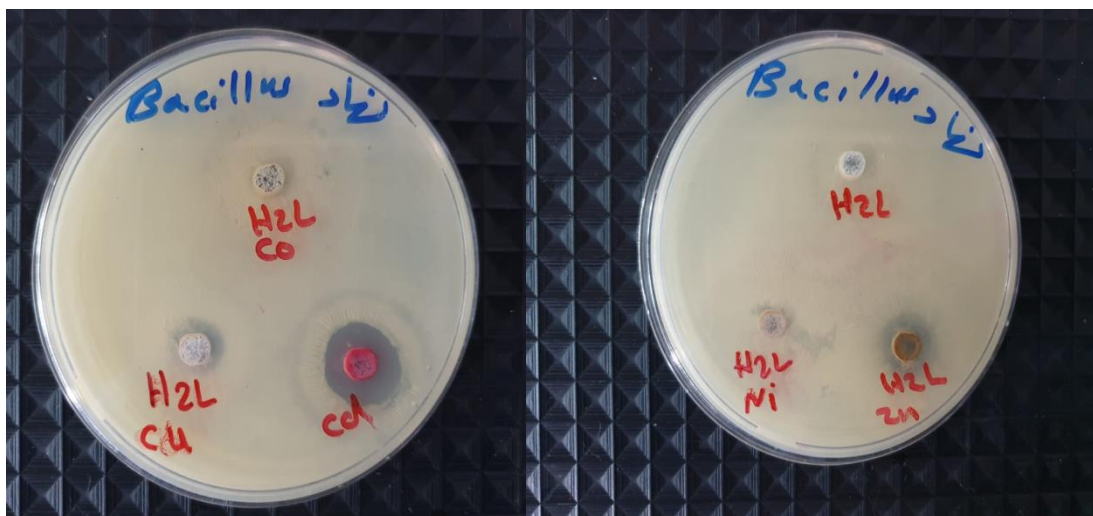


Fig (4.7): The microbiological activity of H_2L^2 and its complexes against *Bacillus subtilis*.

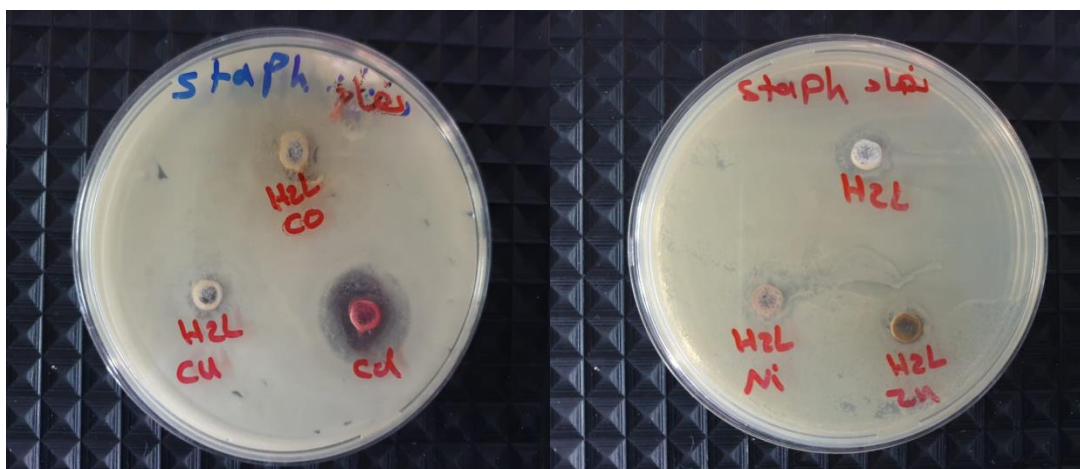


Fig (4.8): The microbiological activity of H_2L^2 and its complexes against *Staphylococcus aureus*.

(4.1.2) Anti-Fungi activity

(4.1.2.1) Anti-fungi activity of HL¹ and its complexes

The antifungal activity of the HL¹ ligand and its metal complexes have been explored against two types of fungi (*Candida* and *Trichomoniasis*). The antifungal activity data of the complexes is listed in Table (4.2), Fig. (4.9 and 4.10) displays the inhibition zones of the synthesised compounds on the tested fungi types. From the obtained data, the ligand indicated no activity against the two types of fungi. Otherwise, some of the complexes revealed activation toward fungi organism. The increase of the anti-fungal activity of complexes could be described by the chelation concept [99], which related to the delocalization of π -electrons across the entire chelate segment. This mean that the polarity of the ligand and the central metal atom decreases, and then results in the incursion of the complex through the lipid tissue of the cell membrane [100,101]. Based on the obtained results, the following conclusion may be pointed out;

1. Some complexes showed higher activity against the tested fungi, compared to the ligand. This could be attributed to the chelation effect [99].
2. The Co(II), Ni(II) and Cu(II) complexes revealed no action against the tested fungi.
3. The Zn(II) and Cd(II) complexes indicated inhibition activity against fungi species (*Candida* and *Trichomoniasis*)

(4.1.2.2) Anti-fungi activity of H_2L^2 and its complexes

The synthesised thiosemicarbazone ligand and its metal complexes were examined for their antifungal activity against (*Candida and Trichomoniasis*). DMSO, which showed no activity against any bacterial strains [98]. The cultured results against the growth of two fungi are listed in Table (4.2). Figure (4.11 and 4.12) displays the antimicrobial effect of the synthesised ligand and its complexes against fungi under survey. The collected data indicated that, the ligand indicated no activity against the two types of fungi. The Cd(II)-complex found to be more active against (*Candida and Trichomoniasis*). Further, the complexes of Ni(II) and Cu(II) ions show no activity against both types of fungi. Accordingly, the following conclusion is pointed out;

1. The tested ligand and its some complexes showed no influence on the activity of (*Candida and Trichomoniasis*)fungi.
2. The complex of Co(II) revealed a comfortable inhibition activity against *Candida*.
3. The Zn(II)-complex indicated a high activity against *Trichomoniasis*.
4. The complexes of Ni(II) and Cu(II) exhibited no activity towards tested fungi.
5. The Cd(II)-complex indicated inhibition activity against fungi species; (*Candida and Trichomoniasis*)

Table (4.2): The inhibition zones (mm) of anti-fungal activity for ligands and thier complexes.

Compounds	<i>Candida</i>	<i>Trichomoniasis</i>
HL ¹	-	-
[Co(HL ¹) ₂]	-	-
[Ni(HL ¹) ₂]	-	-
[Cu(HL ¹) ₂]	-	-
[Zn(HL ¹) ₂]	3	3
[Cd(HL ¹) ₂]	16	7
H ₂ L ²	-	-
[Co(H ₂ L ²) Cl ₂ H ₂ O]	11	-
[Ni(H ₂ L ²) Cl] Cl	-	-
[Cu(H ₂ L ²) Cl ₂ H ₂ O]	-	-
[Zn(H ₂ L ²) Cl] Cl	-	17
[Cd(H ₂ L ²) Cl] Cl	22	14

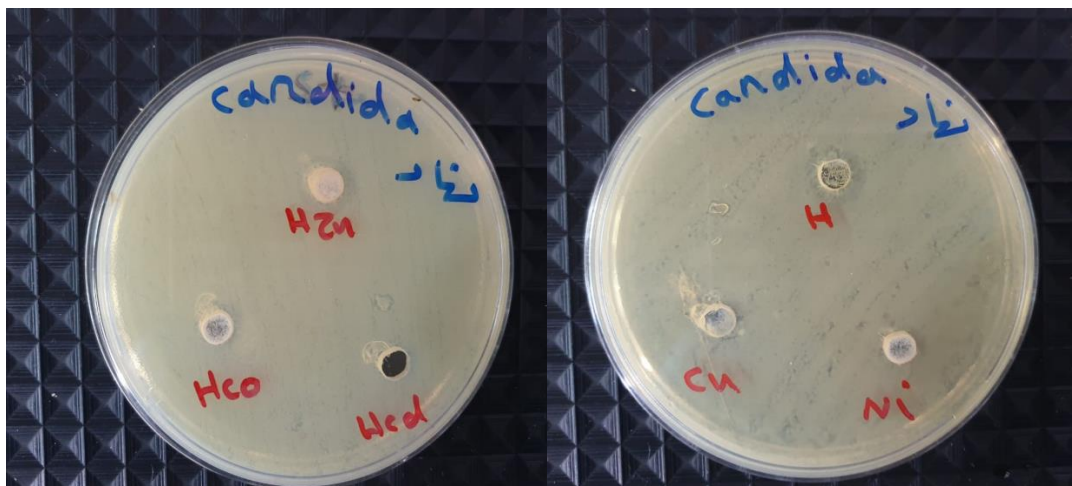


Fig (4.9): The microbiological activity of HL¹ and its complexes against *Candida*.

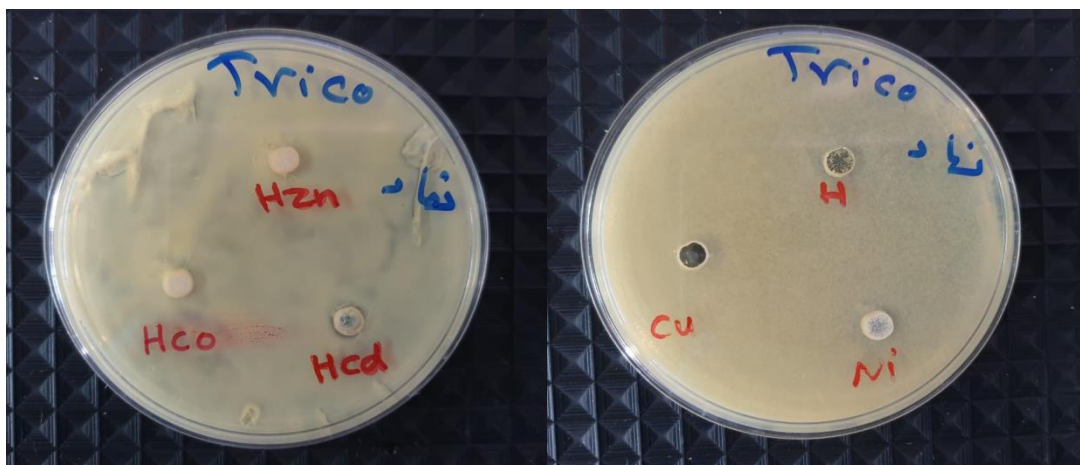


Fig (4.10): The microbiological activity of HL¹ and its complexes against *Trichomoniasis*.

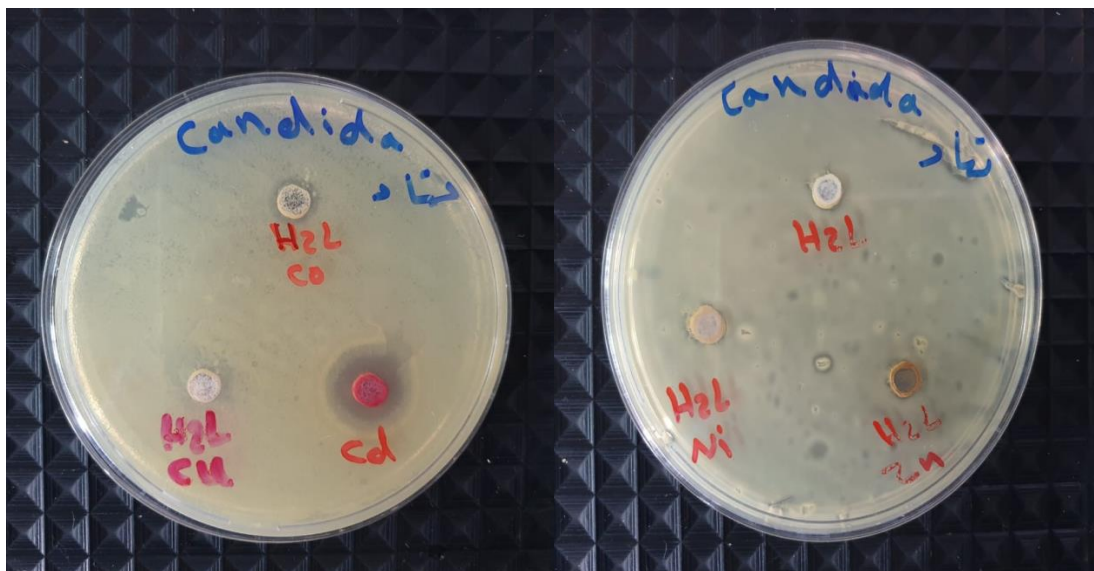


Fig (4.11): The microbiological activity of H_2L^2 and its complexes against *Candida*.

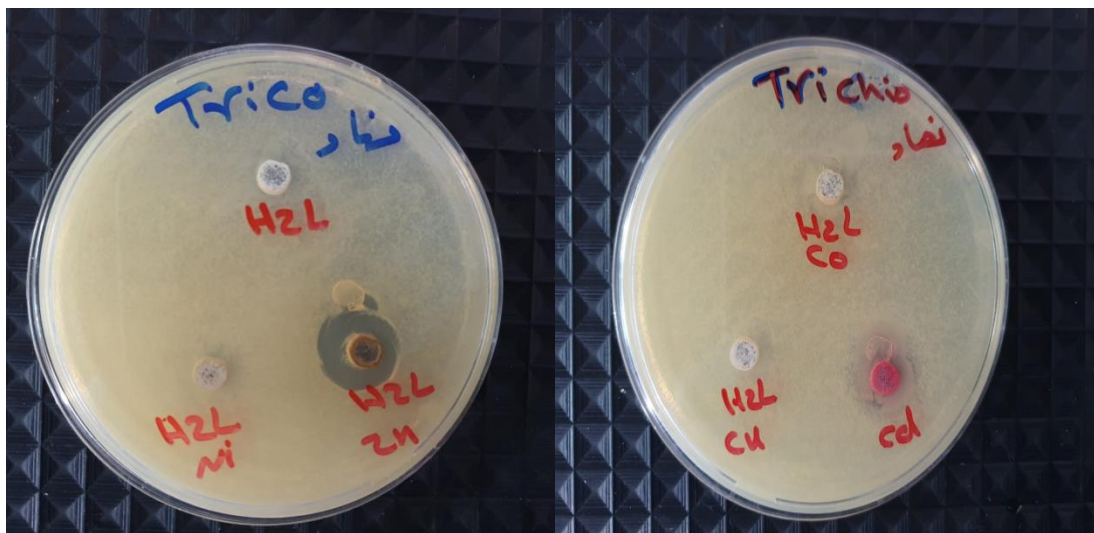


Fig (4.12): The microbiological activity of H_2L^2 and its complexes against *Trichomoniasis*.

(3.12) Conclusions and the proposed molecular structure of ligands and their complexes

The molecular structures of ligands and their metal complexes were deduced and proposed according to their analytical and spectroscopic data as follows:

(3.12.1) FT-IR Spectral data

The FT-IR spectra of ligands and their complexes, Table (3.3), (3.8) and (3.9), were exhibited the following bands:

1. The spectrum of HL^1 , Fig (3.2), revealed the characteristic band of the functional groups including a peak at 3433cm^{-1} assigned to the overlap of peaks (NH) of the secondary amine and OH enol of the carbonyl group which formed as a result of tautomerism between carbonyl-dimedone with a proton for adjacent carbonyl, Further, the spectrum indicated a band at 1647cm^{-1} that assigned to the carbonyl group, compared with peaks at 1694 and 1616cm^{-1} which belongs to carbonyl group of 4-dimethylaminobenzaldehyde and dimedone carbonyl group. The data proved the formation of the HL^1 ligand.

2. The spectrum of H_2L^2 ligand indicated the condensation reaction of HL^1 with thiosemicarbazide moiety. The spectrum indicated two peaks at 1664 and 1622cm^{-1} attributed to the carbonyl group and imine moiety of the thiosemicarbazide, respectively confirming the formation of Schiff-base compound, Fig. (3.4). Further, the spectrum showed peaks at 3371 and 3263 , 3174cm^{-1} , which related to $\nu(\text{N-H})_{\text{hydrazinic}}$ and $\nu(\text{N-H}_2)$ derived from the thiosemicarbazone segment. The band that related to the N-H of secondary amine was detected at 3442cm^{-1} .

3. The spectra of HL¹ complexes displayed facts:

I. The band at 1645cm⁻¹ that related to $\nu(\text{C}=\text{O})_{\text{keto}}$ in free ligand was shifted to higher frequency at 1653,1662,1666,1660 and 1651cm⁻¹ in complexes, respectively. The shifting to higher of the carbonyl moiety may attributed to the coordination of the oxygen atom of the carbonyl to the metal centre in a similar fashion to that reported in literature.

II. The spectra of the metal complexes showed new bands. Which can be attributed to $\nu(\text{M}-\text{O})$ and $\nu(\text{M}-\text{N})$ moiety. Bands observed in the range (598-548)cm⁻¹ assigned to $\nu(\text{Co}-\text{O})$, $\nu(\text{Ni}-\text{O})$, $\nu(\text{Cu}-\text{O})$, $\nu(\text{Zn}-\text{O})$ and $\nu(\text{Cd}-\text{O})$, respectively. The FT-IR spectra showed bands in the range (498-471)cm⁻¹ are attributed to $\nu(\text{Co}-\text{N})$, $\nu(\text{Ni}-\text{N})$, $\nu(\text{Cu}-\text{N})$, $\nu(\text{Zn}-\text{N})$ and $\nu(\text{Cd}-\text{N})$,

4. The spectra of H₂L² complexes displayed facts:

I. The spectra of complexes showed bands at 1612, 1612, 1616, 1618 and 1614cm⁻¹ attributed to the imine group $\nu(\text{C}=\text{N})$ were shifted to lower frequency. The shift to lower frequency may be related to delocalisation of metal electron density into the ligand π -system, HOMO→LUMO. The shifting to lower frequency indicates strong bonding nature between the metal ions and the iminic (C=N) group. The shift in the $\nu(\text{C}=\text{N})$ confirmed the coordination of the ligand through nitrogen atoms of imine moieties to the metal ions.

II. The spectra of complexes revealed peaks that related to $\nu(\text{N}-\text{H})$ stretching of the secondary amine at rungs 3479-3331cm⁻¹ in complexes respectively which were shifted to lower frequency. The shift in the $\nu(\text{N}-\text{H})$ confirmed the coordination of the ligand through nitrogen atoms to the metal ions.

III. The spectra of the metal complexes showed bands allocated between $600\text{-}200\text{cm}^{-1}$ that attributed to $\nu(\text{M-N})$, $\nu(\text{M-S})$ and $\nu(\text{M-Cl})$ moiety. The FT-IR spectra exhibited bands at the range $(498\text{-}405)\text{cm}^{-1}$ were assigned to $\nu(\text{Co-N})$, $\nu(\text{Ni-N})$, $\nu(\text{Cu-N})$, $\nu(\text{Zn-N})$ and $\nu(\text{Cd-N})$ respectively, the bands at the range $(395\text{-}370)\text{cm}^{-1}$ were assigned to $\nu(\text{Co-S})$, $\nu(\text{Ni-S})$, $\nu(\text{Cu-S})$, $\nu(\text{Zn-S})$ and $\nu(\text{Cd-S})$ respectively, Band that belongs to $\nu(\text{M-Cl})$ moiety reported at $(275\text{-}233)\text{cm}^{-1}$ for (Co-Cl) , (Cu-Cl) , (Zn-Cl) and $\nu(\text{Cd-Cl})$ respectively.

(3.12.2) (UV-Vis) Spectra and magnetic susceptibility

1. The electronic spectra data of HL^1 complexes are listed in Table (3.11). The spectra show the following peaks;

I. Peaks detected around $291\text{-}297\text{nm}$ attributed to $\pi \rightarrow \pi^*$, $n \rightarrow \pi^*$ ligand field and $345\text{-}445\text{nm}$ are related to the charge transfer (C.T) transitions, respectively.

II. Additional peaks recorded in the visible region, which assigned to d-d electron-transitions, confirmed the isolation of complexes with octahedral geometries for Co(II) , Ni(II) , Cu(II) , Zn(II) and Cd(II) complexes. The magnetic moment values are in agreement with the proposed structure, Table (3.11). Complexes of Zn(II) and Cd(II) ions (d^{10} configuration) exhibit peaks related to $\pi \rightarrow \pi^*$, $n \rightarrow \pi^*$ and to charge transfer (C.T) transitions only.

2. The electronic UV-Vis spectra data of H_2L^2 complexes were listed in Table (3.12). The complexes spectra show the following peaks:

I. Peaks detected around 267-289nm related to the ligand field $\pi \rightarrow \pi^*$ and $n \rightarrow \pi^*$ transition and peaks in the range of 301-442nm are related to the charge transfer (C.T) transitions, respectively.

II. Additional peaks observed in the visible region confirmed the isolation of four and six-coordinate compounds with square planer for Ni(II) and octahedral geometries about Co(II), Cu(II), Zn(II) and Cd(II). The magnetic moment values are in agreement with the proposed structure, Table (3.12). Complexes of Zn(II) and Cd(II) ions (d^{10} configuration) exhibit peaks related to $\pi \rightarrow \pi^*$, $n \rightarrow \pi^*$ and to charge transfer (C.T) transitions only.

(3.12.3) Conductivity measurements

The molar conductance of the complexes carried out in DMSO solution. The electro-conductivity measurement values of complexes were determined to revealed conductance of (electrolyte or non-electrolyte) (3.24).

(3.12.4) Microanalysis

The microanalysis data (C.H.N.S) along with the chloride and metal content of HL^1 and H_2L^2 complexes Tables (3.5 and 3.7) are in good agreement with the calculated values. These results supported the proposed structure of the complexes.

(3.12.5) NMR data

1. The ^1H -NMR spectra of HL^1 and H_2L^2 confirmed the deduced structure of the ligands and their complexes, Fig (3.29) and (3.30). The spectrum of Zn-HL^1 and $\text{Zn-H}_2\text{L}^2$ complexes indicated the chemical shift values of the ligands with the appropriate shift due to complexation, Fig (3.33) and Fig (3.34)
2. The ^{13}C -NMR spectra of ligands in DMSO-d^6 solvent gave the right number of the resonances confirming the chemical structure and the purity of the compound, Fig (3.31) and (3.32). The spectrum of Zn-HL^1 and $\text{Zn-H}_2\text{L}^2$ complexes indicated the chemical shift values of the ligands with the appropriate shift due to complexation, Fig (3.35) and (3.36).

(3.12.6) Thermal gravimetric analysis

The thermal decomposition of the ligands and some complexes was studied to show the thermal stability of their chemical structure, which assisted in the characterization of compounds.

(3.12.7) Mass spectra

The electrospray (+) mass spectra of ligands; showed fragmentation pattern that confirmed the formation of the prepared compounds.

Based on the above, distorted octahedral structures were suggested for complexes of HL^1 ligand. The data indicated square planer, tetrahedral and distorted octahedral structure was suggested for H_2L^2 complexes.

The proposed molecular structures of complexes were sketched by CS Chem 3D Ultra Molecular Modelling and Analysis Program. The proposed structure $[\text{Co}(\text{HL}^1)_2]$ has been used as an example for the octahedral geometry, Fig (3.42). The proposed structure of $[\text{Co}(\text{H}_2\text{L}^2)\text{Cl}_2\text{H}_2\text{O}]$ and $[\text{Ni}(\text{H}_2\text{L}^2)]\text{Cl}_2$ have been used as an example for H_2L^2 complexes, Fig (3.43 and 3.44).

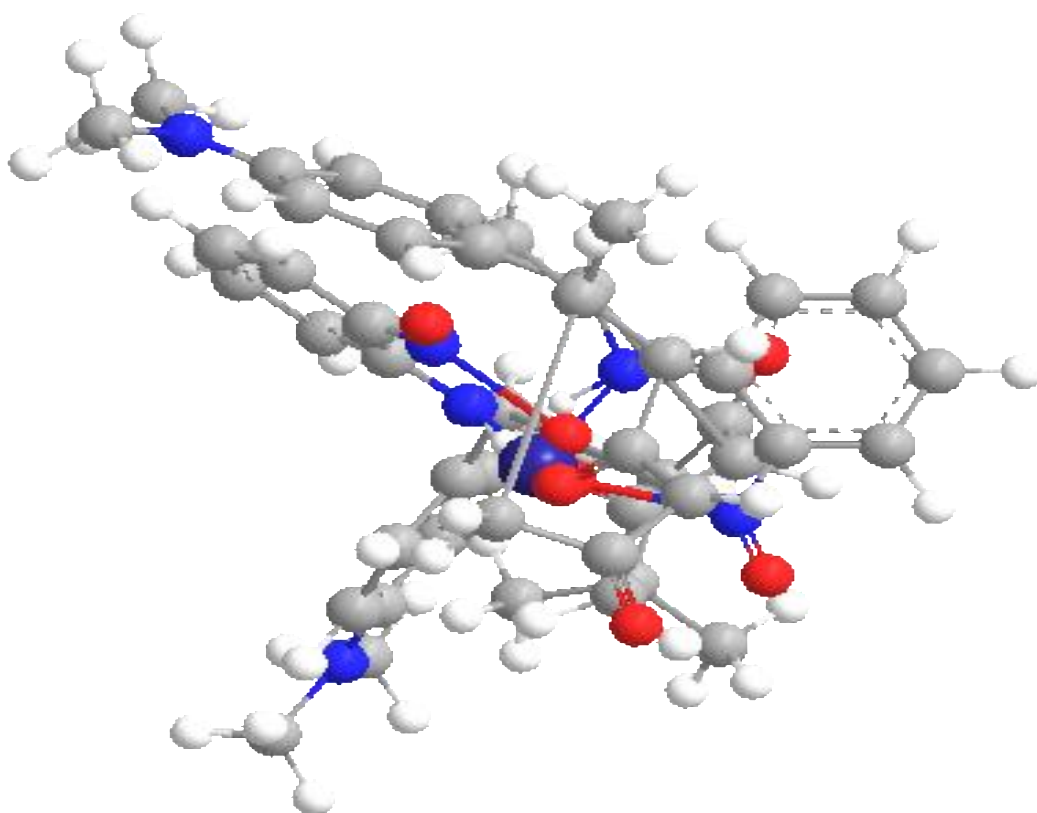


Fig (3.42): The proposed molecular structure of $[\text{Co}(\text{HL}^1)_2]$.

Table (3.25): The important bond length of [Co(HL¹)₂].

atom	Bond length(°/Å)
N-H	1.050
N-CO	1.836
N-O	1.132
C=O	1.208

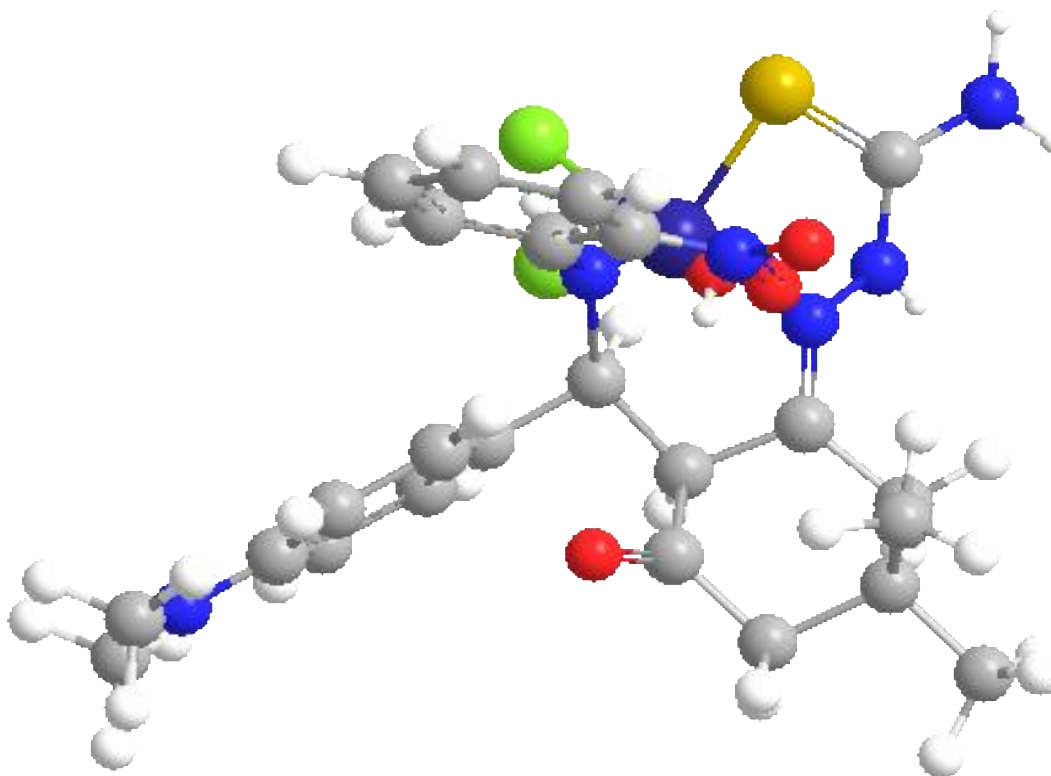
**Fig (3.43): The proposed molecular structure of [Co(H₂L²)Cl₂ H₂O].**

Table (3.26): The important bond length of [Co(H₂L²)Cl₂ H₂O].

atom	Bond length(°/Å)
C=N	1.266
C=O	1.208
Cl-Co	2.150
C-S	3.389
N-N	1.352
N-H	1.012

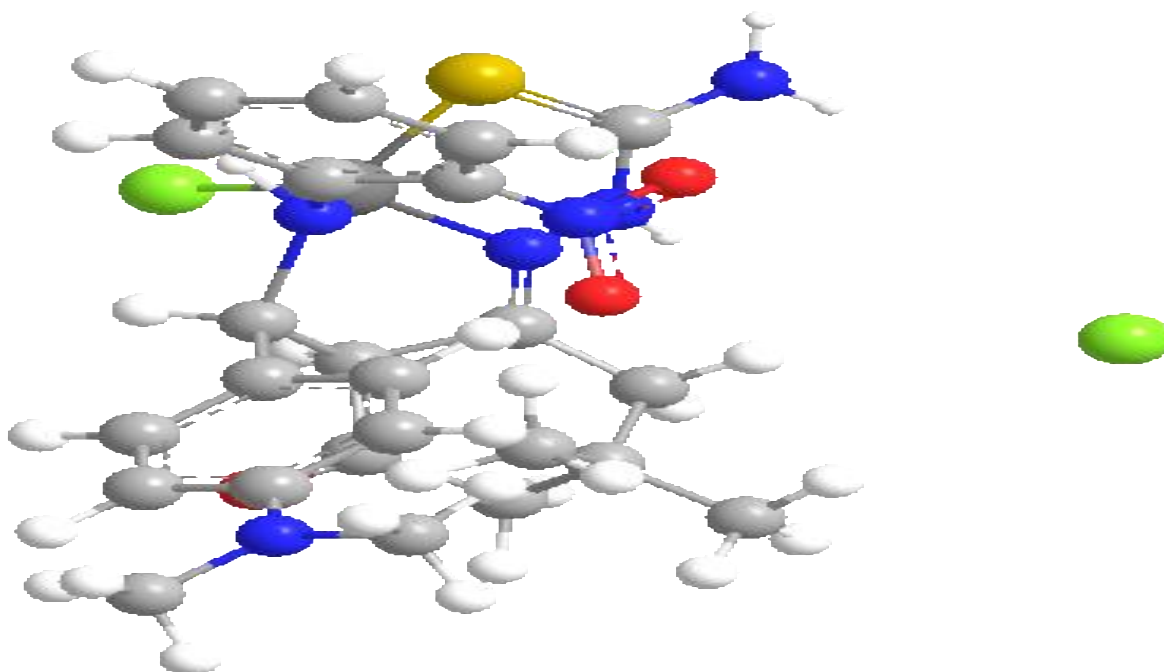
**Fig (3.44): The proposed molecular structure of [Ni(H₂L²) Cl] Cl.**

Table (3.27) : The important bond length of [Ni(H₂L²) Cl] Cl.

atom	Bond length(°/Å)
C=N	1.266
C=O	1.208
S-Ni	2.170
C-S	3.372
N-Ni	1.826
N-H	1.012

(3.13) Prospective studies

1. Preparation of new Mannich-base ligands with different substituents.
2. Preparation of new thiosemicarbazone ligands with different substituents.
3. Preparation of new metal complexes with the above ligand that based on the second and /or third series of transition ions.
4. Working on the recrystallisation of the ligands and their metal complexes to isolate compound suitable for X-ray single crystal.
5. Expanding the microbiological activity study by testing the ligands and their metal complexes against other microorganisms.
6. Studying the anti-cancer activity and DNA cleavage of the prepared compounds.

References

References

1. Souza, P JA Garcia-Vazquez and JR, Masaguer ,*Transition Met. Chem.*1985.**10**:P.410.
2. Lippard S, and Berg JM. *Principles of bioinorganic chemistry*. 1994. University Science Books, California:P.411
3. Kumar, S., Dhar DN and PN, Saxena. *Applications of metal complexes of Schiff bases a review. J Sci. Ind. Res.* 2009, **68**:P.181-187.
4. Sathe, BS., Jaychandran E., Jagtap VA. and Sreenivasa GM.. *Synthesis characterization and anti-inflammatory evaluation of new fluorobenzothiazole schiff's bases*. International Journal of Pharmaceutical Research and Development. 2011. **3**(3):P.164-169.
5. Sondhi, SM., Singh N., Kumar A. A., Lozach O. and Meijer L. *Synthesis, anti-inflammatory, analgesic and kinase (CDK-1, CDK-5 and GSK-3) inhibition activity evaluation of benzimidazole/benzoxazole derivatives and some Schiff 's bases*, Bioorganic and Medicinal Chemistry. 2006. **14**(11):P.3758-3765.
6. Pandey A, Dewangan D, Verma S, Mishra A and Dubey RD. *Synthesis of schiff bases of 2-amino-5-aryl-1,3,4- thiadiazole and its analgesic, anti-inflammatory, antibacterial and antitubercular activity*. International Journal of ChemTech Research. 2011; **3**(1):P.178-184.
7. Chandramouli, C., MR. Shivanand., TB. Nayanbhai., B. Bheemachari and RH. Udupi. *Synthesis and biological screening of certain new triazole schiff bases and their derivatives bearing substituted benzothiazole moiety*, Journal of Chemical and Pharmaceutical Research. 2012. **4**(2):P.1151-1159
8. Chinnasamy, RP., R. Sundararajan and S. Govindaraj, *Synthesis, characterization, and analgesic activity of novel schiff base of isatin derivatives*. Journal of Advanced Pharmaceutical Technology and Research, 2010. **1**(3):P.342-347

References

9. Mounika, K., B. Anupama., J. Pragathi and C. Gyanakumari. *Synthesis, characterization and biological activity of a Schiff base derived from 3-ethoxy salicylaldehyde and 2- amino benzoic acid and its transition metal complexes.* Journal of Scientific Research,2010.**2**(3):P.513-524.
10. Venkatesh, P, *Synthesis, characterization and antimicrobial activity of various Schiff bases complexes of Zn(II) and Cu (II) ions.* Asian Journal of Pharmaceutical and Health Sciences, 2011.**1**(1):P.8-11.
11. Chaubey, AK and SN. Pandeya. *Synthesis & anticonvulsant activity (Chemo Shock) of Schiff and Mannich bases of Isatin derivatives with 2-Amino pyridine (mechanism of action),* International Journal of Pharm Tech Research. 2012.**4**(4):P.590-598
12. Aboul-Fadl,T., FA. Mohammed and EA. Hassan, *Synthesis, antitubercular activity and pharmacokinetic studies of some Schiff bases derived from 1-alkylisatin and isonicotinic acid hydrazide (INH).* Archives of Pharmacal Research, 2003. **26**(1):P.778-784.
13. Miri,R.,N.Razzaghi-asl and MK. Mohammadi, *QM study and conformational analysis of an isatin Schiff base as a potential cytotoxic agent.* Journal of Molecular Modeling. 2013. **19**(2):P.727-735.
14. Ali, SMM, M. Abul Kalam Azad and M. Jesmin, *In vivo anticancer activity of Vanillin semicarbazone,* Asian Pacific Journal of Tropical Biomedicine. 2012.**2**(6):438- 442.
15. Wei, D., N. Li., G. Lu and K. Yao, *Synthesis, catalytic and biological activity of novel dinuclear copper complex with Schiff base.* Science in China B, 2006. **49**(3):P.225-229.

References

16. Avaji, PG., CH. Vinod Kumar., SA. Patil., KN. Shivananda and Cc. Nagaraju, *Synthesis, spectral characterization, in-vitro microbiological evaluation and cytotoxic activities of novel macrocycli bis hydrazone*. European Journal of Medicinal Chemistry, 2009. **49**(9):P.3552-3559.
17. Venugopala, KN and BS. Jayashree. *Synthesis of carboxamides of 2-amino-4-(6-bromo-3-coumarinyl) thiazole as analgesic and antiinflammatory agents*. Indian Journal of Heterocyclic Chemistry, 2003. **12**(4):P.307-310.
18. Emayavaramban, M., K. Kumar ., P. Mani., B. Prabhakaran. and A. Muthuvel, *Synthesis, complexation, spectral and antimicrobial study of some novel 5 bromofluorobenzaldehydeoxime and semicarbazone under ultrasonic irradiation*. International Journal of Advanced Chemistry. 2014. **2**(1):P.20-23.
19. Salman, A.K., M.A. Abdullah., K. Al-Amry and M.A. Malik, *Synthesis, Characterization, Electrochemical Studies, and In vitro Antibacterial Activity of Novel Thiosemicarbazone and Its Cu(II), Ni(II), and Co(II) Complexes*. Hindawi Publishing Corporation Scientific World Journal, 2014. **592375**:P.9.
20. Schiff, H, *eine neue reihe organischer Basen*, Justus Liebigs Annalen der Chemie, Justus Liebigs Annalen der Chemie, 1864. **131**(1):P.118-119
21. Dhar, DN and CL. Taploo. *Schiff bases and their applications*, Journal of Scientific and Industrial Research, 1982:P.501-506
22. Kalaivani, S., NP. Priya and S. Arunachalam, *Schiff bases: facile synthesis, spectral characterization and biotical studies*. Ipampt, 2012. **3**:P.219-223
23. Cozzi PG. *Chem. Soc. Rev.* 2004. **33**:P.410.
24. Du, X., Yu X J *Pol. Sci.: Part A: Polymer Chemistry*. 1997. **35**:P.3249
25. Raeisaenen, M., *thesis Laboratory of Inorganic Chemistry, Department of Chemistry Faculty of Science, University of Helsinki Finland* P.G. Cozzi, *Chem. Soc. Rev.* 2004. **33**:P.410.

References

26. Ray, R., Md. Kudrat-E-Zahan., MM. Haque and Md. Abdul Alim, *Synthesis, characterization and antimicrobial activity of Co(II), Cu(II), and Mn(II) metal complexes of Schiff base ligand derived from cinnamaldehyde and ethylenediamine*. *Int. J. Chem. Stud*, 2015. **3**(2):P.17-19
27. Banu, L. A., Md. Kudrat-E-Zahan., Md. Abul Bashar., MM. Haque., Md. Quamruzzaman. and M. Saidul Islam, *Studies on synthesis and characterization with antimicrobial activity of mixed ligand coordinating co (ii) Complexes with phthalic acid and heterocyclic amines*. *Int. J Chem. Stud*, 2015. **2**(6):P.38-41
28. Costes, JP., F. Dahan ., MBF. Fernandez, MIF. Garcia and AMG. J. Deibe AMG. J, *Sanmartin, Inorg. Chim. Acta*.1998:P. 27473.
29. Kaczmarek, MT., R Jastrza, E. Hoáderna-KĆdzia and W. Radecka- Paryzek. *Inorg. Chim. Acta*. 2009, 362:P.3127.
30. Mukherjee, P., O. Sengupta., MGB. Drew and A. Ghosh. *Inorg. Chim. Acta*. 2009. **362**:P.285.
31. Neelakantana, MA., F. Rusalraj., F. Dharmaraja ., S. Johnsonraja ., T Jeyakumar and MS. Pillai, *Spectrochim. ActaA*. 2008, **71**:P.1599.
32. Busch, DH. J., *Mol. Inclusion Phenom. Recognit. Chem.* 1992.12:389.
33. Mannich, C and W . Krosche , *Arch. Pharm.* 1912: 250 647.
34. Mannich, C and W. Krosche .1912*Ueber ein Kondensationsprodukt aus Formaldehyd, Ammoniak und Antipyrin*. *Arch. Pharm*, 1912:P. 250 647.
35. Irene, B., C. Dubernet and P. Couvreur, *Nanoparticles in cancer therapy and diagnosis*. *Advanced Drug Delivery Reviews*, 2002. **54**:P. 631–651.
36. Dahn, U., H. Hagenmaier., H. Hohne ., WA. Ko¨nig., G .Wolf and H. Zahner 1997 *Arch Microbiol* **107**:P.143.

References

37. Shriner, R. L., and H. R. Todd, *5,5-dimethyl-1,3 cyclohexanedione*. *Organic Syntheses*, 1935. 15:P. 16.
38. Clayden, J., N. Greeves., S. Warren and Wothers. *Peter (2001)*. *Organic Chemistry (1st ed.)*. Oxford University Press :p. 532. isbn 978-0-19-850346-0.
39. Bolte, M and M .Scholtyssik *Dimedone at 133K*. *Acta Crystallogr.* 1997. **53** (10): 9700013. doi:10.1107/S0108270197099423
40. Anslyn, E.V and D. A Dougherty. (2006) *Modern physical organic chemistry*. 2006: University Science Books, Sausalito.
41. Shaygan,S., P.Pasdar Hoda., N. Foroughifar., M. Davallo and Fereshteh. *Cobalt (II) Complexes with Schiff Base Ligands Derived from Terephthalaldehyde and ortho-Substituted Anilines: Synthesis, Characterization and Antibacterial Activity*. *MotieeAppl. Sci.* 2018, 8, **85**: doi:10.3390/app8030385.
42. Pahonțu,E., D. C. Ilieș., S. Shova., C. Paraschivescu ., M. Badea., A. Gulea and T. Roșu. *Synthesis, Characterization, Crystal Structure and Antimicrobial Activity of Copper(II) Complexes with the Schiff Base Derived from 2-Hydroxy-4-Methoxybenzaldehyde*. *Molecules*, 2015. **20**:P 5771-5792.
43. Maihub, A.A., F. S. Alassbaly., M.El-Ajaily and A.M. Etorkil, *Modification on Synthesis of Mixed Ligand Chelates by Using Di- and Trivalent Transition Metal Ions with Schiff Base as Primary Ligand*. *Green and Sustainable Chemistry*, 2014.4:P. 103-110.

References

44. Dubey. R. K., Mishra. C. M and Mishra .A. N., *Synthesis, reactivity and physico-chemical studies of some novel mixed ligand complexes of copper (II)* Indian J. of Chem, 2005. **44**:P. 1159-1164.
45. Al-Jeboori.M.J and S. A Hussain, *New Metal Complexes Derived from Mannich-Base Ligand; Synthesis, Spectral Characterisation and Biological Activity*. Journal of Global Pharma Technology, 2019. **11** (02) :P.548-560.
46. Yousif. E. I., *New Mixed Ligand Complexes ; Synthesis, Spectral Analysis and Biological Activity*. Journal of Global Pharma Technology, 2019. **11**(02) :P.196-203.
47. Liaqat1,M., T.Mahmud., M.Imran., M. Ashraf., U Haq.,M. Muddassar. and T. Ahmad . *Synthesis, characterization and biological activities of a novel Mannich base 2-[(3, 4-dimethoxyphenyl)(pyrrolidin-1-yl)methyl]cyclopentanone and its complexes with Cu(II), Co(II), Ni(II) and Fe(II) ions*. Bulgarian Chemical Communications, 2018. **50**:P. 37 – 43.
48. Al-Jeboori.M.J, E.I. Yousif., R.M. Ahmed., A. H. Hasan., A.S Al-Fahdaw. *Metal Complexes of Heterocyclic Hydrazone Schiff-Bases: Preparation, Spectral Characterisation and Biological Study.*, Iran. J. Sci .Technol Trans.Shiraz University, 2017. **10** (1007):P.017-0187.
49. Goyat, G., S. Garg and K.K. verma, *Complexes of Tellurium(IV) with Isatin-Aniline Schiff Base*. Chemical Science Transactions., 2016, **5**(2):P. 479-487.
50. Balakrishnan.A. and Sankar.A, *studies on the synthesis and Characterization of the transition metal complexes of novel mannich base*. ijpcbs., 2016. **6**(2):P. 150-152.

References

51. Al-Jeboori M. J., R. M. Ahmed., E .I .Yousif , *Co(II) and Cd(II) Complexes Derived from Heterocyclic Schiff-Bases Synthesis, Structural Characterisation, and Biological Activity*. Hindawi Publishing Corporation Scientific World Journal, 2013. **754868**:P.6 .
52. Ramesh .M and A. Sabastiyam , *Synthesis, Characterization and Antimicrobial Studies on a New Mannich Base N-(Morpholinomethyl)phthalimide and its Zinc(II), Cadmium(II) and Mercury(II) Complexes*. Der Chemica Sinica, 2012. **3**(5):P.1297-1304
53. Jameela.A.A., S. A . Palanisamyb.M and M.Padushaa, *Synthesis, characterization and antimicrobial studies of mannich base derived from benzohydrazide and its metal complexes*., Pelagia Research Library., Der Chemica Sinica, 2012. **3**(4):P.864-867
54. Kumar .S. M., M. P. Kesavan ., G.G.V . M.Kumar., M .Sankarganesh., G Chakkaravarthi., G. Rajagopal and J. Rajesh, *New heteroleptic Zn(II) complexes of thiosemicarbazone and diimine Co-Ligands: Structural analysis and their biological impacts*. Journal of Molecular Structure, 2018. **1153** : P 1-11
55. Verma, *Synthesis and Characterization of manganese(II) complexes with Semicarbazide and Thiosemicarbazide based ligands*. International Journal of Pharmaceutical Sciences and Research, 2017. **8**(3):P. 1504-1513.
56. Hossain.Md. S.,C.M. Zakaria., Md. Kudrat-E-Zahan. and B. Zaman, *Synthesis, Spectral and Thermal Characterization of Cu(II) Complexes with Two New Schiff Base Ligand towards Potential Biological Application*. Pelagia Research Library, Der Chemica Sinica, 2017, **8**(3):P.380-392.

57. Tyagi. M and S. Chandra, *Synthesis, characterization and biocidal properties of platinum metal complexes derived from 2,6-diacetylpyridine (bis thiosemicarbazone)*. Open Journal of Inorganic Chemistry, 2012. **2**:P. 41-48.
58. Ahmad .R. M., A. H. Hasan ., E. I. Yousif and D. F. Hussien, *Synthesis , characterize and biological studies of (Cr(III) ,Mn(II) ,Zn(II)and Cd(II)) complexes with Schiff-base ligand*. djps, 2012. **8**:P. 3.
59. Prathimaa. B., Y. S. Raoa., S. A. Reddyb., Y.P. Reddyc and A. V. Reddya , *Copper(II) and nickel(II) complexes of benzyloxybenzaldehyde-4-phenyl-3-thiosemicarbazone:Synthesis, characterization and biological activity*. Spectrochimica Acta Part, 2010. **77** :P.248–252.
60. Xinde Zhu, W.Chenggang, L.Zhiping and D.Yuanlin, *Synthesis, characterization and biological activity of the Schi€ base derived from 3,4-dihydroxybenzaldehyde and thiosemicarbazide, and its complexes with nickel(II) and iron(II)*. Transition Met. Chem,1997. **22**:P.9-13.
61. Balachandrana. C. d., J. Haribabub., K. Jeyalakshmib., S.P. Nattamai.,B.R. Karvembub., N.o.Emia and S.Awaled, *Nickel(II) bis(isatin thiosemicarbazone) complexes induced apoptosis through mitochondrial signaling pathway and G0/G1 cell cycle arrest in IM-9 cells*.Journal of Inorganic Biochemistry, 2018. **182** :P. 208–221.
62. Quevedo, R and B. Moreno-Murillo, *One-step synthesis of a newheterocyclophane family*. Tetrahedron Letters, 2008. **50**(8):P. 936–938.
63. Balakrishnan .A and Dr.A. Sankar, *Study on the Synthesis, Characterization and Antimicrobial studies of the Transition Metal Complexes of the Novel Mannich Base Derived from Pyridazine Derivative*. International Journal of Scientific and Research Publications, 2016. **6** (11):P.2250-3153.

64. Cimerman Z., S. Miljanić. and N. Galić, *Schiff bases derived from aminopyridines as spectrofluorimetric analytical reagents*. Croatica Chemica Acta, 2000 **73** (1) p: 81–95.
65. Galewaki, Z, *Liquid crystalline properties of 4-halogenobenzylidene-4'-alkoxyanilines*. Mol. Cryst. Liq. Crystal, 1994. **249**:P. 43-49.
66. Bong sze hao , *Synthesis and characterization of Schiff base liquid crystals possessing dlalkylAminotermnal unit*. 2011:facult of science unaversiti tunkuabdul rahman may Sc. (Hons.) Chemistry.
67. Liaqat. M., T. Mahmud., A. Hameed., M. Ashraf and H. Asghar, *Synthesis, characterization and antiurease activities of a novel Mannich base 1-[(4-methoxyphenyl)(2- methylidenecyclohexyl)methyl]pyrrolidine (MMP) and its complexes with Cu (II), Ni (II), Co (II), and Fe (II) ions*. Inorganic and Nno-Metal Chemistry, 2017 .**47**:P. 1418-1423.
68. Liaqat. M., T. Mahmud., M. Ashraf., M.Muddassar., M.Imran., T.Ahmad. and L. Mitu, *Synthesis, Characterization and Biological Activities of a Novel Mannich Base 2-[(3,4-dimethoxyphenyl)(pyrrolidinyl) methyl]cyclohexanone and its Complexes with Cu(II), Ni(II), Co(II) and Fe(II) Ions*.REV.CHIM.(Bucharest) ,2017.**68**(12):P.2845-2849.
69. Najmodin. A., A. Fezzeh ., T.Lalleh., Z.Azim and MR. Saidi, *Highly Efficient One-Pot Three-Component Mannich Reaction in Water Catalyzed by Heteropoly Acids*. J. Org. Chem, 2006.**8**:P. 2079-2082.
- 70 . Ramesh.M and .A. Sabastiyam , *Synthesis, Characterization and Antimicrobial Studies on a New Mannich Base N-(Morpholinomethyl)phthalimide and its Zinc(II), Cadmium(II) and Mercury(II) Complexes*. Der Chemica Sinica, 2012, **3**(5):P.1297-1304.

References

71. Al-Fahdawi .M.S., PhD thesis, University of Baghdad. 2006:P. 148-178.
- 72 . Nair M.S., D. Arish and J. Johnson, *Synthesis, characterization and biological studies on some metal complexes with Schiff base ligand containing pyrazolone moiety*. Journal of Saudi Chemical Society, 2016. **20**:P.591–598.
73. Elamathi .C., R. Butcher and R. Prabhakaran, *Preparation, characterizations and biological evaluations of new copper(II) complexes containing ONO pincer type ligands*. Appl Organometal Chem, 2018. **32**(6):P.1-18.
- 74 . Al-Jeboori. M. J., A. H .AL-Dujaili and A. E. Al-Janabi, *Coordination of carbonyl oxygen in the complexes of polymeric N-crotonyl-2-hydroxyphenylazomethine*. Transition Met Chem, 2009. **34**:P.109–113.
75. Thatcher. F. S and W. Simon , *A comparative appraisal of the properties of 'staphylococci' isolated from clinical sites and from dairy products*. Can J Microbiol , 1956. **2** :P.704-709.
76. Nakamoto, K, *Infrared Spectra of Inorganic and Coordination Compounds*. John Wiley and Sons, 1996 New York, 4th Edn.
77. Volkert W. A and T. J. Hofman, *Therapeutic radiopharmaceuticals*. Chem. Rev, 1999. **99**:P.2269.
78. Bal. S and S. S .Bal, *Cobalt(II) and Manganese(II) Complexes of Novel Schiff Bases, Synthesis, Characterization, and Thermal, Antimicrobial, Electronic, and Catalytic Features*. Advances in Chem. 2014, **506851**:P.1-13.
79. Smith .P. H., J. R. Morris. and G. D .Ryan, *Prediction of q-values and conformations of gadolinium chelates for magnetic resonance imaging*. J. Am. Chem. Soc, 1989. **7437**:P. 111.

References

80. Oberhausen. K. J., J. F. Richandon and R. M. Buchanan, *Century-Known Copper Salt Cu(OAc)(OMe) Proven To Be a Unique*. Inorg. Chem,1991. **30**:P.1357.
81. Colchoubian.H., WL. Waltz. and JW. Quail. 1999, *Can .J .Chem.*, 37-77.
82. Ledbetter .JW, *J. Phys. Chem*, 1966:P. 2245 .
83. Ramachandran .E., Gandin. V., Bertani, . Sgarbossa. P., . Natarajan. K., Bhuvanesh. N., Venzo. A., Zoleo A., Glisenti A., Dolmella A., Albinati. A., Marzano and. Marzano. C., “*Synthesis, characterization and cytotoxic activity of novel copper(II) complexes with aroylhydrazone derivatives of 2-Oxo-1,2-dihydrobenzo[h] quinoline-3-carbaldehyde*. *Journal of Inorganic Biochemistry*,2018. **182**:P.18–28.
84. Dong. X-Y., Q-P. Kang ., X-Y. Li., J-C. Ma and W-K Dong ,*Structurally Characterized Solvent-Induced Homotrimeric Cobalt(II) N2O2-Donor Bisoxime-Type Complexes*. 2018,**8**(139):P.1-17.
85. Hassaan .A. M., M. A. Khalifa . and A. K. hehata, *Complexes of some metal ions with a Schiff base ligand derived from Isatin and O-aminophenol*. *Bull. SOC. Chim. Belg*,1995.**104**(3):P. 121-124.
- 86 . Souza,P., M. A Mendiola., A. Matesanz. and .V. Fermindez , *Synthetic and physicochemical studies of divalent metal complexes with cyclic hydrazone and semicarbazone ligands*. *Transition Met. Chem*,1995 .**20**:P.157-161.
- 87 . Lever. *Inorganic Electronic Spectroscopy*, ABP 1984: New York.

References

88. Al-Jeboori M.J., R. M .Ahmed., T.A. Hamdan., A.T .Numan and H. Potgieter .H, *Formation of polymeric assemblies of sixcoordinate metal complexes with mixed bridges of dicarboxylato-azido moieties*, *Complex Metals*, 2014.**1**:(1):P.38-45.
89. Bain. G. A and J. F. Berry, *Diamagnetic Corrections and Pascal's Constants*”, *Journal of Chemical Education*,2008. **85**:P.532-536.
90. Evans .D, *A new type of magnetic balance*, *Journal of Physics E : Scientific Instruments*, 1974. **7**:P.247-249.
91. Ammari, L. K., J. M. Puck, and K. L. McGowan, *Catheter-related Fusarium solani fungemia and pulmonary infection in a patient with leukaemia in remission*. *Clin. Infect. Dis*, 1993. **16**:P.148-150.
92. Housecroft C. E and Sharpe A. G., *Inorganic Chemistry*; Pearson Education Limited: 2008. Vol. 3.
- 93.Kano T., S. Song.,Y.Kubota and K. Maruka, *Highlydiastereandenantioselective mannich reactions of synthetically flexible ketimines with secondary amine organocatalysts.*, *Ang. Chem. Int. Ed.*, 2012. **51**(5): P. 1191 –1194.
94. Himanshu A., L. Francesc and M. Rabindranath, *One-Dimensional Appended Coordination Polymers of Mn^{II}, Cu^{II}, and Zn^{II} Supported by Carboxylate-(2-Pyridyl)alkylamine Ligands – Structure and Magnetism.*, *Euro.J .Inorg. Chem .*, 2009. **22** : P. 3317-3325.

References

95. Qing C., Z. Ming-Hua Z., Lian-Qiang W and Mohamedally K ., *A Multifaceted Cage Cluster, $[Co^{II}_6O_{12} \supset X]^-$ ($X = Cl^-$ or F^-): Halide Template Effect and Frustrated Magnetism* . Chem. Mater, 2010 .**22** : P. 4328-4334.
96. Canpolat E and M. Kaya, *Spectroscopic characterization of N,N-bis(2-[(2,2-Dimethyl-1,3-Dioxolan-4-yl)Methyl]Amino)Ethyl)N',N'Dihydroxyethane diimidamide and its complexes*. Russian J. Coord. Chem, 2005. **31**(7): P. 511-515
97. Geary W.J, *The use of conductivity measurements in organic solvents for the characterisation of coordination compounds*. Russian J. Coord Chem.Rev.1971. **7**: P. 81-122.
98. Rahman. A., M Choudhary and W. Thomsen, *Bioassay Techniques For Drug Development*. 2001: Harwood Academic. Amsterdam. The Netherlands.
99. Singh R.V., R. Dwivedi and S. C Joshi, *Synthetic, magnetic, spectral, antimicrobial and antifertility studies of dioxomolybdenum(VI) unsymmetrical imine complexes having a $N \cap N$ donor system*, Trans .Met .Chemi , 2004. **29** (1) : P.70–74.
100. Tweedy B. G, *Plant extracts with metal ions as potential antimicrobial Agents*. Phytopathology,1964. **55**: P.910–914
101. Ramesh, R and S. Maheswaran, *Synthesis, spectra, dioxygen affinity and antifungal activity of Ru(III) Schiff base complexes*.J.Inorg .Biochem,2003. **96**:P.457–462.

الخلاصة

تضمن البحث تحضير وتشخيص نوعين من الليكاندات ومعقداتها الفلزية. حضر الليكاند الاول وهو من نوع (قاعدة مانخ) باستخدام كلوريد الكالسيوم كعامل مساعد و الكحول الايثيلي كوسط للتفاعل ومن خلال مزج ثلاث مكونات هي : 4- ثنائي- ميثيل- امينو بنزليدهايد ،اورثونايتروأنلين مع الدايميدون و بنسب مولية مقدارها 1:1:1.

حيث : $HL^1 = L^1$

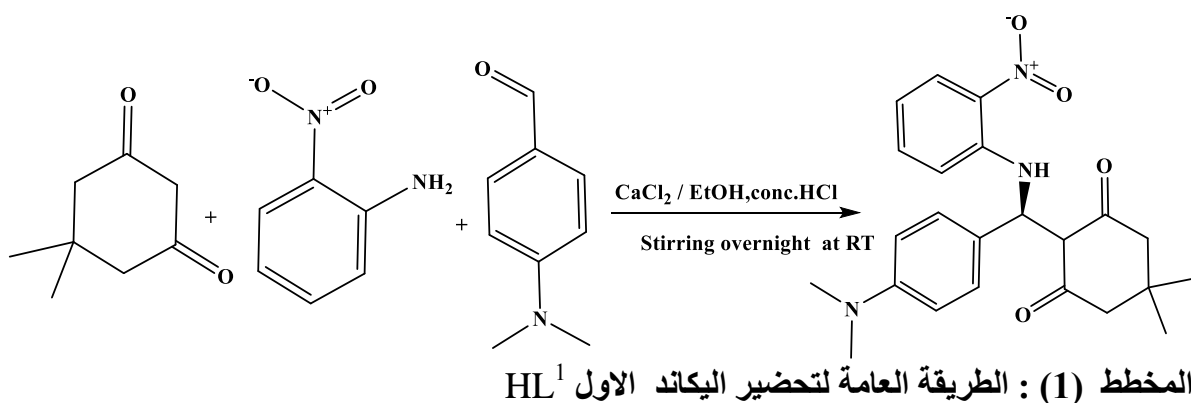
$HL^1 = R$ -2-((4-(dimethylamino)phenyl)((2-nitrophenyl)amino)methyl)-5,5-dimethylcyclohexane-1,3-dione

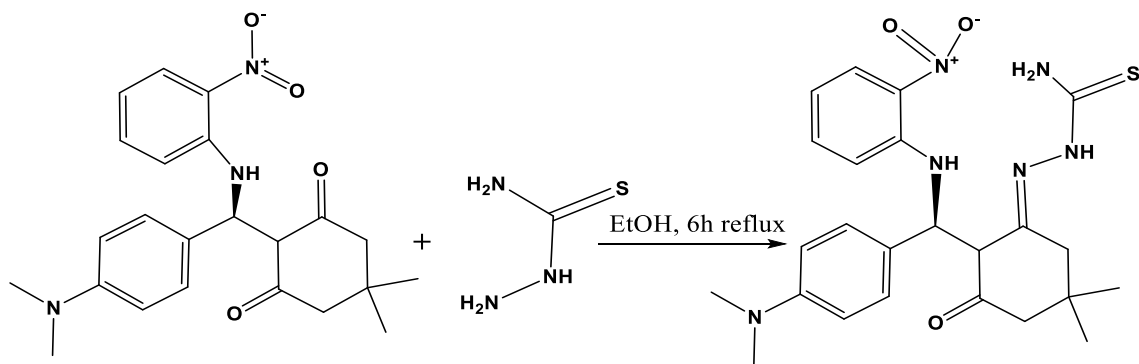
اما الليكاند الثاني فهو (قاعدة شف) وحضر من تفاعل اليكاند الاول مع مادة الثايو سمي كاربازايد و بنسب مولية مقدارها 1:1 .

حيث : $H_2L^2 = L^2$

$H_2L^2 = (E)$ -2-(2-((S)-(4-(dimethylamino)phenyl)((2 nitrophenyl)amino)methyl)-5,5-dimethyl-3-oxocyclohexylidene)hydrazine-1-carbothioamide

والمخططات التالية توضح تحضير اليكاندات HL^1 و H_2L^2





المخطط (2) : الطريقة العامة لتحضير اليكاند الثاني H_2L^2

حضرت المعقدات باستخدام كلا الليكندين لتحضير سلسلة من المعقدات الفلزية مع ايونات :

(Co(II), Ni(II), Cu(II), Zn(II) and Cd(II))

وذلك بمزج نسب مولية مقدارها 2:1 (فلز: ليكاند) باستخدام DMF وسط للتفاعل.

الصيغة العامة لمعقدات اليكاند الاول HL^1 .

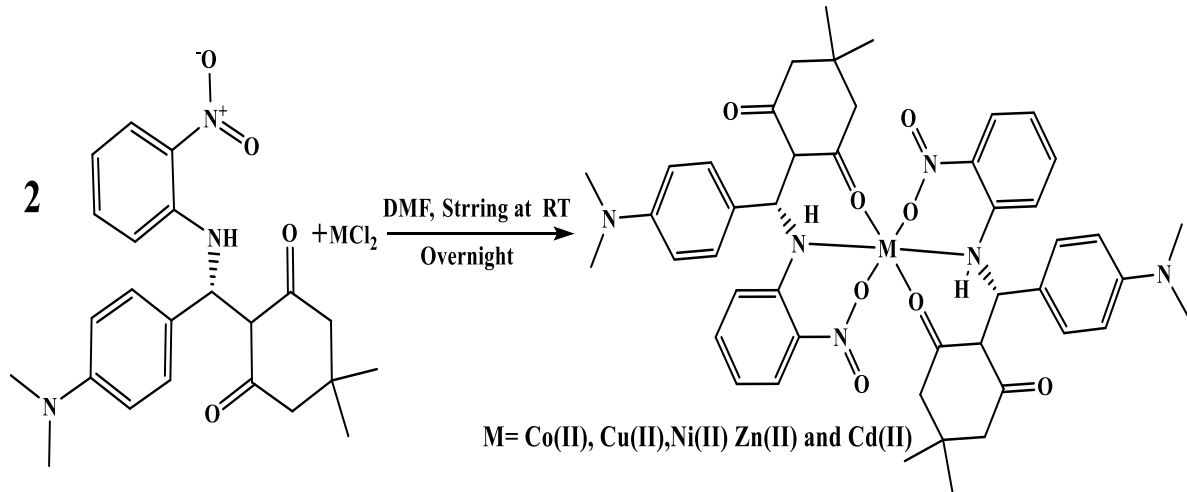
$[M(HL^1)_2]$ where M= Co(II), Ni(II), Cu(II) , Zn(II) and Cd(II)

الصيغة العامة لمعقدات اليكاند الثاني H_2L^2 .

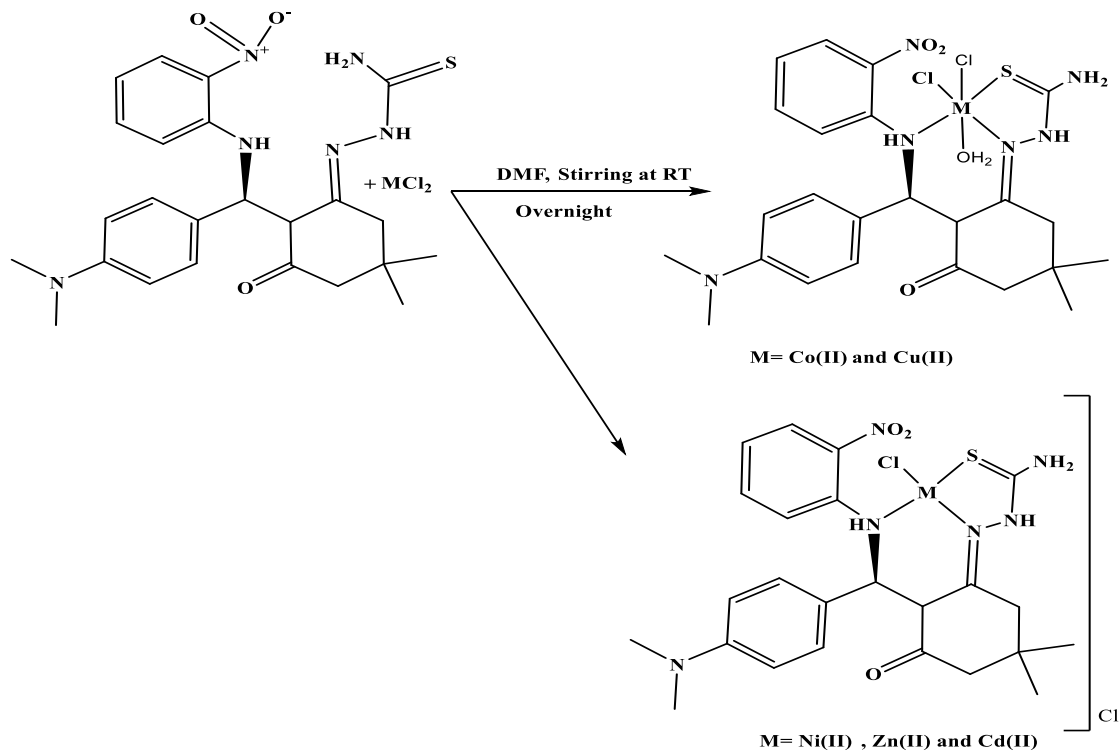
$[M(H_2L^2) Cl_2]$ where M= Co(II), Cu(II), Zn(II) and Cd(II)

$[M(H_2L^2)]Cl_2$ where M= Ni(II)

شخصت الليكاندات والمعقدات بواسطة التحليل الدقيق للعناصر، محتوى المعدن والكلور والتحليل لبعض المعقدات، مطياف الأشعة تحت الحمراء، ومطياف الأشعة فوق البنفسجية والرنين النووي المغناطيسي ومطيافية الكتلة بالإضافة الى فحص الحساسية المغناطيسية، التوصيلية المولارية ودرجة الانصهار.



المخطط (3) : الطريقة العامة لتحضير معقدات الليكاند الاول HL^1



المخطط (4) : الطريقة العامة لتحضير معقدات الليكاند الثاني H_2L^2

واعتمادا على المعطيات التحليلية والطيفية تم اقتراح الاشكال الاتية:

1- اشكال ثمانية السطوح مشوهه بالنسبة لمعقدات اليكاند الاول مع جميع الايونات

Co(II), Ni(II), Cu(II), Zn(II) and Cd(II)

2- اشكال ثمانية السطوح مشوهه بالنسبة لمعقدات الليكاند الثاني مع ايونات الايونات.

Co(II) , Cu(II)

3- شكل مربع مستوي بالنسبة لمعقدات الليكاند الثاني مع ايون.

Ni(II)

4- شكل رباعي السطوح بالنسبة لمعقدات الليكاند الثاني مع ايونات.

Zn(II) , Cd(II)

تم تشخيص الفعالية البايولوجية لكلا اللكندين مع معقداتها الفلزية بالنسبة لنوعين من البكتريا :

موجبة لصبغة :

(*Staphylococcus aureus and Bacillus subtilis*)

وسالبة لصبغة:

(*Escherichia coli and Pseudomonas aeruginosa*)

وكذلك شخصت الفعالية اتجاه نوعين من الفطريات وهي

(*Candida and Trichomoniasis*)



جمهورية العراق
وزارة التعليم العالي والبحث العلمي
جامعة بغداد
كلية التربية للعلوم الصرفة / ابن الهيثم
قسم الكيمياء

التحضير ، التشخيص التركيبي ، الخواص الحرارية والفعالية البيولوجية
للمعقدات الجديدة المشتقة من ليكاندات مع ذرات N و O و S المانحة

رسالة مقدمة الى مجلس كلية التربية للعلوم الصرفة / ابن الهيثم/
جامعة بغداد
وهي جزء من متطلبات نيل درجة الماجستير في الكيمياء

من قبل

نهاد كاظم حسن

بكالوريوس علوم كيمياء (2003) كلية التربية للعلوم الصرفة / ابن الهيثم / جامعة بغداد

بأشراف

أ.م.د. انعام اسماعيل يوسف